**INSTITUTE OF SEISMOLOGY**
**UNIVERSITY OF HELSINKI**
**REPORT S-62**

# LITHOSPHERE 2014

## EIGHTH SYMPOSIUM ON STRUCTURE, COMPOSITION AND EVOLUTION OF THE LITHOSPHERE IN FENNOSCANDIA

***PROGRAMME AND EXTENDED ABSTRACTS***

**edited by**

**Olav Eklund, Ilmo Kukkonen, Pietari Skyttä, Pia Sonck-Koota, Markku Väisänen, David Whipp**

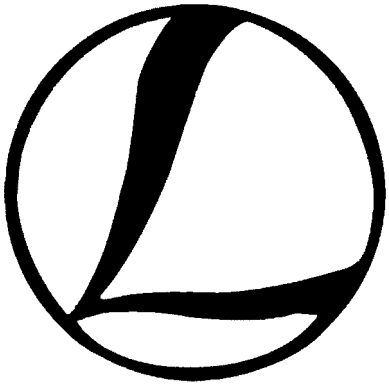





Turun yliopisto
University of Turku


**Åbo Akademi University,**
**Turku, November 4-6, 2014**

**Turku 2014**

Publisher: Institute of Seismology
P.O. Box 68
FI-00014 University of Helsinki
Finland
Phone: +358-294-1911 (switchboard)
Fax: +358-2941-51598
http://www.helsinki.fi/geo/seismo/

ISSN 0357-3060
ISBN 978-952-10-5081-7 (Paperback)
Gosmo Print Oy
Turku 2014
ISBN 978-952-10-9282-5 (PDF)

# LITHOSPHERE 2014

## EIGHTH SYMPOSIUM ON STRUCTURE, COMPOSITION AND EVOLUTION OF THE LITHOSPHERE IN FENNOSCANDIA

***PROGRAMME AND EXTENDED ABSTRACTS***

Åbo Akademi University,
Turku,
November 4-6, 2014

**CONTRIBUTING ORGANIZATIONS**

Finnish National Committee of the International Lithosphere Programme (ILP)
Finnish Geodetic Institute
Geological Survey of Finland
University of Helsinki
University of Oulu
University of Turku
Åbo Akademi University

**ORGANIZING COMMITTEE AND EDITORS**


| | |
|---|---|
| Olav Eklund | Geology and mineralogy, Åbo Akademi University<br>Domkyrkotorget 1, FI-20500 Åbo/Turku, Finland<br>E-mail: olav.eklund [at] abo.fi |
| Ilmo Kukkonen | Department of Physics<br>P.O. B. 64, FI-00014 University of Helsinki, Finland<br>E-mail: ilmo.kukkonen [at] helsinki.fi |
| Pietari Skyttä | Geology Section, Dept. of Geography and Geology<br>FI-20014 University of Turku, Finland<br>E-mail: pietari.skytta [at] utu.fi |
| Pia Sonck-Koota | Geology and mineralogy, Åbo Akademi University<br>Domkyrkotorget 1, FI-20500 Åbo/Turku, Finland<br>E-mail: pia.sonck-koota [at] abo.fi |
| Markku Väisänen | Geology Section, Dept. of Geography and Geology<br>FI-20014 University of Turku, Finland<br>E-mail: markku.vaisanen [at] utu.fi |
| David Whipp | Institute of Seismology, Dept. of Geosciences and Geography<br>P.O.B. 68, FI-00014 University of Helsinki, Finland<br>E-mail: david.whipp [at] helsinki.fi |

**References of Lithosphere Symposia Publications**

*Pesonen, L.J., Korja, A. and Hjelt, S.-E., 2000 (Eds.)*. Lithosphere 2000 - A Symposium on the Structure, Composition and Evolution of the Lithosphere in Finland. Programme and Extended Abstracts, Espoo, Finland, October 4-5, 2000. Institute of Seismology, University of Helsinki, Report S-41, 192 pages.

*Lahtinen, R., Korja, A., Arhe, K., Eklund, O., Hjelt, S.-E. and Pesonen, L.J., 2002 (Eds.).* Lithosphere 2002 – Second Symposium on the Structure, Composition and Evolution of the Lithosphere in Finland. Programme and Extended Abstracts, Espoo, Finland, November 12-13, 2002. Institute of Seismology, University of Helsinki, Report S-42, 146 pages.

*Ehlers, C., Korja A., Kruuna, A., Lahtinen, R. and Pesonen, L.J., 2004 (Eds.).* Lithosphere 2004 – Third Symposium on the Structure, Composition and Evolution of the Lithosphere in Finland. Programme and Extended Abstracts, November 10-11, 2004, Turku, Finland. Institute of Seismology, University of Helsinki, Report S-45, 131 pages.

*Kukkonen, I.T., Eklund, O., Korja, A., Korja, T., Pesonen, L.J. and Poutanen, M., 2006 (Eds.).* Lithosphere 2006 – Fourth Symposium on the Structure, Composition and Evolution of the Lithosphere in Finland. Programme and Extended Abstracts, Espoo, Finland, November 9-10, 2006. Institute of Seismology, University of Helsinki, Report S-46, 233 pages.

*Korja, T., Arhe, K., Kaikkonen, P., Korja, A., Lahtinen, R. and Lunkka, J.P., 2008 (Eds.).* Lithosphere 2008 – Fifth Symposium on the Structure, Composition and Evolution of the Lithosphere in Finland. Programme and Extended Abstracts, Oulu, Finland, November 5-6, 2008. Institute of Seismology, University of Helsinki, Report S-53, 132 pages.

*Heikkinen, P., Arhe, K., Korja, T., Lahtinen,R., Pesonen, L.J. and Rämö, T., 2010 (Eds.).* Lithosphere 2010 – Sixth Symposium on the Structure, Composition and Evolution of the Lithosphere in Finland. Programme and Extended Abstracts, Helsinki, Finland, October 27-28, 2010. Institute of Seismology, University of Helsinki, Report S-55, 154 pages.

*Kukkonen, I.T., Kosonen E.M., Oinonen, K., Eklund, O., Korja, A., Korja, T., Lahtinen, R., Lunkka, J.P. and Poutanen, M., 2012 (Eds.).* Lithosphere 2012 – Seventh Symposium on the Structure, Composition and Evolution of the Lithosphere in Finland. Programme and Extended Abstracts, Espoo, Finland, November 6-8, 2012. Institute of Seismology, University of Helsinki, S-56, 116 pages.

*Eklund, O., Kukkonen, I.T., Skyttä, P., Sonck-Koota, P., Väisänen, M. and Whipp, D., 2014 (Eds.).* Lithosphere 2014 – Eighth Symposium on the Structure, Composition and Evolution of the Lithosphere in Finland. Programme and Extended Abstracts, Turku, Finland, November 4-6, 2014. Institute of Seismology, University of Helsinki, S-62, 126 pages.

***Keywords*** (GeoRef Thesaurus, AGI): lithosphere, crust, upper mantle, Fennoscandia, Finland, Precambrian, Baltic Shield, symposia

# TABLE OF CONTENTS

# PREFACE

The Finnish National committee of the International Lithosphere Programme (ILP) organises every second year the LITHOSPHERE symposium, which provides a forum for lithosphere researchers to present results and reviews as well as to inspire interdisciplinary discussions. The eighth symposium – LITHOSPHERE 2014 – comprises 36 presentations. The extended abstracts (in this volume) provide a good overview on current research on structure and processes of solid Earth. The symposium is international with contributions and participants from the neighbouring countries Estonia, Norway, Russia and Sweden as well as from Algeria, China, Czech Republic and Nigeria. In connection with the meeting, the Geological Society of Finland will have a symposium in Turku in honour of Professor Pentti Eskola (1883–1964) who developed the concept of metamorphic facies.

The three-day symposium is hosted by Åbo Akademi University and it will take place at Arken Campus, Turku in November 4-6, 2014. The participants will present their results in oral and poster sessions. Posters prepared by graduate or postgraduate students will be evaluated and the best one will be awarded. The invited talk is given by Dr. Ritske Huismans from the University of Bergen, Norway.

This special volume ***"LITHOSPHERE 2014"*** contains the programme and extended abstracts of the symposium in alphabetical order.

The organizing committee is grateful for the diverse and comprehensive range of presentations submitted by the participants. We are looking forward to a very interesting meeting with engaging discussions of a wide variety of geological and geophysical topics. Your contributions make this meeting possible.

Turku, October 22, 2014

Olav Eklund, Ilmo Kukkonen, Pietari Skyttä, Pia Sonck-Koota,
Markku Väisänen and David Whipp

Lithosphere 2014 Organizing Committee

# LITHOSPHERE 2014 Symposium
# Programme

## Tuesday, November 4

09:00 - 10:00 Registration at Arken Campus, Åbo Akademi University, Turku, Auditorium Armfelt

**10:00 - 10:15 Opening: Olav Eklund**

**10:15 - 11:00 Invited speaker: R.T. Huismans**
Advances in geodynamic modelling of rifted margin formation and lithosphere scale inversion and mountain building

**11:00 - 12:30 Session 1: Analogue and numerical modeling of lithospheric evolution**
Chair: David Whipp

11:00 - 11:30 **A. Soesoo, P.D. Bons and S. Hade**
Partial melting from the point of numerical and analogue modelling
11:30 - 12:00 **L. Kaislaniemi, J. van Hunen, M.B. Allen and I. Neill**
Modelling post-collisional magmatism – Results from integrated thermo-mechanical mantle convection and thermodynamic geochemical melting models
12:00 - 12:30 **K. Moisio and A. Kaikkonen**
Some remarks about the focal depths and rheological models in the POLAR ; profile, Northern Finland.

**12:30 - 13:30 Lunch**

**13:30 - 14:30 Session 2: Analogue and numerical modeling of lithospheric evolution (continued)**
Chair: Annakaisa Korja

13:30 - 14:00 **K. Nikkilä, A. Korja, H. Koyi and O. Eklund**
Analogue modeling of asymmetric gravitational spreading – a case from Fennoscandia
14:00 - 14:30 **D. M. Whipp, Jr., C. Beaumont and J. Braun**
Orogen-parallel mass transport along the arcuate Himalayan front into Nanga Parbat and the western Himalayan syntaxis

**14:30 - 15:00 Coffee/Tea**

**15:00 - 16:30 Session 3: Orogenies: Structure, deformation, magmatism and metamorphosis**
Chair: Markku Väisänen

15:00 - 15:30 **M. Sayab, J.-P. Suuronen, P. Hölttä, R. Lahtinen, N. Kärkkäinen and A.P. Kallonen**
X-ray computed micro-tomography: a holistic approach to metamorphic fabric analyses and associated mineralization
15:30 - 16:00 **F. Chopin, A. Korja, P. Hölttä, O. Eklund and O.T. Rämö**
The Vaasa dome: its tectonic and metamorphic evolution during the Svecofennian orogeny
16:00 - 16:30 **A. Korja and MIDCRUST Working Group**
Svecofennian orogeny in an evolving convergent margin setting

18:00 - 21:00 **Eskola symposium and ice breaker at Geologicum, Åbo Akademi**

## Wednesday, November 5

**09:30 - 11:00 Session 4: Orogenies: Structure, deformation, magmatism and metamorphosis (continued)**
Chair: Alvar Soesoo

09:30 - 10:00 **T. Korja, K. Vaittinen, M. Abdel Zaher, M. Pirttijärvi, A, Korja, M. Smirnov and I. Lahti**
Crustal conductors in a complex accretionary orogen in Fennoscandia
10:00 - 10:30 **J. Engström and K.E.S. Klin**
Ductile deformation and Continental Collision Structures of the Kangerlussuaq area in the Southern Part of the Nagssugtoqidian Orogeny, Central West Greenland
10:30 - 11:00 **S. Sjöblom**
Thermobarometric study on genesis of Ca-Ti-rich micas in shoshonitic lamprophyres in Fennoscandia

**11:00 - 11:30 Coffee/Tea**

**11:30 - 12:30 Session 5: Precambrian and Phanerozoic evolution of the Fennoscandian lithosphere**
Chair: Raimo Lahtinen

11:30 - 12:00 **A. Arzamastsev**
Paleozoic magmatic events in the north-eastern Fennoscandian Shield: Estimation
12:00 - 12:30 **L. Arzamastseva**
Paleozoic magmatic events in the north-eastern Fennoscandian Shield

**12:30 - 13:30 Lunch**

**13:30 - 16:30 Session 6: Precambrian and Phanerozoic evolution of the Fennoscandian lithosphere (continued)**
Chair: Pietari Skyttä

13:30 - 14:00 **P. Mikkola, E. Heilimo, T. Halkoaho and A. Käpyaho**
Neoarchaean alkali enriched gabbros and diorites of the Karelian Province as part of the diversification of the plutonic activity

14:00 - 14:30 **E. Heilimo and P. Mikkola**
Neoarchaean alkaline rich igneous magmatism as a part of cratonization of the western Karelia

14:30 - 15:00 **Å. Johansson and M. Stephens**
Timing of magmatism and migmatization in the 2.0–1.8 Ga Svecokarelian orogen, Uppland, south-central Sweden

**15:00 - 15:30 Coffee/Tea**

15:30 - 16:00 **O. Eklund**
Spatial and temporal connection between TIB and post-collisional shoshonites

16:00 - 16:30 **A.B. Vrevsky**
Non-subduction geodynamics of the Neoarchean continental lithosphere: geochemical, isotopic and petrologic signatures of the Kolmozero-Voro'ya greenstone belt, Kola–Norwegian province, Fennoscandian Shield

**16:30 - 17:00 Session 7: Poster introductions**
Two-minute talks with two slides in the auditorium
Chair: Olav Eklund

**17:00 - 19:00 Poster viewing and networking with refreshments**

**P1** **R. Aho, T. Kauti, H. Penttinen, P. Skyttä and M. Väisänen**
A multi-disciplinary approach to unravel the tectonic setting of the bedrock in the Salo area, SW Finland

**P2** **J. Kinnunen, P. Skyttä, N. Tenovuo and T. Kilpeläinen**
Structural mapping with terrestrial laser scanner. Case study: folding in skerry of Vekara, SW-Finland

**P3** **N. Koittola**
Detailed geolgical 3D modelling - investigation niche 3 in ONKALO, Olkiluoto

**P4** **S. Leinonen**
Shear tectonic features of Archean Portti Soapstone formation

**P5** **J. Nevalainen and E. Kozlovskaya**
Seismic tomography for microseismic data from Pyhäsalmi Mine, Pyhäjärvi

**P6** **J. Palosaari, S. Raunio, R. Rundqvist, R-M. Latonen, J.-H. Smått, R. Blomqvist and O. Eklund**
High quality flake graphite in the Fennoscandian shield

**P7** **S. Piippo, M. Kaartinen and P. Skyttä**
Structural evolution of the southern part of the Peräpohja Belt in the Tornio region, northern Finland

**P8** **M. Väisänen, Simelius, C., H. O'Brien, M. Kyllästinen and J. Mattila**
Late Svecofennian mafic magmatism in southern Finland

**P9** **L. Vecsey, J. Plomerova, H., Munzarova, V. Babuška and LAPNET Working Group**
Velocity Images of the Lithosphere and Structure of Fennoscandian Upper Mantle

**P10** **W. Zhang, D. Roberts and V. Pease**
Detrital zircon age record in sandstones from three Caledonian nappes in NE Finnmark, northern Norway

## Thursday, November 6

**10:00 - 11:00 Session 8: Geothermal studies in Fennoscandia**
Chair: Francis Chopin

10:00 - 10:30 **Y. Maystrenko, O. Olesen and H.K. Elevebakk**
New geothermal data from the Fyllingsdalen, Ullrigg and Årvollskogen boreholes, located in southern Norway

10:30 - 11:00 **I. Kukkonen**
Mantle heat flow in the Fennoscandian Shield

**11:00 - 11:30 Coffee/Tea**

**11:30 - 12:30 Session 9: Natural resources and metallogeny**
Chair: Ilmo Kukkonen

11:30 - 12:00 **F. Molnár, H. O`Brien, J. Lahaye, A. Käpyaho and G. Sakellaris**
Sulphur and copper isotope characteristics of the orogenic gold deposits in the Archaean Hattu schist belt, eastern Finland

12:00 - 12:30 **M. Ahven, J. Hokka and T. Halkoaho**
Kiviniemi ferromonzodiorites - a new type of Sc-Zr-Y occurrence

**12:30 - 13:30 Lunch**

**13:30 - 14:30 Session 10: Neotectonics, seismicity, deglaciation and postglacial uplift of Fennoscandia**
Chair: Toivo Korja

13:30 - 14:00 **S. Gradmann, M. Keiding, O. Olesen and Y. Maystrenko**
NEONOR2 – Neotectonics in Nordland, NW Norway

14:00 - 14:30 **P. Skyttä and K. Korkka-Niemi**
Bedrock structures controlling the spatial occurrence and geometry of glacial deposits; example from First Salpausselkä, Hyvinkäänkylä, Finland

**14:30 - 15:00 Coffee/Tea**

**15:00 - 15:30 Session 11: Other lithospheric topics and short communications**
Chair: Olav Eklund

15:00 - 15:30 **B. Lund and K. Högdahl**
Old shear zone reactivation: The 15 September 2014 M4.1 Sveg earthquake, Central Sweden

**15:30 - 16:00 Final discussions and poster awards**

# EXTENDED ABSTRACTS

# A multi-disciplinary approach to unravel the tectonic setting of the bedrock in the Salo area, SW Finland

Riku Aho, Tuomas Kauti, Heidi Penttinen, Pietari Skyttä and Markku Väisänen

Department of Geography and Geology, 20014 University of Turku, Finland
E-mail: pietari.skytta@utu.fi

This paper presents a number of hypotheses on the crustal evolution of the Salo area in SW Finland. The working hypotheses will be tested using a multi-disciplinary approach comprising structural analysis, 3/4D-modelling, isotope geology and geochemistry. The project is expected to provide new insights into the complex orogenic evolution of the Fennoscandian Shield at 1.9-1.8 Ga.

**Keywords:** structural analysis, 3D-modelling, isotope geology, geochemistry

## 1. Introduction

This investigation addresses the evolution of the Svecofennian crust in the Salo area in SW Finland, which is characterised by gently-dipping structures and voluminous 1.85-1.80 Ga granitoids (Figure 1A; e.g. Kurhila et al., 2010). The significance of the study arises in particular from the need to understand the timing and origin of the sub-horizontal structures which have been interpreted resulting from e.g. emplacement of the 1.85-1.80 Ga granitoids (Stålfors and Ehlers, 2006) or homogeneous flattening during crustal extension (Skyttä and Mänttäri, 2008). Furthermore, the observed bimodal nature of magmatism and some relatively young magmatic ages at 1.83-1.81 Ga (Väisänen et al. 2014) are not in concert with the earlier results. The research activities started with systematic field mapping and will proceed towards 3/4D-modelling and isotopic work on structurally controlled samples. The results will provide new insights into the complex Svecofennian evolution in southern Finland.

## 2. Working hypotheses

The following hypotheses will be tested:

a) The Salo area represents an intra-orogenic rift that developed between two major orogenies that affected the Svecofennian domain of the Fennoscandian Shield at 1.9-1.8 Ga, the 1.89-1.87 Ga Fennian and the 1.84-1.80 Ga Svecobaltic orogenies (Lahtinen et al. 2005). Hence, the area would correlate with the setting of the approximately 1.87-1.84 Ga intraorogenic sedimentary basins in the Svecofennian domain of Finland and Sweden (Bergman et al. 2008, Lahtinen and Nironen, 2010) and the coeval mafic magmatism in SW Finland (Väisänen et al., 2012).
b) Sub-horizontal structures were generated during homogeneous crustal extension (around 1.83 Ga) of the crust that was thickened during the Fennian orogeny (Skyttä and Mänttäri, 2008).
c) The sub-horizontal structures relate to Fennian (1.89-1.87 Ga) thrust tectonics, similar to that described from the Kemiö area further south-west (Van Staal and Williams, 1983).
d) The sub-horizontal structures were generated during the syn-transpressional emplacement of the 1.85-1.80 Ga granites (Ehlers et al., 1993; Väisänen and Hölttä 1999, Skyttä et al. 2006). The process has been characterized by magma ascent along major sub-vertical shear zones, followed by emplacement into sub-horizontal sheets (Stålfors and Ehlers, 2006).

To test the hypotheses, we aim at constructing a comprehensive crustal evolution model which attributes i) the evolution of the major shear zones and regional-scale strain partitioning, and their effects on the granite emplacement and subsequent deformation, ii) the structural-metamorphic transitions leading to exposure of variable crustal depths across the area, and iii) the ages of the deformation events and the significant lithological units, as well as their geochemistry and Lu-Hf -isotopes to trace their sources.

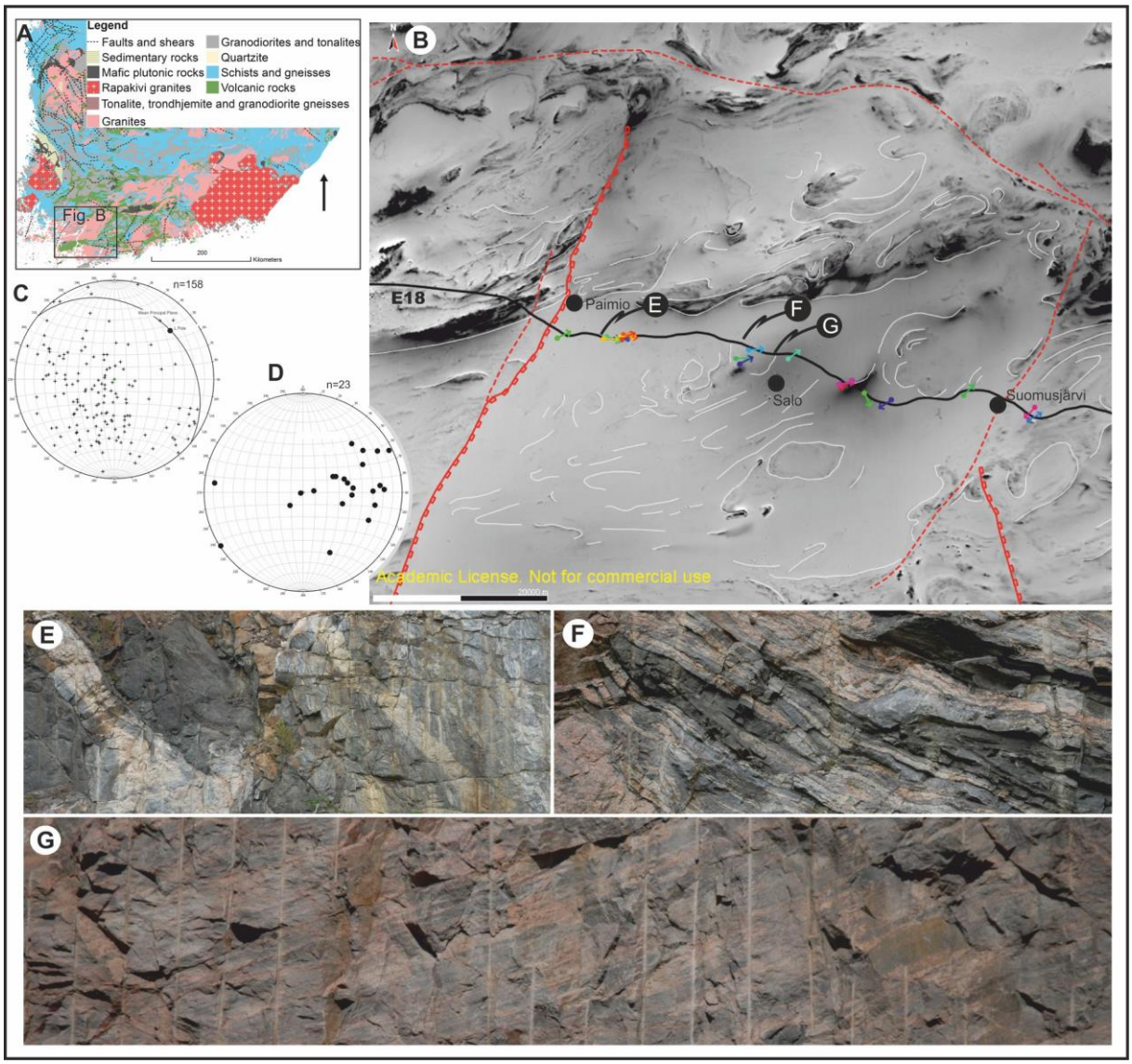


**Figure 1**. A. Simplified geology of southern Finland. B. An overview of the study area with magnetic form lines, most significant shear zones and fold axes indicated (Map source in A and B: GTK). C and D. Streographic projections of the measured foliations (C; mean plane and β-axis indicated) and fold axes (D). E. Mica-gneiss with volcanic interlayers. F. Recumbent isoclinal folds. G. Gently-dipping banding in granite.

## 2. Methods and data

The backbone of the project's current research activities is formed by structural mapping of the road cuts along the motorway #1 between Turku and Helsinki, which in the section between Paimio and Suomusjärvi form a semi-continuous chain of high-quality

outcrop across the study area (Figure 1x). Prior to the field mapping, the outcrops with clearly contrasting lithologies and discernible structures were photographed into panoramic images which served as mapping templates (Figure 1x). Photography also ensured that the road cuts are systematically documented for future usage while they still are fresh and optimal for geological observations. The collected structural measurements have been complemented by collecting oriented samples which aim at defining the kinematics of the shear zones, fabric development in the fold hinges, and providing petrographic data for distinguishing the lithological units. Structural data from available bedrock maps has been digitized, evaluated and incorporated into the structural data set. The first stages of the structural analysis involve subdivision of the study area into structural domains and specification of the internal characteristics within each of the domains. Thereafter, the work proceeds into making correlations between the domains which will ultimately require geochronological constraints. The structural analysis is carried out as the MSc project of Riku Aho.

The structural data and results derived from the structural analysis will be further developed into digital 3D-models. A major effort will be placed upon model building and 3D-visualisation of the structural framework of the area. The following work will comprise unfolding the upright (D3) folds, block restoration of the structural domains and testing the emplacement setting of the lateorogenic granitoids. Furthermore, alternative structural successions will be modelled, including testing the kinematics of the major shear zones. The regional-scale work will be complemented by laser-scanning of selected key localities for detailed geometrical analysis of the folds and deformation zones. The 3/4D-modelling is performed with MOVE$^{TM}$ software, by Tuomas Kauti as part of his MSc thesis.

Geochronological determinations will aim at i) defining the crystallization ages of lithological units, ii) providing constraints on the age of deformation leading to the generation of the sub-horizontal structures, and iii) constraining the timing of the metamorphic peak. The age determinations will use the U-Pb systems on zircon and monazite.

In connection with the zircon dating, the same grains will be also analysed on the Lu-Hf isotopes in order to trace the source of the rocks. The isotopic analyses will be conducted in the Finnish Geosciences Research Laboratory (SGL) at the Geological Survey of Finland, Espoo. The isotope part of the study forms the MSc project of Heidi Penttinen. During the project, a large number of samples for chemical analyses will be collected.

**3. Preliminary results and future work**

The first results are based on the structural mapping and analysis, and will be later complemented by analytical data during the progress of the project.

Field mapping has revealed that the area is lithologically and structurally more complex than previously considered. The main lithologies comprise migmatitic metasedimentary (Figs. 1D, E) and metavolcanic rocks, and intrusive rocks with compositions ranging from granite to gabbro. Particularly significant is the strong heterogeneity of the granites, the different types characterized by mingling with mafic magmas, intense banding (Figure 1F), and homogeneous appearances.

The foliation measurements collected in the project define a gently NE-dipping mean orientation and a gently NE-plunging statistical fold axis (Figure 1C). The measured fold axes (Figure 1D) cluster along a sub-vertical WSW-ENE striking girdle, with the densest clustering plunging moderately towards E-ENE. The measured fold axes reflect the upright D3-folding with sub-horizontal, curvilinear, approximately E-W trending fold axes characteristic for southern Finland (e.g. Skyttä and Mänttäri, 2008). In contrast, the statistical fold axis determined from the foliation data (Figure 1C) is further affected by deflections into more N-S striking shear zones (Figure 1B).

For further analysis, the area has been subdivided into structural domains, characterized by: i) upright folds with axes plunging towards E-NE, ii) sub-horizontal attitudes defined by banding within the granitoids or recumbent folding in supracrustal units, iii) steep to sub-vertical structural grain, and iv) areas with structural complexity.

The next step in the structural analysis will be a more detailed delineation of the approximately SW-NE striking shear zones, and their kinematic analysis based on microstructural observations. Furthermore, the above constraints will be linked to the observed fold vergences and the derived deformation kinematics.

**Acknowledgements**

The Finnish Cultural Foundation, Varsinais-Suomi Regional Fund is acknowledged for financial support and Midland Valley Exploration Ltd. for the use of MOVE™ modelling software under the Academic Software Initiative.

**References:**

Bergman, S., Högdahl, K., Nironen, M., Ogenhall, E., Sjöström, H., Lundqvist, L. and Lahtinen R., 2008. Timing of Palaeoproterozoic intra-orogenic sedimentation in the central Fennoscandian Shield; evidence from detrital zircon in metasandstone. Precambrian Research, 161, 231–249.

Ehlers, C., Lindroos, A., and Selonen, O., 1993. The late Svecofennian granite-migmatite zone of southern Finland-a belt of transpressive deformation and granite emplacement. Precambrian Research, 64, 295-309.

Kurhila, M., Andersen, T. and Rämö, O. T., 2010. Diverse sources of crustal granitic magma: Lu-Hf isotope data on zircon in three Paleoproterozoic leucogranites of southern Finland. Lithos, 115, 263–271.

Kurhila, M., Vaasjoki, M., Mänttäri, I., Rämö, T. and Nironen, M. 2005. U-Pb ages and Nd isotope characteristics of the lateorogenic migmatizing microline granites in southwestern Finland. Bulletin of the Geological Society of Finland, 77, 105–128.

Lahtinen, R., Korja, A. and Nironen, M. 2005. Palaeoproterozoic tectonic evolution. In: M. Lehtinen, P. A. Nurmi and O. T. Rämö, (eds.) Precambrian Geology of Finland — Key to the Fennoscandian Shield. Elsevier B.V., 481–532.

Lahtinen, R. and Nironen, M. 2010. Paleoproterozoic lateritic paleosol–ultra-mature/mature quartzite–meta-arkose successions in southern Fennoscandia—intra-orogenic stage during the Svecofennian orogeny. Precambrian Research, 183, 770-790.

Skyttä, P., Väisänen, M., Mänttäri, I., 2006. Preservation of Palaeoproterozoic early Svecofennian structures in the Orijärvi area, SW Finland–Evidence for polyphase strain partitioning. Precambrian Research, 150, 153–172.

Skyttä, P., Mänttäri., I., 2008. Structural setting of late Svecofennian granites and pegmatites in Uusimaa Belt, SW Finland: Age constraints and implications for crustal evolution. Precambrian Research, 164, 86–109.

Stålfors, T. and Ehlers C. 2006. Emplacement mechanisms of Late-orogenic granites - Structural and geochemical evidence from southern Finland. International Journal of Earth Sciences, 95, 557-568.

Väisänen, M. and Hölttä, P., 1999. Structural and metamorphic evolution of the Turku migmatite complex, southwestern Finland. Bulletin of the Geological Society of Finland, 71, 177–218.

Väisänen, M., Eklund, O., Lahaye, Y., O'Brien, H., Fröjdö, S., Högdahl, K. and Lammi, M. 2012. Intra-orogenic Svecofennian magmatism in SW Finland constrained by LA-MC-ICP-MS zircon dating and geochemistry. GFF, 134, 99–114.

Väisänen, M., Simelius, C., O'Brien, H., Kyllästinen, M. and Mattila, J., 2014. Late Svecofennian mafic magmatism in southern Finland. Lithosphere 2014 – 8th Symposium on the Structure, Composition and Evolution of the Lithosphere inFennoscandia. Programme and Extended Abstracts, Turku, Finland, November 4-5, 2014. Institute of Seismology, University of Helsinki, Report S-62, 107-110.

Van Staal, C. R., and Williams, P. F., 1983. Evolution of a Svecofennian-mantled gneiss dome in SW Finland, with evidence for thrusting. Precambrian Research, 21, 101-128.

# Kiviniemi ferromonzodiorites – a new type of Sc-Zr-Y occurrence

M. Ahven, J. Hokka and T. Halkoaho

Geological Survey of Finland, P.O. Box 1237, FI-70211 Kuopio, Finland
E-mail: marjaana.ahven@gtk.fi

The Kiviniemi 1.86 Ga mafic intrusion in the Eastern Finland has been subjected to a meandering yet gradually proceeding study since its discovery by the Geological Survey of Finland in 2008. In this article we shortly describe the general features of the intrusion together with a brief look into the mineral resource estimation. While the intrusion consists of several rock types with somewhat similar geochemical and mineralogical characteristics, the special features (high Fe, Ti and P together with elevated Sc, Zr, Y, Hf, Ba and K as well as low compatible elements) are most pronounced in the area of 2.5 hectare melanocratic main deposit. Multiple whole-rock and mineral analyses were carried out in order to examine the distribution of Sc and Zr in the intrusion and further on to detect the process of scandium enrichment. Preliminary mineral resource estimation based on the analyses from the main deposit area introduces a fairly homogeneous deposit with an average Sc grade of 154.3 g/t (14.3 Mt). Although some feeble ideas exist concerning the connection of Sc with fluid activity and metamorphosis, it is clear that more diverse tools and time are needed to understand the Sc enrichment in Kiviniemi intrusion.

**Keywords:** ferromonzodiorite, ferrodiorite, scandium, zirconium, Central Finland Granitoid Complex

## 1. Geological setting and general features

The Kiviniemi mafic intrusion is located on the northeastern border of Central Finland Granitoid Complex (Figure 1). It consists of relatively coarse-grained, melanocratic garnet-bearing fayalite ferromonzodiorites and ferrodiorites surrounded by slightly more leucocratic ferromonzodiorites and ferrodiorites. A few two meter thick pyroxenite cumulate bodies with similar mineralogy but distinctive mesocumulate texture were found amongst the melanocratic ferromonzodiorites. A heterogeneous group of small-grained diorites extends further to the south, and the mafic body as a whole is surrounded by coarse porphyritic granite. The graded and mingled contacts between the mafic body and the surrounding granite indicate comagmatism of some sort, which is supported also by the overlapping ages (ferromonzodiorite 1857±2 Ma, granite 1859±9 Ma; Ahven 2012, Halkoaho et al. 2013). However, differences in the εNd values (+0.1 and -2.5, respectively; Ahven 2012, Halkoaho et al. 2013) indicate involvement of Archean crustal component in the granite.

All of the ferromonzodiorites and ferrodiorites show broadly similar mineral paragenesis. Main minerals (>10%) are (ferro)hedenbergitic clinopyroxene, almandine garnet, fayalitic olivine ($Fo_{1-4}$), amphibole (ferrohastingsite and ferroactinolite) and plagioclase (average An content ca. 40%). Minor (3-10%) amounts of biotite, potassium feldspar, zircon, ilmenite, fluorapatite and pyrite are present. Accessory (<3%) amounts of pyroxferroite, clinoferrosilite, secondary chlorite and stilpnomelane were identified with electron microprobe analyses. The group of heterogeneous diorites shows less iron-rich mineralogy, having orthopyroxene and amphibole as the main mafic minerals. The strong metamorphic overprint is visible as corona textures and protomylonitic appearance in (melanocratic) ferromonzodiorites and ferrodiorites.

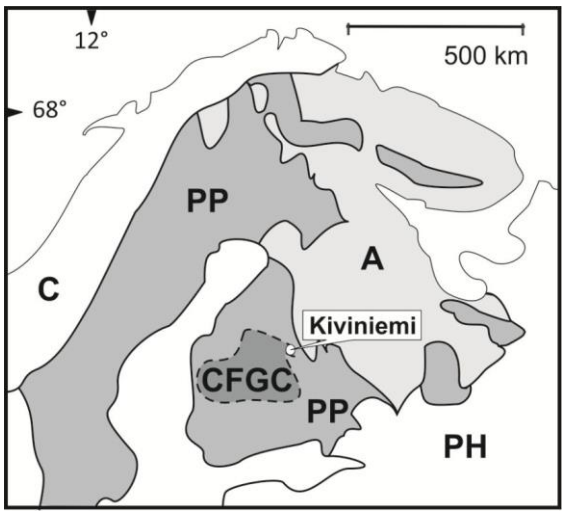


**Figure 1.** Location of the Kiviniemi intrusion in the Fennoscandian shield. A=Archaean Kola-Karelian Domain, PP=Paleoproterozoic (mainly Svecofennian) Domain, CFGC=Central Finland Granitoid Complex, PH= Phanerozoic rocks, C=Caledonides.

The Kiviniemi intrusion consists of highly evolved tholeiitic rocks with shoshonitic, alkaline and metaluminous affinities. Average Mg-number for ferromonzodiorites and ferrodiorites is 8.4 and they contain up to 3% $TiO_2$ and 1.5% $P_2O_5$. The group of heterogeneous diorites has more primitive composition with average Mg-number 20 and up to 4% $TiO_2$ and 2.2% $P_2O_5$. The peak of iron enrichment is achieved in pyroxenite cumulates (Figure 2). Compatible elements Ni and Cr show comparably low concentrations mostly below detection limits (Ni 20 ppm and Cr 30 ppm) throughout the intrusion. Concentration of Zn, however, can reach the maximum of 780 ppm in the melanocratic rocks.

## 2. Curious elements

The ferromonzodiorites and ferrodiorites are characterized by elevated concentrations of metallic scandium (36-281ppm), zirconium (235-5600 ppm) and yttrium (max 189 ppm). Highest values 293 ppm, 6760 ppm and 255 ppm, respectively, were determined by ICP-OES from solutions after sodium peroxide fusion of 0.2 g samples in a Ni crucible (Halkoaho et al. 2013). Zr concentrations remain varied but high throughout the intrusion, while Sc elevation seems to be restricted to the melanocratic main deposit. As comparison, Sc (element 21) occurs widely scattered in the Earth's crust, typically in ferromagnesian minerals as a trace element (5-100 ppm) and thus common Sc concentration in mafic rocks is only 20-40 ppm.

Currently, scandium enrichment aside from laterite deposits is reported mainly from granite-related hydrothermal veins and metasomatic rocks, pegmatites and carbonatites, as the enrichment process is considered hydrothermic (e.g. Bernhard 2001 and references therein). Since its lanthanide-like behaviour and similar properties to aluminium and yttrium, it is usually concentrated in phosphate and aluminium compounds yet also forms rare minerals such as thortveitite [$(Sc,Y)_2Si_2O_7$]. Revealed by the electron microprobing, the main carriers of $Sc_2O_3$ in the Kiviniemi melanocratic main deposit are ferrohastingsite (max 2088 ppm, average 1053 ppm, n=24), ferrohedenbergite (max 1736 ppm, average 1180 ppm, n=25) and apatite (1068-1133 ppm, n=2). The amount of Sc in zircon (average 190 ppm, n=13) seems to correlate positively with a yellow fluorescent phenomenon. Garnet, plagioclase and pyroxferroite also host minor concentrations of Sc.

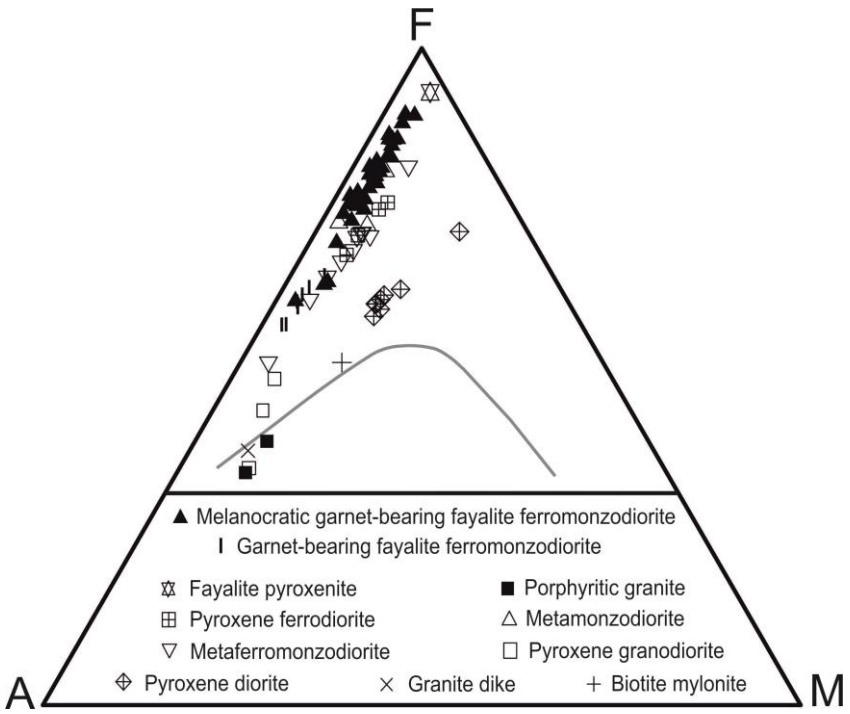


**Figure 2.** AFM (alkalis, iron and magnesium) ternary diagram showing the composition of all Kiviniemi intrusion samples, including the wall rock granite.

## 3. Economical point of view

Scandium is mostly used in lightweight aluminium alloys for aerospace and high-performance sporting components. It reduces grain growth when heated, but is often substituted in the alloy with more affordable titanium. Sc is also utilised in fuel cells, metal halide light bulbs and structural ceramics. The isotope $^{46}$Sc serves as a tracing agent in oil refineries. Hitherto, the global demand has been met by processing mine tailings and residues (e.g. uranium refining, fluorite and tungsten tailings). The biggest producers are China, Russia, Ukraine and Kazakhstan but the global consumption level is still low, estimated 2-10 tonnes per year. The development of new technologies and the use of Sc in solid oxide fuel cells are hoped to raise new interest in Sc worldwide, as prominent resources are found also in Norway, Australia and Madagaskar (Gambogi 2014). New high-grade laterite-hosted sources in Australia (Metallica Minerals LTD, EMC Metals Corp.) are believed to establish a reliable primary product supply which would end up to a more organized and stable markets. Regular resources would also promote the research of scandium appliances.

According to the preliminary mineral resource estimation, the Kiviniemi occurence contains estimated 14.3 Mt at 154.3 g/t Sc. The mineral resource estimation was calculated with the inverse distance method. Since the main deposit melanocratic ferromonzodiorites and ferrodiorites have rather homogeneous Sc concentrations, significant tonnage loss occurs only after 100-150 g/t cut-off levels. The block model, albeit is based on a limited amount of data (drill holes R1-R4; Figure 3) and should therefore be treated as low level of confidence, serves as a useful indication of exploration potential.

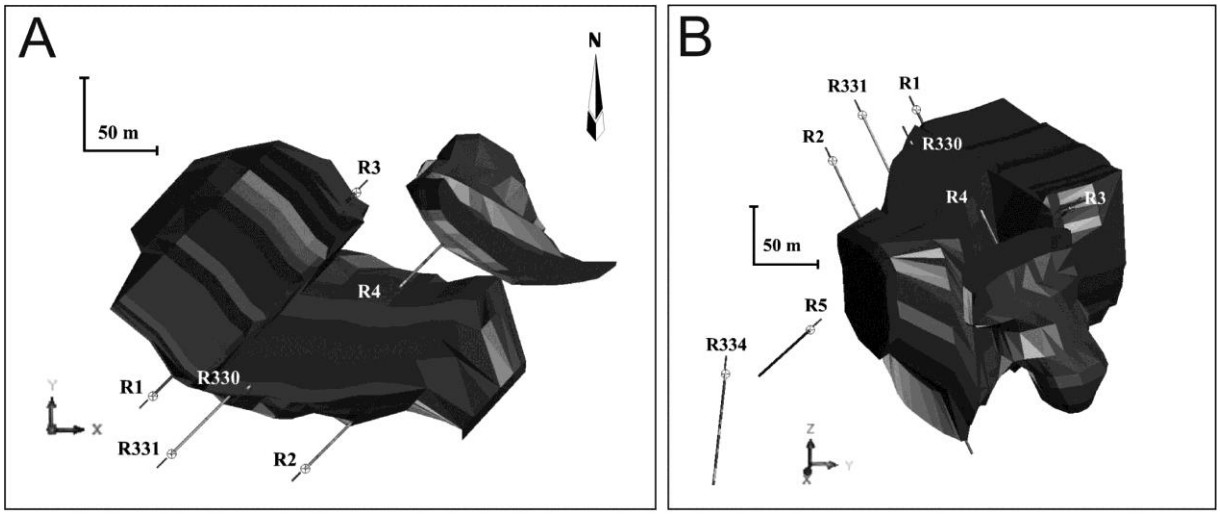


**Figure 3.** The wireframe model of Kiviniemi occurrence. A. View vertically downwards. B. Birdseye view from east. Model by Janne Hokka (2013).

## References:

Ahven, M., 2012. Petrology and geochronology of the Kiviniemi garnet-bearing fayalite ferrogabbro, Rautalampi. Unpublished M.Sc. Thesis, University of Helsinki, Department of Geosciences and Geography. 62 p.

Bernhard, F., 2001. Scandium mineralization associated with hydrothermal lazulite-quartz veins in the Lower Austroalpine Grobgneis complex, Eastern Alps, Austria. In: Piestrzynski A. et al. (eds) Mineral Deposits at the Beginning of the 21st Century. Proceedings of the joint sixth biennial SGA-SEG meeting. Kraków, Poland. A. A. Balkema Publishers, 935-938.

EMC Metals Corp. Nyngan Scandium Project, available at: http://www.emcmetals.com/i/pdf/EMCTechRptNynganApr2010.pdf

Gambogi, J., 2014. U.S. Geological Survey Mineral Commodity Summaries 2014: Scandium. Available at: http://minerals.usgs.gov/minerals/pubs/commodity/scandium/mcs-2014-scand.pdf

Halkoaho, T., Ahven, M. and Rämö, O. T., 2013. A New Type of Magmatic Sc-Zr Occurrence located in the Kiviniemi area, Rautalampi, Central Finland. In: Erik Jonsson et al. (eds) Mineral deposit research for a high-tech world. 12th Biennial SGA Meeting, 12–15 August 2013, Uppsala, Sweden, Vol. 4, 1717−1719.

Hokka, J. and Halkoaho, T., 2014. Mineral resource estimation for the Kiviniemi Sc-Zr-Y-deposit. In: Lauri, L.S. et al. (eds) Current Research: 2nd GTK Mineral Potential Workshop, Kuopio, Finland, May 2014. Geological Survey of Finland, Report of Investigation, 207, 39-40.

SCONI Project by Metallica Minerals LTD, available at: http://www.metallicaminerals.com.au/sconi (page visited: 01.10.2014)

# The Vaasa dome: its tectonic and metamorphic evolution during the Svecofennian orogen

F. Chopin[1], A. Korja[1] and P. Hölttä[2], Olav Eklund[3] and Osmo Tapani Rämö[1]

[1]Department of Geosciences and Geography, P.O. Box 68, FI-00014 University of Helsinki, Finland
[2]Geological Survey of Finland GTK, P.O. Box 96, FI-02151 Espoo, Finland
[3]Department of Geology and Mineralogy, Åbo Akademi University, FI-20500 Turku, Finland
E-mail: francis.chopin@helsinki.fi

This study focuses on the tectono-metamorphic evolution of the 100 km wide Vaasa dome in the Svecofennian orogen (Finland). This field–based and quantitative lab study (U/Pb geochronology, petrological modelling) brings information on thermal and material transport at crustal scale during this Paleoproterozoic orogenesis.

**Keywords:** Vaasa dome, Svecofennian orogen, migmatite, middle crust

## 1. Geological setting

The Vaasa dome in bothnia (or Vaasa migmatitic complex) is cored by diatexite migmatites and "S-type" granitoids and gradually mantled by metatexite migmatites and mica schist derived from pelites and greywackes with thin metabasite-andesite intercalations (e.g. Korsman et al., 1997). Geochemical data have demonstrated that the metasediments are the sources of the melted core: it have been suggested that the dome have been formed by in-situ melting of the crust (e.g., Mäkitie et al., 2012; Suikkanen et al., 2014).

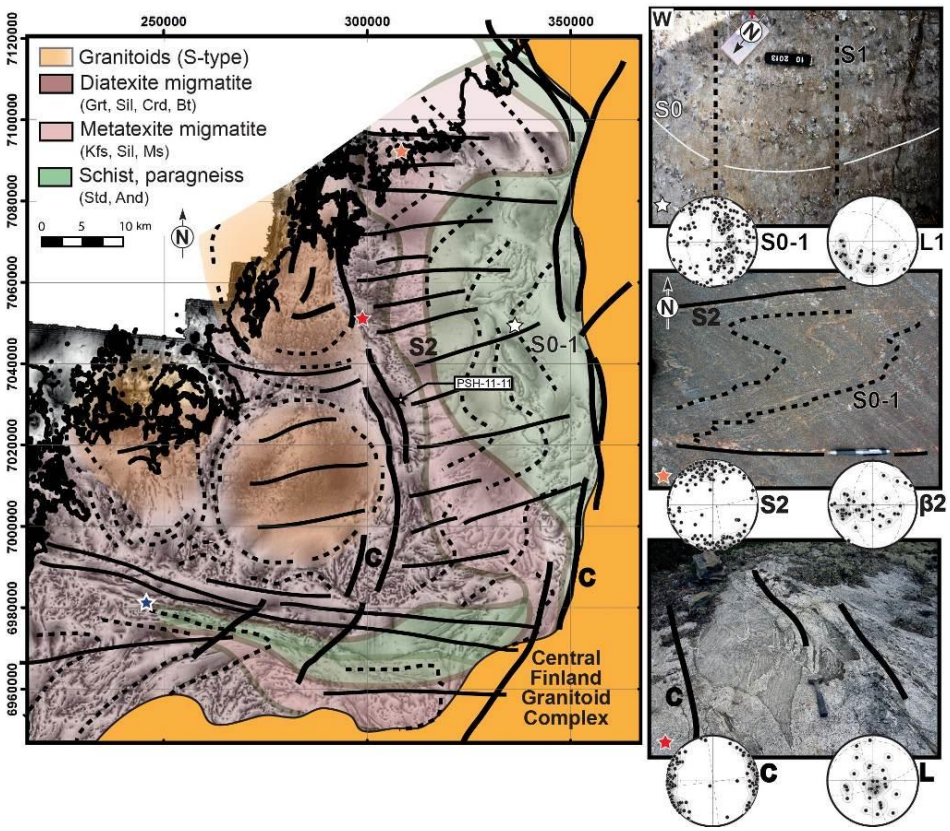


**Figure 1.** Simplified structural map of the Vaasa dome. Background: aeromagnetic map (courtesy of Markku Pirttijärvi).

## 2. Tectonic

The field work study (Figure 1) highlights the early formation (D1) of a first metamorphic fabric S1, generally moderately dipping toward the West. Kinematic indicators suggest a top-to-the-(N)E kinematic during D1. A strong lateral increase of the in-situ melt content is already observed at this stage towards the core of the dome. This early layered and partially melted fabric is then affected by a regional N-S shortening (D2) forming km- to outcrop-scale E-W striking folds and new S2 sub-vertical foliation. Late sub-vertical shear zone with vertical kinematic (D3) are visible along the dome border and within the diatexitic zone. No late detachment structures have been observed.

## 3. Metamorphism

In the metamorphic belt, the grade increases from medium-T amphibolite facies to low-P granulite facies towards the core of the dome. Pseudosections using Perple_X in the MnNCKFMASHTO system have been performed in one mica schist (Grt+BtPl+Qz±Std+Sill+And) and one metatexite migmatite (Bt+Liq+Crd+Pl+Kfs+Grt+Qz±Sill+And). The metamorphic peaks are bracketed at 560°C at 5 kbar and 750-770°C at 4.5-5 kbar, respectively, whereas the retrograde conditions, calculated at 540°C and <3 kbar is similar for both lithologies (Figure 2). This implies an isobaric increase of the metamorphic grade towards the core of the dome. An isothermal decompression for the schist and a retrograde PT path for the migmatites are observed. Idealized PT paths are shown in Figure 2.

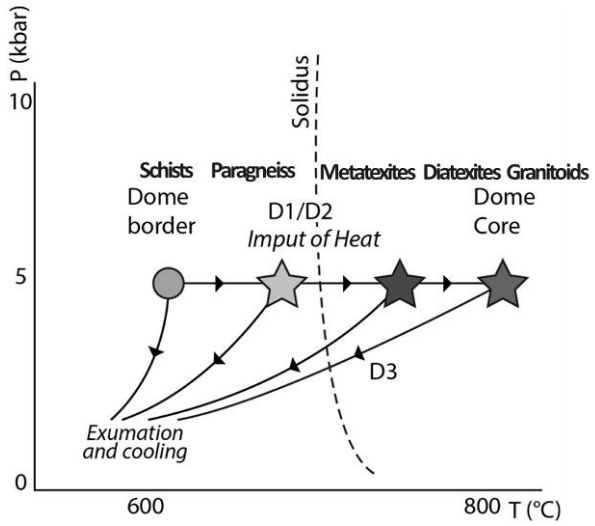


**Figure 2.** Idealized PT path of the metamorphic rocks from the Vaasa dome.

## 4. Geochronology

New U/Pb geochronological analysis on monazite from metatexite migmatites and mica schists from different part of the metamorphic belt have been carried out at the Geological Survey of Finland. Most of the ages clustered at 1860–1865 Ma (Figure 3). They are similar to other monazite ages obtained from the dome core (courtesy of MIDCRUST members and GTK) whereas U/Pb ages from metamorphic and magmatic zircons are older and clustered at 1875 Ma. This might represent the peak of melting process and associated metamorphism whereas younger ages (1860–1865 Ma) might be related to the cooling of the orogenic middle crust. This has to be compared to U/Pb zicons ages from igneous rocks of the Central Finland Granitoid Complex (CFGC) showing a strong peak at 1880 Ma (not shown). It has to be

noticed that few monazites from metamorphic rocks of the dome mantle gave ages similar to those of pegmatites, i.e about 1800 Ma. A similar evolution has been observed in Swedish part of the bothnian basin (Skiöld & Rutland, 2006).

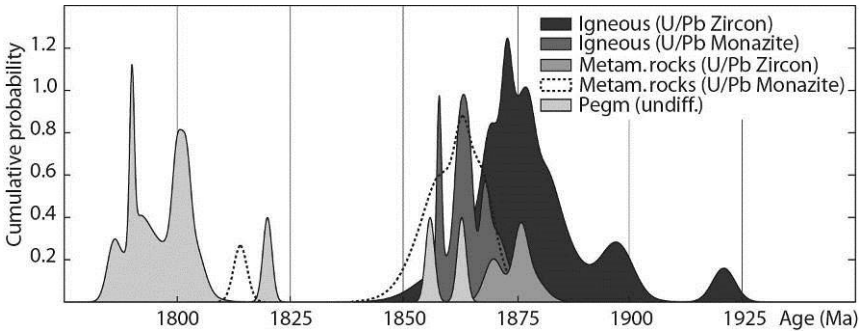


**Figure 3.** Probability curves of age data for the Vaasa dome. Source: MIDCRUST project, Public database (GTK) and unpublished ages from the GTK (Courtesy of Hannu Huhma). Ages of metamamorphic rocks include schistes and migmatites.

## 5. Discussion

The formation of the Vaasa dome may be the result of distributed thickening followed by shortening during a persistent high-temperature thermal anomaly. It forms a layered middle crust with a strong lateral increase of in-situ melt (Figure 4), followed by a regional N–S horizontal shortening (D2). The culmination of the thickening and the associated metamorphism takes place at 1875 Ma. Exhumation and concomitant cooling of the dome along subvertical shear zone is bracketed at 1860–1865 Ma. This might be correlated with the geodynamic setting of the Svecofenian orogen (Lahtinen et al., 2014). After its formation in a back-arc setting at around 1910 Ma, the Bothnia basin is thickened within a fore arc system in front of the pre-existing arc (CFGC). An orogenic scale N-S shortening, possibly associated with the formation of an orocline at 1870–1860 Ma might be responsible for the final configuration of the orogen (Lahtinen et al., 2014). The origin of the thermal anomaly in the Vaasa dome (and in Paleoproterozoic orogens in general), is still disputed. Heat source inherited from the back-arc basin (e.g. Thomson et al., 2001), radioactive decay, thickening, magma underplating in lower crust and/or delamination might have generated the thermal positive anomaly.

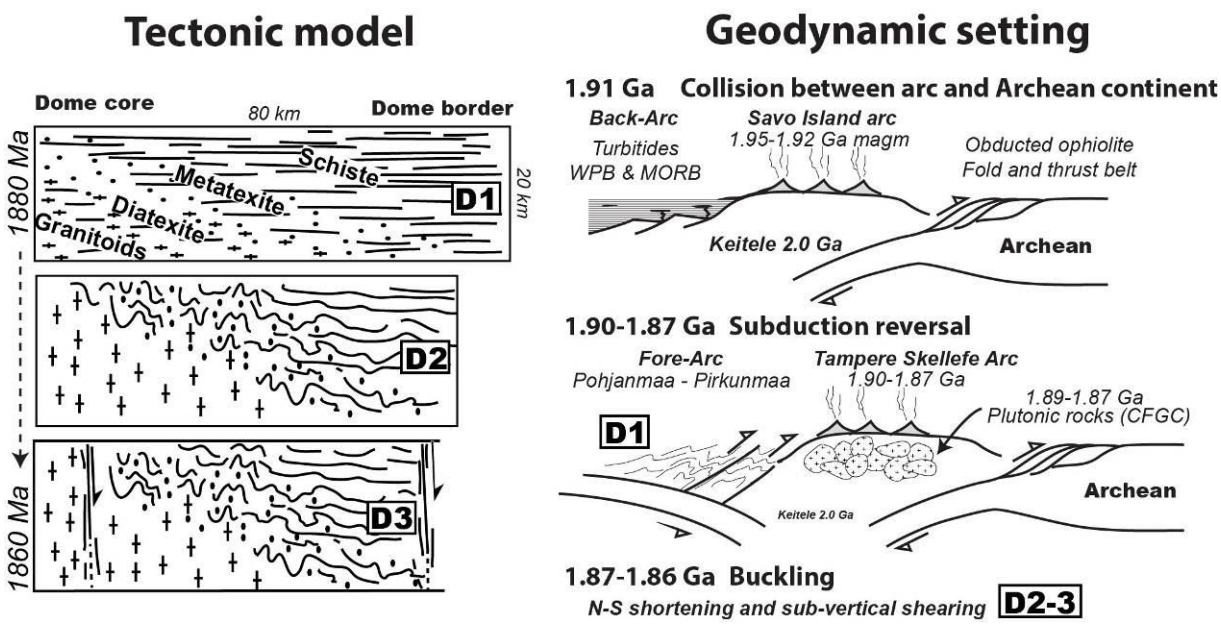


**Figure 4.** Tectonic model (left) and geodynamic setting from back-arc to fore-arc (right) of the Vaasa dome

## References:

Korsman, K., Koistinen, T., Kohonen, J., Wennervirta, M., Ekdahl, E., Honkamo, M., Idman, H. and Pekkala, Y., 1997 (Eds). Bedrock map of Finland 1:1.000.000, Geological Survey of Finland, Espoo, Finland.

Lahtinen, R., Johnston, S.T., Nironen, M., 2014. The Bothnian coupled oroclines of the Svecofennian Orogen: a Palaeoproterozoic terrane wreck. Terra Nova, 26, 330–335.

Mäkitie, H., Sipilä, S., Kujala, H., Lindberg, A. and Kotilainen, A., 2012. Formation mechanism of the Vaasa Batholith in the Fennoscandian Shield: petrographic and geochemical constraints. Bulletin of the Geological Society of Finland, 84, 141–166.

Skiöld and Rutland., 2006. Successive ~1.94 Ga plutonism and ~1.92 Ga deformation and metamorphism south of the Skellefte district, northern Sweden: Substantiation of the marginal basin accretion hypothesis of Svecofennian evolution. Precambrian Research, 148, 181–204.

Suikkanen, E., Huhma, H., Kurhila, M. and Lahaye, L., 2014. The age and origin of the Vaasa migmatite complex revisited. Bulletin of the Geological Society of Finland, 86, 41–55.

Thompson, A.B., Schulmann, K., Jezek, J. and Tolar, V., 2001, Thermally softened continental extensional zones (arcs and rifts) as precursors to thickened orogenic belts. Tectonophysics, 332, 115–141.

# Ductile deformation and Continental Collision Structures of the Kangerlussuaq area in the Southern Part of the Nagssugtoqidian Orogeny, Central West Greenland

J. Engström[1], and K.E.S. Klint[2]

[1]Geological Survey of Finland, P.O. Box 96, SF-02151 Espoo, Finland.
[2]Geological Survey of Denmark and Greenland, Øster Voldgade 10, DK-1350 Copenhagen K, Denmark
E-mail: jon.engstrom@gtk.fi

This study focuses on the results of a detailed structural investigation of a field area located close to the southern margin of the c. 1.85 Ga old collisional Nagssugtoqidian orogeny and has been subjected to several episodes of deformation. These episodes were compiled into a local structural deformation history of the study area that recognizes seven different deformation phases, including two stages of folding and one major intrusive stage during which the Kangâmiut mafic dykes were formed 2.05 Ga. Two types of shear zones are especially studied; one semi-ductile type trending E-W with a dextral sense of shear and an impressive shear zone outlining the Kangerlussuaq-Russell thrust fault. The absolute ages of the different types of ductile and brittle deformations are uncertain because of lack of radiometric ages. However, in relative terms, it is suggested that the E-W trending semi-ductile shear zones and the Kangerlussuaq-Russell thrust fault are ancient features related to the Nagssugtoqidian orogeny.

**Keywords:** Continental collision structures; Kangerlussuaq-Russell thrust fault; Tectonic structural model; Nagssugtoqidian orogeny; West Greenland

## 1. Introduction

The Nagssugtoqidian Orogeny has formed mainly between 1.92 and 1.75 Ga (Garde and Hollis 2010) as a consequence of convergence and collision of the North Atlantic Craton and a poorly defined craton to the north (van Gool et al., 2002). The Palaeoproterozoic reworking in the orogeny extends from Kangerlussuaq to southern Disko Bugt (Ramberg, 1949; Escher and Pulvertaft, 1976; Marker et al., 1995). Several studies has been performed in the central and northern end of the Nagssugtoqidian orogen (e.g. Garde and Hollis, 2010; Connely et al., 2006), while the southern end of the orogeny at the northern margin of the North Atlantic Craton in the proximity of Kangerlussuaq has been largely unexplored. The study site is located in area along the Greenland Inland Ice, at the southern end of the orogeny in the near vicinity of the North Atlantic Craton.

## 2. Geology of the study area

The study area have been subjected to two phases of folding (Klint et al., 2013) which are separated from each other by an extensional phase of deformation defined by intrusion of Kangâmiut mafic dykes (Mayborn and Lesher, 2006). Close to the ice sheet margin, in the north-eastern part of the area, the bedrock is characterised by folded mafic garnet gneiss that defines an open, NNW-trending and shallowly plunging (c. 14°) F1 fold structure. The F1 folds is gradually turning into tight/isoclinal steeply dipping overturned folds that can be traced south and westward around an open and steeply-plunging, kilometre-scale F2 fold structure with a steeply dipping foldaxis (c. 70-60°) towards N - NW. The large scale F2 fold structures are repeated several times going from east to west in the northern part of the study area. Whereas, the southern part of the study area is dominated by E-W trending 10-100 m wide foliation parallel semi-ductile shear zones (system 1). The rock type to the west and south is mainly felsic orthogneiss with varying amount of garnet. The 10-100 m wide foliation

parallel shear zones are believed to be syntectonic with the formation of the F2 folding and these shear zones may have acted as decollemént plane for the folding.

The onset of the brittle deformation is defined by several ENE-WSW trending thrusts or reverse faults (system 2). At the southern end of the study area several of these thrust faults are spaced at regular interval building up thrust sheets with hanging wall thrusted towards SSE. These thrusts are crosscutting all aforementioned features but they are also representing a gradual rotational shift from a general strike slip (passive plate boundary's) towards classic collisional structures. These thrust faults are especially prominent along the Kangerlussuaq–Russell thrust fault, with a general moderate to steep dip towards NW, accordingly these thrust sheets have been rotated towards a more steeply dipping position from the original location.

The system 3, 4, 5 and 6 are shear zones and faults with a more brittle character than the previously described deformation phases. The system 3 faults are overprinting system 1, 2 and the F2 folds. The system 4 normal faulting and NNE trending pegmatites indicates either a general extensional stress regime or local transtension during strike slip movements. Finally the youngest geological events are related to the type 5 and 6 faults and shear zones forming two generally brittle strike slip fault systems, which is also regarded the primary hydraulic zones in the area.

## 3. Summary and Conclusion

The results of a detailed structural investigation with a detailed geological mapping at key locations facilitated the construction of a tectonic structural model showing the geological development of the Kangerlussuaq area. The area has undergone several episodes of deformation, which have been compiled into an event succession for the study area that recognizes 8 tectonic events overprinting each other. Two stages of folding (F1 and F2) are identified along with one major episode of intrusion of the Kangâmiut mafic dyke swarm 2.05 Ga (Mayborn and Lesher, 2006) and 6 pronounced shearing/faulting events postdating the Kangâmiut dykes extending from ductile deformation shearing events to brittle deformation with extensive faulting, covering both the collisional and post collisional tectonic history of the area.

## References:

Connelly, J.N., Thrane, K., Krawiec, A. W. and Garde, A. A., 2006. Linking the Palaeoproterozoic Nagssugtoqidian and Rinkian orogens through the Disko Bugt region of West Greenland. Journal of the Geological Society, London., 163, 319–335

Escher, A. and Pulvertaft, T. C. R., 1976. Rinkian mobile belt of West Greenland, 104–119.

Garde, A.A. and Hollis, J.A., 2010. A buried Palaeoproterozoic spreading ridge in the northern Nagssugtoqidian orogen, West Greenland. Geological Society Special Publications (London), 338, 213–234.

Klint K.E.S., Engström J., Parmenter A., Ruskeeniemi T., Claesson Liljedahl L. and Lehtinen A., 2013. Lineament mapping and geological history of the *Kangerlussuaq* region, southern West Greenland. Geological Survey of Denmark and Greenland Bulletin. 28, 57–60.

Marker, M., Mengel, F., van Gool, J. and field party, 1995. Evolution of the Palaeoproterozoic Nagssugtoqidian orogen: DLC investigations in West Greenland. Rapp. Grønlands. Geol. Unders., 165, 100–105.

Mayborn, K.R. and Lesher, C.E., 2006. Origin and evolution of the Kangâmiut mafic dyke swarm, West Greenland. In: Garde, A.A.; Kalsbeek, F. (eds): Precambrian crustal evolution and Cretaceous-Palaeogene faulting in West Greenland. Geological Survey of Denmark and Greenland Bulletin, 11, 61-86.

Ramberg, H., 1949. On the petrogenesis of the gneiss complexes between Sukkertoppen and Christianshaab, West Greenland. Meddelelser fra Dansk Geologisk Forening, 11, 312–327.

van Gool, J.A.M., Connelly, J.N., Marker, M. and Mengel, F.C. 2002. The Nagssugtoqidian orogen of West Greenland: tectonic evolution and regional correlations from a West Greenland perspective. Canadian Journal of Earth Sciences, 39, 665–686.

# NEONOR2 - Neotectonics in Nordland, NW Norway

S. Gradmann, M. Keiding, O. Olesen and Y. Maystrenko

Geological Survey of Norway (NGU), Trondheim, Norway
E-mail: sofie.gradmann@ngu.no

## 1. Introduction

The Nordland area in NW Norway is one of the tectonically most active areas in Fennoscandia (Olesen et al., 2004). Neotectonic deformation processes constitute a geohazard, shape the present-day landscape and influence the behaviour of hydrocarbons on the Norwegian continental shelf. An earlier study showed that patterns of enhanced seismicity in this region coincide with mapped fractures and escarpments and with deviations from the long-wavelength pattern usually attributed to glacial isostatic adjustment. E-W tensional stresses dominate the deformation pattern (Hicks et al., 2000a,b), which is peculiar with respect to the first-order, NW-SE compressional stress pattern in Fennoscandia resulting from ridge-push effects. A link most likely exists to enhanced Pleistocene erosion, which may have caused flexural uplift and extension in the coastal regions (Bungum et al., 2010; Olesen et al., 2013). The Pleistocene sediment redistribution is well recorded in the 1.5 kilometers thick Naust formation offshore (Dowdeswell et al., 2010).

## 2. Project Description

The NEONOR2 project aims to better map the present-day neotectonic activity in the Nordland area and to evaluate the contribution of sediment erosion/deposition on the present-day stress pattern. A seismic array of 25 stations is recording seismicity around the Nordland area for over two years (Figure 1a). Initial data analysis confirms high seismic activity along the coast and the offshore areas, separated by a zone of reduced activity in the Vestfjorden. The data set will be used for detailed mapping of seismic activity as well as calculation of fault plane solutions and stress orientation. The detailed monitoring of seismicity will be linked to observations of surface deformation obtained through geodetic measurements. In-situ stresses are measured from boreholes, either as principal stress directions or, where possible, as the full stress tensor. A numerical modelling approach is employed to quantify the contributions of ridge-push, glacial isostatic adjustment, topography and Pleistocene sediment redistribution on the present-day stress field. A 3D subsurface model is developed that best matches the present-day observations. Furthermore will the knowledge of Pleistocene sedimentation patterns allow us to evaluate palaeo-stress patterns and palaeo-temperatures along the Nordland margin.

## 3. Results from Geodetic Data Analysis

The regional surface deformation is recorded by a network of permanent GPS stations as well as differential SAR interferometry (InSAR). The establishment of a permanent GPS network Norway began in the early 1990s. An updated GPS velocity field using 150 stations in and around Norway has been published by Kierulf et al. (2014), including the BIFROST stations (Scherneck et al., 1989), a number of high-quality sites from central and eastern Europe as well as a large number of permanent GPS stations installed for navigation purposes in Norway (Figure 1b).

In 2013-2014, the European Space Agency launched a new set of SAR satellites (Sentinel), which record images over entire Norway every 12 days. A joint analysis of the high temporal resolution GPS data and the high spatial resolution InSAR data provides detailed information about the near-surface strain rate field, hopefully allowing us to distinguish between different sources of deformation acting at varying wavelengths.

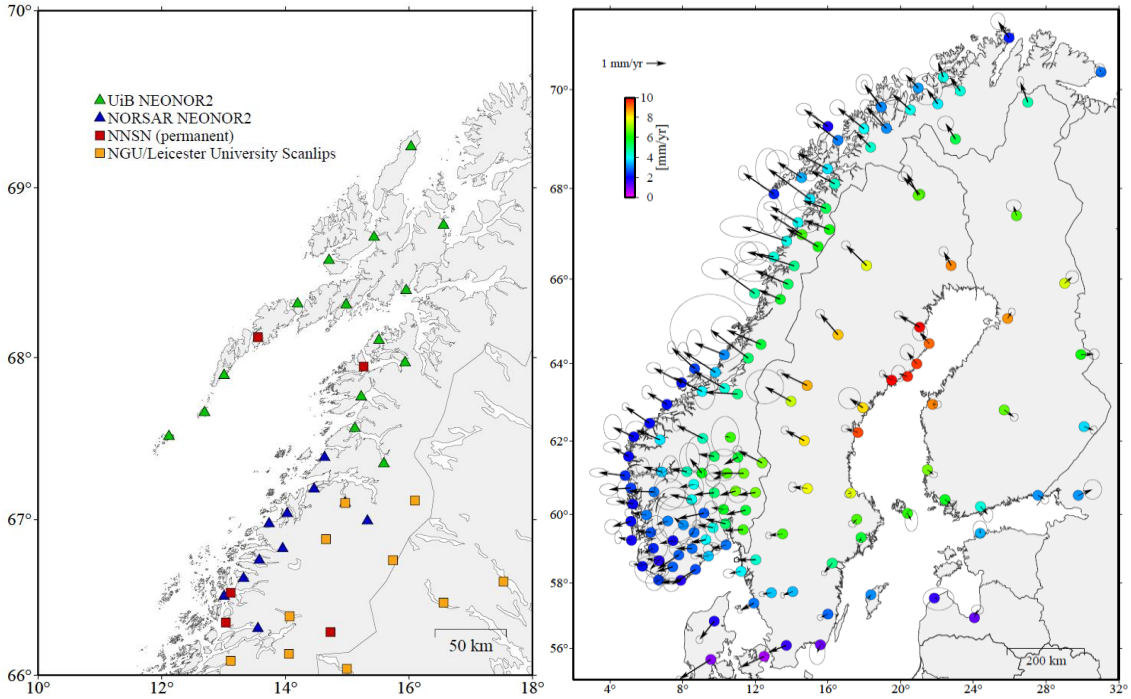


**Figure 1.** (a) The NEONOR2 seismic network covering the Nordland area. It comprises an array of 25 temporal broadband seismic stations and permanent stations of the Norwegian National Seismological Network and uses data from the British-Norwegian Scanlips project. (b) GPS velocity field over Fennoscandia showing horizontal and vertical components as arrows and coloured dots, respectively (from Kierulf et al., 2014).

We use the new geodetic and seismological data to investigate how the deformation observed at the surface relates to the seismic deformation at depth. As a first approach, we have estimated the strain rate field in and around Norway from the GPS velocity field (Kierulf at al., 2014), as well as the seismic strain rate field from previously published focal mechanisms (Hicks et al. 2000a) as well as unpublished data. Figure 2 shows the maximum shear strain rates and the areal strain rate computed by first interpolating the horizontal GPS on to a regular grid, and then taking the spatial derivative (method by Beaven and Haines, 2001). The strain rates show a clear first-order pattern of extensional strain on land and compressional strain offshore, in agreement with the expected deformation from the glaciostatic rebound. We have estimated the seismic strain rate from a summation of the published focal mechanism moment tensors (Kostrov, 1974). The seismic strain rate field is dominated by the larger events which almost exclusively occur offshore and have reverse to strike-slip mechanisms.

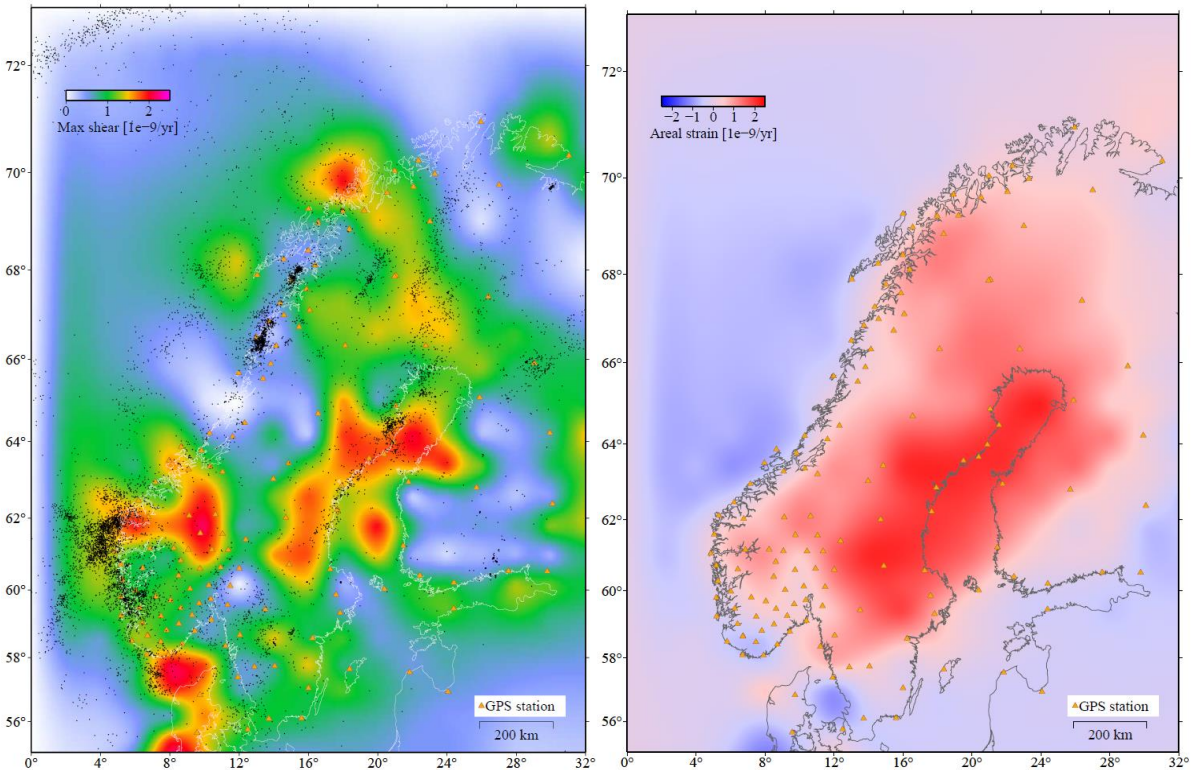


**Figure 2.** (a) Maximum shear strain rates and (b) areal strain rates computed from the horizontal GPS velocities in Figure 1b. The black dots in (a) show earthquakes during 1980-2011 from the FENCAT data base, University of Helsinki.

## 4. Results from Numerical Stress Modelling

We study the interaction of stress field components acting on a continental margin and their contribution to the present-day stress-field. In the Nordland region, the regional stress field stems from the interaction of ridge push and GIA; the local stress field mainly results from lateral density variations (primarily topography and Moho) as well as the isostatic effects of sediment unloading and loading (Fejerskov and Lindholm, 2000). Additional stress field contributions (e.g. tectonic) cannot be ruled out. Whereas the first three effects are fairly well constrained or merely add to the regional stress field, the present-day stress effect of the Pleistocene sediment redistribution is only poorly known and is the focus of this study.

We use COMSOL Multiphysics to perform a 3D finite element analysis of a coupled system of differential equations (Stokes equation, incompressibility, rheological constraints, heat conduction) on an adaptable mesh. The models are at crustal scale and include surface topography, basement and Moho depths taken from literature and seismic profiles. The ‘background’ stress state originating only from internal body forces (e.g. variations in topography) already shows significant deviatoric stresses, which are very often omitted in stress models (Figure 3). We apply the far-field stress fields (GIA, ridge-push, sediment redistribution) as effective force boundary conditions to the sides or base of the model. This approach allows us to account for all stress sources at once but also to vary them separately in order to examine their relative contributions to the observed stress and strain concentration and orientation. A reference model is built that best fits the calculated stress fields to the observed ones derived from seismological and geodetic data. Major faults are included as pre-existing weakness zones, here represented by fault-like, internal mesh boundaries. Their effects on local stress localization or distribution are studied in connection to the areas of enhanced and reduced seismic activity, respectively.

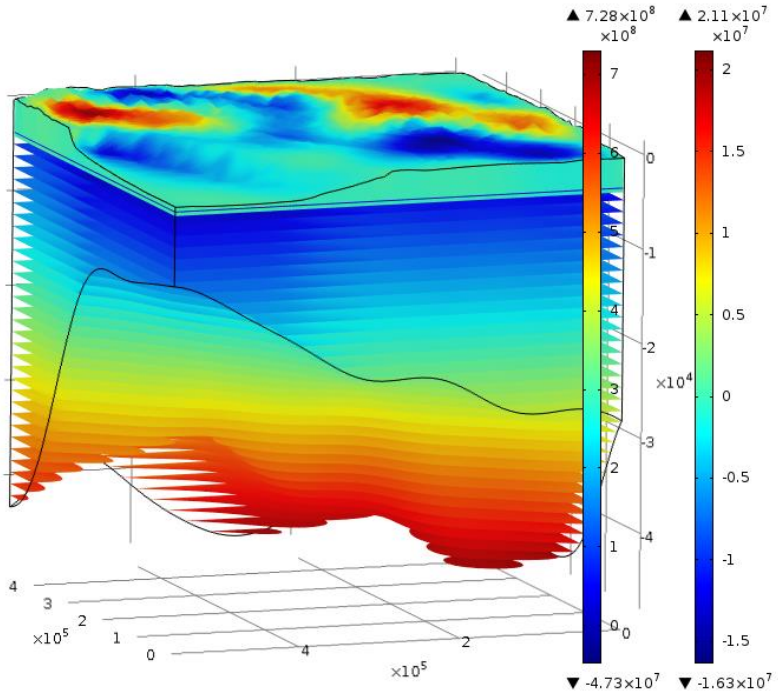


**Figure 3.** Preliminary stress model of the Nordland area, reaching from the surface (topography) to the base of the crust (Moho). Horizontal stresses are plotted at the surface (left legend), mean stress is plotted elsewhere (right legend).

## References:

Beaven, J. and Haines, J., 2001. Contemporary horizontal velocity and strain rate fields of the Pacific-Australian plate boundary zone through New Zealand. J. Geophys. Res. 106.

Bungum, H., Olesen, O., Pascal, C., Gibbons, S., Lindholm, C. and Vestøl, O., 2010. To what extent is the present seismicity of Norway driven by postglacial rebound? Journal of the Geological Society, London, 167, 373-384.

Dehls, J.F., Olesen, O., Bungum, H., Hicks, E., Lindholm, C.D. and Riis, F., 2000. Neotectonic map, Norway and adjacent areas 1:3 mill. Geological Survey of Norway, Trondheim.

Dowdeswell, J.A., Ottesen, D. and Rise, L., 2010. Rates of sediment delivery from the Fennoscandian Ice Sheet through an ice age. Geology, 38, 3–6.

Fejerskov, M. and Lindholm, C.D., 2000. Crustal stress in and around Norway; an evaluation of stress-generating mechanisms. In Nøttvedt. A. (ed.): Dynamics of the Norwegian margin, Geological Society, London, Special Publications, 167, 451-467.

Hicks, E.C., Bungum, H. and Lindholm, C.D. 2000a. Stress inversion of earthquake focal mechanism solutions from onshore and offshore Norway. Norsk Geologisk Tidsskrift, 80, 235-250.

Hicks, E.C., Bungum, H. and Lindholm, C.D. 2000b. Seismic activity, inferred crustal stresses and seismotectonics in the Rana region, northern Norway. Quaternary Science Reviews, 19, 1423-1436.

Kierulf, H.P., Steffen, H., Simpson, M.J.R., Lidberg, M., Wu, P. and Wang, H., 2014. A GPS velocity field for Fennoscandia and a consistent comparison to glacial isostatic adjustment models. J. Geophys. Res. 119.

Kostrov, V. V., 1974. Seismic moment and energy of earthquakes, and seismic flow of rock. Earth Phys., 1, 23-40.

Olesen, O., Blikra, L.H., Braathen, A., Dehls, J.F., Olsen, L., Rise, L., Roberts, D., Riis, F., Faleide, J.I. and Anda, E., 2004. Neotectonic deformation in Norway and its implications: a review. Norwegian Journal of Geology 84, 3-34.

Olesen, O., Bungum, H., Dehls, J., Kierulf, H.P., Lindholm, C., Pascal, C. and Roberts, D., 2013. Neotectonics, seismicity and contemporary stress field in Norway - mechanisms and implications. In Quaternary Geology of Norway, L. Olsen & Slagstad, T. (eds.), Nor. Geol. Unders. Spec. Publ. 13.

Scherneck, H.-G., Johansson, J.M., Mitrovica, J.X. and Davis, J.L., 1989. The BIFROST project: GPS determined 3-D displacement rates in Fennoscandia from 800 days of continuous observations in the SWEPOS network. Tectonophysics, 294, 305-321.

# Neoarchaean alkaline rich igneous magmatism as a part of cratonization of the western Karelia

E. Heilimo[1] and P. Mikkola[1]

[1]Geological Survey of Finland, P.O. Box 1237, 70211 Kuopio, Finland
E-mail:esa.heilimo@gtk.fi

We have studied a group of granitoids, mainly quartz syenites, from the western Karelia subprovince of the Fennoscandian shield. Characteristic compositional features of the rocks are high contents of alkalis (Na, K), LILE (Ba, Sr), associated with low contents of Mg, Ni, and Cr. The quartz syenites represent a group of late phase intrusions overlapping in age with the other Neoarchaean felsic, intermediate, and mafic igneous rocks: sanukitoids, quartz diorites, and alkali-rich gabbros, derived from heterogeneously enriched lithospheric mantle. The $\delta^{18}O$ values vary from mantle-like values to ones indicating involvement of source(s) which have undergone low temperature fractionation. This study provides new evidence of the heterogeneity of Neoarchaean plutonism and has implications for the cratonization process of the Archaean Karelia Province.

**Keywords:** Quartz syenite, Archaean, Karelia Province, Geochemistry, U-Pb, Sm-Nd, O

## 1. Introduction

Alkali-rich igneous rocks are volumetrically minor component of the geological record. Their parental magmas rocks are proposed to be derived via variable degrees of partial melting of metasomatized lithospheric or asthenospheric mantle (e.g. Sutcliffe et al., 1990). In some cases partial melting of thickened lower crust, with minor middle and upper crust contamination has been proposed as a possible source (Smithies and Champion, 1999). Regardles of the source, effective mineral fractionation plays a significant role in the formation of alkaline rich “syenitic” or “monzonitic” magma compositions.

## 2. Geology of the quartz syenites

Seven felsic alkaline intrusions have been recognized from the Lentua complex of the Archaean western Karelia subprovince (Fig. 1). Temporally and spatially they are part of the Neoarchaean late phase plutonism, whose other members are sanukitoids, quartz diorites, and alkali rich gabbros, all likely to be derived from enriched mantle source (Käpyaho et al., 2006, Heilimo et al., 2010, Mikkola et al., 2011a, Mikkola et al., 2014). The fore mentioned suites are coeval with anatectic leucogranitoids (e.g. Mikkola et al., 2012).Typical mineralogical compositions vary from syenite to quartz syenite, but the group also includes a small number of quartz monzonites, monzonites and granites. Intrusions often display weaker deformation than the older granitoids. The mafic minerals are also more abundant and richer in alkalis than in the other granitoids. The intrusions are generally less than 3 km in diameter, although the largest intrusion is 10 km in length.

## 3. Elemental composition

Majority of the analyzed rocks have higher contents of alkaline ($K_2O+Na_2O$ 7.97–11.23 wt. %) and LIL elements (Ba up to 5000 ppm and Sr up to 2000 ppm), which separates them from the sanukitoids and quartz diorites, although there is high variation between individual intrusions. Another compositional feature separating the sanukitoids and quartz diorites from the quartz syenites is the low content of Mg, Ni, and Cr of the latter. Despite scatter there is clear compositional resemblance to the Archaean syenites and monzonites from Yilgarn and Abitibi provinces (Smithies and Champion, 1999)

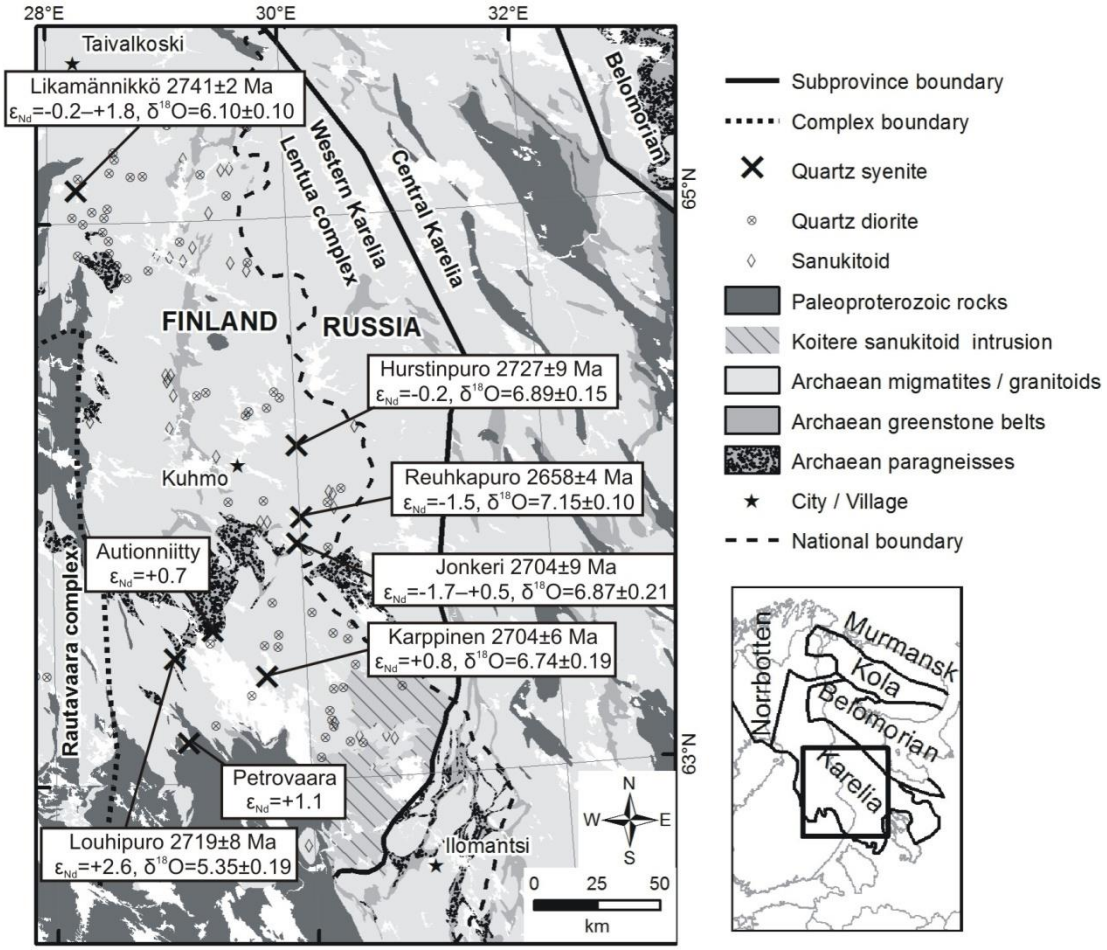


**Figure 1.** Generalized geological map of the Western part of the Karelia Province (Koistinen et al., 2001) pointing the quartz syenite intrusions and available isotopic data, as well as location of the Neoarchaean sanukitoids and quartz diorites, based on National Electronic Bedrock Map of Finland (DigiKP) database. Inset map shows the Archaean Provinces of the Fennoscandian shield. Data for the Likamännikkö intrusion from Mikkola et al. (2011b).

## 4. **Geochronological and isotopic data**

The in situ U-Pb analyses on zircons were performed with laser ablation multicollector inductively coupled plasma mass spectrometer (LA-MC-ICPMS) at the Finnish Isotope Geosciences Laboratory. The Sm-Nd analyses on whole-rocks were performed using VG Sector 54 thermal ionization multiple collector mass spectrometer and isotope dilution (ID-TIMS) at the isotope laboratory of the Geological Survey of Finland. The O-isotope ratios of zircons were measured using Cameca IMS 1280 multi-collector ion microprobe at the Nordsim facility, National Museum of Natural History, Stockholm, Sweden.

Based on U–Pb results the emplacement ages of the quartz syenites vary from 2.74 Ga to 2.66 Ga (Fig. 1). Thus, the quartz syenite group overlaps temporally with other late phase intrusions. Initial whole-rock $\varepsilon_{Nd}$-values vary between -1.8 and 2.6, and do not indicate a major contribution of significantly older crust. Zircon O-isotope data show that quartz syenite and sanukitoid intrusions display similar, highly variable $\delta^{18}O$ values, 5.3−7.2 vs. 5.1−8.5 ‰

respectively (Heilimo et al., 2013). Most samples from both groups yield $\delta^{18}O$ values similar to mantle source zircons, but the highest ratios strongly indicate contribution from sources with high $\delta^{18}O$, i.e. one that have undergone low temperature fractionation.

## 6. Discussion

As earlier mentioned the quartz syenites differ as a group from the other late phase granitoid groups of Karelia, such as sanukitoids and quartz diorites, the most significant differences being the higher contents of alkaline elements (Na, and K) and LILE (Ba, and Sr). Their composition is likely a result of evolution by effective fractional crystallization of mafic minerals, most evidently hornblende. Ba vs. Sr and Cr vs. V diagrams in logarithmic scale (Fig. 2) indicate that hornblende fractionation may have played a significant role in magma evolution a minor contribution from pyroxenes phases is also possible. The lack of clear negative Eu-anomaly in composition rules out the possibility of significant plagioclase and K-feldspar fractionation in the magma evolution. Due to the strong fractionation of mafic minerals, estimations of the parental magma composition and it's source are difficult based only on elemental composition. The lowest $\delta^{18}O$ values 5.3−6.1 ‰ of quartz syenites zircons can be explained via partial melting of mantle peridotite or unaltered mid-ocean ridge basalt (MORB). However, the highest $\delta^{18}O$ values 6.7−7.2 ‰ indicate involvement of a component that has undergone low temperature fractionation. Similar variation is also observed in the sanukitoids of the Karelia province.

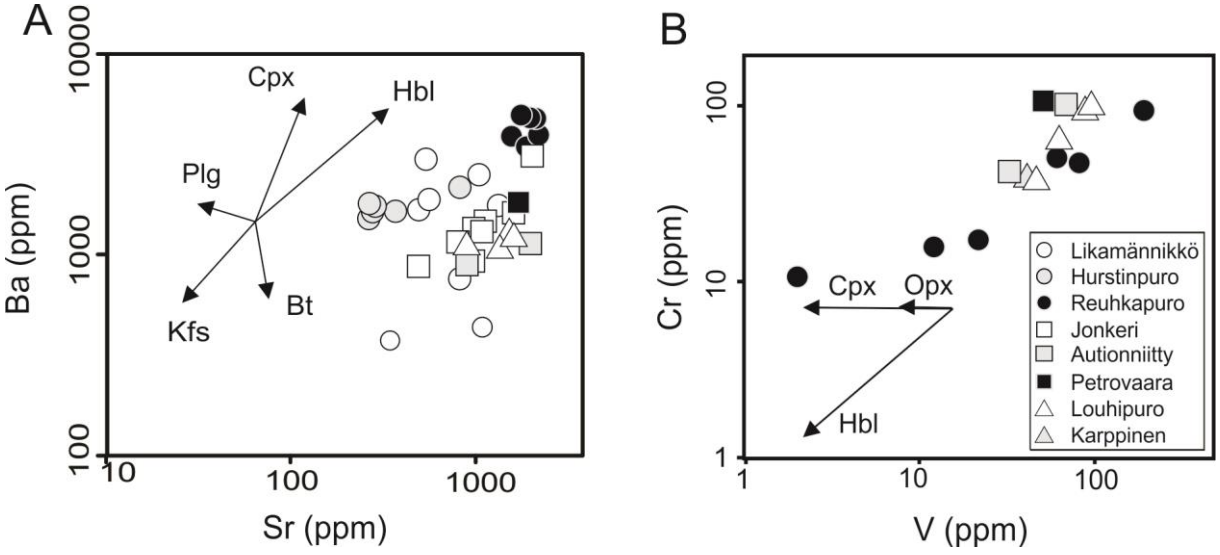


**Figure. 2.** Selected bivariate diagrams with logarithmic scales and qualitative mineral vectors for studied intrusions. a) Ba vs. Sr, b) Cr vs. V. Distribution coefficients from Rollinson (1993). Abbreviations for minerals Plg – plagioclase, Kfs – K-feldspar, Biot − biotite, Hbl – hornblende, Opx – orthopyroxene, Cpx – clinopyroxene.

The quartz syenite group is part of final cratonization events of the western Karelia. The compositional, and isotope characteristics of the quartz syenites display similarities with the other late phase plutonic rocks; sanukitoids, quartz diorites, and alkali rich gabbros. Although, unlike the more intensively studied local sanukitoid intrusions, they seem not to present a well established event(s). Crystallisation ages of the intrusions span 80 Ma (2.74−2.66 Ga) making a single triggering event unrealistic. Instead the quartz syenites require a tectonic process/setting that allow mantle several times during the last stages of the cratonization in the western Karelia subprovince. Regardless of the tectonic setting the quartz syenites are a part of diversification of magmatic activity the Archaean-Proterozoic boundary (~ 2.7–2.5 Ga) after long lived voluminous TTG magmatism that is recorded both locally and globally.

**References:**

BEDROCK OF FINLAND - DigiKP. Digital map database [http://ptrarc.gtk.fi/digikp200/]. Espoo: Geological Survey of Finland [referred 31.12.2013]. Version 1.0.

Bindeman, I., 2008. Oxygen Isotopes in Mantle and Crustal Magmas as Revealed by Single Crystal Analysis. Reviews in Mineralogy & Geochemistry, 69. 445–478.

Heilimo, E., Halla, J., and Hölttä, P., 2010. Discrimination and origin of the sanukitoid series: geochemical constraints from the Neoarchean western Karelian Province (Finland). Lithos, 115, 27−39.

Heilimo, E., Halla, J., Andersen, T., and Huhma, H., 2013. Neoarchean crustal recycling and mantle metasomatism: Hf-Nd-Pb-O isotope evidence from sanukitoids of the Fennoscandian shield. Precambrian Research, 228, 250−266.

Käpyaho, A., Mänttari, I., and Huhma, H., 2006. Growth of Archaean crust in the Kuhmo district, eastern Finland : U-Pb and Sm-Nd isotope constraints on plutonic rocks. Precambrian Research, 146, 95–119.

Koistinen, T., Stephens, M. B., Bogatchev, V., Nordgulen, Ø., Wennerström, M., and Korhonen, J., 2001 (Comp.). Geological map of the Fennoscandian shield, scale 1:2000 000. Geological survey of Finland, special maps, 48.

Mikkola, P., Huhma, H., Heilimo, E., and Whitehouse, M., 2011a. Archean crustal evolution of the Suomussalmi district as part of the Kianta Complex, Karelia; constraints from geochemistry and isotopes of granitoids. Lithos, 125, 287−307.

Mikkola, P., Salminen, P., Torppa, A., and Huhma, H., 2011b. The 2.74 Ga Likamannikko complex in Suomussalmi, East Finland: Lost between sanukitoids and truly alkaline rocks? Lithos, 125, 716−728.

Mikkola, P., Heilimo, E., Halkoaho, T., and Käpyaho, A., 2014. Neoarhaean enriched gabbros and diorite of the Karelian Province as part of the diversification of the plutonic activity. Lithosphere 2014 – 8th Symposium on the Structure, Composition and Evolution of the Lithosphere inFennoscandia. Programme and Extended Abstracts, Turku, Finland, November 4-5, 2014. Institute of Seismology, University of Helsinki, Report S-62, 61-64.

Rollinson, H. R., 1993. Using Geochemical Data: Evaluation, Presentation, Interpretation, Longman, UK. 352 p.

Smithies, R. H., and Champion, D. C., 1999. Late Archaean felsic alkaline igneous rocks in the Eastern Goldfields, Yilgarn Craton, Western Australia: a result of lower crustal delaminating? Journal of Geological Society, London, 156, 561–576.

Sutcliffe, R. H., Smith, A. R., Doherty, W., and Barnett, R. L., 1990. Mantle derivation of Archaean amphibole-bearing granitoid and associated mafic rocks: evidence from the southern Superior Province, Canada. Contributions to Mineralogy and Petrology, 105, 255–274.

# Advances in geodynamic modelling of rifted margin formation and lithosphere scale inversion and mountain building

R. S. Huismans

Department of Earth Sciences, University of Bergen, Allégaten 41, N-5007 Bergen, Norway
E-mail: Ritske.Huismans@geo.uib.no

In this presentation I will use numerical models to provide insights in two fundamental parts of the Wilson cycle: continental extension leading to rifted margin formation and mountain building resulting from continental convergence.

**Keywords:** Wilson cycle, rifted margin, orogenesis, numerical modelling, geodynamics

Contrasting end members of volcanic and non-volcanic passive margin formation show a large variability in structural style and associated subsidence history that imply strong variability in the underlying thermo-mechanical conditions at the time of rifting. For instance the Iberia-Newfoundland non-volcanic conjugate margin system has evolved from initial wide to late stage narrow, most probably asymmetric rift, leading to exhumation of mantle lithosphere and sub-lithospheric mantle in a wide ocean-continent transition zone under essentially cold conditions. In contrast rifting in for instance the North or the Central South Atlantic conjugate passive margins resulted in very wide (> 250 km) strongly thinned crustal conjugates. Volcanic rifted margins such as in the North and South Atlantic show excess magmatic activity and shallow water conditions at the rift-drift transition implying even higher geothermal gradients. Here thermo-mechanical finite element model experiments are used to investigate factors that are potentially important controls during volcanic and non-volcanic passive margin formation, which may explain these characteristic differences. Focus is on factors that control the degree of magmatism and structural style during lithosphere extension and passive margin formation.

Similarly not all convergent orogens are the same. In recent work we focus on the relationships between tectonic deformation and sedimentary basin formation. Resolving the interaction and feedback between tectonic crust-lithosphere scale deformation and surface processes through erosion of elevated areas and formation of sedimentary basins over multiple scales has been a long-standing challenge. While forward process based models have been successful at showing that a feedback is expected between tectonic deformation and redistribution of mass at the earth's surface by erosion, transport, and deposition, demonstrating this coupling for natural systems has been an even greater challenge and is strongly debated. Observational constraints on crust-lithosphere deformation and surface processes are typically collected at highly varying spatial and temporal scales, while forward process based models are typically run at either very large lithosphere-mantle scale, or at the scale of the sedimentary basin making it difficult to investigate and explore the detailed interaction and feedback between these systems. Here I will report on recent advances in forward modelling linking crust-lithosphere deformation with surface processes over a large range of scales resolving tectonic plate scale deformation and sedimentary basin formation at stratigraphic scales. The forward numerical models indicate a linkage and interaction between the structural style of thick-skinned large-scale mountain belt and rift-passive margin formation, erosion-transport-deposition processes operating at the surface, and the thin-skinned deformation occurring in the associated sedimentary basins.

# Timing of magmatism and migmatization in the 2.0–1.8 Ga Svecokarelian orogen, Uppland, south-central Sweden

Å. Johansson[1] and M.B. Stephens[2]

[1]Swedish Museum of Natural History, Box 50 007, SE-104 05 Stockholm, Sweden
[2]Geological Survey of Sweden, Box 670, SE-751 28 Uppsala, Sweden, and
Division of Geosciences, Luleå University of Technology, SE-971 87 Luleå, Sweden
E-mail: ake.johansson@nrm.se

U-Pb dating of zircon (10 samples) or monazite (1 sample) using the NORDSIM ion microprobe technique has been carried out on migmatized ortho- and paragneisses as well as less deformed felsic intrusive rocks from four separate areas (Rimbo, Hedesunda–Tierp, Skutskär and Forsmark) in the Uppland region, south-central Sweden. The rocks in this region belong to the 2.0-1.8 Ga Svecokarelian (a.k.a. Svecofennian) orogen in the Fennoscandian Shield. Most of the magmatic crystallization ages (N=7) range between 1.91 Ga (Rimbo area) and 1.86 Ga (Hedesunda area); a homogenous leucogranite intruded paragneiss in the Rimbo area at 1.84 Ga. Metamorphic ages could only be obtained from three samples at Rimbo (zircon), Tierp (monazite) and Skutskär (zircon), all falling at 1.87-1.86 Ga. In addition, individual zircons in some other samples yielded mixed or metamorphic ages down to 1.85 Ga. Zircons from the remaining samples either lacked metamorphic overgrowths or had U-rich and metamict overgrowths, from which only highly discordant ages were obtained. No unequivocal evidence for a later metamorphic event around 1.8 Ga was obtained from the samples in this study.

**Keywords:** orthogneiss, crystallization age, metamorphic age, Svecokarelian, U-Pb, zircon

## 1. Background, aims, methods and sample areas

Andersson et al. (2006) and Högdahl et al. (2008, 2012) have previously addressed the timing of metamorphism, including migmatization, in the 2.0-1.8 Ga Svecokarelian (a.k.a Svecofennian) orogen, in the central part of Sweden, and found evidence for two separate episodes of high-grade metamorphism around 1.87-1.86 Ga and 1.83-1.82 Ga. Furthermore, Hermansson et al. (2007, 2008) showed that penetrative ductile deformation under medium-grade conditions commenced and reached its waning stage in the Forsmark area, northern Uppland, at 1.87-1.86 Ga; subsequent deformation under low-grade conditions in this area was inferred to be confined to discrete ductile shear zones. Recently, Stephens and Andersson (2012) have provided new data on the timing of migmatization in the area between Stockholm in the north and Loftahammar to the south, confirming the polyphase metamorphism.

The primary aim of the present investigation was to constrain the timing of migmatization in the high-grade rocks north of Stockholm and in the northern part of Uppland, using U-Pb SIMS geochronology on zircon from selected samples of ortho- and paragneiss. This investigation complements the studies by Andersson et al. (2006) and Stephens and Andersson (2012) in south-central Sweden; it also joins together the areas studied by Stephens and Andersson (2012) mainly south of, and Högdahl et al. (2008, 2011) north of the Uppland region. A second aim was to determine the protolith ages of the orthogneisses. Samples were collected from four separate areas: (1) The Rimbo area, north of Stockholm, located close to a boundary between high- and medium-grade rocks; (2) The Hedesunda–Tierp area surrounding the 1.87 Ga Hedesunda granite massif in northern Uppland; (3) The Skutskär and (4) Forsmark areas, both located within the predominantly high-grade rocks along the northern coast of Uppland affected by strong ductile deformation with WNW–ENE trend (Stephens et al. 2009). An important question concerned whether evidence could be found for two high-grade metamorphic events in these areas.

## 2. Results

The results are presented in Table 1 and summarized visually in Figure 1. Unfortunately, only limited information could be obtained on the timing of metamorphism, as metamorphic rims or recrystallized domains within the zircons were, in many cases, too narrow to analyse or very U-rich and metamict, providing only highly discordant data. Furthermore, the relatively small age gap between protolith ages and metamorphic ages is a complicating factor. Nevertheless, important new information both on the magmatic and metamorphic evolution of the Uppland area in south-central Sweden has been obtained from this study.

Two orthogneiss samples (ÅJ12:03 and 04) from the Rimbo area both yielded magmatic crystallization ages around 1.91 Ga, which is slightly older than the early-orogenic Svecokarelian granitoids previously dated in south-central Sweden, and similar in age to or older than most of the volcanic rocks in this region (see compilation in Stephens et al. 2009). Metamorphic domains in zircons from one of these orthogneisses yielded an age of 1865±8 Ma. A migmatized paragneiss sample (ÅJ12:01) from the Rimbo area had detrital cores (n=4) falling between 2.11 and 1.94 Ga, and highly discordant metamorphic rims. A leucogranite body (ÅJ12:02), which intruded the paragneiss, yielded a weighted average $^{207}Pb/^{206}Pb$ age of 1844±3 Ma, similar to the crystallization age of leucogranite that intruded a diatexitic migmatite of sedimentary origin south of Stockholm (Stephens and Andersson 2012).

Along the southern margin of the 1.87 Ga phase of the so-called Hedesunda granite massif, zircons from a migmatitic, fine-grained orthogneiss of possible volcanic origin (ÅJ12:05) yielded a range of $^{207}Pb/^{206}Pb$ ages between 1900 and 1850 Ma, interpreted as a mixture of a magmatic protolith age around or slightly above 1.90 Ga, and a migmatization age around or possibly even after 1.85 Ga. A felsic dyke from the same outcrop area (ÅJ12:06) gave a well-defined weighted average $^{207}Pb/^{206}Pb$ age of 1872±2 Ma, similar in age to the spatially associated Hedesunda granite (1869±9 Ma, U-Pb TIMS, Bergman et al. 2004), to which the dyke may be related. A nearby felsic intrusive rock with inclusions of gneissic amphibolite (ÅJ12:07) yielded an uncertain magmatic crystallization age in the range 1.88-1.86 Ga. The uncertainty concerns the possible presence of inherited magmatic zircons close in age to 1.88 Ga with actual crystallization of the felsic intrusive rock around 1.86 Ga or, alternatively, a metamorphic resetting event around 1.86 Ga after crystallization around 1.88 Ga. The field relationships at this locality support the former interpretation. Along the eastern rim of the Hedesunda granite massif, north of Tierp, a strongly foliated migmatitic gneiss of uncertain origin (ÅJ12:08) failed to give any zircons, but monazite from this sample yielded a concordant age of 1862±1 Ma, interpreted as the timing of migmatization.

Further north, at Långsand east of Skutskär, a strongly foliated and fractured migmatitic fine-grained orthogneiss of presumed volcanic origin (ÅJ12:09) and a cross-cutting granitic dyke (ÅJ12:10) were sampled inside the complex shear belt with WNW–ESE trend along the northern coast of Uppland. The orthogneiss zircons were highly fractured and altered, but three different generations of zircon could be clearly discerned visually; inherited cores, a magmatic main phase, and metamorphic overgrowths. The magmatic zircons yielded a weighted average $^{207}Pb/^{206}Pb$ age of 1893±4 Ma, interpreted to date the magmatic protolith, with mixed or metamorphic data points scattering down to 1850 Ma. Only two zircons crystals were retrieved and analysed from the cross-cutting granitic dyke, and no conclusions on its magmatic crystallization age could be made. To the south, along the Gårdskär road, a sample of migmatitic orthogneiss (ÅJ12:11) of presumed intrusive origin yielded a weighted average $^{207}Pb/^{206}Pb$ protolith age of 1886±3 Ma and a metamorphic age of 1866±3 Ma, with a few recrystallized domains or metamorphic overgrowths ranging down to 1840 Ma. Finally, a migmatitic orthogneiss from Rönngrundet (ÅJ12:12), close to the Forsmark nuclear power

plant and north of the Singö deformation zone (Stephens et al. 2009), yielded a magmatic protolith age of 1899±3 Ma, with a single spot in a metamorphic overgrowth at 1870 Ma.

**Table 1.** U-Pb zircon and monazite age data from orthogneisses and felsic intrusive rocks in the Uppland region, south-central Sweden.

| Area | Rock type | Sample no. | Interpretation | Weighted average $^{207}Pb/^{206}Pb$ age | | |
|---|---|---|---|---|---|---|
| | | | | Age ± 2σ (Ma) | MSWD | n |
| **Rimbo** | Leucogranite | ÅJ12:02 zr | Magmatic age | 1844 ± 3 | 0.97 | 10 |
| | Migmatitic orthogneiss (intrusive) | ÅJ12:03 zr | Magmatic age | 1907 ± 3 | 0.67 | 6 |
| | | | Metamorphic age | 1865 ± 8 | 0.00 | 3 |
| | Orthogneiss (intrusive) | ÅJ12:04 zr | Magmatic age | 1909 ± 4 | 0.41 | 12 |
| **Hedesunda** | Migmatitic, fine-gr. orthogneiss (volcanic?) | ÅJ12:05 zr | Magmatic age | Around or older than 1.90 Ga | | |
| | | | Metamorphic age | Around or possibly after 1.85 Ga | | |
| | Felsic dyke | ÅJ12:06 zr | Magmatic age | 1872 ± 2 | 1.2 | 11 |
| | Felsic intrusive rock | ÅJ12:07 zr | Magmatic age | 1.86 – 1.88 Ga | | |
| **Tierp** | Migmatitic gneiss | ÅJ12:08 mz | Metamorphic age | 1862 ± 1 | 1.0 | 21 |
| **Skutskär** | Migmatitic, fine-gr. orthogneiss (volcanic?) | ÅJ12:09 zr | Magmatic age | 1893 ± 4 | 0.97 | 16 |
| | Migmatitic orthogneiss (intrusive) | ÅJ12:11 zr | Magmatic age | 1886 ± 3 | 1.1 | 19 |
| | | | Metamorphic age | 1866 ± 3 | 0.18 | 5 |
| **Forsmark** | Migmatitic orthogneiss | ÅJ12:12 zr | Magmatic age | 1899 ± 3 | 1.3 | 7 |

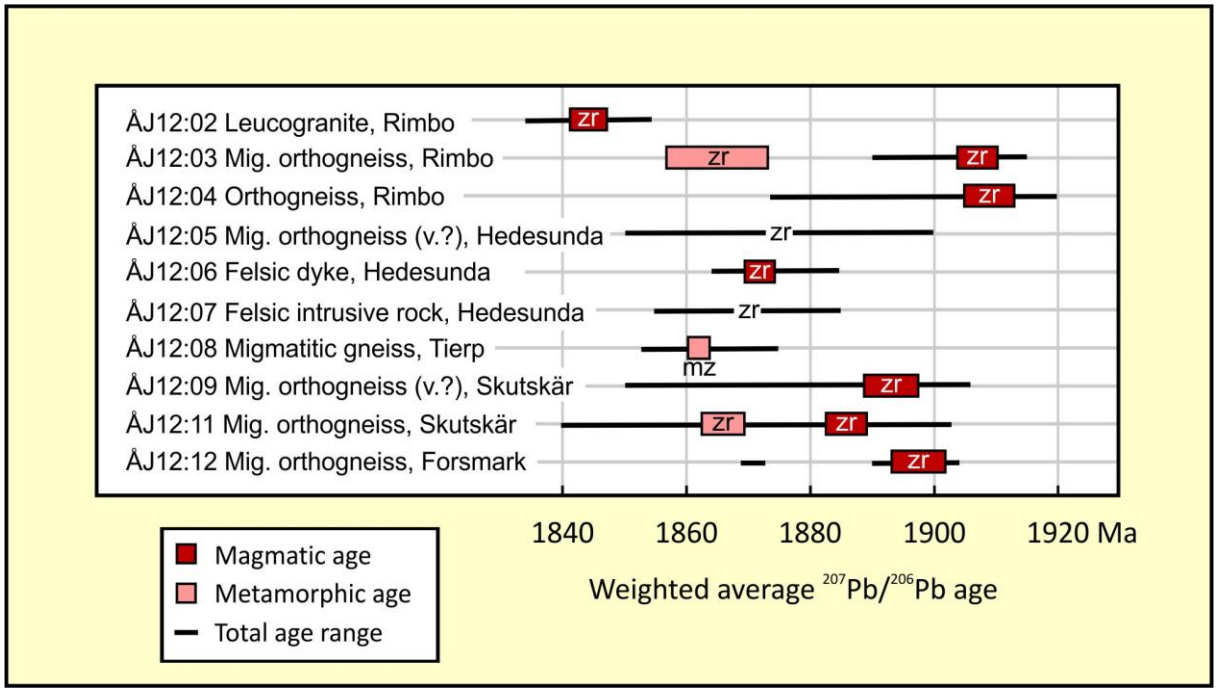


**Figure 1.** Summary of U-Pb zircon (zr) and monazite (mz) ages from orthogneisses and felsic intrusive rocks in the Uppland region, south-central Sweden. Boxes represent weighted average $^{207}Pb/^{206}Pb$ ages with 2 σ uncertainty. (v.?) = volcanic?

## 3. Discussion and conclusions

It is apparent from Table 1 and Figure 1 that, apart from the 1.84 Ga leucogranite at Rimbo (ÅJ12:02), all the magmatic crystallization ages fall in the range 1.91 to 1.86 Ga, irrespective of whether the rocks are intrusive or extrusive in origin. These ages are similar to or slightly older than the ages of other early Svecokarelian volcanic and intrusive rocks in south-central Sweden (see compilation in Stephens et al. 2009). The two oldest ages, at around 1.91 Ga, obtained from two orthogneisses of intrusive origin in the Rimbo area, are the oldest intrusive

rock ages so far obtained from this part of Sweden, and may mark the onset of subduction-related magmatism in this region. These granitoids have generally been considered intrusive into the nearby metasedimentary rocks (e.g. paragneiss sample ÅJ12:01). However, without any direct field observations of the contact relationships and bearing in mind the youngest detrital cores in the paragneiss sample around 1.94 Ga, the relative time relationship remains elusive. The 1.87 Ga felsic dyke at Hedesunda is similar in age to the spatially associated Hedesunda granite massif.

Metamorphic zircon in the studied samples may be subdivided into three textural types: (1) BSE-bright recrystallized domains within older magmatic zircons, which normally retain a relatively high inherited magmatic Th/U-ratio and yield metamorphic or mixed ages; (2) BSE-dark, recrystallized, U-rich domains within older magmatic zircons, which have become altered and metamict, and yield highly discordant, geologically meaningless ages; and (3) BSE-dark or zoned newly grown zircon overgrowths with low Th/U, which, if sufficiently thick to be analysed, turn out to be metamict and, once again, yield discordant and geologically meaningless results.

Thus, only limited data on the timing of migmatitization could be obtained, with the best defined ages (two from zircons, one from monazite) at 1.86-1.87 Ga, similar to the older metamorphic ages obtained by Andersson et al. (2006), Högdahl et al. (2008, 2012) and Stephens and Andersson (2012) in central Sweden, as well as the intrusive ages of the older phase of the Hedesunda granite (Bergman et al. 2004), the Ljusdal batholith (Högdahl et al. 2008) and the oldest phase of the Transscandinavian Intrusive Belt (see compilation in Stephens et al. 2009). In several of the other investigated samples, individual analytical spots show a range of mixed or metamorphic ages down to around 1.85 Ga, with the leucogranite from the Rimbo area providing a well-defined youngest end point at 1844±3Ma. No unequivocal evidence for a separate, younger metamorphic event at around 1.8 Ga could be found in the new data.

**References:**

Andersson, U.B., Högdahl, K., Sjöström, H. and Bergman, S., 2006. Multistage growth and reworking of the Palaeoproterozoic crust in the Bergslagen area, southern Sweden: evidence from U-Pb geochronology. Geological Magazine, 143, 679-697.

Bergman, S., Persson, P.-O., Delin, H., Stephens, M.B. and Bergman, T., 2004. Age and significance of the Hedesunda granite and related rocks, south-central Sweden. GFF, 126, 18-19.

Hermansson, T., Stephens, M.B., Corfu, F., Andersson, J. and Page, L., 2007. Penetrative ductile deformation and amphibolite facies metamorphism prior to 1851 Ma in the western part of the Svecofennian orogen, Fennoscandian Shield. Precambrian Research, 153, 29-45.

Hermansson, T., Stephens, M.B., Corfu, F., Page, L. and Andersson, J., 2008. Migratory tectonic switching, western Svecofennian orogen, central Sweden: Constraints from U/Pb zircon and titanite geochronology. Precambrian Research, 161, 250-278.

Högdahl, K., Sjöström, H., Andersson, U.B. and. Ahl, M., 2008. Continental margin magmatism and migmatisation in the west-central Fennoscandian Shield. Lithos, 102, 435-459.

Högdahl, K., Majka, J., Sjöström, H., Persson Nilsson K., Claesson, S. and Konecný P., 2012. Reactive monazite and robust zircon growth in diatexites and leucogranites from a hot, slowly cooled orogen: implications for the Palaeoproterozoic tectonic evolution of the central Fennoscandian Shield, Sweden. Contributions to Mineralogy and Petrology, 163, 167-188.

Stephens, M.B. and Andersson, J., 2012. Contrasting orogenic systems in the Fennoscandian Shield, southern Sweden. LITHOSPHERE 2012 Symposium, November 6-8, 2012, Espoo, Finland, 4 pp.

Stephens, M.B., Ripa, M., Lundström, I., Persson, L., Bergman, T., Ahl, M., Wahlgren, C.-H., Persson, P.-O. and Wickström, L., 2009. Synthesis of bedrock geology in the Bergslagen region, Fennoscandian Shield, south-central Sweden. SGU Ba 58, Uppsala, 259 pp.

# Modelling post-collisional magmatism – Results from integrated thermo-mechanical mantle convection and thermodynamic geochemical melting models

L. Kaislaniemi, J. van Hunen, M. B. Allen, P. Bouilhol, I. Neill

Durham University, Durham, United Kingdom
E-mail: lars.kaislaniemi@iki.fi

We present models of mantle convection dynamically coupled with thermodynamic models of mantle melting. This tool is used to study the anatexis of lower crust during post-collisional lithospheric thinning. Complex feedback mechanisms between lithospheric thinning, melt weakening, crustal melting and melt removal induced depletion stiffening are found. Crustal anatexis induced by lithospheric thinning has a positive feedback mechanism that can lead to the collapse of the crust, extensional tectonic regime and sudden granitic plutonism.

**Keywords:** post-collisional magmatism, mantle convection, thermodynamic modelling, orogenic collapse

## 1. Introduction

Generation of late- to post-orogenic (post-collisional) mafic magmatism has invoked a multitude of explanations, from slab break-off (Davies and von Blanckenburg 1995) and whole mantle delamination (Pearce et al. 1990) to small-scale convection (Kaislaniemi et al. 2014). The source of these rocks, however, is generally agreed to be in the depleted subduction-modified lithospheric mantle, based on the isotopic and REE characteristics of the rocks. The generation of the associated felsic magmatism, on the other hand, remains a debated issue. A review by Bonin (2004) argues for a same mantle source for the post-orogenic mafic and felsic rocks. The transition from post-collisional to post-orogenic–marked by extensional episodes, gravitational collapse of the crust and transition from high-K calc-alkaline bimodal magmatic suites into alkaline magmatic suites–shows a decreasing role of the crust in this magmatism. Contrary to this, Liegeois et al (1998) suggest that the differences between post-collisional high-K suites and post-orogenic alkaline suites are linked to the sources themselves, and only to a lesser degree to the differentiation process.

In addition, the heat source for the extensive melt production in post-orogenic setting has been a subject of extensive research. It is now generally agreed that unless a significant crustal thickening (~doubling the thickness) takes place, the increased radiogenic heating alone cannot produce extensive crustal melting (Thompson and Connolly 1995). It is probable that the anomalously thick crust of the Tibet contains partially molten layers (Nelson et al. 1996). Also, thermal modelling (Kukkonen and Lauri 2009) of the Paleoproterozoic Svecofennian orogeny has shown that a rapid thickening of the crust up to 70 km total thickness could produce temperatures high enough for partial crustal melting and granite production. However, in cases like the Variscan orogeny, with high temperature and low pressure metamorphism, implying only modest amounts of crustal thickening, lithospheric thinning (e.g. Franke 2000) and underplating of mafic magmas (Williamson et al 1992) have been considered perhaps more probable causes for crustal melting. Seismic studies showing strong reflections at the moho level have been used to argue for magmatic underplating, as for example is the case in the south-western of the Svecofennian orogeny (Korsman et al 1999). Mafic enclaves within these post-collisional granitoids (e.g. Couzinié et al 2014), called vaugnerites, in the French Massif Central and the Bohemian Massif of the Variscan, evidence

mingling of mafic and felsic magmas, interpreted to show coeval crustal anatexis and intrusion of mantle-derived melts.

Inherently associated with continental collisions is the formation of migmatite-granite terrains, exposed at locations of eroded mountain belts (e.g. Vanderhaeghe et al 1999). The formation of these belts is caused by the heating of the orogenic event, whether by radiogenic or mantle derived heating, as discussed above. These terrains crop out as so called core complexes or domes sometimes with associated with extensive granitoid intrusions (e.g. Velay dome of the Massif Central in France or the Southern part of the Svecofennian orogeny). The exhumation process of these formations remain discussed, but in all cases the exhumation is associated with a late-orogenic "collapse" of the thickened crust and formation of extensional structures.

In the Velay dome region the collapse of the orogen is evidenced by migmatite terrains and granitic intrusions (Couzinié et al 2014): Migmatization (340 Ma to 310 Ma) after collisional peak (340-335 Ma) was followed by a period of granitic magmatism at about 310-300 Ma. The granitic suites are closely associated with mantle-derived Mg-K-rich diorites, cropping out as intrusive bodies or enclaves within the felsic rocks. In the southern part of the Paleoproterozoic Svecofennian orogeny, a granite-migmatite zone comprises the Southern Finland (Väisänen et al. 2000). The main collisional stage took place at 1.89-1.87 Ga. High temperature low pressure granulites, indicating high heat flow, and shoshonitic bimodal magmatism is present throughout the migmatite zone. Extension took place at 1.83-1.82 Ga (e.g. Nironen and Kurhila, 2008). U-Pb ages of the leucogranites within the belt show emplacement during a 70 Myrs period from 1.86 Ga to 1.79 Ga (Kurhila et al. 2010).

Common to both the Variscan Velay migmatite dome and the Svecofennian southern Finland migmatite belt are an extended period of partial crustal melting ending in formation of granitic plutons and extensional tectonics (orogenic collapse). Both have closely associated mantle-derived mafic rocks implying involvement of mantle melting in the generation of the crustal melts.

**2. Methods and results**

We present a thermo-mechanical model of mantle convection coupled with thermodynamic modelling of crustal melting. The aim is to produce a general model of post-collisional/-orogenic lithosphere-asthenosphere dynamics and to examine the effects of mantle hydration during subduction, convective lithospheric thinning and underplating of mafic melts at moho level to the production of mantle and crustal melts. Dynamic feedback mechanisms between melting, depletion, melt weakening, depletion stiffening and residue/melt composition evolution during melt removal are taken into account.

Our results show that minor amounts of water released from the preceding subduction to the upper mantle lowers the mantle viscosity enough to initiate sub-lithospheric small-scale convection. This leads to localized lithospheric thinning and melting of lithospheric and asthenospheric mantle. Partial melting of the lower crust caused by the added conductive heating by lithospheric thinning has a positive feedback on the lithosphere erosion (Fig. 1). Once started, the lithospheric thinning is sustained by the weakening effects of partial crustal and mantle melts. Underplating of mafic mantle melts at the moho level increases the moho temperatures and enhances crustal anatexis momentarily, but a high viscosity residue left in the lithospheric mantle "shields" the lower crust from extensive melting. Our models show periods of tens of millions of years of partial melting at the lower crust before the melt degrees exceed the threshold for melt removal, i.e. plutonism at upper crustal levels.

Convective removal of the lithosphere causes dynamic topography effects. A more variable topography is produced by the melt weakening enhanced lithospheric thinning.

The composition of the partial crustal melts vary during the thinning of the lithosphere, as the pressure and temperature of melting changes and the composition of the residue evolves. On a TAS diagram, the melts overlap with the fields of tonalite, (quartz)monzonite, granodiorite and, to a lesser degree, granite. There is a tendency to decreasing peraluminous nature of the melts (Fig. 2) with time, although anatexis timing is varying horizontally and thus geochemical trends are diachronous as well.

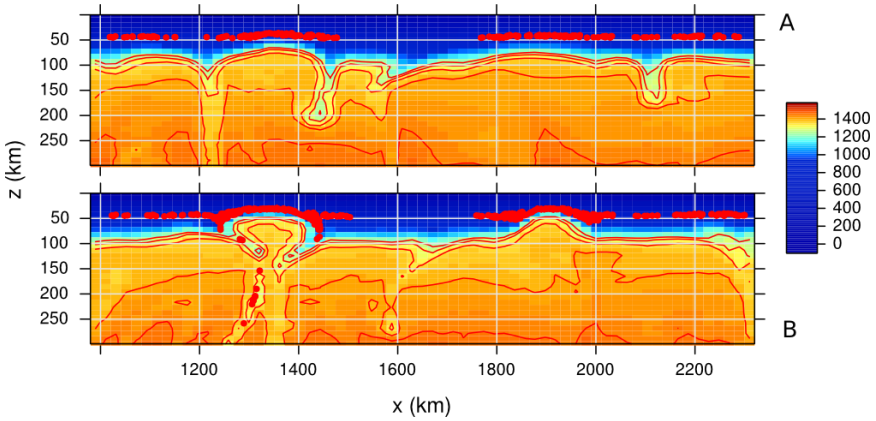


**Figure 1.** The temperature field of the uppermost mantle and lithosphere showing the sub-lithospheric small-scale convection and localized thinning of the lithosphere. Red dots show locations of partial crustal melting in the lower crust. A) Melt weakening effects not taken into account. B) Melt weakening enabled, prociding positive feedback to the lithosphere removal.

## 3. Conclusions

Mafic and felsic magmatism typical to post-collisional settings can be generated by following steps: **1)** Hydrous activation of the asthenosphere-lithosphere boundary by fluids from the preceding subduction leads to sub-lithospheric small-scale convection and local convective thinning of the lithosphere. **2)** Thinning causes mafic potassic mantle-derived magmatism and increasing temperatures in the lithosphere and lower crust. Crustal anatexis starts, possibly augmented by underplating magmas at the moho level. **3)** Crustal anatexis is sustained for long periods (up to tens of millions of years) before the degree of melting exceeds a critical threshold for melt extraction. This melt extraction forms the granitic plutons at upper crustal levels. **4)** Crustal anatexis has a positive feedback, via melt weakening, in the lithospheric thinning. This works as a trigger for the whole mantle delamination, enhanced crustal anatexis and destabilization, "collapse", of the crust. **5)** Removal of melts from the mantle and crustal sources forms depleted high viscosity residue layers in the lithospheric mantle and lower crust. This greatly reduces further melting events.

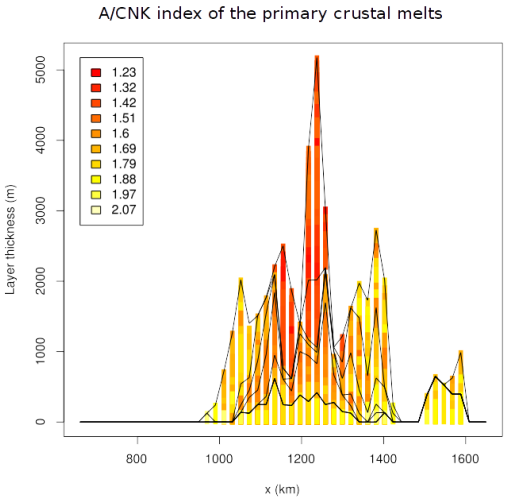


**Figure 2.** The A/CNK index of the extracted crustal melts as a function of location (cf. Fig 1). Columns represent "stratigraphic" columns assuming melts have extruded on to the surface and piled on top of each other. Black lines are isochrons with 10 Myrs interval.

## References:

Bonin, B. 2004. Do coeval mafic and felsic magmas in post-collisional to within-plate regimes necessarily imply two contrasting, mantle and crustal, sources? A review. Lithos, 78, 1–24.

Couzinié, S., Moyen, J.-F., Villaros, A., Paquette, J.-L., Scarrow, J. H., and Marignac, C. 2014. Temporal relationships between Mg-K mafic magmatism and catastrophic melting of the Variscan crust in the southern part of Velay Complex (Massif Central, France). Journal of GEOsciences, 59, 69–86.

Davies, J. H., and von Blanckenburg, F. 1995. Slab breakoff: A model of lithosphere detachment and its test in the magmatism and deformation of collisional orogens. Earth and Planetary Science Letters, 129, 85–102.

Franke, W. 2000. The mid-European segment of the Variscides: tectonostratigraphic units, terrane boundaries and plate tectonic evolution. Geological Society, London, Special Publications, 179, 35–61.

Kaislaniemi, L., van Hunen, J., Allen, M. B., and Neill, I. 2014. Sublithospheric small-scale convection--A mechanism for collision zone magmatism. Geology, 42, 291–294.

Korsman, K., Korja, T., Pajunen, M., Virransalo, P., and Group, G. W. 1999. The GGT/SVEKA Transect: Structure and evolution of the Continental Crust in the Paleoproterozoic Svecofennian Orogen in Finland. International Geology Review, 41, 287–333.

Kukkonen, I., and Lauri, L. 2009. Modelling the thermal evolution of a collisional Precambrian orogen: High heat production migmatitic granites of southern Finland. Precambrian Research, 168, 233–246.

Kurhila, M., Andersen, T., and Rämö, O. T. 2010. Diverse sources of crustal granitic magma: Lu–Hf isotope data on zircon in three Paleoproterozoic leucogranites of southern Finland. Lithos, 115, 263–271.

Liégeois, J.-P., Navez, J., Hertogen, J., and Black, R. 1998. Contrasting origin of post-collisional high-K calc-alkaline and shoshonitic versus alkaline and peralkaline granitoids. The use of sliding normalization. Lithos, 45, 1–28.

Nelson, K. D., Zhao, W., Brown, L. D., Kuo, J., Che, J., Liu, X., … Edwards, M. 1996. Partially Molten Middle Crust Beneath Southern Tibet: Synthesis of Project INDEPTH Results. Science, 274(5293), 1684–1688.

Nironen, M., and Kurhila, M. 2008. The Veikkola granite area in southern Finland: emplacement of a 1.83-1.82 Ga plutonic sequence in an extensional regime. Bulletin of the Geological Society of Finland, 80, 39–68.

Pearce, J. A., Bender, J. F., Delong, S. E., Kidd, W. S. F., Low, P. J., Guner, Y., … Mitchell, J. G. 1990. Genesis of collision volcanism in Eastern Anatolia, Turkey. Journal of Volcanology and Geothermal Research, 44, 189–229.

Thompson, A. B., and Connolly, J. A. D. 1995. Melting of the continental crust: Some thermal and petrological constraints on anatexis in continental collision zones and other tectonic settings. Journal of Geophysical Research, 100(B8), 15565–15579.

Väisänen, M., Mänttäri, I., Kriegsman, L. M., and Hölttä, P. 2000. Tectonic setting of post-collisional magmatism in the Palaeoproterozoic Svecofennian Orogen, SW Finland. Lithos, 54, 63–81.

Vanderhaeghe, O., Burg, J.-P., and Teyssier, C. 1999. Exhumation of migmatites in two collapsed orogens: Canadian Cordillera and French Variscides. Geological Society, London, Special Publications, 154, 181–204.

Williamson, B. J., Downes, H., and Thirlwall, M. F. 1992. The relationship between crustal magmatic underplating and granite genesis: an example from the Velay granite complex, Massif Central, France. Transactions of the Royal Society of Edinburgh: Earth Sciences, 83, 235–245.

# Structural mapping with terrestrial laser scanner: a case study from Vekara, SW-Finland

Kinnunen Jussi, Skyttä Pietari, Tenovuo Niklas and Kilpeläinen Timo

Geology section, Department of Geography and Geology, FI-20014 University of Turku, Finland
E-mail: jpkinn@utu.fi

Terrestrial laser scanning is comparatively new land surveying method but already widely used in producing highly accurate 3D- and digital elevation model. In this article we describe a method how to apply terrestrial laser scanning as an implement in the geological structure mapping.

**Keywords:** terrestrial laser scanning, 3D-modelling, structural geology, Precambrian, Paleoproterozoic, Svecofennian, supracrustal, Finland

## 1. Introduction

The rapid advances in data acquisition, processing and mobile technologies during the last years have challenged the methods of traditional field mapping. Consequently, digital mapping has become an increasingly attractive alternative. However, the digital methods have most commonly been applied at regional scale which is why they may fail in using the full potential of modern technology.

The current project aims at innovative integration of detailed digital on- and off-shore elevation models (DEM) and detailed aerial photographs with investigations on geological structures controlling the topographic features. The research project will be conducted on the Vekara Island, SW Finland (Fig. 1), which is characterized by ice-polished outcrops perfectly suitable for geological observations (Kinnunen et al., 2014). This presentation concentrates on introducing terrestrial laser scanning on one 50 by 100 m skerry SW of the Vekara island. The bedrock of the skerry is characterized by folds and joints which may be recognized from the aerial images, and which orientations may be defined in detail by laser-scanning due to the control they have on the local-scale topography (Fig. 2a).

## 2. Objectives

This project aims at detailed characterization of geological structures by combining high-resolution digital elevation models and aerial photographs with structural mapping and analysis. The prime tool for the base data acquisition in the project is Riegl VZ-400 terrestrial laser scanner, which generates accurate point clouds. The main objective is to produce digital elevation models overlain by high-resolution aerial photos, which can be used for virtual outcrop mapping, especially for observing geological structures in all different scales. Further goals of this ongoing project include development of scientific understanding of the processes which contributed to the ductile and brittle deformation structures in rocks metamorphosed under medium to high-grade conditions, and applicability of the developed method for the variety of end-users, including research and use of the coastal areas of the Baltic Sea.

## 3. Methods

*a) Fundamentals of the laser scanning:*

Terrestrial laser scanner is positioned in the top of the adjustable tripod. When measuring scanner transmits invisible and eye-safe laser rays. Scanner registers all rays reflected back and calculates coordinates of the single reflection point. With high speed mode Riegl laser

scanner produces dense xyz point cloud from 100° x 360° area up to 350 m range. Effective measurement rate is up to 122 000 measurements/second and given precision is 3 mm.
Also, calibrated Nikon D800 digital camera is attached to scanner and after the each full scan it shoots 36,3 Mpx photographs around whole scanned area, usually five photos partly one on the other. With these photographs it is possible to colour point cloud so that it produces photorealistic model of the scanned area.

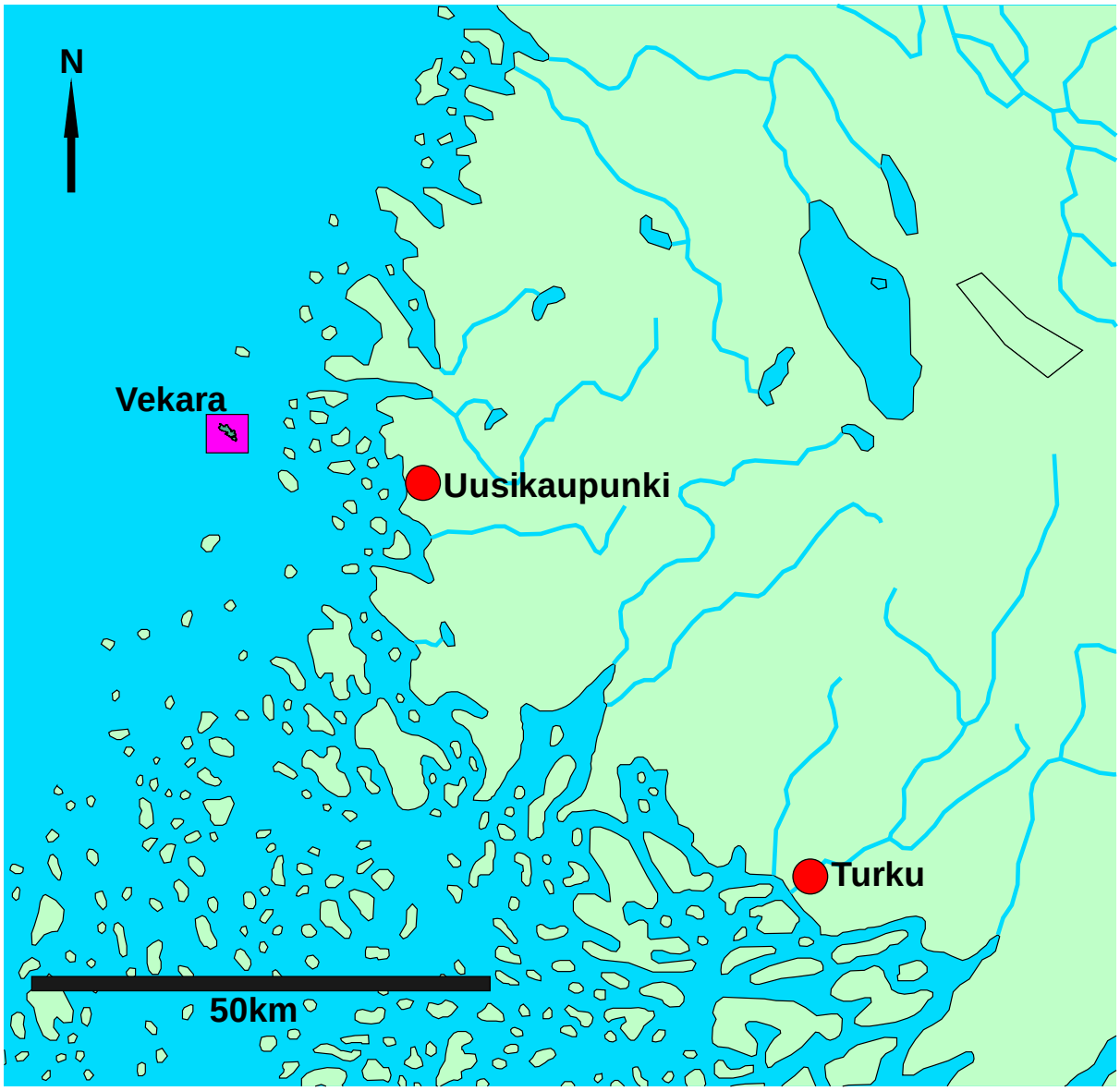


**Figure 1.** Vekara island, about 20 km from Uusikaupunki to WNW in fuchsia coloured rectangle.

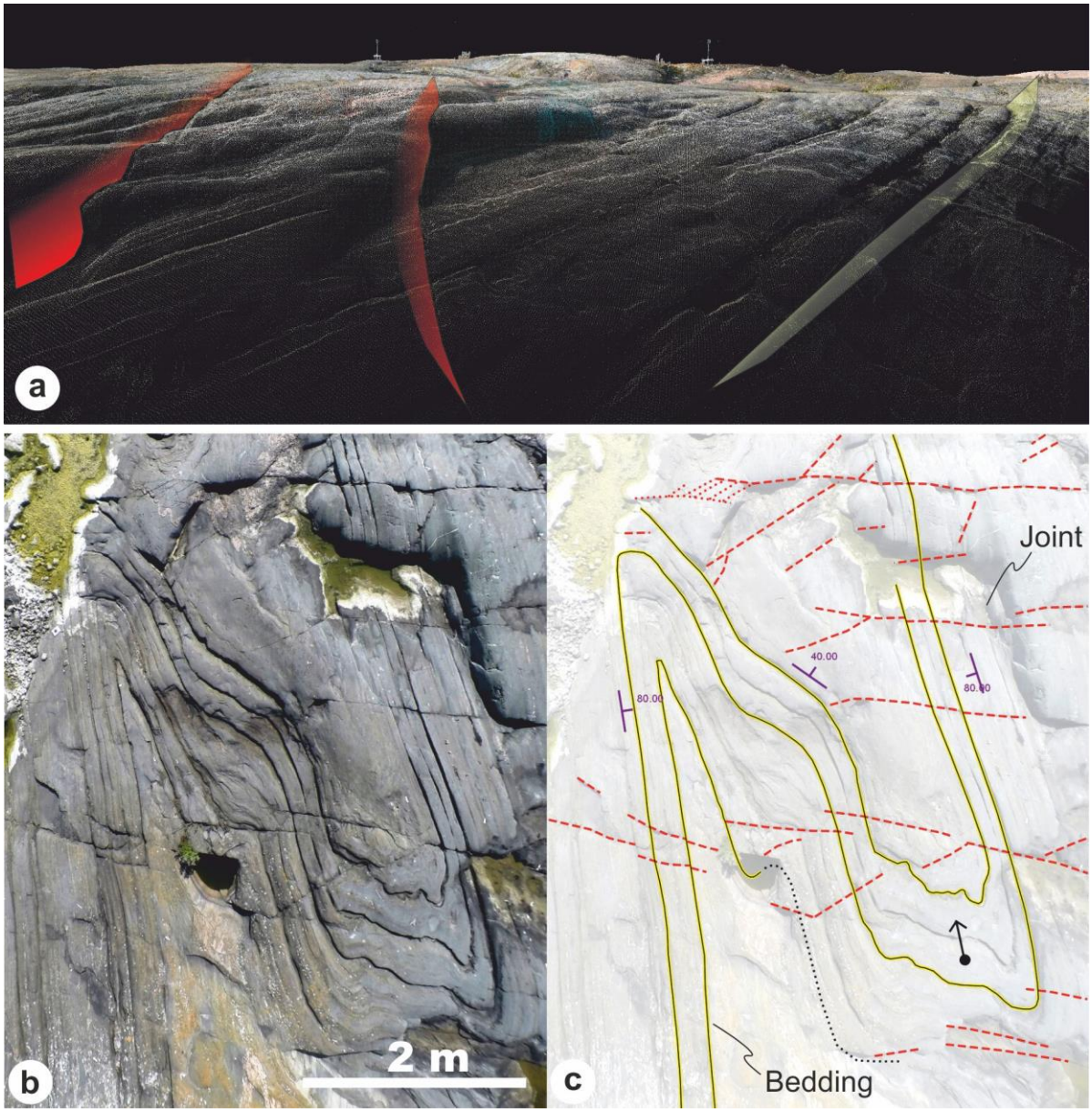


**Figure 2a.** Oblique picture taken from photo-coloured point cloud in RiScan Pro™. Direction of the two joints marked with red planes and folded bedding with green plane. **Figure 2b.** Aerial photograph taken from DJI Phantom 2 Vision -quadcopter with GoPro 3+ -camera. **Figure 2c.** Digitized structural form lines over the Figure 2 b photograph.

*b) Job description:*

First we decided positions for the scan stations. The skerry has numerous small pits and topographic depressions, and, consequently, a dense network of 18 scanning stations was chosen to avoid shadowing in scans. Subsequently, 18 marking nails were placed on the outcrop surfaces between the stations, and their exact positions were measured with a tachymeter. The initial positions of southernmost and northernmost nails were acquired with Trimble R8 RTK-GPS. Reflectors composing of reflector sticks on self-made adjustable tripods were placed upon the marking nails. 10 reflectors were used in all the measurements, with 6-8 tiepoints common with the measurements from the adjoining measurement locations.

*c) Scandata postprocessing:*
Individual point clouds from one scan station may be registered on a coordinate system (in this project ETRS89-TM35FIN) and the point clouds may be combined using the common tiepoints with native Riegl postprocessing software RiScan Pro™. It is possible to cut, filter, repair and colour point clouds. Surface triangulation can be made in RiScan Pro™ with 2D-Delaunay algorithm or later in other modelling applications.
After the preprocessing data can be exported for example as commonly accepted .las or .laz format and carried out in digital GIS- and 3D-modelling environment making use of the increased data processing capacity of the up-to-date modelling software packages. These include ESRI ArcMap™, Midland Valley Move™ and Blue Marble Geographics™ Global Mapper™.

## 4. Results

Each point cloud was registered according to known reference points in 10 reflectors in RiScan Pro™. For each point cloud application counts automatically internal standard deviation, which fluctuated between 0,00148 m to 0,00219 m before any corrections. Average radial, theta (vertical) and phi (horizontal) deviations varied between 0,0000 to 0,0068 m averaging around 1 mm. Standard deviation for all combined 18 point clouds was 0,0002 m and corresponding radial, theta and phi deviations were all 0,0000 (sic!). It is impossible to separate point cloud borders visually from each other and despite of careful searching we have not noticed any discontinuities in linear objects.

From photograph rendered digital elevation model (DEM) linear objects (e.g. faults, cracks, contacts, striation) of >1mm size can be clearly distinguished and their 3D determined. All erosional surfaces are not structure surfaces and cross checking between desktop mapped structures and real ones has to be made.

With the integrated model comprising of the laser-scans and aerial photographs (Fig. 2b), realistic structural form lines may be digitized to serve as modelling layers in the 3D-modelling software packages (Fig. 2c).

## 5. Conclusions

Using nails and tachymeter to mark and georeference the reflector places, as well as the use of 10 reflectors in each scan was very successful as indicated by the low errors. Three reasons for deviations (minimal though) can be; 1.) wind, 2.) adjustment of the reflector sticks and 3.) impossibility to follow quadrant rule in reflector arrangement. Hard wind could swing the thin reflector sticks and disturb the exact measurements. The reflector sticks were 110 cm high (distance between stick tip and middle point of 5 cm diameter reflector was 107,5 cm) and it should be situated exactly perpendicular to avoid systematic error, which could be 1-2 cm estimated. Also reflectors should be arranged so that there should be at least one reflector in each quadrant of the scan area. This was usually impossible in beach scan sites and corners in the island.

Terrestrial laser scanning is the best contemporary method to produce highly accurate digital elevation model. Combined together with high resolution photography it is ultimate tool for any virtual 3D-modelling including geological virtual outcrop modelling.

## References:

Kinnunen, J., Kilpeläinen, T., and Skyttä, P., 2014. Use of modern 3D modelling in research on the ductile and brittle structural evolution of Vekara Island, SW Finland. In: Ed. Virtasalo, Joonas and Tuusjärvi, Mari. 1st Finnish National Colloquium of Geosciences Espoo 19–20 March 2014 Abstract Book. Opas 58. Geological Survey of Finland.

# Detailed geological 3D-modelling - investigation niche 3 in ONKALO, Olkiluoto

N. Koittola

Posiva Oy Olkiluoto, 27160 Eurajoki, Finland
E-mail: noora.koittola (at) posiva.fi

The aim of this study was to create a detailed geological 3D-model of one of the ONKALO's investigation niche. The niche is one of the main study areas in ONKALO and for that reason the small scale geological model was required for the supporting the rock mechanical and geophysical test results. Totally, four separate geological models were created with geological and geophysical data. The modelling itself was carried out with Geovia Surpac software. The main aspects of the study were the quality control of the data and methods and the goal was to get more information of the small scale lithological features, structural features and the physical features of rock.

**Keywords:** 3D-modelling, POSE-experiment, Surpac, structural geology, geophysics, Olkiluoto

## 1. Introduction

Posiva Oy is responsible for implementing the final disposal programme for spent low-active nuclear fuel of its owners Teollisuuden Voima Oy and Fortum Power & Heat Oy. The planned site is Olkiluoto Island where Posiva Oy is carrying out the site studies for the characterization of the bedrock. This study is a part of the ongoing rock mechanical POSE (Posiva's Olkiluoto Spalling Experiment) experiment, whose goals are to define the *in situ* stress conditions and the spalling strength of the bedrock. The results of the POSE experiment were complicated to interpret and the back analysis cannot be completed without a detailed geological 3D model of the investigation niche 3, where the POSE experiment was carried out (Figure 1).

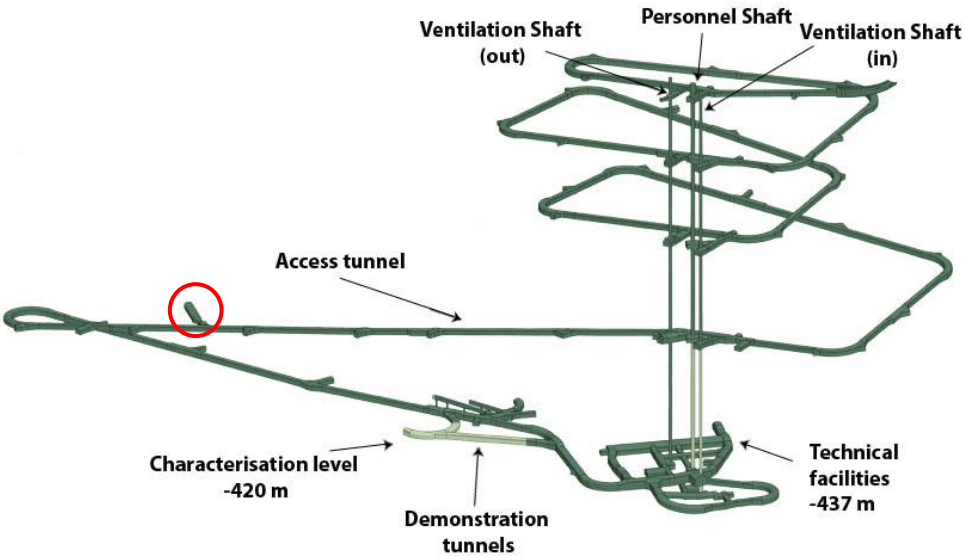


**Figure 1.** ONKALO and investigation niche 3.

## 2. Data and methods

The investigation niche 3 is one of the most studied areas in ONKALO so that diverse geological and geophysical data were available. Geological mapping was carried out after the excavation in 2009 and also the 3D-photogrammetry model from the surface of the niche occurred. Totally 97 drill cores were drilled from the niche's area and three almost full scale (1.5 m x 7.2 m) deposition holes (ONK-EH1...3) were drilled on the floor of the niche. Also at the south end of the niche an EDZ-field is located which consists of 30 1 m deep drill holes. It is mostly used in excavation damage zone studies. Several geophysical tests have been carried out around the niche but the selected methods to this study were ground penetrating radar, Mise-á-la-Masse and drill hole geophysics.

## 3. 3D geological modelling process

Based on the needs of rock mechanical back analysis of the Pose experiment and the selected data, totally 4 separate models were created: lithological model, foliation model, fracture model and a model of physically anomalous zones. Modelling was decided to be carried out with Geovia Surpac software because it is one of the most common modelling software in geo-industry and most of the geological and geophysical data was already in a form supported by Surpac.

In this study the modelling method was quite unique because the traditional numerical or cutting profile modelling did not work, because the used data was strongly connected to certain areas in the niche. There was also a need to keep the model as exact as possible especially on the areas, where there were most data. For that reason, for example, the lithological model of the niche was created as four separate detailed blocks, which were combined afterwards as one solid-block. The modelled lithological rocks were veined gneiss (VGN) as blue, pegmatite granite (PGR) as red, diatexitic gneiss (DGN) as greenish blue and quartz gneiss (QGN) as dark blue (Figure 2). The foliation and fractures were modelled as discs. Physically anomalous zones were modelled as planes.

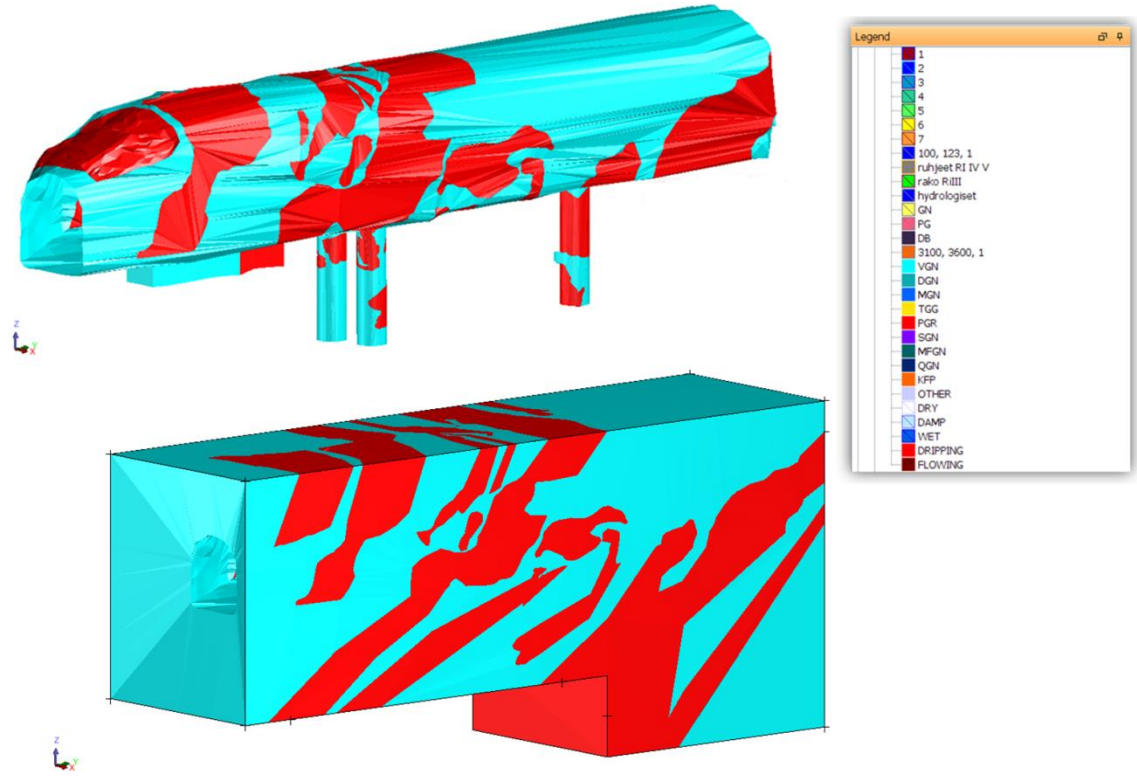


**Figure 2.** Lithological models of the investigation niche 3, viewed to northwest.

**Figure 3. F**racturing of the niche viewed to northwest. Green = filled fracture, yellow = slickenside fracture, brown = grain-filled fracture, red = clay-filled fracture.

## 4. Conclusions

The modelling gave information of the detailed lithological variation, main foliation and fracture sets and the locations of anomalous rock masses. Also some interpretation of these zones was made.

Two main foliation directions were identified (164/46 and 62/39, dip direction/dip) which indicate possible folding in the area. Fracturing was more randomly oriented, but three main directions exist (156/34, 270/85 and 342/83). The first set (156/34) follows foliation and most of the fractures are slickenside fractures. This slickenside fracture set was interpreted as

a continuation of a local fault zone OL-265. However, this feature needs more characterization.

During the study, quality control of the used data and methods was one of key references. In modelling, understanding of geological processes and geophysical features of geological units is needed.

In the investigation niche 3, the lithology at the south end of the niche was extremely complicated and for that reason additional drillings to that area (ONK-EH1…2) was proposed. If these drillings take place, it is possible to update the model. However, that is really time-consuming. The modelling programs are developing but still the modelling requires handwork, whose quality depends on the understanding of the geology and data.

**References:**

Aaltonen, I. (ed.), Lahti, M., Engström, J., Mattila, J., Paulamäki, S., Gehör, S., Kärki, A., Ahokas, T., Torvela, T., and Front, K., 2010. Geological model of Olkiluoto Site Version 2.0. Posiva Oy. Olkiluoto. Finland. 280 p.

Heikkinen, E. and Kantia P., 2011. Suitability of Ground Penetrating Radar for Locating Large Fractures. Working Report 2011-92. Posiva Oy. Olkiluoto, Finland. 64 p.

Nordbäck N., 2013. Outcome of the Geological Mapping of the ONKALO Undeground Research Facility, Chainage 3116-4986. Working Report 2013-11. Posiva Oy. Olkiluoto, Finland. 106 p.

Posiva Oy., 2011. Olkiluoto Site Description 2011. Posiva 2011-02. Posiva Oy. Olkiluoto, Finland. 1032 p.

Valli, J., Hakala, M., Wanne, T., Kantia, P. and Siren, T. 2011. ONKALO POSE experiment – Phase 3: Execution and monitoring. Working Report 2012-41. Posiva Oy. Olkiluoto, Finland. 163 p.

# Svecofennian orogeny in an evolving convergent margin setting

A. Korja and MIDCRUST Working Group

Institute of Seismology, Dept. Geosciences and Geography, Univ. Helsinki, Finland
E-mail: annakaisa.korja@helsinki.fi

It is suggested that the long-lived Svecofennian orogen records a change in the style of subduction from short lived subduction to long lived subduction zone. The change is recorded as change in crustal architecture imaged by crustal scale seismic reflection profiles. The architecture is compared with several existing theories: external-internal orogenies, advancing-retreating subduction systems, young cold-old hot orogenies. An example of a complex system where several processes interact is given from Vaasa Dome, western central Svecofennian orogen.

**Keywords:** Svecofennian, crustal architecture, orogenic model, crustal architecture

## 1. General

In Fennoscandian, the dominant tectonic mode changes from extension to convergence at around 1.9 Ga (Lahtinen et al., 2005; Korja et al., 2006). The rock record is characterized by subduction-related magmatism and modern style accretional and collisional orogens. At around 1.8 Ga the subduction systems seem to have stabilized implying that modern type full-scale convection is at operation (Korja and Heikkinen, 2008). The evolution of the convergent margin is recorded in the rock record and crustal architecture of the long lived Svecofennian orogeny (1.9-1.7 Ga).

## 2. Svecofennian orogen and orogenic models

It is suggested that the initial phase of the Svecofennian orogeny (1.92-1.88 Ga) - the compilation of the nucleus - has similarities with internal orogeny and the main phase (1.88-1.7 Ga) - continuous subduction - is more compatible with external orogeny as defined by Collins et al., (2011). A change from internal to external orogeny type implies that Baltica has drifted from a position above a convection cell to the outer rim of the convection cell. This may have implications on how orogenies evolve in time and space. It is suggested that Svecofennian orogen is one of the first examples of external orogenic systems that formed after the initiation of full-scale convection.

A closer look at the internal structure of the Svecofennian orogen reveals distinct regional differences. The northern and central parts of the Svecofennian orogen (Central Finland) that have been formed during the initial accretionary phase – or compilation of the nucleus – have a thick three layer crust (Fig. 1). The area has not only thick crust (55-65 km) but also thick mafic lower crust (10-30 km) and block–like internal architecture (e.g. SVEKA; SVEKALAPKO; Hyvönen et al., 2007; Grad and Tiira, 2009). Reflection profiles (FIRE1-3) image listric structures flattening on crustal scale décollement zones at the upper-middle crust and middle-upper crust boundaries (Korja et al., 2009). The crustal architecture together with large volumes of exposed granitoid rocks suggests the spreading of the orogen and the development of an orogenic plateau in Central Finland. The architecture is reminiscent of a large hot orogen in Jamieson and Beaumont's (2013) classification of orogens.

Within the western and southwestern part of the Svecofennian orogen, which is envisioned to have formed during continuous subduction phase, the crust is thinner (45-50 km) and it is hosting crustal blocks with one or two crustal layers. Those crustal blocks, where

the layering is poorly developed, host crustal scale reflective structures dipping to NE. Such blocks are found south-southwest of NE-dipping mantle reflections previously interpreted as paleo-subduction zones (BABEL Working group, 1990; Korja and Heikkinen, 2005). Crustal blocks with well-developed two layer crust are located N-NE of the mantle reflections interpreted as paleo-subduction zones (BABEL B, 1, 2, 3&4,). Altogether the architecture suggests a long-lived southwesterly retreating subduction system, with continental back-arc formation in the rear parts. The architecture is similar to that imaged by Collisions et al. (2002) large hot orogens.

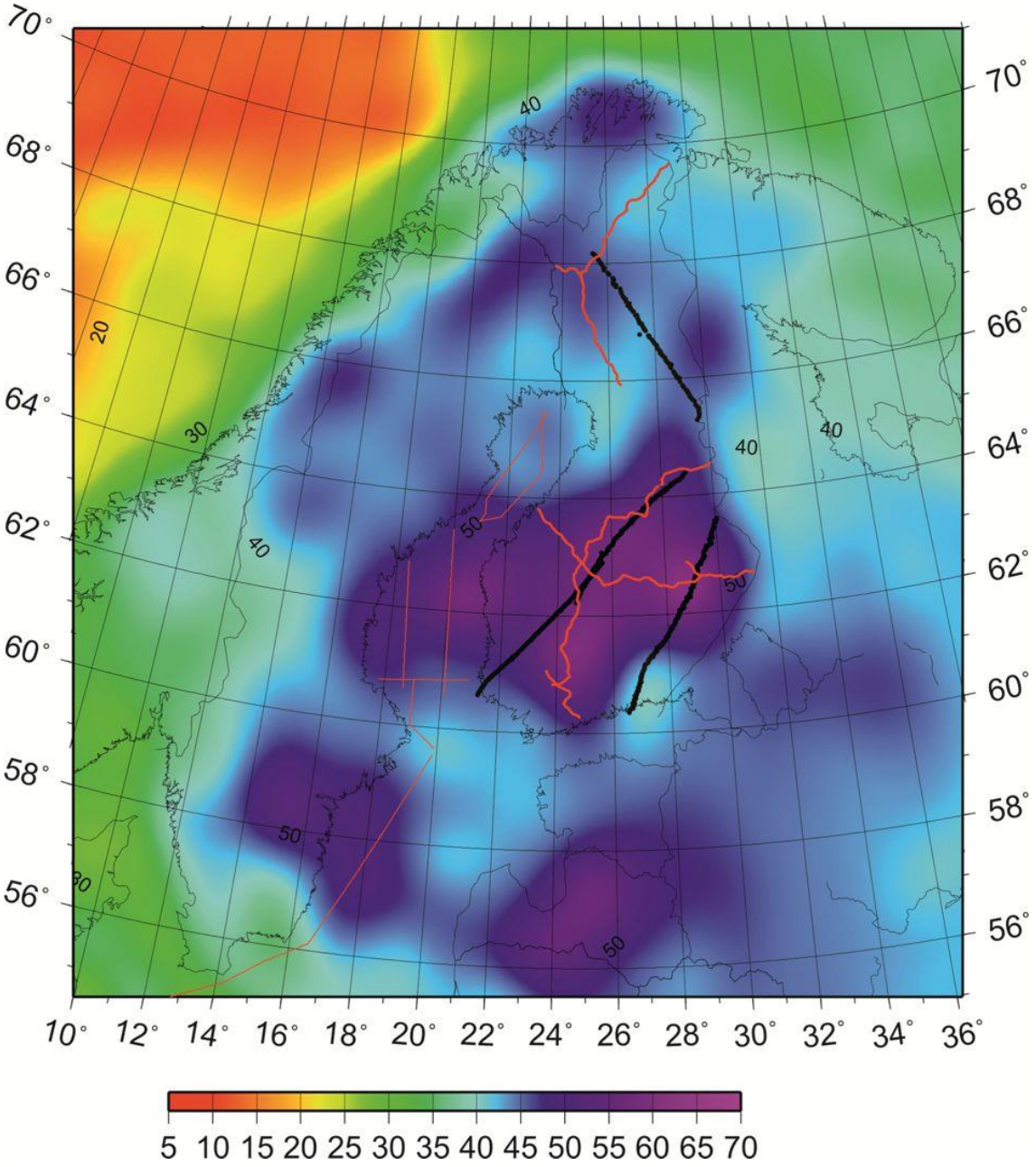


**Figure 1.** Seismic lines on a map of the depth to the Moho boundary of Fennoscandia (Grad and Tiira, 2008). Svecofennian orogen coincides broadly with the dark blue to purple colors (45-70 km). Black lines are refraction lines, wider red lines are FIRE onshore reflection lines and thin red lines are BABEL off-shore reflection lines.

Formation of back-arc basins implies that the lower plate i.e. the subduction zone is retreating at a greater speed than the upper plate is advancing. The fast retreating rate of the subduction zone is not only forming the continental back arc environment but also probably restricting the thickening of the upper plate and the growth rate of the orogen. This may have resulted in the present architecture that is reminiscent of young and cold orogen in Gulf of Bothnia area (BABEL 2,3&4; Korja and Heikkinen, 2005) and in the transitional orogen in the Bothnian Sea and Baltic Sea areas (BABEL 1,6,B; Korja and Heikkinen, 2005) as defined by Jamieson and Beaumont (2013). Changes in the relative velocities of the upper and lower plate may have resulted in repetitive extensional and compressional phases of the orogen (Collins, 2002) as suggested by Hermansson et al. (2008) for southern part of the Svecofennian orogen.

**3. An example from the Vaasa dome**

Svecofennian orogen can be used as a proxy to study the change from initial accretionary stage to continuous retreating subduction zone, or the change from hot to cold orogeny within a relatively limited space and time. It can also be used to study, how orogenic blocks in different orogenic evolutionary stages interact and impact each other when juxtaposed in a convergent setting.

One area, where the complex interaction of nearby areas in different tectonic phase can be studied, is Bothnian basin in the western central part of the Svecofennian orogen. The Bothnian basin is dominated by large scale granitic dome structure - Vaasa Dome – surrounded by supracrustal belts (Chopin et al, 2012). The development of the dome structure is controversial. It is located at a junction of thick and thin crust and at junction of N-NE and E-SE dipping crustal scale structures. Seismic interpretations suggest that it may also locate at a junction of an older large hot orogen in the east and a young cold orogen in the west.

On BABEL 3&4 line, the Vaasa dome is situated above an old paleo subduction and collision zone dipping to NE. Paleo back-arc extension setting is viable as tectonic setting for the dome. In this scenario an extensional setting is formed when the subduction zone is retreating southwestwards and or the subduction slab is detached. Vaasa dome is placed within the paleo accretion prism that has taken part in a young cold orogeny in Jamieson and Beaumont's (2013) classification.

On FIRE3a line, the seismic sections indicate thickening of the crust via thick skin stacking and modified by westward flow of the middle crust. Midcrustal flow towards away from the Central Finland plateau towards the orogenic hinterland in the west could be the driving force for the doming of the Vaasa dome. In this scenario the Vaasa Dome is part of a large hot orogeny in Jamieson and Beaumont's (2013) classification.

More detailed geological and geophysical studies of the Vaasa dome will give more insight into the complex interaction of crustal terranes at different evolutionary stages. More detailed descriptions and discussion of the dome can be find in MIDCRUST project presentations by Chopin et al. 2014, Nikkilä et al. 2014, Rämö et al. 2014, Kurhila et al. 2014, Kotilainen et al. 2014 (all in this volume).

## References:

Chopin, F., Korja, A., Hölttä, P., 2012. Tectonometamorphic evolution of the Bothian belt within the Svecofennian orogen - a case study for the building of a large dome in the Paleoproterozoic. Lithosphere 2012 − Seventh Symposium on the Structure, Composition, and Evolution of the Lithosphere in Finland. Programme and Extended abstracts (Edited by I. Kukkonen et al.), Espoo, Finland, 6−8 november, Institute of Seismology, University of Helsinki, Report S-56, 5-8.

Collins, W.J., 2002. Hot orogens, tectonic switching, and creation of continental crust. Geology, 30, 535- 538.

Collins, W. J., Belousova, B. A., Kemp, A. I. S. & Murphy, J. B. 2011, Two contrasting Phanerozoic orogenic systems revealed by hafnium isotope data. Nature Geosci., 4, 333–337.

Grad, M., Tiira, T. & ESC Working Group, 2009. The Moho depth map of the European Plate. Geophys. J. Int., 176, 279–292.

Hyvönen, T., Tiira, T., Korja, A., Heikkinen, P., Rautioaho, E. and SVEKALAPKO Seismic Tomography Work, 2007. A tomographic crustal velocity model of the central Fennoscandian Shield. Geophys J. Int., 168, 1210-1226.

Jamieson, R.A., and Beaumont, C., 2013. On the origin of orogens. Geol. Soc. Am. Bull., doi:10.1130/B30855.1.

Korja, A. and Heikkinen, P., 2005. The Accretionary Svecofennian Orogen-Insight from the BABEL profiles. Precam. Res., 136, 241-268.

Korja, A. and Heikkinen, P.J., 2008. Seismic images of Paleoproterozoic microplate boundaries in Fennoscandian Shield. Chapter 11. Geol. Soc. Am. Special Paper, 440, p. 229–248.

Korja, A., Kosunen, P. and Heikkinen, P.J. 2009. A Case Study of Lateral Spreading the Precambrian Svecofennian Orogen. Geol. Soc., Special Paper, 321, 225–251.

Korja, A., Lahtinen, R. and Nironen, M., 2006. The Svecofennian Orogen: a collage of microcontinents and island arcs. In: D. Gee, R. Stephenson (eds) European Lithosphere Dynamics. Geological Society, London, Memoirs, 32, 561-578.

Hermansson, T., Stephens, M.B., Corfu, F., Page, L.M. & Andersson, J., 2008. Migratory tectonic switching, western Svecofennian orogen, central Sweden: Constraints from U/Pb zircon and titanite geochronology. Precamb. Res., 161, 250–278.

Lahtinen, R., Korja, A. and Nironen, M., 2005. Paleoproterozoic tectonic evolution. In: M. Lehtinen, P.A. Nurmi & O.T. Rämö (eds.), Precambrian Geology of Finland – Key to the Evolution of the Fennoscandian Shield. Elsevier B.V., Amsterdam, 481–532.

Korja, A. and Heikkinen, P.J., 2008. Seismic images of Paleoproterozoic microplate boundaries in Fennoscandian Shield. Chapter 11. Geol. Soc. Am. Special Paper, 440, p. 229–248.

Korja, A., Lahtinen, R. and Nironen, M., 2006. The Svecofennian Orogen: a collage of microcontinents and island arcs. In: D. Gee, R. Stephenson (eds) European Lithosphere Dynamics, Geological Society, London, Memoirs, 32, 561-578.

# Crustal conductors in a complex accretionary orogen in Fennoscandia

T. Korja[1], K. Vaittinen[2], M. Abdel Zaher[3], M. Pirttijärvi[1], A. Korja[4], M. Smirnov[1] and I. Lahti[5]

[1]University of Oulu, Finland
[2]Boliden Mineral AB, SE-93681 Sweden
[3]National Research Institute of Astronomy and Geophysics, Egypt
[4]University of Helsinki, Finland
[5]Geological Survey of Finland, Rovaniemi
E-mail:toivo.korja@oulu.fi

The crustal conductivity structure of the Central Svecofennian Orogen is studied in an extended Bothnian region. 2-D inversion of magnetotelluric data revealed a set of conductors that can be associated with different types of closed basins in passive margin and arc settings. The conductors mark the boundaries of accreting units. The comparison of the models with airborne electromagnetic data and lithological maps suggests that conductors are composed of graphite- and sulphide-bearing metasedimentary rocks.

**Keywords:** electrical conductivity, magnetotellurics, airborne electromagnetics, crust, accretionary orogen, Svecofennian, black shales, Fennoscandia, Bothnian region

We have studied conductivity structures within the Svecofennian orogen, a complex accretionary orogen in the Fennoscandian Shield. The accreting units comprise a subducting plate carrying passive margin sequences and two island arc complexes with possible forearc, backarc and accretionary prism sequences. Conductors are interpreted as representing different types of closed basins (Figure 1) and thus mark the boundaries between the accreting units. We have compiled old and new data from seven BB MT-profiles transecting palaeo-basins: the Kiiminki, Bothnian, Savo, and Kainuu belts in the central part of the orogen.

The data comprise c. 240 BMT soundings (Figure 2). Older data from 1980's (Korja et al., 1986; Vaaraniemi, E., 1989; Hjelt et al., 1992; Korja and Koivukoski, 1994; Lahti et al., 2002) were inverted for the first time. The new inversions of the old and new data (Vaittinen et al., 2012a, b) revealed the sets of conductors with opposing dips. Conductors associated with the passive margin dip W/SW-wards whereas arc-affiliated conductors dip E/SE-ward. The Botnian belt represents a palaeo-accretionary prism within which a large dome structure with a granitic core (Vaasa dome) has developed. The eastern part of the dome is characterized by deep conductors dipping E and below the neighbouring tectonic unit. On the surface, the prism sequences are dipping W-wards at low angles. Sub-horizontal conductors mark the bottom of the granitic core of the dome. A comparison of the conductivity models with airborne electromagnetic data (Arkimaa et al., 2000; Pirttijärvi et al., 2014) and lithological maps suggest that deeper conductors are composed of graphite- and/or sulphide-bearing metasedimentary rocks.

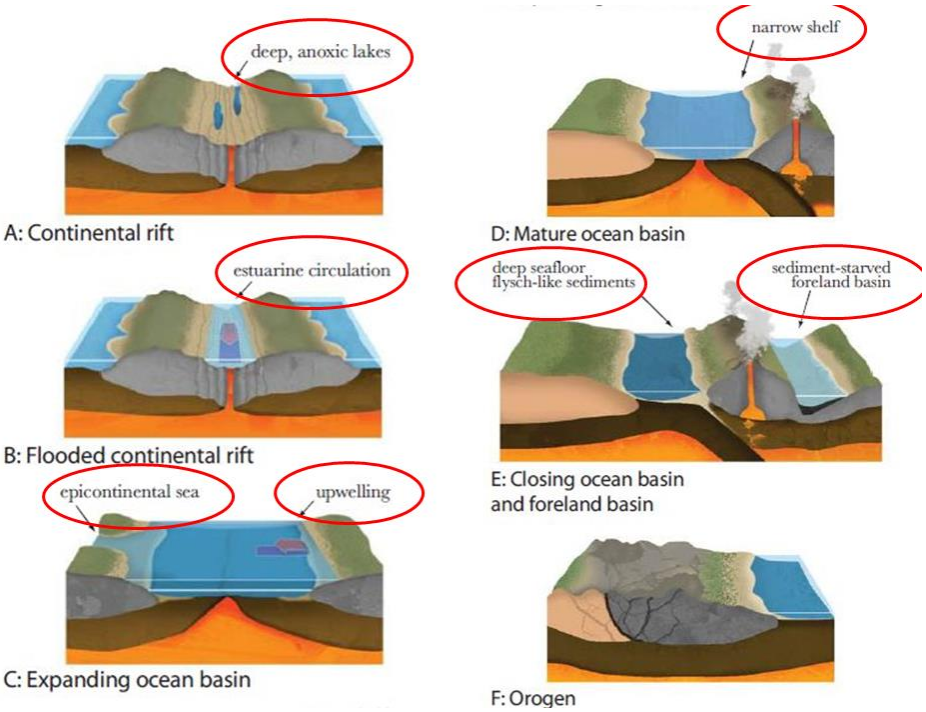


**Figure 1.** Wilson Cycle. Annotations refer to environments where black shales may accumulate. Due to various depositional environments, the conductive black schist formations can be used to delineate different stages of the orogen. Figure from Trabucho-Alexandre al, 2012.

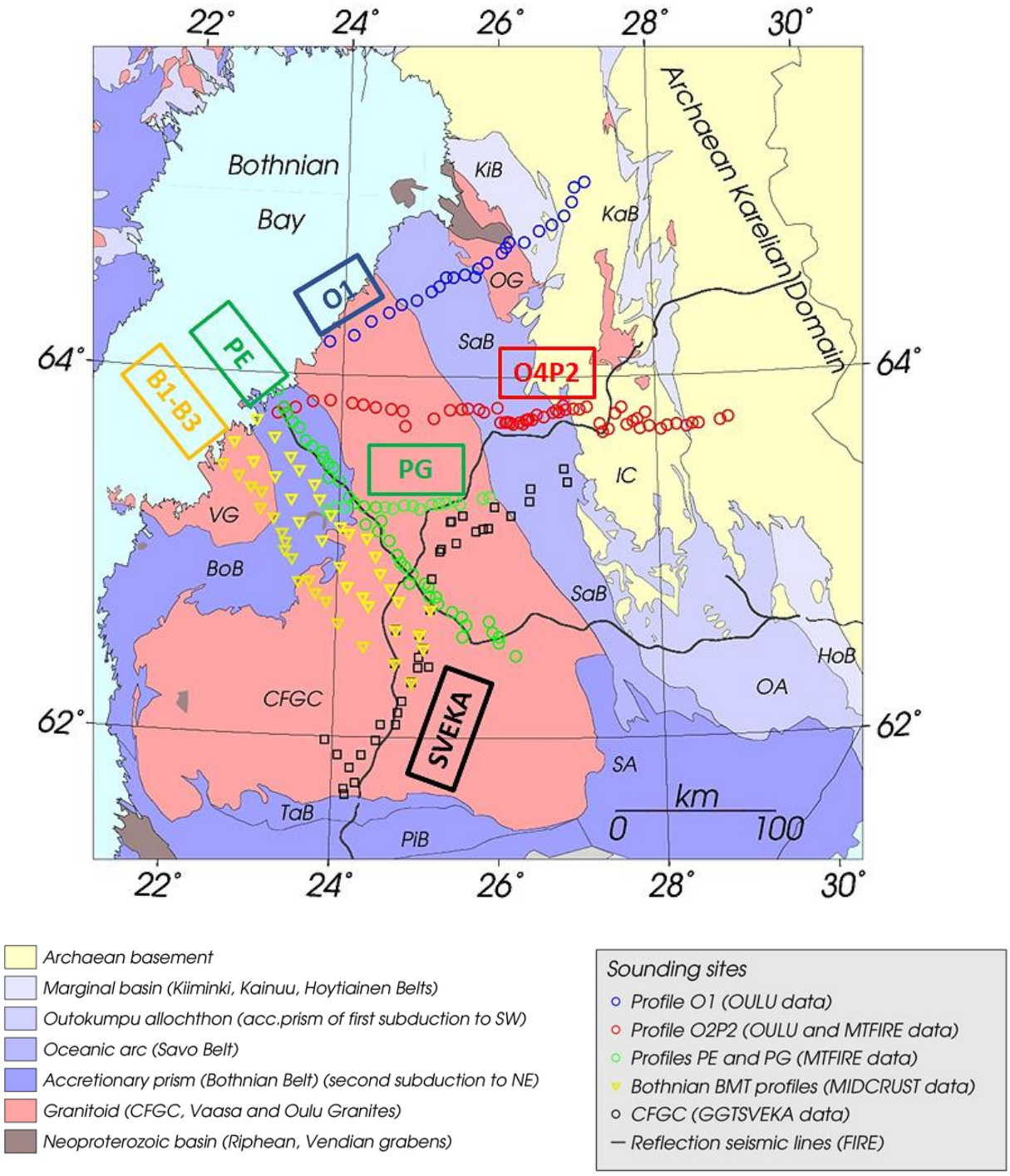


**Figure 2.** Broad-band magnetotelluric data (1/300-1000 s) in the extended Bothnian region. The lithology of the research area is modified from Koistinen et al., (2001).Magnetotelluric data from: O1 – (Korja et al., 1986); O4 – (Vaaraniemi, E., 1989; Hjelt et al., 1992; SVEKA – (Korja and Koivukoski, 1994; Lahti et al., 2002); P2, PG, PE, and B1-B3 – (Vaittinen et al., 2012a,b).

## References:

Arkimaa, H., Hyvönen, E., Lerssi, J., Loukola-Ruskeeniemi, K., and Vanne, J. 2000. Proterozoic black shale anomalies and aeromagnetic anomalies in Finland, 1:1 000 000. Geological Survey of Finland, Espoo.

Hjelt, S.-E., Korja, T. and Vaaraniemi, E. (Compilers), 1992. Magnetovariational and magnetotelluric results. Map 11, in Freeman, R. and Mueller, St. (eds.): A Continent Revealed: The European Geotraverse. Cambridge University Press. Cambridge.

Koistinen, T., Stephens, M.B., Bogatchev, V., Nordgulen, Ø., Wennerstrom, M. and Korhonen, J., 2001. Geological Map of the Fennoscandian Shield, Scale 1:2000000, Geological Survey of Finland, Espoo; Geological Survey of Norway, Trondheim; Geological Survey of Sweden, Uppsala; North-West Department of Natural Resources of Russia, Moscow.

Korja, T., Zhang, P., and Pajunpää , K., 1986. Magnetovariational and magnetotelluric studies of the Oulu-anomaly on the Baltic Shield Finland. Journal of Geophysics, 59, 32-41.

Korja, T. and Koivukoski, K., 1994. Magnetotelluric investigations along the SVEKA profile in central Fennoscandian Shield, Finland. Geophys. J. Int., 116, 173-197.

Lahti, I., Korja, T., Pedersen, L.B., and BEAR Working Group, 2002. Lithospheric Conductivity along GGT/SVEKA Transect: Implications from the 2-D Inversion of Magnetotelluric Data. In: Lithosphere 2002. Programme and extend abstracts. Lahtinen, R., Korja, A., Arhe, K., Eklund, O., Hjelt, S.-E. and Pesonen, L.J. (eds). Institute of Seismology, University of Helsinki, Helsinki, Finland, Report S-42, 75-78.

Pirttijärvi, M., Abdel Zaher, M. and Korja, T. 2014. Combined inversion of airborne electromagnetic and static magnetic field data. Submitted to Geophysica.

Trabucho-Alexandre, J., Hay, W.W., and de Boer, P.L., 2012. Phanerozoic environments of black shale deposition and the Wilson Cycle. Solid Earth, 3, 29-42.

Vaaraniemi, E., 1989. Electromagnetic studies of the lithosphere on the Northern Segment of the EGT (in Finnish), M.Sc. Thesis, Department of Geophysics, University of Oulu.

Vaittinen, K., Korja, T., Kaikkonen, P., Lahti. I. and Smirnov, M. Yu., 2012a. High-resolution magnetotelluric studies of the Archaean-Proterozoic border zone in the Fennoscandian Shield, Finland. Geophys. J. Int., 188, 908-924.

Vaittinen, K., Korja, T., Abdel Zaher, M., Pirttijärvi, M., Smirnov, M., Lahti, I and Kaikkonen, P., 2012b. Vintage and retro conductivity models of the Bothnian Bay region: implications for the crustal structure and processes of the Svecofennian orogen. In: Kukkonen, I., Kosonen, E., Oinonen, K., Eklund, O., Korja, A., Korja, T., Lahtinen, R., Lunkka Juha Pekka and Poutanen, M. (Eds.), 2012. Lithosphere 2017 – Seventh Symposium on the Structure, Composition and Evolution of the Lithosphere in Finland. Programme and Extended Abstracts, Helsinki, Finland, November 6-8, 2012. Institute of Seismology, University of Helsinki, Report S-56, 105-108

# Mantle heat flow in the Fennoscandian Shield

I.T. Kukkonen[1]
[1]Department of Physics, University of Helsinki, P.O.B 64, FI-00014 University of Helsinki
E-mail: ilmo.kukkonen@heslinki.fi

Mantle heat flow in the Fennoscandian shield was determined earlier using thermal models calibrated with pressure and temperature (pT) data on mantle-xenoliths in the Kuopio-Kaavi kimberlite province, eastern Finland. In the present work, I discuss representativeness of the point-like observation with isostatic lithosphere models. Mantle density is temperature dependent by heat expansion. If the mantle heat flow varied in the study area at large it would create variations in the elevation of the lithosphere. The results suggest that the mantle heat flow is probably stable in a wide area in the Fennoscandian Shield in Finland and in the sediment covered platform in NE Russia and Estonia.

**Keywords:** geotherm, mantle heat flow, lithosphere, upper mantle, Fennoscandian Shield

## 1. Introduction

Mantle heat flow is an important parameter applied in thermal modelling of the lithosphere. It strongly affects the lithosphere thickness and temperature estimates of the upper mantle. Mantle heat flow is usually derived from the thermal models themselves by removing the effect of crustal heat sources from the measured surface heat flow value. Due to uncertainties in crustal heat production and thermal conductivity, the calculated geotherm is sensitive for biases in the parameter values input to the model. These complications may result in circumferential results.

On the other hand, independent data is obtained from mantle xenolith data which provide direct evidence of the temperature gradient in the mantle. Applying information on mantle thermal conductivity the value of the mantle heat flow density is obtained. Mantle-derived kimberlite-hosted xenoliths were applied earlier for geotherm determination in the central part of the Fennoscandian Shield in the Kuopio-Kaavi kimberlite province (Kukkonen and Peltonen, 1999; Kukkonen et al., 2003). The obtained mantle heat flow value is low, 12 $mWm^{-2}$, and it has been uncertain how far from the kimberlite province the result actually is applicable. In this work I study the problem with simple isostatic calculations on topography expected to arise from varying the mantle heat flow value.

## 2. Xenolith derived geotherm and mantle heat flow

The lithospheric geotherm calibrated with pT data on mantle xenoliths is shown in Figure 1a. Thermal conductivity of the mantle was estimated with a geometrical mean of the conductivities of the rock-constituting minerals and their modal composition. In the thermal model conductivity was assumed to be temperature dependent and to consist of both phonon conduction and radiative heat transfer (for details see Kukkonen and Peltonen, 1999). The obtained values for the temperature gradient and mantle heat flow density were 4 K/km and 12 $mWm^{-2}$, respectively.

## 3. Modeling and results

Two variants of mantle heat flow density were applied in the modelling (Figure 1b), first the value obtained from the xenolith studies (12 $mWm^{-2}$) and second, a value two times as big (24 $mWm^{-2}$). The high value represents results obtained in typical thermal modelling of shield areas.

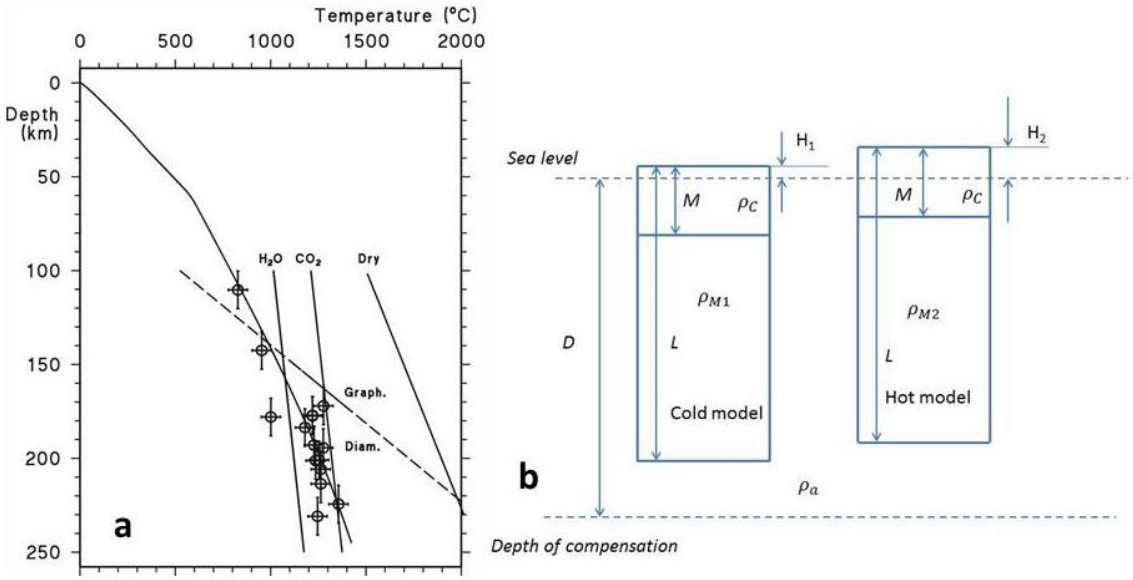


**Figure 1.** a) Lithospheric geotherm for the Kuopio-Kaavi kimberlite province, central Fennoscandian Shield, derived with a 2D conductive model calibrated with pT-data on mantle xenoliths (Kukkonen et al., 2003), b) Isostatic 1D models of lithosphere with the mantle density being temperature dependent via thermal expansion of rock. In the case of a low mantle heat flow and temperature gradient (Cold model) the elevation of the lithosphere is smaller than in the case of high mantle heat flow (Hot model).

The lithosphere thickness was taken as 250 km and the crust as 50 km. Due to the applied contrast in mantle temperature gradient, the average density of the mantle in the cold model has a density of 3332 kg $m^{-3}$ and 3311 kg $m^{-3}$ in the hot model, respectively. Assuming the lithosphere is in isostatic equilibrium a difference in elevation of 1.3 km results due to heat expansion. However, the elevation and bathymetry data of Fennoscandia do not indicate such a variation in a wide area surrounding the kimberlite province. A relatively flat area extends about 1000 km in N-S direction and 500 km in E-W direction. The conclusion is that the low mantle heat flow value determined with mantle xenolith data is very probably representative in an extensive area in the central and eastern part of the Shield and the sediment-covered platform.

## 4. References

Kukkonen, I.T. and Peltonen, P., 1999. Xenolith-controlled geotherm for the central Fennoscandian Shield: implications for lithosphere-asthenosphere relations. Tectonophysics, 304, 301-315.

Kukkonen, I.T., Kinnunen, K. and Peltonen, P., 2003. Mantle xenoliths and thick lithosphere in the Fennoscandian Shield. Phys. Chem. Earth, 28, 349-360.

# Shear tectonic features of the Archaean Portti soapstone formation

S. Leinonen

Geologian tutkimuskeskus, Neulaniementie 5, 70211 KUOPIO
E-mail: seppo.leinonen@gtk.fi

Soapstone is a low metamorphic, carbonated ultramafic rock containing talc, magnesite, dolomite, chlorite and iron oxides, also in places serpentine and amphibole; however in a broader sense of the use including also non-carbonated talcose compositions. Soapstone has usually fine to medium grained and massive nature, also found as easily cleavable schistose structures. This study considers structural features of the Portti soapstone and how the schistosity is formed during ductile shearing and how observed textures are able to be considered as kinematic indicators.

**Keywords:** Ultramafic, Soapstone, Metamorphism, Structural geology, Shear tectonics

## 1. Geology of the Portti area soapstone

The Portti soapstones occur in the Archaean Suomussalmi greenstone belt south from Saarikylä, near Portinvaara. Portti area consist seven separate north-south trending soapstone bodies (Figure 1). Formations represent more probably different parts of one komatiite flow sheet than separate magmatic events. Portti occurrence has highest magnesium content, 32.55 wt-% MgO, Sivuportti highest calcium, 4.26 wt-% CaO and aluminium, 3.18 wt-% $Al_2O_3$ content. All the formations are entirely altered to soapstone, serpentinite found only in the western side of Sivuportti and middle of Hoikkalampi occurrences. Soapstones after komatiitic lavas belong to Saarikylä Formation, which contains also komatiitic basalts, Cr basalts and local felsic volcanoclastic units Papunen et al. (2009). Supracrustal rocks of the Tipasjärvi, via Kuhmo to Suomussalmi continuing greenstone belt are 2.84–2.79 Ga oceanic plateau type komatiitic and tholeiitic basalts, sediments, banded iron formations and felsic arc type volcanoclastics Hölttä et al. (2008). Pressure temperature conditions have been at highest 6-7 kbar and 660 °C, degreasing to 500 °C in the inner parts of greenstone belt synclinorium. There have been three main metamorphic events, two Archaean in amphibolite facies and one Proterozoic in greenschist facies conditions Tuisku (1988).

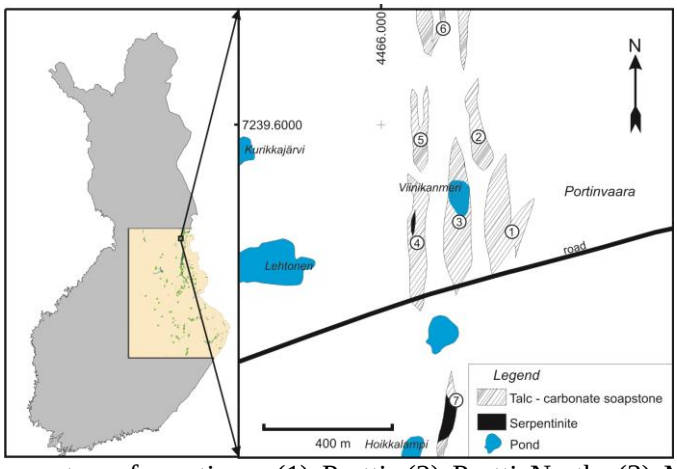


**Figure 1.** Portti area soapstone formations: (1) Portti, (2) Portti North, (3) Middle Portti, (4) Side Portti, (5) Side Portti North, (6) Haaposenmeri and (7) Hoikkalampi.

## 2. Soapstone

The Portti formation comprises compositional variation of talc-magnesite-dolomite-chlorite soapstone types. Talc-magnesite type contains in average talc 50 wt-%, magnesite 35 wt-% and chlorite 8 wt-%. Dolomite content is 0.8 wt-%. Talc-dolomite soapstone shows some higher talc 55 wt-% and chlorite 14 wt-% than that of talc-magnesite. Dolomite content is relatively low 28 wt-%, magnesite found only in some percentages. Bulk rock chemistry of talc-magnesite sequences has 37.0 $SiO_2$, 33.8 MgO and 0.6 CaO as weight-%. The iron content 8.3 wt-% $Fe_2O_3$ is mostly included in the oxide phase, i.e. magnetite, also in carbonates of the lower oxidation state. Talc-dolomite types are higher in silica 46.0 wt-% $SiO_2$, calcium 6.0 wt-% CaO and iron 9.1 wt-% $Fe_2O_3$ compared to talc-magnesite; also aluminium 3.4 wt-% $Al_2O_3$ and titanium 0.2 wt-% $TiO_2$ shows some higher values. Magnesium content is relatively low, in average 26.9 wt-% MgO.

## 3. Metamorphism

Soapstone, here a talc-carbonate composition appears trough a fluid-rock reaction at the expense of serpentine (1). The paragenesis is formed as well in prograde or retrograde regional metamorphic events at low to high pressure levels (P=10 kbar). Serpentine marks the lowest temperature of the talc-carbonate (T=200 °C) and orthopyroxene the highest (T=570 °C), i.e. the talc out reaction (2).

According thermodynamic modelling, the temperature limit of the serpentine to talc-magnesite reaction is directed by the mole fraction of carbon dioxide ($XCO_2$) in pore fluids. Talc-carbonate is stable with high carbon dioxide fractions (0.024-0.023) along regional metamorphic kyanite geotherm from low greenschist up to high grades of middle amphibolite facies conditions (T=550 °C, P=5 kbar), but in presence of low-$CO_2$ fluids (0.02) only at relatively low, below 2.5 kbar pressures and not until in high-grade temperatures (T=520 °C) Leinonen (2013). At these low-pressure, high-temperature levels olivine reacts readily to talc-magnesite below temperatures T=520 °C (3) and tremolite to dolomite already at below 1 kbar and that higher temperatures T=600 °C (4). At low-temperatures tremolite reacts with serpentine and carbon dioxide to the talc-dolomite soapstone (5). A very high carbon dioxide fluid ($XCO_2 \geq 0.023$) is not stable with talc giving growth to the quartz by the reaction (6).

(1) 2 serpentine + 3 $CO_2$ ↔ 3 magnesite + talc + 3 $H_2O$
(2) talc +magnesite ↔ 2 enstatite + $CO_2$ + $H_2O$
(3) 4 forsterite + $H_2O$ + 5 $CO_2$ ↔ talc + 5 magnesite
(4) 5 tremolite + 12 forsterite + 20 $CO_2$ + 8 $H_2O$ ↔ 13 talc + 10 dolomite
(5) tremolite + 4 serpentine +8 $CO_2$ ↔ 3 talc + 4 dolomite+4 $H_2O$
(6) talc + $CO_2$ ↔ 3 magnesite + 4 quartz + $H_2O$

Soapstone alteration of the Portti formation proceeded after serpentine to talc-carbonate reaction, in the beginning by re-crystallization of carbonate tails and growth of pressure shadow talc, followed lastly by decarbonation and the formation of schistose chlorite. Shear tectonic deformation is localized near contacts and to cross-cutting structures.

## 4. Shear tectonic features

The foliation of the Portti soapstones has developed by multi-stage metamorphic deformation processes during and after talc-carbonate alteration. The foliation initially appeared by orientated growth of talc to the lowest pressure direction of the stress field and finally structures were sheared parallel to north-south trending Saarikylä strike-slip fault. Textures of

the local shear tectonics are seen like anastomosing foliation, asymmetric carbonate porphyroclasts and pressure shadow talc (Figure 2).

Outcrop scale structures show well developed shear banding and the latest deformation phases occurred above a ductile brittle transition zone, during which chlorite filled the main schistosity crosscutting slip cleavage joints. The chlorite growth occurred partly contemporaneously with the late re-crystallization of talc and that after. Shear tectonic deformation caused mainly through going schistosity to previous unoriented soapstone, locally also talc-carbonate alteration of serpentinite sequences.

Shear deformation stages most likely express retrograde conditions, however at first occurred in P-T conditions of talc-carbonate stability, overprinting and further modifying previous soapstone textures. Late stages shows decarbonation events of hydrous fluids, like formation of talc-chlorite schistosity and in the latest event formation of all the former foliations and carbonate porphyroclasts crosscutting chlorite slip cleavage.

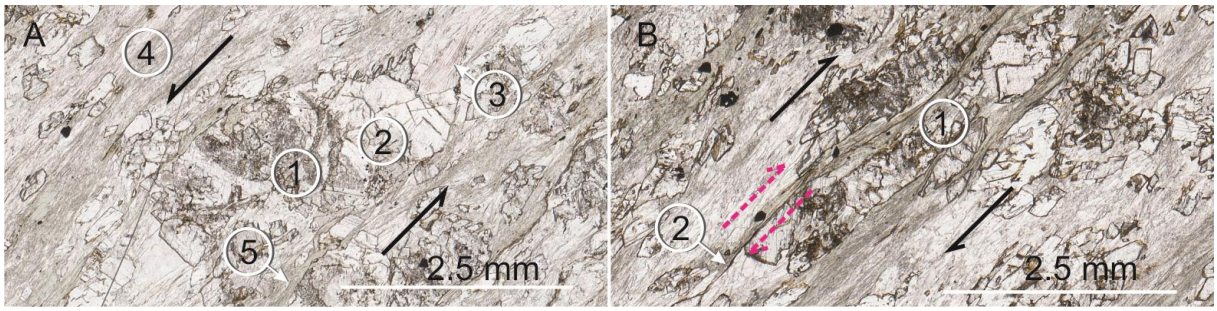


**Figure 2.** A shear textures pointing scanned thin section of soapstone, sample 4513-P20-6.20, Porttivaara, Suomussalmi, plain polarized light. A) In order of forming: an asymmetric dust fine Fe-oxide filled magnesite porphyroclast (1), pressure shadow tails of transparent looking Fe-bearing magnesite (2) and the subsequent growth of flaky talc (3). The fine grained foliation composes talc and chlorite (4), places only chlorite (5). The shape of the tailed carbonate porphyroclast indicates sinistral sense of shear. B) A chlorite walled boudinage sector and broken carbonate crystals indicates the extensional deformation (1). A micro-scale cross-cutting dextral fault through a carbonate crystal displays at least 1 mm offset (2).

## 5. Deformation events

All the lithological contacts of adjacent country rocks, schistosity and felsic veins trends parallel to main shear zone N-S (360), overprinting weak $D_{n+2}$ foliation NE (20) and that later crenulation cleavage $D_{n+3}$ NNE (40-50). The $D_{n+1}$ structures appear in soapstone as a slight schistosity and a talc-carbonate striping N (05), which trends nearly to the same direction than the lithological contacts and relict schistosity of country rocks. This basic soapstone orientation is overprinted by through going NNE (20) $D_{n+2}$ cleavage, appearing with the former cleavage as an oblique polygonal jointing. Carbonate-talc veining and cleavage planes of the $D_{n+3}$ deformation strikes also north as the main shear structures (360) and cuts at the same all the former $D_{n+1}$ and $D_{n+2}$ foliations (Figure 3). Carbonate veins indicate, that at least in the beginning of $D_{n+3}$ event the fluid contained carbon dioxide and tension fractures originated in local extension stress field. During late stages of strike-slip deformation metamorphic fluid turned to hydrogen rich. This is seen as chlorite walled carbonate veins and chlorite filled slip surfaces. Shear along these N-S trending structures caused NE (40) $D_{n+3}$ shear banding of former foliation, also to the carbonate veins. The most foliated and chloritized soapstones are localized to contact zones. Latest $D_{n+4}$ deformation features are occasional riedel joints, north passing R (05) and north-west R´ (330).

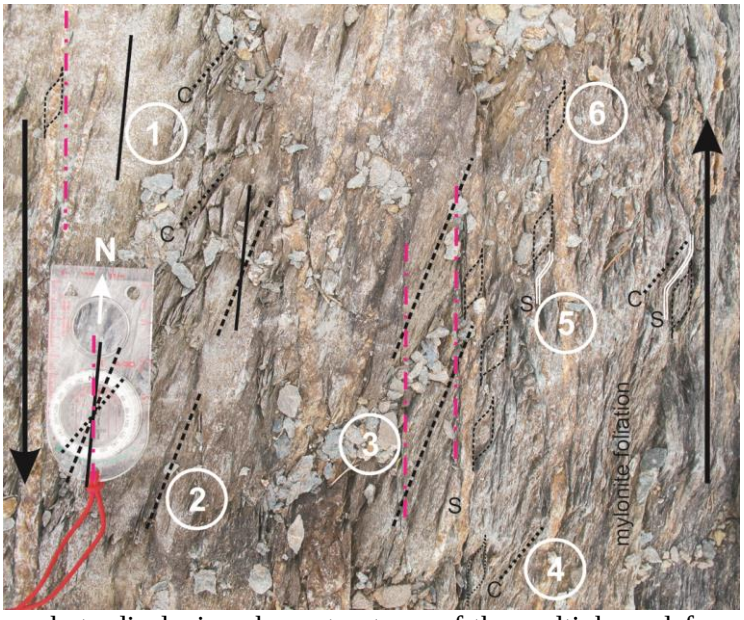


**Figure 3.** An outcrop photo displaying shear structures of the multiphase deformed Portti soapstone, Suomussalmi. A slight north-striking (05) $D_{n+1}$ first order foliation (1 / solid lines) is seen in less deformed parts with the $D_{n+2}$ foliation (2 / dashed lines). N-S trending mylonitic $D_{n+3}$ foliation is also found along chlorite walled carbonate veins (3 / dash-dot lines). $D_{n+3}$ event caused locally SC-structures: the NNE striking shear banding (C) (4 / dot lines), the rotated foliation (S) (5 / double lines) and the fish like boudins (6 / dashed lines) into the most sheared sectors of the formation. All the foliations are west-dipping (at 85°).

## 6. Conclusions

Soapstone is a talc-carbonate metamorphic ultramafic rock; fine to medium grained and has massive and schistose structures. The Portti formation, like many other soapstone occurrences in the study area are weakly or intensively foliated. Schistosity has shear tectonic features and indications of a sinistral sense of movement. The growth of a pressure shadow carbonate and a subsequent talc tails around magnesite porphyroclasts evolved at first the retrogressive metamorphism from peak of low amphibolite facies to greenschist facies conditions. Sheared structures got the maturity after decarbonation and the contemporaneous chlorite growth. Trough going $D_{n+1}$ and $D_{n+2}$ foliation trends N and NNS direction. Chlorite filled $D_{n+3}$ shear planes run parallel to north-striking main shear. $D_{n+3}$ deformation is also seen as weak NE-SW shear banding. The best kinematic indicators appeared to be a shear banding, asymmetric porphyroclasts and boudins, also observations of the sense of movement along fault planes.

## References:

Hölttä, P., Balagansky, V., Garde A., A., Mertanen, S., Peltonen, P., Slabunov, A., Sorjonen-Ward, P. and Whitehouse, M. 2008. Archean of Greenland and Fennoscandia. Episodes, 31, no. 1.

Leinonen, S. 2013. Exploration for Soapstone Occurrences: Use of Bulk Chemical Analyses to Select Potential Formation Areas. In: Luis Guerra Rosa, Zenaide Carvalho G. Silva and Luis Lopes (Eds), Global Stone Congress. Key Engineering Materials, 548, 10-19.

Papunen, H., Halkoaho, T. and Luukkonen, E. 2009. Archaean evolution of the Tipasjärvi-Kuhmo-Suomussalmi Greenstone Complex, Finland. Geological Survey of Finland, Bulletin, 403, 68 p.

Tuisku, P. 1988. Geothermobarometry in the Archean Kuhmo-Suomussalmi greenstone belt, eastern Finland. In: Marttila, E. (ed.) 1988. Archaean geology of the Fennoscandian Shield: Proceedings of a Finnish-Soviet symposium in Finland on July 28-August 7, 1986. Geological Survey of Finland, Special Paper, 4, 171-172.

# New geothermal data from the Fyllingsdalen, Ullrigg and Årvollskogen boreholes, located in southern Norway

Yuriy P. Maystrenko, Odleiv Olesen and Harald K. Elvebakk

Geological Survey of Norway (NGU), Trondheim, Norway

E-mail: yuriy.maystrenko@ngu.no

Knowledge about the temperature distribution within the upper crystalline crust is an important issue in the geosciences. The changes in temperature control the major properties of crystalline rocks, sediments and fluids as a result of increasing temperature with depth. We have made an attempt to understand the major characteristics of the subsurface temperature distribution in southern Norway.

**Keywords:** lithosphere, crust, heat flow, thermal modelling, groundwater flow, Norway

## 1. Introduction

New geothermal data have recently been obtained for three boreholes, Fyllingsdalen, Ullrigg and Årvollskogen, which are located in southern Norway near Bergen, Stavanger and Moss, respectively (Figure 1).

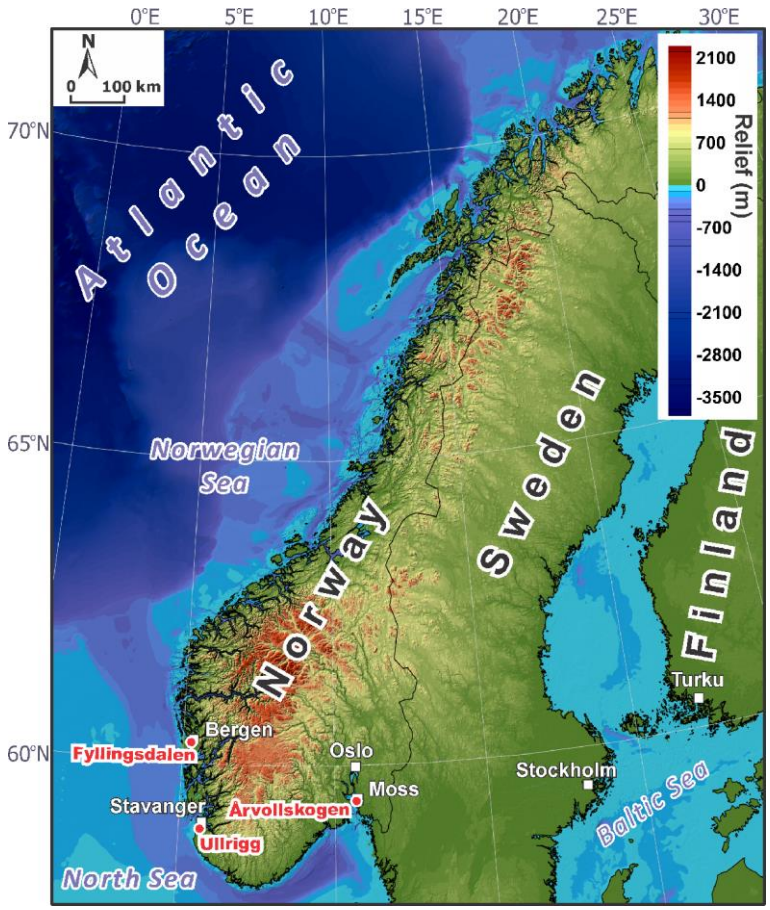


**Figure 1.** Location of the investigated boreholes (topography and bathymetry are from Norwegian Mapping Authority).

Thermal well logging (Figure 2) has been performed in Ullrigg, Fyllingsdalen and Årvollskogen boreholes during 2011-2013.

Based on 2D gravity and magnetic modelling, the lithosphere-scale 2D structural models have been constructed for the Bergen, Stavanger and Moss areas. These data-based 2D models were used during the 2D thermal modelling to understand the thermal regime within the crystalline crust of the study areas. The 2D structural models have been used as a realistic approximation of the geometries of the underlying crystalline crust and lithospheric mantle during the 2D thermal modelling.

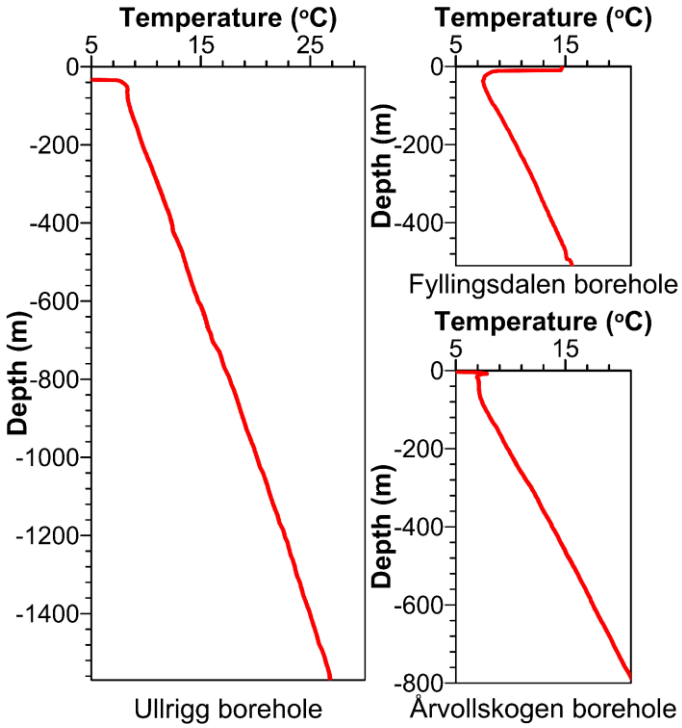


**Figure 2.** The measured temperatures in the Ullrigg, Fyllingsdalen and Årvollskogen boreholes (modified after Maystrenko et al., under review[b]).

## 2. Data and methods

All available shallow and deep data have been used to construct these 2D structural models which, therefore, represent a current state of our knowledge of the bedrock structure beneath these three study areas. Construction of the 2D models has been done by use of recently published/released structural data. For the upper part of the models, the surface geology and borehole data have been used (Ragnhildstveit and Helliksen, 1997; Jorde et al., 1995; Lutro and Nordgulen, 2008). The lithosphere-asthenosphere boundary has been determined from previously published data (Artemieva et al., 2006; Gradmann et al., 2013; Maystrenko et al., 2013). Configuration of the crystalline crust and the Moho topography have been derived from the published interpretations of deep seismic lines (Stratford et al., 2009) and validated by a 2D density and magnetic modelling.

2D gravity and magnetic modelling have been carried out by use of the commercial software package GEOSOFT Oasis montaj. During 2D density and magnetic modelling, the GM-SYS Profile Modelling module was used to model the geological structure along four 2D profiles by changing the geometries, densities and magnetic properties of the layers to obtain

a fit between the observed potential fields and the modelled gravity and magnetic responses of the 2D models.

The 2D thermal modelling has been performed by use of the commercial software package COMSOL Multiphysics. For the upper boundary, the time-dependent temperature at the Earth's surface and sea bottom has been applied. This has been done by taking into account palaeoclimatic changes during the last 200,000 years. The lithosphere-asthenosphere boundary has been chosen as a lower thermal boundary which corresponds to the 1300 °C isotherm. More detailed information about the methodology can be found in Maystrenko et al., under review[a, b].

## 3. Results and conclusions

According to the results of the 2D thermal modelling, a significant decrease of the Earth's surface temperatures during the two last Weichselian and Saalian glaciations still affects the subsurface thermal field of the study areas in terms of the reduced temperatures within the uppermost part of the crystalline crust. Tentative palaeoclimatic corrections of the heat flow for the investigated boreholes vary from 21-23 to 26-28 mW/m². The calculated palaeoclimatic corrections are generally in agreement with those based on the regional-scale estimates for this part of Scandinavia (Majorowicz and Wybraniec, 2010). Furthermore, the advective cooling due to groundwater flow is an additional factor for the reduction of temperatures within the Bergen and Stavanger areas where the normal annual precipitation is one of the highest in Europe, reaching locally more than 4000 mm/year (NMI, 2013). On the other hand, the influence of the groundwater flow on subsurface temperatures is most likely relatively low within the Moss area.

According to the results of 2D thermal modelling, the modelled temperatures are higher in the Fyllingsdalen and Årvollskogen boreholes compared to the Ullrigg borehole. This difference is in agreement with the low measured thermal gradient in the Ullrigg borehole which is less than 13.0 °C/km compared to 16.5 °C/km in the case of the Fyllingsdalen borehole and 19.3 °C/km in the Årvollskogen borehole. The difference in radiogenic heat production of the crystalline crust is one of the main reasons for the higher measured and modelled temperatures within the Bergen and Moss areas in comparison to the Stavanger area. This resulted in a higher heat flux in the Fyllingsdalen and the Årvollskogen boreholes in comparison with the Ullrigg borehole. The results of 2D thermal modelling demonstrate that potential for the geothermal energy is higher within the Bergen and Moss areas compared to the Stavanger region.

## Acknowledgements

The authors would like to acknowledge the appreciated support from BayernGas, BKK, ConocoPhillips, Det norske, Eni, E.ON, GdF Suez, Lundin, Maersk, NGU, Noreco, NPD, Repsol, RWE-Dea, Statoil, Total, VNG and Wintershall which helped us to investigate the Ullrigg and Fyllingsdalen boreholes in the framework of "Crustal Onshore-Offshore Project (COOP)". We would also like to acknowledge the support from Statkraft Varme AS which helped us to investigate the Årvollskogen borehole in the framework of the project "Evaluation of the deep geothermal potential in Moss area, Østfold county".

## References:

Artemieva, I.M., Thybo, H., and Kaban, M.K., 2006. Deep Europe today: geophysical synthesis of the upper mantle structure and lithospheric processes over 3.5 Ga. In: Gee D.G., Stephenson, R.A. (Eds.), European Lithosphere Dynamics, Geol. Soc, London, Mem. 32, The Geological Society Publishing House, Bath, pp. 11-41.

Gradmann, S., Ebbing, J., and Fullea, J., 2013. Integrated Geophysical Modeling of Boundary Zone in Lithospheric Mantle under Norway and Sweden, Geophysical Journal International, 194, 1358-1373.

Jorde, K., Sigmond, E.M.O., and Thorsnes, T., 1995. Geologisk kart over Norge, berggrunnskart Stavanger. Norges geologiske undersøkelse, Trondheim, Norway, scale 1: 250 000, 1 sheet.

Lutro, O., and Nordgulen, Ø., 2008. Oslofeltet, berggrunnskart Oslo. Norges geologiske undersøkelse, Trondheim, Norway, scale 1: 250 000, 1 sheet.

Majorowicz, J., and Wybraniec, S., 2010. New terrestrial heat flow map of Europe after regional paleoclimatic correction application. International Journal of Earth Sciences, doi: 10.1007/s00531-010-0526-1.

Maystrenko, Y., Olesen, O., and Ebbing, J., 2013. Deep structure of the northern North Sea and adjacent areas according to regional-scale 3D density and thermal modeling: EGU General Assembly, Geophysical Research Abstracts, 15, EGU2013-2159.

Maystrenko, Y.P., Elevbakk, K.H., Ganerød, G.V., Lutro, O., Olesen, O., and Rønning, J.S, under review[a]. 2D structural and thermal models in south-eastern Norway based on the recently drilled Årvollskogen borehole and 2D density, magnetic and thermal modelling. Geothermal Energy.

Maystrenko, Y.P., Slagstad, T., Elevbakk, K.H., Ganerød, G.V., Olesen, O., and Rønning, J.S, under review[b]. New heat flow data from three boreholes near Bergen, Stavanger and Moss, southern Norway. Geothermics.

NMI, 2013. Kart med nedbørnormal for Norge. Gjelder for normalperioden 1961-1990. http://met.no/Klima/Klimastatistikk/Klimanormaler/Nedbor/.

Ragnhildstveit, J., and Helliksen, D., 1997. Geologisk kart over Norge, berggrunnskart Bergen. Norges geologiske undersøkelse, Trondheim, Norway, scale 1: 250 000, 1 sheet.

Stratford, W., Thybo, H., Faleide, J.I., Olesen, O., and Tryggvason, A., 2009. New Moho Map for onshore southern Norway. Geophysical Journal International, 178, 1755-1765.

# Neoarchaean alkali enriched gabbros and diorites of the Karelian Province as part of the diversification of the plutonic activity

P. Mikkola[1], E. Heilimo[1], T. Halkoaho[1] and A. Käpyaho[2]

[1]Geological Survey of Finland, P.O. Box 1237, 70211 Kuopio, Finland
[2]Geological Survey of Finland, P.O. Box 96, 02151 Espoo, Finland
E-mail: perttu.mikkola@gtk.fi

Neoarchaean alkali rich gabbros and diorites from the western Karelia Province of the Fennoscandian Shield are characterized by variably elevated REE, $K_2O$, Ba and Sr. Compositional data, zircon O-isotope values and Sm-Nd data imply a magma source that was heterogeneous due to subduction related metasomatism. The alkali enriched gabbros and diorites are an additional piece in the puzzle formed by compositionally diverse magmatism derived from heterogeneously enriched mantle during the Neoarchaean period in the Karelia craton of Fennoscandian and associated with the cratonization of the area.

**Keywords:** Neoarchaen, Plutonism, Karelia province, Geochemistry

## 1. Geological setting

We have studied Neoarchaean gabbro and diorite intrusions and two dykes displaying variable enrichment in alkalis and REE from the Lentua Complex, which is part of the Western Karelia subprovince (Fig. 1). The Lentua Complex is a typical Archaean crustal block dominated by 2.83−2.78 Ga tonalite-trondjhemite-granodiorites (TTGs) hosting variably sized greenstone belt slivers of similar age. The Neoarchaean marks a significant diversification of magma compositions in the Western Karelian subprovince (as well as globally). Sanukitoids of the Karelia province form two distinct zones, the 2.74 Ga intrusions of the Central Karelia subprovince and 2.72 Ga intrusions of the Western Karelia subprovince (Heilimo et al., 2011; Fig. 1). Third, less voluminous, 2.69 Ga sanukitoid event, is known only from central parts of the Lentua complex (Mikkola et al., 2014). Quartz diorites, which cannot be included in to the sanukitoid suite due to their lower Mg#, LILE and REE enrichment and they are also mainly slightly younger (ca. 2.7 Ga). However temporal overlap with the main sanukitoid zones exists and both suites have been interpreted to represent melts from variably metasomatized mantle (Heilimo et al., 2011; Mikkola et al., 2011). The 2.74–2.66 Ga quartz syenite suite is volumetrically the smallest and temporally the most scattered of the Neoarchaean mantle derived suites of the Lentua complex (Heilimo et al., 2014). Subprovince wide migmatization and intrusion of anatectic leucogranitoids at 2.7 Ga are all associated with the collisional assembly of the Archaean craton (Käpyaho et al. 2006; Mikkola et al., 2011).

## 2. Field geology and petrography

The separate intrusions are ellipsoidal in shape and the lengths are less than 1000 m and they form positive anomalies on the aerogeophysical maps. The intrusions consist of medium-grained (2-5 mm) dark-greyish to dark-greenish gabbros and diorites. Small pegmatitic patches (<50 cm across) were observed in Änäkäinen. Some of the samples display distinct orientation, whereas others are unoriented. Main minerals (>5 %) are plagioclase ± amphibole ± biotite ± pyroxene ± quartz with variation both within an individual intrusion as well as between the intrusions. Apatite is abundant enough to account as main mineral in some of the samples from Änäkäinen, in other samples it is present as an accessory phase. Variably abundant magnetite explains the positive anomalies on aeromagnetic maps. Both of the dyke samples are ultramafic and consist of hornblende and biotite.

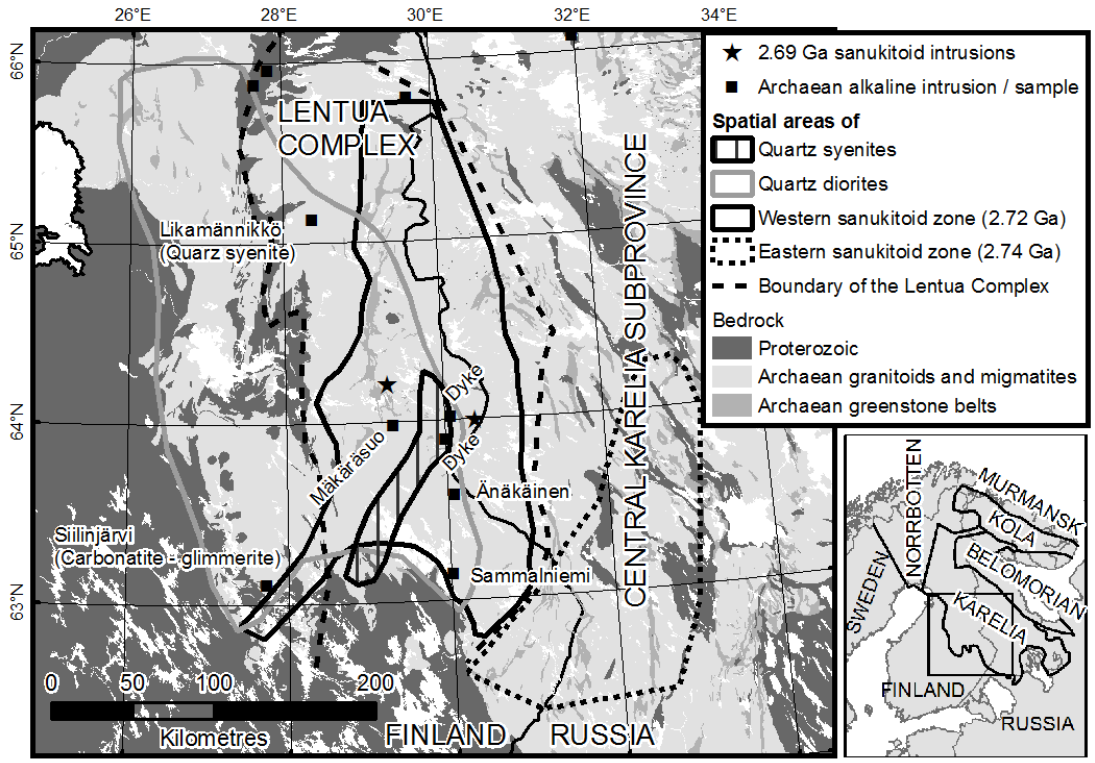


**Figure 1.** Location of the studied intrusions and dykes on geological map. Also shown are the areal extents of the other Neoarchaean mantle derived plutonic suites. In inset the Archaean provinces of the Fennoscandian Shield.

### 3. Whole-rock geochemistry and isotope data

Compositionally the samples form a hetereogeneous group, the common nominators being the varying degree of enrichement in alkalis. They vary from ultrabasic to intermediate ($SiO_2$=37.6–61.6 wt. %) and from ultrapotassic to calc-alkaline, majority being shoshonitic ($K_2O$=0.2–10.6 wt. %, $Na_2O$=0.5–6.3 wt. %; Fig. 2). In respect to $SiO_2$, the MgO, Ni and Cr concentrations and especially the Mg# of the samples are relatively low (Fig. 2). Samples from Änäkäinen display two separate trends in respect to e.g. MgO, $P_2O_5$ and $K_2O$ suggesting the involvement of more than one magma pulse. Most of the samples display high but variable concentrations of Ba (237–1905 ppm), Sr (147–1623 pm), Zr (56–514 ppm) and (1.5–45.6 ppm) All samples display varying enrichment in LREE ($La_N$=55−575 and an outlier 1910; Fig. 2) and moderate LREE/HREE fractionation ($(La/Yb)_N$=4−80).

Crystallization age of the Änäkäinen has been defined as 2711±2 Ma by Huhma et al. (2012a). Whole-rock Sm-Nd analyses done on three samples (Huhma et al., 2012b; unpublished data) indicate involvement of older material in the genesis of the gabbros as initial $\varepsilon_{Nd}$ values vary between +0.7 and -1.2 and respective depleted mantle model ages from 2876 to 3063 Ma. These values are in the same range as those reported for the surrounding TTG granitoid dominated basement and other coeval granitoids i.e. sanukitoids, quartz diorites and quartz syenites. Based on 14 in situ analyses the average $\delta^{18}O$ value of the zircons from the Änäkäinen age determination sample is 7.34±0.10 ‰, which indicates involvement of material that has experienced low temperature oxygen isotope fractionation.

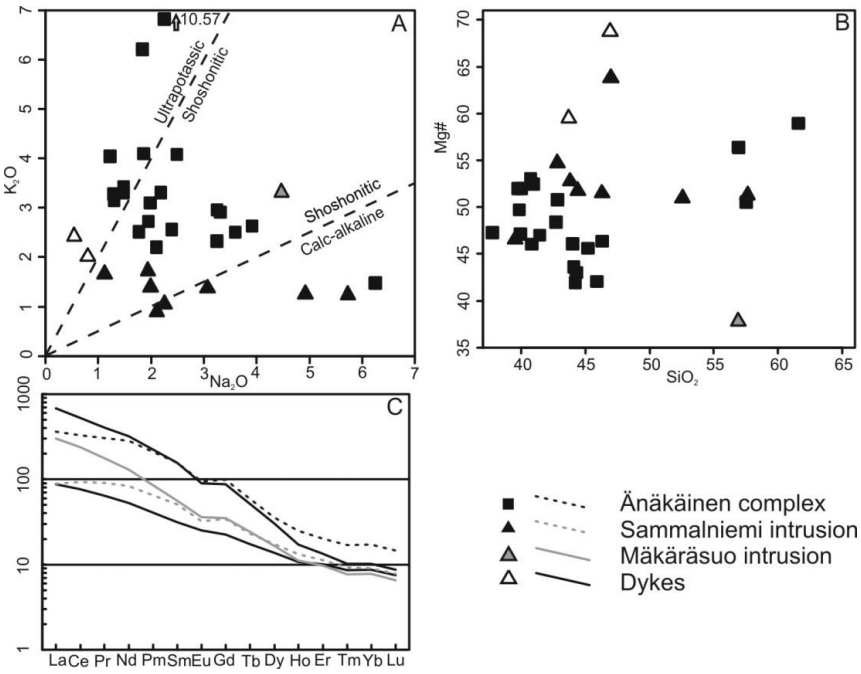


**Figure 2.** Studied samples plotted on A) $Na_2O$ (wt. %) vs. $K_2O$ (wt. %) diagram, B) $SiO_2$ (wt. %) vs. Mg# diagram and C) Chondrite normalized REE diagram. In C median values are used for Änäkäinen and Sammalniemi intrusions.

## 5. Discussion

Contamination of mantle derived mafic to ultramafic magma or partial melting of pre-existing crust cannot explain the observed enrichment of LREE, LILE and $P_2O_5$ combined with ultrabasic to basic compositions as the available contaminants/melt sources are either distinctly more felsic and/or less enriched in the mentioned elements. Thus these characteristics must originate from the mantle. Compositionally our samples cannot be included into the sanukitoid suite although certain similarities are evident i.e. enrichment in REE, $K_2O$, Ba, and Sr. The observed low Mg#, Cr and Ni, especially in the case of the Änäkäinen complex, could be explained with fractional crystallization of olivine and clinopyroxene. Based on geochemical modelling Laurent et al. (2014) showed that low MgO, high FeO and high $K_2O$ magmas could indicate a combination of two sources: metasomatized lithospheric mantle (i.e. the source of sanukitoids) and astenospheric mantle (i.e. the source of tholeites). Samples from the Sammalniemi intrusion could have been produced this way, but the high LILE and LREE characteristics of the Änäkäinen complex do not fit this model. Low Zr/Sm and Hf/Sm ratios could indicate carbonate metasomatism of the source, especially for the Änäkäinen complex with elevated $P_2O_5$ contents. Negative anomalies of Nb and Ti can be interpreted to indicate sediments as the metasomatizing agent of the mantle wedge, these features are present in the samples from Änäkäinen, but the negative Ti-anomaly is missing from the Sammalniemi samples. The whole-rock Sm-Nd data yielding model ages older than crystallization ages and elevated $\delta^{18}O$ values suggest involvement of older crustal material that had undergone low temperature isotope fractionation.

The alkali enriched gabbros and diorites are an additional piece in the all ready significant compositional heterogeneity of the Neoarchaean plutonic rocks related to the final stages of the accretionary orogeny of the Fennoscandian Shield. Spatially the Neoarchaean suites overlap, but also display certain differences in their distribution (Fig. 1). Neoarchaean subduction characterized by frequent slab-break offs and cessations of plate movements,

possibly in time scale well below 10 Ma and associated small scale convection cells (Magni et al., 2012) would have been able to produce heterogeneity of source compositions and melting conditions. Kaislaniemi et al. (2014) suggested that chaotic sublithosperic convection could explain the continuation of heterogeneous magmatism in post-collisional environment.

It would be unrealistic to construct the Neoarchaean geological history of the Lentua Complex (mere 400 km by 100 km) without taking into account for example the proposed ca 2.7 Ga Belomorian subduction event, only 300 km further east, marked by the existence of eclogites (Mints et al., 2010), instead we must look at Lentua and its neighbouring blocks as an entity. The Archaean domain of the Fennoscandian Shield and Tibetan Plateau are of roughly similar size, i.e. 1000 km by 500 km, and show similarities both in diversity and overall timespan of the mantle derived magmatism. Thus the combination regional scale processes e.g. slab roll back, slab break-off and crustal delamination following subduction related metasomatism suggested as explanation for the sifts in place and composition of the alkaline magmatism within Tibetan Plateau (Chung et al. 2005) seems like a plausible option for the Archaean of the Fennoscandian Shield.

**References:**

Chung, S.-L., Chu, M.-F., Zhang, T.-Q., Xie, Y.-W., Lo, C.-H., Lee, T.-Y., Lan, C.-Y., Li, X.-H., Zhang, Q., and Wang, Y.-Z., 2005. Tibetan tectonic evolution inferred from spatial and temporal variations in post-collisional magmatism. Earth-Science Reviews, 68, 173−196.

Heilimo, E., Halla, J., and Huhma, H., 2011. Single-grain zircon U-Pb age constraints of the western and eastern sanukitoid zones in the Finnish part of the Karelian Province. Lithos, 121, 87−99.

Heilimo, E., and Mikkola, P., 2014. Neoarchean alkaline rich igneous magmatism at cratonization stage of western part of Karelian (Baltic) Province. In: 31th Nordic Geological Winter Meeting Lund, Sweden, January 8–10 2014. p. 112.

Huhma, H., Kontinen, A., Mikkola, P., Halkoaho, T., Hokkanen, T., Hölttä, P., Juopperi, H., Konnunaho, J., Luukkonen, E., Mutanen, T., Peltonen, P., Pietikäinen, K., and Pulkkinen, A., 2012b. Nd isotopic evidence for Archaean crustal growth in Finland. In: Hölttä, P. (ed) The Archaean of the Karelia Province in Finland. Geological Survey of Finland Special Paper, 54, 175–212.

Huhma, H., Mänttäri, I., Peltonen, P., Kontinen, A., Halkoaho, T., Hanski, E., Hokkanen, T., Hölttä, P., Juopperi, H., Konnunaho, J., Lahaye, Y., Luukkonen, E., Pietikäinen, K., Pulkkinen, A., Sorjonen-Ward, P., Vaasjoki, M., and Whitehouse, M., 2012a. The age of Archaean greenstone belts in Finland. In: Hölttä, P. (ed) The Archaean of the Karelia Province in Finland. Geological Survey of Finland, Special Paper, 54, 73–174.

Kaislaniemi, van Hunen, J., Allen, M.B., and Neill, I., 2014. Sublithospheric small-scale convection—A mechanism for collision zone magmatism. Geology, 42, 291−294.

Käpyaho, A., Mänttäri, I., and Huhma, H., 2006. Growth of Archaean crust in the Kuhmo district, eastern Finland: U-Pb and Sm-Nd isotope constraints on plutonic rocks. Precambrian Research, 146, 95–119.

Koistinen, T., Stephens, M.B., Bogatchev, V., Nordgulen, Ø., Wennerström, M., and Korhonen, J., 2001. Geological map of the Fennoscandian Shield, scale 1:2 000 000. Geological Survey of Finland: Geological Survey of Norway: Geological Survey of Sweden: Ministry of Natural Resources of Russia.

Laurent, O., Rapopo, M., Stevens, G., Moyen, J.F., Martin, H., Doucelance, R. and Bosq, C., 2014. Contrasting petrogenesis of Mg–K and Fe–K granitoids and implications for post-collisional magmatism: Case study from the Late-Archean Matok pluton (Pietersburg block, South Africa). Lithos, 196–197, 131−149.

Magni, V., van Hunen, J., Funiciello, F., and Faccenna, C., 2012. Numerical models of slab migration in continental collision zones. Solid Earth, 3, 293–306,

Mikkola, P., Huhma, H., Heilimo, E. and Whitehouse, M., 2011. Archean crustal evo-lution of the Suomussalmi district as part of the Kianta Complex, Karelia: constraints from geochemistry and isotopes of granitoids. Lithos, 125, 287–307.

Mikkola, P., Heilimo, E., and Huhma, H., 2014. Relationships between sanukitoids and crust-derived melts and their implications for the diversity of Neoarchaean granitoids: a case study from Surmansuo and nearby areas, Eastern Finland. East Finland. Bulletin of the Geological Society of Finland, 86, 23–40.

Mints, M.V., Konilov, A.N., Dokukina, K.A., Kaulina, T.V., Belousova, E.A., Natapov, L.M., Griffin, W.L., and O'Reilly, S.Y., 2010. The Belomorian Eclogite Province: Unique Evidence of Meso-Neoarchaean Subduction and Collision. Doklady Earth Sciences, 434, 1311–1316.

# Some remarks about the focal depths and rheological models in the POLAR profile, Northern Finland.

K. Moisio and P. Kaikkonen

Geophysics, Oulu Mining School, University of Oulu
P.O. Box 3000
FI-90014 University of Oulu
Finland
E-mail: kari.moisio@oulu.fi

Relations between the focal depths of the earthquakes and the calculated rheological strengths were analyzed together with the stress intensity estimates for the seismic POLAR profile in northern Fennoscandia. The values of the calculated rheological brittle strength in the crust were reduced by changing e.g., the pore fluid factor, friction coefficient and assumed stress regime. These reductions enabled low enough brittle strength in relation to stress field estimates in order to allow earthquake occurrence in a rheological sense.

**Keywords:** lithosphere, Fennoscandia, focal depths, rheology

## 1. Introduction

The relations between the earthquakes and the calculated rheological strengths were analysed. The continental lithosphere is usually old, cold, having a multilayer rheology and rheological behaviour is determined by the brittle and ductile properties of the constitutive rocks that form the lithosphere. Seismicity is an indication of brittle deformation in the lithosphere and earthquakes are confined to so-called seismogenic layer, usually located in the uppermost brittle part of the crust in the continental lithosphere.

Depth distribution of seismic activity can be compared with the rheological models, as it is generally assumed that seismicity is usually limited to brittle layers, and above the depth of the brittle-ductile transition (e.g., Chen and Molnar 1983). This transition depth is located at the depth where the brittle strength reaches its maximum value and the ductile behaviour becomes the dominating deformation mechanism. Maximum earthquake depth can have correlation with the long-term brittle layer thickness which is controlled by the depth to the brittle–ductile transition and thus also by the temperature (e.g., Ranalli 1995; Burov 2011). This is further conditioned by the intraplate stress levels. However, seismicity is physically related to frictional instabilities not to changes in rheological properties. Another definition for the lower boundary of the seismicity is assumed to be controlled by change in the frictional behaviour (Blanpied et al. 1991; Scholz 2002). This is a temperature controlled sliding stability transition. Thus seismicity is not an adequate criterion for the relative strength of rocks on the lithospheric scale as it can be understood to be induced by frictional and viscous instabilities arising from strain-dependent changes in the rheology of the fault rocks with respect to that of the host rock (Handy and Brun, 2004).

## 2. Methods and motivation

First, rheological strength profiles (Moisio and Kaikkonen, 2013) were calculated for the seismic POLAR profile adopting a rheological classification for the crust and mantle based on the seismic velocities and compositional analysis done for the POLAR profile (Janik et al., 2009). Several thermal models with varying crustal heat production and lithosphere thickness were used in the determination of the rheological models.

Next the earthquake focal depth data was analysed. Earthquakes around the POLAR profile are mostly confined to the upper crust (Fig 1). Mean focal depth value is 7.1 km for the 93 events evaluated from a 100 km wide zone around the POLAR profile. Spatially focal depths show twofold distribution (Fig 2). In the SW earthquakes are situated slightly deeper, few of them deeper than 20 km, which for intraplate region can be considered rather deep. In the central and NE parts most of the earthquakes are at depths less than 10 km.

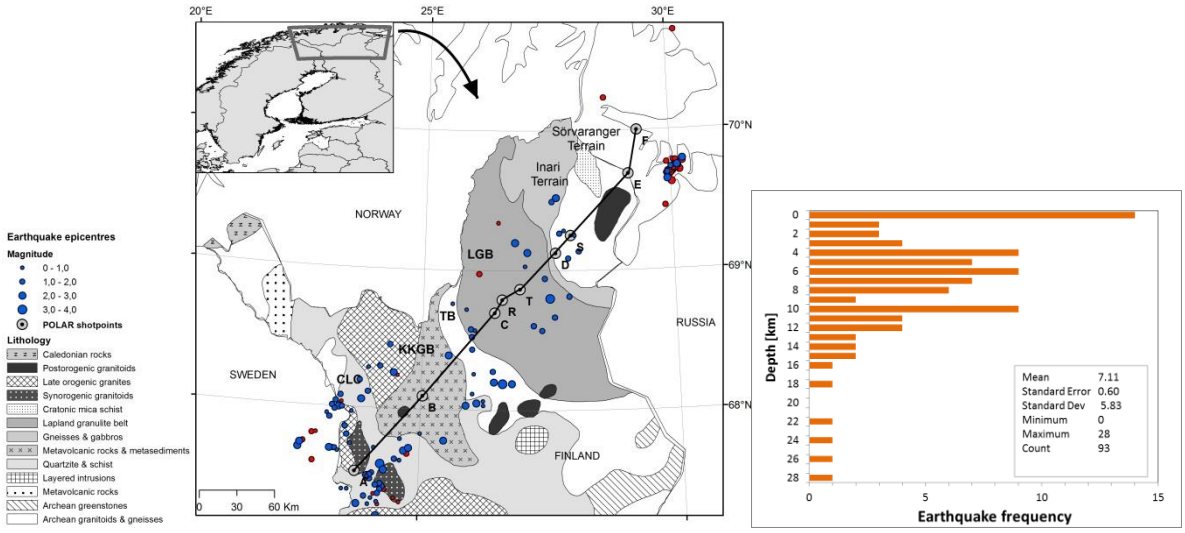


**Figure 1.** Location of the seismic POLAR profile together with the geological map (© Geological Survey of Finland, 2003). Bold letters refer to shotpoint locations. The locations of the seismic events during the period of 1965-2011 with magnitudes (Institute of Seismology 2013) are shown for about a 100 km wide zone along the profile. On the right focal depth distribution of the selected earthquake events with relevant statistics.

The calculated rheological strength in a compressional stress regime following the linear brittle mechanism relationship described by Byerlee's law suggests as high as 1 GPa differential stresses already at the depth of 20 km. These high values indicate that only very shallow earthquakes should appear around the POLAR profile as critical stresses in the crust are unlikely to exceed values of 200 MPa (Lamontagne and Ranalli 1996; Ranalli 2000). If assuming that the maximum lithospheric critical stresses and the earthquake depths are within the error bounds then the strength values should be reduced considerably to explain the earthquake occurrence at these depths.

## 3. Results

Relations between the focal depths of the earthquakes and the calculated rheological strengths together with the calculated stress intensity estimates were analyzed. The conventional rheological model for the POLAR profile seems to be too strong to explain satisfactorily the earthquake occurrence in the crust as only less than 20 % of the analysed earthquake events are located in this very shallow region of conventional failure (Fig. 2, blue region). Several factors which decrease the value of the rheological strength e.g., smaller friction coefficient, higher pore fluid pressure and different assumed stress regime, and their effects were analysed. It seems that most of the earthquake events can be explained by reverse stress regime if high pore pressure conditions exist. However, for the deepest events it seems that also changes both in the stress regime to strike-slip one and in the friction coefficients to lower one are needed (Fig 2).

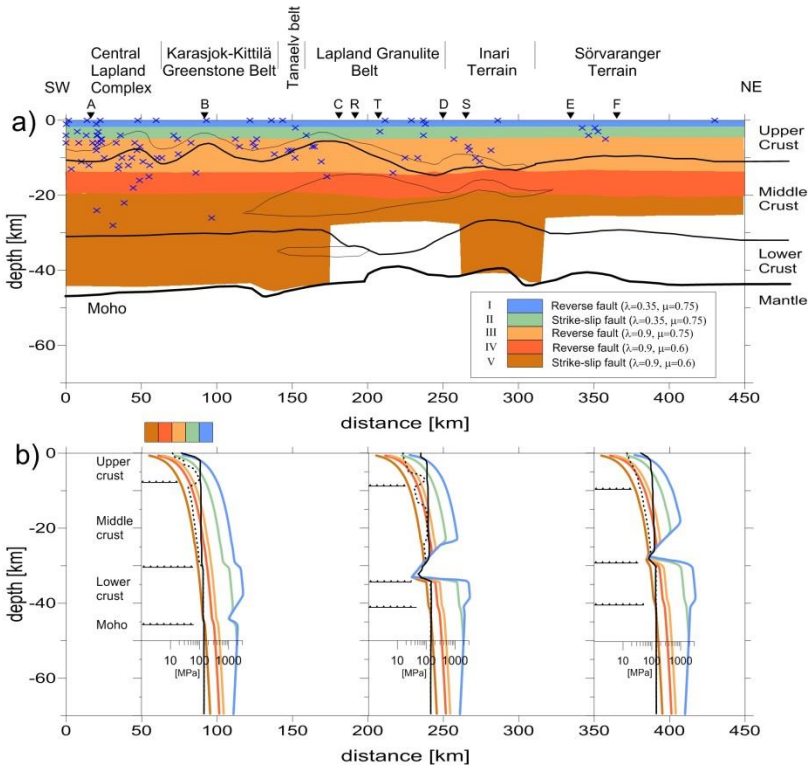


**Figure 2.** a) Earthquake focal depths with blue crosses and the depth ranges where frictional failure of rock is possible, i.e., stress exceeds rheological strength. Regions of failure due to changes in stress regime, pore fluid factor λ or friction coefficient μ are shown with different colours and numbers (I−V) and are explained in legend.
b) Influence of the different parameters on the individual strength profiles (I−V) and the calculated stress intensities (black curves) for the locations of 50, 200 and 350 km along the POLAR profile. Intersection of the strength and the stress intensity defines the depth above which failure is possible. (from Moisio and Kaikkonen, 2014)

## References:

Blanpied, M., Lockner, D. and Byerlee, J., 1991. Fault stability inferred from granite sliding experiments at hydrothermal conditions. Geophys Res. Lett., 18, 609-612.

Burov, E.B., 2011. Rheology and strength of the lithosphere. Mar. Pe.t Geol., 28, 1402-1443.

Chen, W. and Molnar, P., 1983. Focal depths of intracontinental and intraplate earthquakes and their implications for the thermal and mechanical properties of the lithosphere. J. Geophys. Res., 88, 4183-4214.

Handy, M.R. and Brun, J.-P., 2004. Seismicity, structure and strength of the continental lithosphere. Earth Planet Sci. Lett., 223, 427-441.

Institute of Seismology, 2013. Catalog of earthquakes in Northern Europe 1375-. (Read 1.4. 2013). http://www.helsinki.fi/geo/seismo/english/bulletins/index.html.

Janik, T., Kozlovskaya, E., Heikkinen, P., Yliniemi, J. and Silvennoinen H., 2009. Evidence for preservation of crustal root beneath the Proterozoic Lapland-Kola orogen (northern Fennoscandian shield) derived from P and S wave velocity models of POLAR and HUKKA wide-angle reflection and refraction profiles and FIRE4 reflection transect. J. Geophys. Res., 114, B06308.

Lamontagne, M. and Ranalli, G., 1996. Thermal and rheological constraints on the earthquake depth distribution in the Charlevoix, Canada, intraplate seismic zone. Tectonophys, 257, 55-69.

Moisio, K. and Kaikkonen, P., 2013. Thermal and rheological structures along the seismic POLAR profile in the northern Fennoscandian Shield. Terra Nova, 25, 2–12.

Moisio, K. and Kaikkonen, P., 2014. Stress, rheological structure and earthquakes in the POLAR profile in the northern Fennoscandian Shield. Int. J. Earth Sci., DOI 10.1007/s00531-014-1061-2

Ranalli, G., 1995. Rheology of the Earth (2nd edit.), Chapman & Hall, London.

Ranalli, G., 2000. Rheology of the crust and its role in tectonic reactivation. J. Geodyn., 30: 3-15.

Scholz, C.H., 2002. The mechanics of earthquakes and faulting. Cambridge university press.

# Sulphur and copper isotope characteristics of the orogenic gold deposits in the Archaean Hattu schist belt, eastern Finland

F. Molnár[1], H. O`Brien[1], J. Lahaye[1], A. Käpyaho[1] and G. Sakellaris[2]

[1]Geological Survey of Finland, Finland
[2]Endomines Oy., Finland
E-mail: ferenc.molnar@gtk.fi

$^{34}S/^{32}S$ ratios in pyrrhotite, pyrite and chalcopyrite, as well as $^{65}Cu/^{63}Cu$ ratios in chalcopyrite were analysed by LA MC ICPMS technique with high spatial resolution in polished thin sections of ore specimens. Results of these studies suggest that sulphur and copper isotope data determined by this technique could effectively be applied to monitor reductive-oxidative conditions of ore forming processes and sources of fluids.

**Keywords:** orogenic gold deposits, sulphur isotope, copper isotope, Archaean, Fennoscandia

## 1. Geology and gold deposits in the Hattu schist belt

The Hattu schist belt (HSB) is a part of the Ilomantsi greenstone belt of Archaean age in the western part of the Karelian Province of the Fennoscandian Shield. The extension of the N-S oriented HSB in Eastern Finland is approx. 50 km in length with max. 20 km width and is continuous for a further ~200 km to the North in the Kostamushka greenstone belt in Russia. The HSB consists of felsic volcanic and epiclastic sedimentary units of around 2.75 Ga age with local intercalations of mafic and ultramafic volcanic rocks in the vicinity of the Pampalo mine (Sorjonen-Ward, 1993; Figure 1). These units are aligned between tonalite, granodiorite and leucogranite intrusions of similar ages (2.75-2.73 Ga; Sorjonen-Ward, 1993). Lower amphibolite facies metamorphism at 4-6 kbars pressures and at 500-600°C temperatures affected rocks of HSB at ca. 2.70-2.63 Ga (O`Brien et al., 1993). Emplacement of NW-trending gabbroic dikes took place from 2.3 to 2.0 Ga in relation to the Paleoproterozoic rifting of the Archaean craton. Between ca. 1.85 and 1.7 Ga, tectonothermal processes affected the western part of the Karelian Province due to overthrust of the up to 5-6 km thick east-verging Svecofennian nappe complex (Kontinen et al., 1992). The nappe complex was completely eroded away from the western part of the Karelian Province during the Neoproterozoic exhumation.

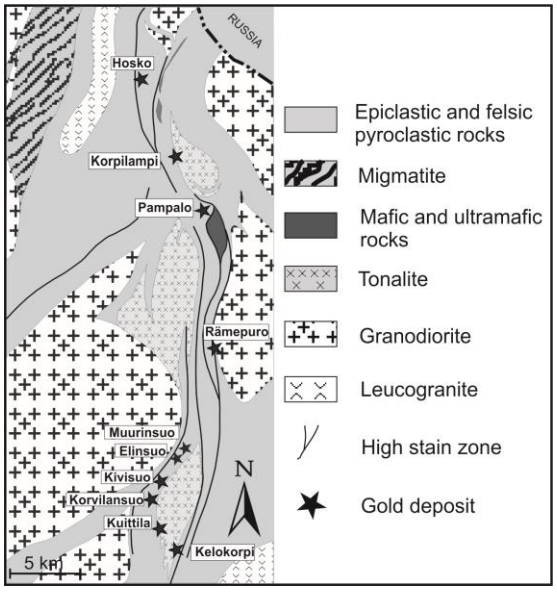


**Figure 1.** Geology of the HSB.

The gold deposits in the HSB are located along N-S and NE-SW trending shear zones which cut across folded epiclastic sedimentary and volcanogenic units, as well as intrusive rocks (Fig. 1). The known cumulative mineral resource of deposits in the HSB is 3,81 Mt. Currently, the deposits at the Pampalo mine (0.505 Mt @ 2.31 g/t Au reserve) and at Rämepuro (0.169 Mt @ 2.1 g/t Au) are being exploited. According to the host rocks and ore mineralogy, the gold deposits of the HSB can be divided into two major groups. In the first group, the major Fe-sulphide mineral is pyrrhotite (PO) with less common pyrite (PY) and arsenopyrite (APY) and the mineralization is mostly hosted by tourmalinized, sericitized and

biotitized metasedimentary units (Korvilansuo, Muurinsuo, Rämepuro and Hosko deposits). Locally, the felsic porphyry dikes cutting the metasedimentary units are also mineralized (e.g. Rämepuro, Korvilansuo). In the second group, tonalitic and felsic porphyry intrusive rocks (Kuittila and Pampalo) and intermediate-felsic clastic volcanic units (Pampalo) are the major host rocks. Tourmalinization is less extensive and biotite(-sericite) with albite-K-feldspar alteration is prevailing. The major sulphide mineral is PY with subordinate occurrences of PO in these deposits. The mineralization has disseminated-stockwork character in each deposit.

**2. Aims and methods of studies**

The major factors affecting fractionations of sulphur and copper isotopes during hydrothermal processes are the variations in temperature and changes in the oxidation state of fluids. In addition to those effects, ratios of $^{34}S/^{32}S$ in PO, PY and CPY, as well as $^{65}Cu/^{63}Cu$ in CPY may also be influenced by the sources of fluids and the interaction of these fluids with the host rocks of the ore. We analysed ratios of these isotopes for determining whether the observed variations in the major Fe-sulphide mineralogy and host rocks of gold deposits in the HSB could be correlated with sulphur and copper isotope data. Regional scale evaluation of stable isotope signatures of ore forming processes also supports assessments of ore potential.

PO, PY and CPY usually occur in complex intergrowths with each other and other minerals, and their individual grains (especially in the case of CPY), have relatively small (< 200µm) sizes in most of the ore samples in the HSB. Therefore we applied *in situ* LA MC ICPMS analyses for determination of sulphur and copper isotope ratios in polished thin sections. The high spatial resolution of the analytical technique (e.g. 50-80 µm laser beam diameter) allowed us to perform analyses on small sulphide grains and to check homogeneity of isotope ratios within the larger individual grains, taking into account that the 2σ precision of analyses are 0.37 ‰ (CPY) and 0.54 ‰ (PY, PO), as well as 0.12 ‰ (CPY) for $^{34}S/^{32}S$ and $^{65}Cu/^{63}Cu$ isotope ratios, respectively. Sulphur isotope ratios were analysed in 443 spots of 44 samples whereas copper isotope ratios were analysed in 64 spots of 10 samples. The advantage of the applied analytical technique is that the textural settings and parageneses of minerals could be recorded during the analyses.

**3. Results**

The average (AVE) $\delta^{34}S_{CDT}$ values in PO are between +0.7 and +5.1 ‰ in the Hosko, Rämepuro, Muurinsuo and Korvilansuo deposits where PO is the predominant Fe-sulphide mineral and the ore is hosted by metasedimentary rocks (Fig. 2). Felsic dike hosted ore in some of these deposits and the PO-dominated ore paragenesis in the tonalite hosted Kuittila deposit have similar range of AVE $\delta^{34}S_{CDT}$ values of PO. Ranges of AVE $\delta^{34}S_{CDT}$ data for PY and CPY associated with PO in metasediment hosted ores are +1.6 - +5.7 ‰ and +0.4 – +2.4 ‰, respectively. PY and CPY from felsic dikes of predominantly metasediment hosted ore have also positive AVE $\delta^{34}S_{CDT}$ values within these latter ranges. In the Pampalo deposit, where in contrast, PY is the major Fe-sulphide mineral and the ore is hosted by felsic porphyry and volcanoclastic units, the AVE $\delta^{34}S_{CDT}$ values for PY are between -6.0 and +3.5 ‰, as well as between -8.0 and -2.0 ‰, respectively. Data for CPY and rare PO-associated with PY are also mostly in these ranges both in the intrusive and volcanoclastic units at Pampalo, although CPY has even more negative values in some samples. The observed within grain variations of $\delta^{34}S_{CDT}$ data for PO, PY and CPY are usually in the range of the analytical precision except for some PY and CPY grains from the Pampalo deposit, which can show up

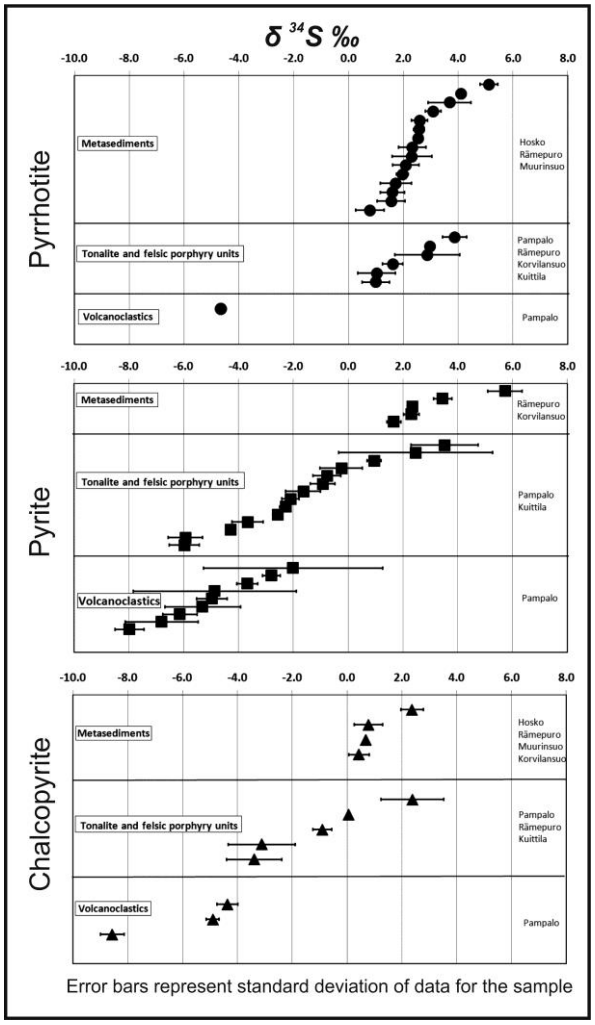


**Figure 2:** Sulphur isotope data for PO, PY and CPY according to localities and host rocks in the Hattu schist belt.

to 6 ‰differences between cores and rims of individual grains.

The AVE $\delta^{65}Cu_{NIST978}$ values for CPY from samples of the metasedimentary rock hosted ore (e.g. Rämepuro, Muurinsuo and Korvilansuo deposits) are between -0.35 and 0 ‰, whereas data from intrusive and volcanoclastic rock hosted ore samples (e.g Pampalo and Kuittila deposits) are more variable between -0.5 and +0.6 ‰, but the most common values are higher than 0 ‰. The within sample and within grain variation of $\delta^{65}Cu_{NIST978}$ values is up to 0.8‰. The negative AVE $\delta^{65}Cu_{NIST978}$ values in CPY grains of samples from metasedimentary rock hosted ores are associated with positive AVE $\delta^{34}S_{CDT}$ values and the positive AVE $\delta^{65}Cu_{NIST978}$ values are associated mostly with negative AVE $\delta^{34}S_{CDT}$ values in the intrusive and volcanoclastic rocks (Fig.3).

## 4. Discussion

Orogenic gold deposits in Archaean greenstone belts are usually characterized by rather uniform $\delta^{34}S_{CDT}$ values: data for PY usually fall between 0 and +9‰ (Hodkiewicz et al., 2008). This uniformity of sulphur isotope compositions suggests a common, average crustal source of fluids with reductive character. However, local deviation from this general characteristic with occurrences of -10 to 0 ‰ $\delta^{34}S_{CDT}$ values also occur in some deposits of ore districts which are otherwise characterised by positive $\delta^{34}S_{CDT}$ values for iron sulphides. The significant negative shift of $\delta^{34}S_{CDT}$ values could generally be explained by precipitation of sulphides from more oxidative fluids.

In the Hattu schist belt, the variation in oxidation state of fluids is reflected by the predominant sulphide mineralogy, and accordingly, the < 0‰ $\delta^{34}S_{CDT}$ values of PY and CPY are typical for the PO-absent ores at the Pampalo mine. The relatively oxidative character of fluids may reflect involvement of magmatic fluids in the ore forming processes, or tectonically induced pressure variations causing effervescence of reducing gases from the ore forming fluids (Hoskiewitz et al, 2008). Boiling of parent fluids of ore have not been detected by fluid inclusion studies either at the Pampalo mine or in the other gold deposits of the Hattu schist belt (Poutiainen and Partamies, 2003; Molnár et al., 2013), thus variation in oxidation state of fluids due to the effect of phase separation processes is a less plausible interpretation. Therefore the role of magmatic fluids, at least in some stages of ore deposition, cannot be excluded at Pampalo. The occurrence of syn-magmatic ore formation at Pampalo is also

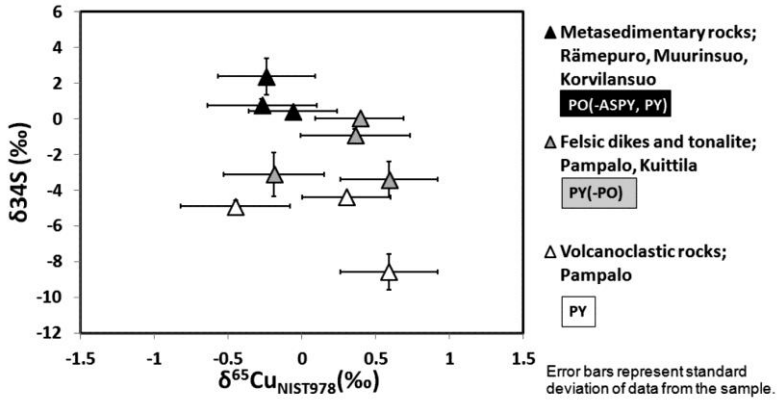


**Figure 3:** Cu and S isotope data for CPY according to localities, host rocks and mineral associations in the Hattu schist belt.

supported by the observation that the mineralized felsic porphyry unit is intruded by an unmineralized tonalite. On the other hand, the variations in sulphur isotope compositions of PO, PY and CPY can also be correlated with the compositions of host rocks, which suggests importance of rock buffering on the fluid chemistry. This is in agreement with the disseminated-stockwork nature of ores in the Hattu schist belt.

The range of $\delta^{65}Cu_{NIST978}$ values between -1 and +1 ‰ is typical for CPY in felsic intrusion related shallow and granite intrusion related deep hydrothermal systems. More negative values occur in sediment-hosted copper ores whereas more positive values are typical for volcanogenic massive sulphide deposits (Larson et al, 2003). Thus the copper isotope data also appear to support involvement of magmatic fluids in the formation (of the precursor ores) of gold deposits in the Hattu schist belt. The relatively large variation in $\delta^{65}Cu_{NIST978}$ data in ores hosted by intrusive and volcanoclastic rocks with <0‰ AVE $\delta^{34}S_{CDT}$ values probably reflects the influence of variation in redox conditions on fractionation of copper isotopes under hypogene hydrothermal conditions.

## 5. Conclusions

The $\delta^{34}S_{CDT}$ data of PO, PY and CPY and $\delta^{65}Cu_{NIST978}$ values of CPY in the orogenic gold deposits of the Hattu schist belt can be correlated with the ore mineral paragenesis and compositions of host rocks. The ore of the Pampalo mine deposited under more oxidative conditions in comparison to the other deposits in the belt and magmatic fluids were probably also involved in the formation of the polygenic ore. Our results also suggest that paired sulphur and copper isotope studies of chalcopyrite from orogenic gold deposits may help to constrain the origin and chemistry of hydrothermal fluids.

## References:

Hodkiewicz, P.F., Groves, D.I., Davidson, G..J., Weinberg, R.F. and Hagemann, S.G., 2008. Influence of structural setting on sulphur isotopes in Archean orogenic gold deposits, Eastern Goldfields Province, Yilgarn, Western Australia. Mineralium Deposita, 44, 129-150.

Kontinen, A., Paavola, J. and Lukkarinen, H., 1992. K-Ar ages of hornblende and biotite from late Archean rocks of eastern Finland: interpretation and discussion of tectonic implications. Geol. Surv. Finland Bull. 365 p.

Larson, P., Maher, K., Ramos, F., Chang, Z., Gaspar, M., and Meinert, L., 2003. Copper isotope ratios in magmatic and hydrothermal ore forming environments. Chem. Geol., 201, 337–350.

Molnár, F., O`Brien, H.E., Lahaye, Y., Käpyaho, A., Sakellaris, G.., 2013. Signatures of overprinting mineralisation processes in the orogenic gold deposit of the Pampalo mine, Hattu schist belt, eastern Finland. 12th Biennial SGA Meeting, Proceedings, vol. 3, 1160-1163.

O`Brien, H.E., Huhma, H., Sorjonen-Ward, P., 1993. Petrogenesis of the late Archean Hattu schist belt, Ilomantsi, eastern Finland. Geol. Surv. Finland Spec. Paper 17, 133-146

Poutiainen, M. and Partamies, S., 2003. Fluid evolution of the late Archean Rämepuro deposit in the Ilomantsi greenstone belt in eastern Finland. Miner. Deposita, 38,196-207.

Sorjonen-Ward, P., 1993. An overview of structural evolution and lithic units within and intruding the late Archean Hattu schist belt, Ilomantsi, eastern Finland. Geol. Surv. Finland Spec. Paper, 17, 193-232.

# Seismic tomography for microseismic data from Pyhäsalmi Mine, Pyhäjärvi

J. Nevalainen and E. Kozlovskaya

Sodankylä Geophysical Observatory, Laboratory of Applied Seismology, University of Oulu, Finland
Pentti Kaiteran katu 1, 90570 Oulu
E-mail: jouni.nevalainen@oulu.fi

The study presented here describes a seismic tomography applied for microseismic data from Pyhäsalmi mine, Pyhäjärvi, to obtain seismic velocity structure within the mine. The data is recorded from 2002 when the passive microseismic monitoring network was installed in Pyhäsalmi mine and over one hundred thousand microseismic events within mine have been observed since. The interest of this study is to research how well tomography will work on passive seismic data where event-geophone geometry is based on natural occurring events. Furthermore a double-difference technique will be applied to enchant both seismic velocity structure modelling as well the relocation of the seismic events.

**Keywords:** Seismics, tomography, time-lapse, double-difference, Finland, Pyhäsalmi, mine

## 1. General

In this study a time-lapse tomography is presented and the initial results for data from Pyhäsalmi mine at Pyhäjärvi. The purpose of the work is to study how well seismic data from passive microseismic network can be used to study seismic velocity within mine using seismic tomography. The results are then compared to the known boundaries of Pyhäsalmi deep ore body to consider the reliability of the algorithm.

Another task for this study is to apply seismic tomography for conjugated data series to observe secular chances in seismic velocity structure within Pyhäsalmi mine. The seismic velocity within certain rock type is not exactly a constant and is affected by numerous factors like pressure and intactness of the rock (Reynolds, 2011). In the mining environment the change of the pressure distribution within rock due mining operation affects directly seismic velocities of the rock. In general, the increase of pressure increases seismic velocities as well. At some point the rock cannot handle increased pressure but fails and cracks, which can lead to hazardous accidents within mine (Brady, 2004). Thus tracking changes in the seismic velocity modelling using time-lapse seismic tomography will assist in monitoring pressure changes in the rock and provide information both for safety and continuity of mining operation.

To enhance the modelling further the double-difference technique will be applied to tomography algorithm. This will make not only tomography result more accurate but also the accuracy of location of observed seismic events through relocation in Pyhäsalmi mine.

## 2. Time-lapse seismic tomography method and double-difference technique

The aim of the Time-lapse seismic tomography (both traditional linear travel-time seismic tomography and novel double-difference seismic tomography) is to detect of changes in seismic velocities in mining environment (Luxbacher, 2008). For the linear traveltime seismic tomography I'm using technique descripted by Lu & Inderwiesen (1994). Used tomography is based on mathematical solution of seismic velocity's structures using Kacmarz's method and a technique, which uses this method directly, the SIRT (Simultaneous iterative reconstruction technique). This method requires, like any other tomography, to have sufficient amount of seismic events and observations to make whole model area covered with seismic rays

between event-geophones. On model parts where the ray coverage is poor the tomography will produce mathematical artefacts which do not image the true seismic velocity of area.

Double-difference techniques for microseismic events relocation has been used during past decade in regional as well in teleseismic event location algorithms to make the relocation more accurate. The fundamental equation of this iterative least-squares procedure relates the residual between the observed and predicted phase travel time difference for pairs of seismic events observed at common stations to changes in the vector connecting their hypocenters through the partial derivatives of the travel times for each event with respect to the unknown. When the earthquake location problem is linearized using the double-difference equations, the common mode errors cancel, principally those related to the receiver-event structure. This way it is avoided the need for station corrections or high-accuracy of predicted travel times for the portion of the raypath that lies outside the focal volume. This approach is especially useful in regions with a dense distribution of seismicity, i.e. where distances between neighboring events are only a few kilometers or less as in mines. (Waldhauser & Ellsworth, 2000)

## 3. Microseismic data in Pyhäsalmi mine

Microseismic event data from Pyhäsalmi mine has been measured since 2002, when the microseismic monitoring network was installed to the mine. The networks main goal is to locate frequently occurring microseismic events for monitoring and for safety for mining operations. The hardware for microseismic system at Pyhäsalmi mine was acquired from Integrated Seismic System International (ISSI) Company and software is maintained from Institute of Mine Seismology (IMS). Geophones installed in Pyhäsalmi mine are mostly one component (vertical) but few 3-component geophones are also installed. Geophones have been placed around Pyhäsalmi deep ore body. The data contains calculated hypocenters of microseismic events as well the arrival times of body waves (P- and S-waves) for all seismic stations belonging to microseismic monitoring network within the mine. The microseismic networks event localization accuracy has been determinated by the Pyhäsalmi Mining Ltd and also by Pyy (2007) in his Master's Thesis work. In Pyy's thesis the best accuracy for the seismic location are located at upper and central part of the deep ore body and the poorer location accuracy outside microseismic system and in bottom part of the mine where the production (rock crushing) within mine is made. The average event location accuracy is 30 m.

## 4. Appling Seismic tomography and initial results

Model sizes for tomography are determined by the coverage of microseismic systems located events-geophone pairs. Multiple different modelling areas have been tested. The Seismic tomography algorithm for Pyhäsalmi data event-geophone geometry has been tested through synthetic models. The result for one synthetic model is shown in Figure 1. The Fig. 1A presents synthetic model from 4 vertically sliced layers (50 m thick elements) and black dots presents events used in tomography. The Fig. 1B presents the results of seismic tomography based on traveltimes calculated from synthetic model. The event-geophone geometry is from third quarter of year 2008. From Fig. 1 can be seen that the major elements of the synthetic model are present in tomography model. Calculated velocities, however, are not as sharp on the boundaries but does "phase" into the "true" model. This is due the averaging effect of tomography itself. Nevertheless the tomography works well on synthetic data.

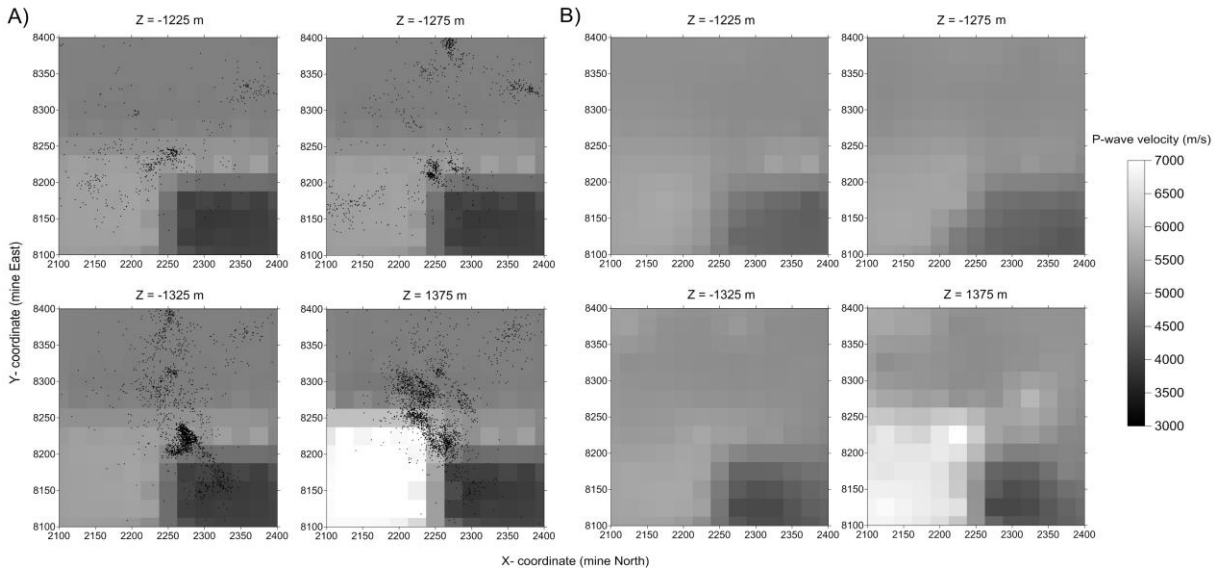


**Figure 1.** Results of SIRT tomography on synthetic model using real data geometry. A) The synthetic model and B) The result of SIRT tomography. The dots present used seismic events. The images have been plotted in XY-direction into 25 m grid.

After examination of the data, the sufficient amount of event-geophone pairs for modelling the surroundings of the deep ore body is data from three months and in some periods of time even down to few weeks. The tomography algorithm demands a known total traveltime for every event-geophone pairs which has been calculated for true data using the default velocity model of the mine (P-wave 5500 m/s, S-wave 3500 m/s). Now the information of the true geology is within the "false" locations of the events since they have been calculated using this default velocity model. By applying seismic tomography on data the heterogeneous of velocity structure will be revealed. Other source for velocity structure information, not yet applied, is the time difference between P- and S-waves.

In Figure 2 is presented results for Pyhäsalmi data from third quarter of year 2008 in four z-layers and model images are plotted in 25 m grid. The size of the tomography model is 300 m x 300 m in XY-direction (X, mine North Y, mine East), in vertical direction 200 m (-1200 m − -1400 m, a bottom part of the deep ore body) and the element size is 50 m for all dimensions. The tomography founds a solution quickly (1-2 iteration) and after that extra iterations (if allowed) only enhance mathematical artefacts for poorly ray-covered cells. In comparison boundaries of deep ore body (white polygons) of corresponding depth one can distinguish the higher velocity structures of the ore body from the tomography model. In interpretation it is necessary to look also the information of areas that has been already mined and refilled with filling which has very slow seismic velocity. This is still to be done.

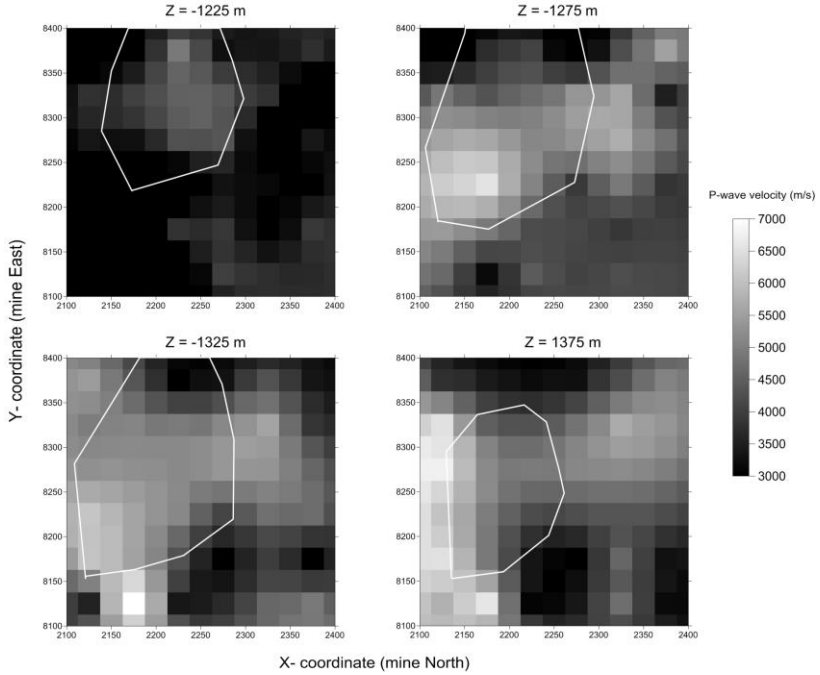


**Figure 2.** Results of tomography for data from third quarter of year 2008. The average boundaries for Pyhäsalmi deep ore body are presented in with polygon.

## 5. Conclusion

Seismic tomography works results on passive seismic data recorded in Pyhäsalmi mine. Interpretation of models, despite mathematical artifacts, is trustworthy and correlate well with real boundaries of deep ore body of Pyhäsalmi mine.

Next step is to apply double-difference method iteratively with tomography to adjust the event locations and enhance the seismic velocity model. Other task to be done is make use of the S-wave observations which are observed mainly from 3-componenet geophones to increase further velocity model accuracy.

## References:

Brady, B. H. G. and Brown, E. T., 2004. Rock mechanics for underground mining. Third edition. Kluwer Academic Publishers, Netherlands, 628 p.

Lo, T. and Inderwiesen, P., 1994. Fundamentals of Seismic Tomography, Geophysical Monograph Series, Society of exploration geophysics, No 6.

Luxbacher, K. M., 2008. Time-Lapse Passive Seismic Velocity Tomography of Longwall Coal Mines: A Comparison of Methods, dissertation of Doctor of philosophy, faculty of Virginia Polytechnic Institute & State University.

Pyy, A., 2007. TUTKIMUS PYHÄSALMEN KAIVOKSEN MIKROSEISMISEN HAVAINTOVERKON PAIKANNUSTARKKUUDESTA (A study for localization accuracy of Microseismic networks at Pyhäsalmi mine). Master's thesis, Department of physics, University of Oulu.

Reynolds, J, 2011. An introduction to applied and enviromental geophysics, Second edition. Wiley-Blackwell imprint of John Wiley & sons Ltd, England, 796 p.

Waldhauser F. and Ellsworth, W.L., 2000. A Double-Difference Earthquake Location Algorithm: Method and Application to the Northern Hayward Fault, California.

# Analogue modeling of Asymmetric Gravitational Spreading – a case from Fennoscandia

K. Nikkilä[1], A. Korja[1], H. Koyi[2] and O. Eklund[3]
[1]University of Helsinki, Institute of Seismology
[2]Hans Ramberg Tectonic Laboratory, Uppsala University, Department of Earth Sciences
[3]Åbo Akademi University, Geology and Mineralogy
E-mail: kaisa.nikkila@helsinki.fi

Orogenesis can develop at different scales and between different plate types and may result in overthickening of the crust and thus post-collisional extension (Beaumont et al. 2001). This paper presents crustal scale structures of unilateral gravitational spreading in three-layered crust at post-collisional stage using analogue centrifuge models.

**Keywords:** Svecofennian orogen, post-collisional extension, analogue models, three-layer crust

## 1. Introduction

In the late stage of orogeny, the continental crust has substantially thickened and may result in gravitational instabilities and post-collisional extension. The post-collisional extension in the middle- and lower crust is possible due to radioactive heating (England and Thompson, 1986) which reduce the viscosity of the crust enabling large-scale lateral flow (Beaumont et al., 2001). The post-collisional extension have been studied in modern orogenies like in Himalayas and Alps (Beaumont et al., 2001; Collins, 2002; Frisch et al., 2000), but also in ancient ones like in Trans-Hudson orogenic belts and Caledonian (Jamieson and Beaumont, 2011; Fossen, 2010). This study is inspired by Svecofennian orogen and our purpose have been to test what kind of large-scale structures post-collisional extension may produce to the crust with contrasting mechanical properties.

We have studied post-collisional extension of an over-thickened crust with the help of analogue models. The analogue models were designed to represent asymmetric post-convergence extension of two rheologically different terranes, representing a cold cratonic nucleus and warm collided block, respectively. We have assumed that before spreading the crust has attained a three-layer structure and that the middle crust has been partially molten (Royden, 1996, Beaumont et al., 2004), therefore the middle layer had lowest viscosity in our models. The main flow direction was dictated by free space and thus experiments were one-way spreading, although the extension direction varied between the models (Figure 1).

The two mechanically different terrane blocks were named after Archean (A) and Paleoproterozoic (P) crusts. The layer thicknesses - upper layer (UC) of 10km –middle layer (MC) of 30 km-lower layer (LC) of 20 km, have been adapted from the Svecofennian orogen, where three-layer are observed in the seismic studies (e.g. Korja et al., 1993, Korja et al,. 2009). In addition, effect of reactivation of shear zones were tested by pre-existing cuts, and models 4 and 5 had a set of orthogonal cuts dipping 60° (Figure 1).

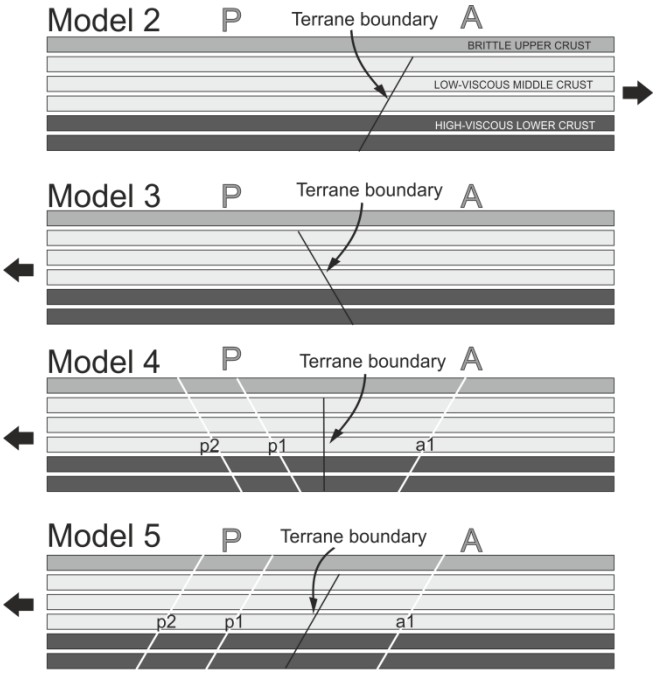


**Figure 1.** Schematic illustrations of the initial set-up of three-layer models. Black arrows show stretching direction. Black line represents the boundary between A and P, and white lines are pre-existing cuts (p2, p1 and a1).

## 2. Results

The amount of extension varied between the different crustal layers during experiments. The weak ductile middle layer (MC) flowed with highest amount of extension. The MC flow rotated block boundary and pre-existing cuts towards flow direction resulting in both listric structures and changes in dip direction (zigzag pattern).

Deeper units exposed faster in the weak block (P) compared to strong block (A), and therefore formed dome structures into block models with pre-existing cuts. The middle layer formed dome structures because of fracturing in the the UC. The MC thickened below the UC fractures and thinned between the gaps causing UC subsidence. This co-operation had influence of the total model thickness, and regardless of the high amount of extension (e.g. 50 %) the decrease of thickness was less than half of the amount of stretching. The blocks flattened approximate 20 % from the extension side and 10 % from the fixed side (Fig. 2).

The pre-existing cuts assisted the extension and thus the extension rate was higher. When we convert the time in models to nature, extending the crust by 50 % would take 12 my, if pre-existing shear zones are resent and 25 my, if not.

The pre-existing cuts enabled large-scale block rotation in a stronger block A. The block rotation caused subsidence of UC, uplift of MC and compression in LC.

P. The exposure level of the domes were deeper in

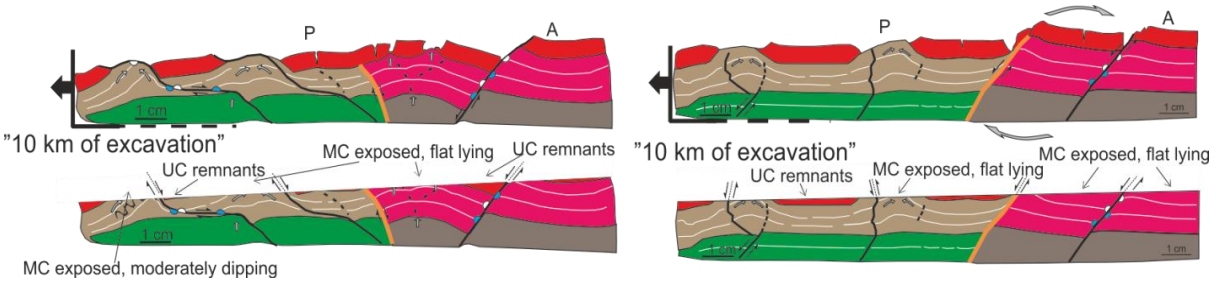


**Figure 2.** Line tracings of models 4 and 5. Both models are accompanied by a section from which a ca. 10 km slice has been removed from the top. In the model 4, left, uplift occurred in the footwall and subsidence on the hanging wall. The pre-existing cuts deformed as active faults and main movement occurred along the cuts, which extended and formed ramp- and flat structure. In the model 5, right figure, cuts rotated and formed zigzag – pattern in the middle layer. The cut offset are marked with white and blue circles.

## 3. Correlations to Svecofennian orogen and conclusions

The modeling results presented above can also be used for interpretation of the structures of Svecofennian orogen and here we discuss of these features.

The modeling results propose that middle crustal flow rotate terrane boundaries and inherited weakness zones towards extension direction. This may imply that the Archean-Paleoproterozoic boundary and Raahe-Ladoga shear complex dip eastward in the middle crustal level.

The listric shape in models and reflection profile FIRE3a, and middle layer doming in models and Bothnian belt (BB) area (Hölttä, 2013, Chopin et al., 2012) show similarities, therefore we propose that post-collisional extension have been a part of BB tectonic evolution and have caused the shape of the seismic reflections.

The crustal scale block rotation is likely occurred at Outokumpu area. The metamorphic grade is increasing westward (Kontinen et al., 1992; Sorjonen-Ward, 2006), like the modeling results suggest, and low-grade Höytiäinen belt (Kohonen, 1995) may represent a subsided block. In addition, we propose the block rotation and inherited structures may cause steps at Moho boundary, when the crustal block slides downward along pre-existing weakness zone. This kind of Moho step locates below Outokumpu area.

Based on similarities between models and Svecofennian orogen we estimate 50 % westward extension in the area. 50 % of extension is achieved in ca 12 my, and it thinned the Paleoproterozoic crust approximate 20 % and Archean crust by 10 %. If we compare the thickness changes in models to the present crustal thickness in Svecofennian orogen, we can propose that after collision the Paleoproterozoic crustal thickness was 66 km, suture zone thickness was 72 km and Archean crust was 55 km thick.

## References:

Beaumont, C., Jamieson, R. A., Nguyen, M. H. and Lee, B. 2001. Himalayan tectonics explained by extrusion of a low-viscosity crustal channel coupled to focused surface denudation. Nature, 414(6865), 738-742.

Beaumont, C., Jamieson, R. A., Nguyen, M. H. and Medvedev, S. 2004. Crustal channel flows: 1. numerical models with applications to the tectonics of the himalayan-tibetan orogen. Journal of Geophysical Research: Solid Earth, 109(B6), - B06406. doi:10.1029/2003JB002809

Chopin, F., Korja, A. and Hölttä, P. 2012. Tectonometamorphic evolution of the Bothian belt within the Svecofennian orogen - a case study for the building of a large dome in the Paleoproterozoic. S-56: Lithosphere meeting 2012

Collins, W. J. 2002. Hot orogens, tectonic switching, and creation of continental crust. Geology, 30, 535-538.

England, P. C. and Thompson, A. 1986. Some thermal and tectonic models for crustal melting in continental collision zones. Geological Society, London, Special Publications, 19, 83-94.

Fossen, H., 2010. Extensional tectonics in the North Atlantic Caledonides: a regional view. Geological Society, London, Special Publications,335, 767–793.

Frisch, W., Dunkl, I. and Kuhlemann, J. 2000. Post-collisional orogen-parallel large-scale extension in the Eastern Alps. Tectonophysics, 327, 239-265

Hölttä, P. 2013. Svecofennian metamorphism in Pohjanmaa, western Finland, 198.

Jamieson, R. A. and Beaumont, C. 2011. Coeval thrusting and extension during lower crustal ductile flow - implications for exhumation of high-grade metamorphic rocks. Journal of Metamorphic Geology, 29, 33-51.

Kohonen, J. 1995. From continental rifting to collisional crustal shortening: Paleoproterozoic kaleva metasediments of the höytiäinen area in north karelia, finland. Geological Survey of Finland,

Kontinen, A., Paavola, J. and Lukkarinen, H. 1992. K-ar ages of hornblende and biotite from late Archaean rocks of eastern Finland: Interpretation and discussion of tectonic implications. Geologian tutkimuskeskus, Espoo.

Korja, A., Korja, T., Luosto, U. and Heikkinen, P. 1993. Seismic and geoelectric evidence for collisional and extensional events in the Fennoscandian shield implications for Precambrian crustal evolution. Tectonophysics, 219, 129-152.

Korja, A., Kosunen, P., and Heikkinen, P. 2009. A case study of lateral spreading: The Precambrian Svecofennian orogen. Geological Society, London, Special Publications, 321, 225-251.

Royden, L. 1996. Coupling and decoupling of crust and mantle in convergent orogens; implications for strain partitioning in the crust. Journal of Geophysical Research, 101, 17-17,705.

Sorjonen-Ward, P. 2006. Geological and structural framework and preliminary interpretation of the FIRE 3 and FIRE 3A reflection seismic profiles, central Finland. Geological Survey of Finland, Special Paper, 43, 105-159.

# Magmatism in northern part of Central Finland granitoid complex

K. Nikkilä[1], I. Mänttäri[2], P. Kosunen[3], O. Eklund[4] and A. Korja[1]

[1]University of Helsinki, Institute of Seismology
[2]Geological Survey of Finland
[3]Posiva Oy
[4]Åbo Akademi University, Geology and Mineralogy
E-mail: kaisa.nikkila@helsinki.fi

In the Paleoproterozoic Svecofennian orogenic domain of the Fennoscandian shield, the large Central Finland Granitoid Complex (CFGC) consists of plutonic rocks and minor amounts of supracrustal rocks. The CFGC has a geological history that is only vaguely known. The metamorphic culmination of the Svecofennian orogen occurred at about 1890 Ma. The resultant magmatism was associated with syn- and post-collisional orogenic events at 1890-1870 Ma and the latest granitoid rocks of the CFGC seem to have intruded into uppermost, brittle part of the crust in an extensional tectonic setting (Nironen et al, 2000). However the age data have been defective in the area and the magmatism have been divided into these orogenic events by using deformation stage. In this study we represent new U-Pb zircon age data from Karstula-Saarijärvi area.

**Keywords:** Svecofennian orogen, U-Pb, zircon, magmatism

## 1. Introduction

The bedrock of the research area is mainly composed of plutonic igneous rocks of granitoid composition (Figure 1). These can be roughly divided into two groups: the typically massive coarse-porphyritic granites (the so-called postkinematic granites, 1885-1875 Ma, Nironen 2003) and the typically foliated, even-grained or porphyritic granites and granodiorites and even-grained tonalites (the so-called synkinematic granitoids, 1890-1880 Ma; Nironen, 2003). Intermediate to mafic plutonic rocks are much more rare and are represented by few small intrusions (gabbroic to quartz dioritic), mainly in the northern part of the area. Relatively felsic rocks dominate also the supracrustal associations of the area. The supracrustal rocks are thought to be slightly older than the synkinematic granitoids (Nironen, 2003).

We have studied the rocks in the northern part of the Central Finland granitoid complex to find out the relationship between different magmatism in the area and to define the syn- and post-collisional events in the area.

## 2. Methods

We have collected 27 sample, which include felsic (sub)volcanic rocks from the Kalmari complex, intermediate volcanic rocks from the Bothnian belt – CFGC boundary, both even-grained and porphyritic granites, diabase, granodiorites, diorite, quartz-diorite and tonalite. In addition of this we have used ca. 150 samples (©GTK) as background data for geochemical purposes.

The U-Pb isotope analyses were made from eight of the samples using the Nordic Cameca IMS 1280 (SIMS) at the Swedish Museum of Natural History, Stockholm. The samples were felsic volcanic and subvolcanic rocks, granodiorites, granite, diorite and tonalite.

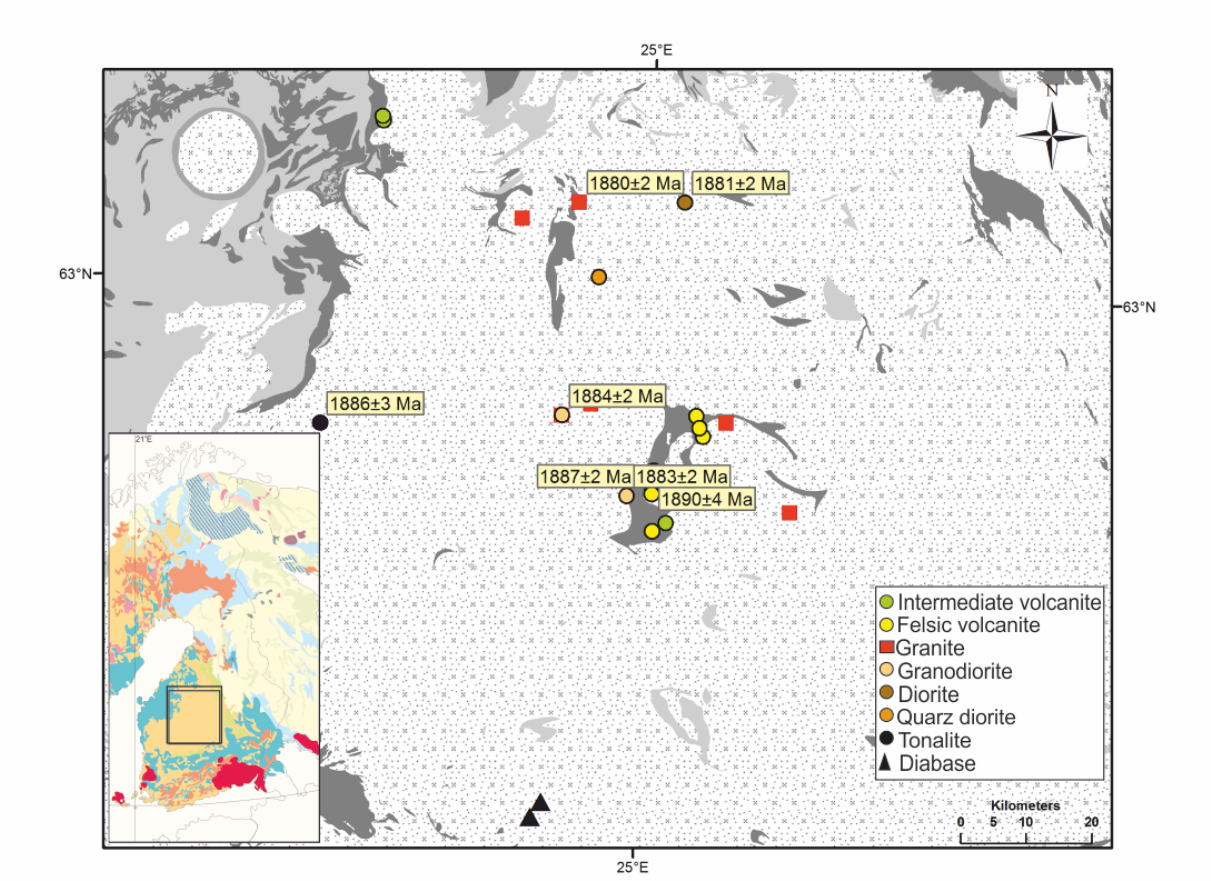


**Figure 1.** Simplified lithological map of Central Finland granitoid complex (CFGC) and the sample locations.

## 3. Results: Geochemistry

The felsic rocks show calc-alkaline trend, are peraluminous and have volcanic arc- pattern. There is a clear relationship between the felsic (sub)volcanic and granitic rocks, although the plutonic rocks are more enriched to the crust. The porphyritic granites have higher SiO2 – content, otherwise the rocks have same trend as other felsic rocks.

Granodiorites are more complex. The rocks are mostly consistent with each other, but not always. Massive granodiorite is closer to tonalite than gneissic granodiorite. However, it seems that granodiorites are more enriched with crustal material than tonalite and forms own group.

Tonalite is metaluminous and show more high-Al TTG series affinity (low-Sr/Y vs Y).

Diorite is clearly from mantle and quartz-diorite presents crustal contaminated version from same source.

Diabases are tholeitic and represents oceanic material.

## 4. Results: U-Pb zircon ages

The results show that different magmatic events show overlapping ages with a decreasing age trend. In general, the tonalite and the (sub)volcanic rocks show "older ages" of 1894-1883Ma, whereas the 1886-1878 Ma dioritic to granitic rocks are the "youngest" ones and are clearly younger that the oldest volcanic rocks (Figure 2).

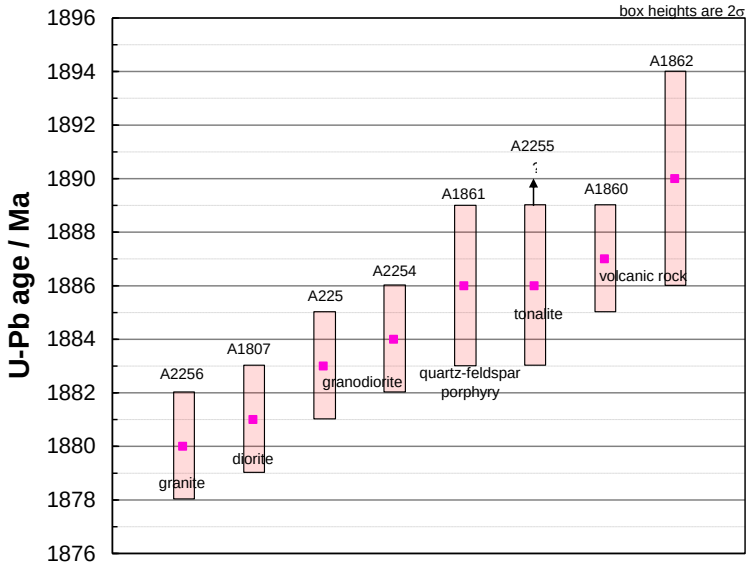


**Figure 2.** Summary diagram of the age results.

## 5. Summary

The geochemistry indicates that the CFGC is a well-developed volcanic arc. Only exception is diabases with MORB characteristics that most probably represent a later extensional event. Clear is that they are not associated with the Kalmari volcanites. The felsic volcanic rocks in the Kalmari complex are all from same source although they differ from structure and texture, and likely the rocks represent both volcanic and subvolcanic sequences.

Felsic plutonic rocks are younger than their supracrustal counterparts. This and earlier studies/unpublished results indicate ca 1880 Ma emplacement ages for deformed, even-grained (synkinematic) and porphyritic granitic (postkinematic) rocks (Rämö et al., 2001). It differs from earlier interpretations, which suggested that the deformed rocks are older (e.g. Nironen 2003). However other studies from CFGC show that the porphyritic granites cross-cut the foliated granites (Elliott, 2001), but we have not found field evidence of that in Karstula area.

In the study area, two types of granodiorite were identified. The typical granodiorite is gneissic and sometimes sheared and the other is massive with intermediate/mafic enclaves. Granodiorites are coeval. Tonalite is the oldest intrusive rock in the area and likely represents syncollisional magma. The tonalite is massive and both massive granodiorite and tonalite may represent undeformed blocks or upper crustal exhumation level whereas the deformed granodiorite represents deeper crustal level.

## References:

Elliott, B.A., 2001. The Petrogenesis of the 1.88-1.87 Ga Post-kinematic Granitoids of the Central Finland Granitoid Complex.

Nironen, M., 2003. Keski-Suomen Granitoidikompleksi, Karttaselitys. Summary: Central Finland Granitoid Complex - Explanation to a map. Geological Survey of Finland, Report of Investigation, 157, 45 p.

Nironen, M., Elliott, B.A. and Rämö, O.T., 2000. 1.88–1.87 Ga postkinematic intrusions of the Central Finland Granitoid Complex: a shift from C-type to A-type magmatism during lithospheric convergance. Lithos, 53, 37–58

Rämö, O.T., Vaasjoki, M., Mänttäri, I., Elliott, B.A. and Nironen, M., 2001, Petrogenesis of the post-kinematic magmatism of the Central Finland Granitoid Complex I; radiogenic isotope constraints and implications for crustal evolution Journal of Petrology, 42, 1971-1993.

# High quality flake graphite in the Fennoscandian shield

J. Palosaari[1], S. Raunio[1], R. Rundqvist[1], R-M. Latonen[2], J-H. Smått[3], R. Blomqvist[4] and O. Eklund[1]

[1] Department of Geology and mineralogy, Åbo Akademi University
[2] Laboratory of analytical chemistry, Åbo Akademi University
[3] Laboratory of physical chemistry, Åbo Akademi University
[4] Fennoscandian Resources Oy
E-mail: jenny.palosaari@abo.fi

**Keywords:** flake graphite, graphite, high-P/high-T metamorphism, Fennoscandia

In 2013, the European Commission defined 20 raw materials fundamental to Europe's economy based on the Economic importance and the supply risk of the materials. One of these "critical" raw materials is NATURAL GRAPHITE[1]. Natural graphite can be sub-divided into amorphous graphite, flake graphite and vein graphite. Among these graphite types, flake graphite can be used for several applications like batteries, carbon brushes, heat sinks, coated conductors, lubricant additives, pencils, refractory applications, graphite shapes, coated conductors brake pads, clutches, foundry applications, powder metallurgy, drilling mud additives, nuclear reactors, flame retardants, synthetic diamonds and – not but not least – raw material for graphene[2].

The demand for graphite is enormous. Paul Gorman, CEO at Great Lakes Graphite state in an interview in Market Watch sept 16 2014 that "With the advancement of battery storage, mobile battery systems and alternative energy infrastructure, it is estimated that 20 new graphite mines will be required to keep up with demand by the year 2020"[3].

The conversion from amorphous graphite to flake graphite takes place during metamorphism in amphibolite to granulite facies. The Fennoscandian shield is a Precambrian shield area where extensive parts of the bedrock have been exposed to high grade metamorphism. This means that a major part of the graphite schists (or black schists) may have developed flake graphite. Previously, the black schists in the Fennoscandian shield have been the target for exploration, since the black schists use to be the trap for sulphide ores. Because of this, it exist a lot of information from black schist areas (maps, drill cores, analyses). However, our project is looking for graphite rich areas depleted in sulfides to get flake graphite with as high quality as possible from the bedrock. Recently, flake graphite mines have opened in Norway and Sweden in areas where the geology is similar to the geology in Finland. For this reason, there is a future for flake graphite exploration in Finland.

Since 2012, a project between the companies Norwegian graphite, Fennoscandian resources Oy and Åbo Akademi University (Geology and mineralogy, Physical- and Analytical chemistry) have developed a route for flake graphite research – from exploration to nanotechnological applications (financed by K.H. Renlund foundation). The most important results from this project are:

- There are potential ores in the Fennoscandian shield for flake graphite exploration
- Some of these areas contain up to 28% flake graphite
- High quality flake graphite appears in areas with high metamorphism (figure 1).

- The lattice parameters of high quality flake graphite are identical to the theoretical parameters for flake graphite. I.e. The flake graphite consists of infinite layers of graphene. The lattice parameters are determined with XRD and Raman spectrometry.
- By using electric shock waves, the graphite ore is gently fragmentized with few damages on the flake graphite grains
- By using the Haarla flotation route, the end product is close to pure flake graphite.

Our research indicates that the hypothesis "the higher metamorphic area – the higher quality of flake graphite" is correct. Until now, the highest quality flake-graphite was found in the Vesterålen area in north western Norway, where the metamorphism reached granulite facies (Palosaari, 2014). Current research indicates that high metamorphic areas in eastern Finland will give similar results as the findings in Norway.

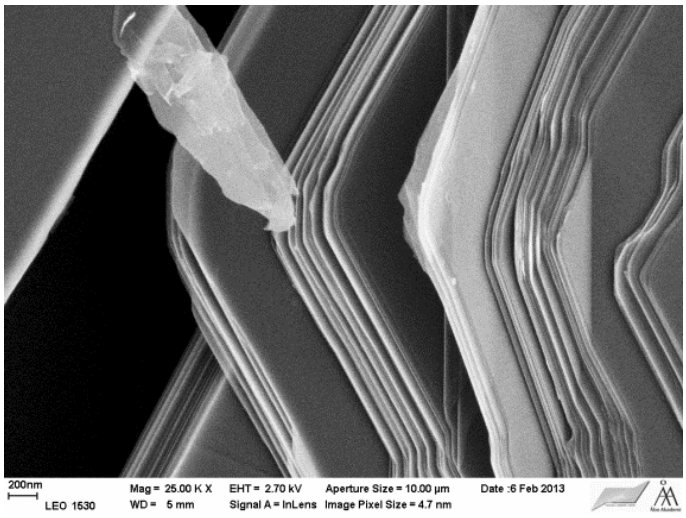


**Figure 1**. SEM image of high quality flake graphite from a granulite facies area in eastern Finland.

## References:

[1] http://ec.europa.eu/enterprise/policies/raw-materials/critical/index_en.htm
[2] European Commission: Report on critical raw materials for the EU, critical raw material profiles http://ec.europa.eu/enterprise/policies/raw-materials/files/docs/crm-critical-material-profiles_en.pdf
[3]http://www.marketwatch.com/story/tesla-gigafactory-will-require-8-new-graphite-mines-great-lakes-graphite-is-fast-tracked-to-production-2014-09-16
Palosaari, J., 2014. Flakgrafit i Sortland, nordvästra Norge. Master's thesis. Åbo Akademi University.

# Structural evolution of the southern part of the Peräpohja Belt in the Tornio region, northern Finland

Simo Piippo[1], Maiju Kaartinen[2] and Pietari Skyttä[2]

[1]Deparment of Geosciences and Geography, 00014 University of Helsinki, Finland
[2]Department of Geography and Geology, 20014 University of Turku, Finland
E-mail: pietari.skytta@utu.fi

The work reported here aims at defining the structural geology of the southern part of the Peräpohja Belt for the purposes of belt-scale structural interpretations and structural restorations within the belt. Potential variations in the thickness of the supracrustal units could be used for recognition of normal faults that acted as pathways for mineralizing fluids. This work relates to an ongoing research project focusing at understanding the structural control of mineral deposits in the Peräpohja Belt by the means of structural analysis and 3/4D-modelling.

**Keywords:** structural analysis, 3/4D-modelling, Peräpohja Belt, Archaean, Palaeoproterozoic

## 1. Introduction

The Peräpohja Belt in Northern Finland comprises Palaeoproterozoic supracrustal rocks deposited on the Archaean basement. On the metallogenetic map of Finland, the belt is identified as a critical Cu (± Au) province (Eilu et al., 2013), with potential for large-scale stratabound copper deposits (Hitzman et al., 2010; Kyläkoski et al., 2012). Evolution of the Peräpohja Belt as a Palaeoproterozoic basin is inferred to comprise syn-depositional extension in a failed rift setting (Kyläkoski et al., 2012), characterized by normal faulting. When the extension subsequently shifted to shortening, the original growth faults were inverted, which makes their identification difficult. For this reason, only 4D-modelling will enable us to understand the coupling between the deformation structures and the stratigraphy, and hence outline the inverted or reactivated normal faults. As the normal faults are considered the main pathways for fluid flow through the crust, they can, after successful recognition, be used as exploration targets for Cu (+Au). An additional aspect to the modelling is given by a working hypothesis attributing the structural discontinuities within the Peräpohja Belt to deformation along major shear zones within the underlying Archaean basement.

The work reported here aims at defining the structural geology of the southern part of the belt for the purposes of belt-scale structural interpretations and structural restorations aiming at recognition of thickness variations of supracrustal units. Furthermore, the work also aims at geological correlations across the national border between Finland and Sweden; this part of the work will be supported by geochemistry and geochronological data processed during the progress of the project. Selection of the study area is based on the vicinity of the Archaean-Proterozoic contact and the potential to correlate the structures with potential basement deformation characteristics (Skyttä et al., 2014) and deformation patterns in structural domains with a similar setting further east (Nieminen et al., 2014).

## 2. Data and methods

Field work within this project aims at i) evaluating the reliability of the existing structural data for the modelling purposes and ii) collecting new data for developing the understanding on the structural geometry and evolution of the southern part of the belt. After data validation, structural analysis will proceed to compilation of form line maps (Fig. 1) and building of 3D-models (Fig. 2), based on structural point data and geophysical maps and profiles. Future

modelling aims at restoring the younger deformation events masking the older ones, and at providing alternative solutions to explain the crustal evolution in the area.

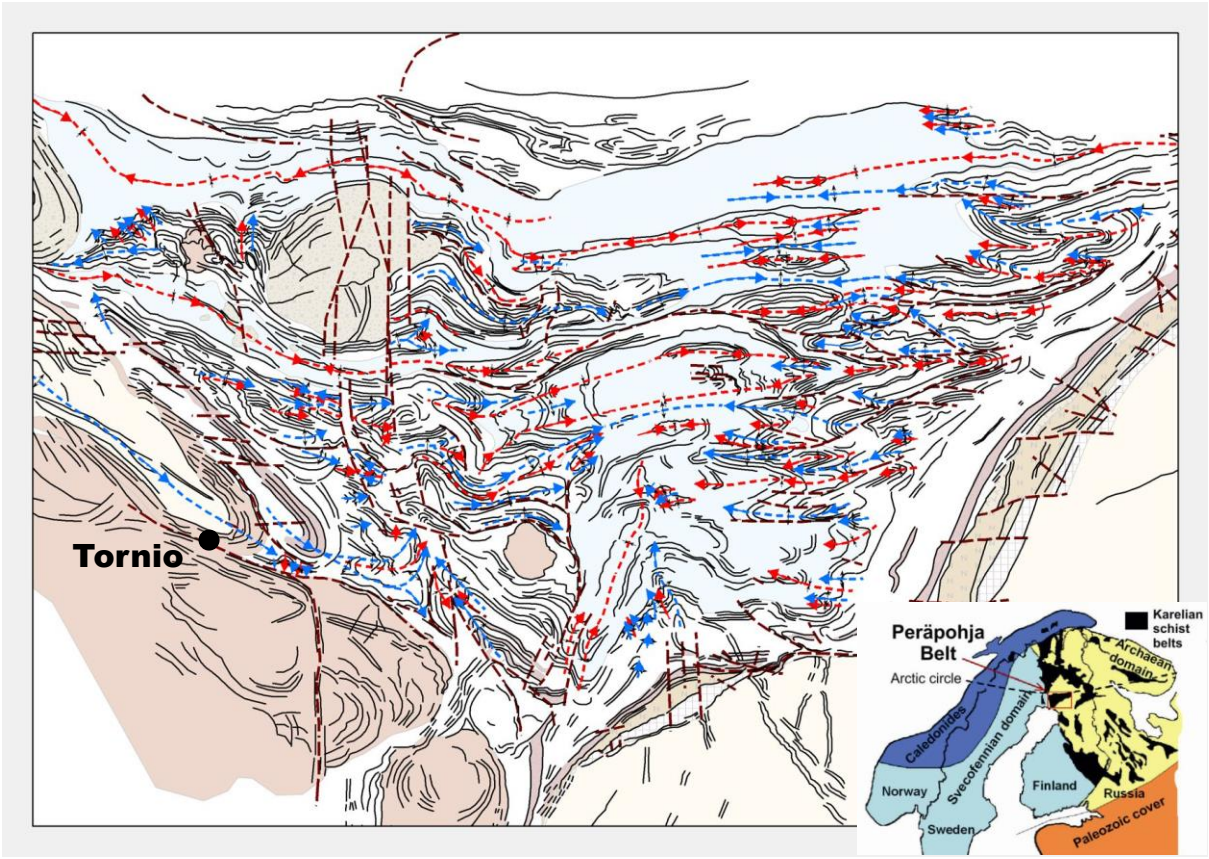


**Figure 1**. A form line draft of the southern part of the Peräpohja Belt illustrating the systematic pattern of curvilinear anti- and synclines (blue and red dashed lines) and larger faults and shear zones (dashed brown lines). The thin lines stand for lithological contacts and magnetic form lines. Inset: Location of the Peräpohja Belt (Kyläkoski, 2007).

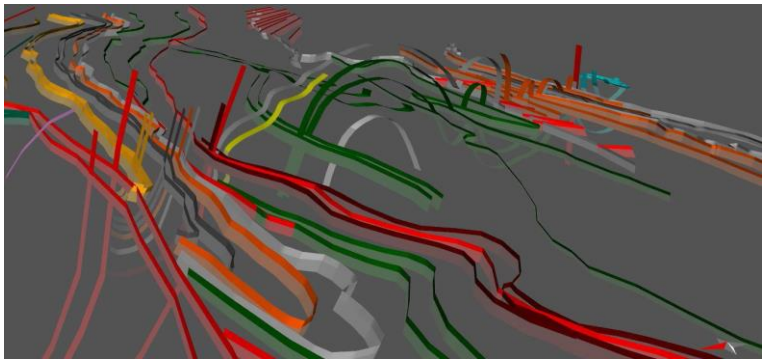

**Figure 2**. A preliminary 3D-model illustrating the structural geometry related to the main folding of supracrustal rocks in the Peräpohja Belt.

### 3. Preliminary results and discussion

Initial analysis of the Peräpohja rocks in the study area indicates that the map-scale folds are dominantly asymmetric with vergences towards SSW to SSE, and spatially closely associated

with reverse faults. Based on the form line interpretations (Fig. 1), the dominant fault population occurs parallel with the axial traces of the folds. In the central parts of the study area, away from the contact with the Archaean basement, the axial surfaces are roughly planar but the axes show variable curvatures leading to repeated axial culminations and depressions, nonetheless all attributed to one deformation event. In this structural domain, fold axes are characteristically sub-vertical, which we link to sub-vertical tectonic transport, tentatively attributed to corner flow within the triangular area defined by the Proterozoic-Archaean contacts in the SW and SE. Towards the contact with the Archaean rocks in the SW and NE, the axial surfaces curve and deflect towards parallelism with the contact while the fold axes are moderately to gently plunging.

Observations on the mineral composition and texture of rocks units on both the Finnish and Swedish side allow making the following correlations (see also Bergman et al., 2014): Sockberget Group – Kvartsimaa and Palokivalo formations; Råneå Group – Martimo Formation; Vitgrundet formation – Rantamaa formation; Lina Suite – Kierovaara granite.

Summing up, the observations indicate that folding within the Peräpohja Belt is controlled by reverse faults, compatible with southward directed thrust-like deformation. Furthermore, as the NW-SE striking domal structures close to Tornio are continuous from Finland to Sweden, and the style and geometries of folds above the Archaean basement are similar along both the SE and SW margins of the Peräpohja Belt, we infer that the southern part of the Peräpohja Belt was initially symmetric. This is in contrast to the dominant WSW-ENE strike of the Proterozoic-Archaean contact further east.

The work conducted in the near-future will concentrate at detailed correlation of shear zones across the study area, defining the pattern of strain localisation, transitions in the metamorphic grade across the area, and more detailed constraints on the stratigraphy of the Martimo formation, the under- and overlying units and its potential interlayers.

**Acknowledgements**

K. H. Renlund foundation is acknowledged for financial support for the project, First Quantum Minerals Ltd. for funding the field work and Mawson Resources for access to research data. Thanks to Midland Valley Exploration Ltd. for the use of MOVE™ modelling software under the Academic Software Initiative.

**References:**

Bergman, S., Bergström, U., Bastani, M., Jönberger, J., Juhojuntti, N. and Johansson, P., 2014. Regionalkartering i kartområdet 25N Haparanda, tidigare arbeten och resultat från fältarbetet 2013. SGU-rapport 2014:07, 30 pp. (in swedish)

Eilu, P., Bergman, T., Bjerkgård, T., Feoktistov, V ., Hallberg, A., Korsakova, M., Krasotkin, S., Litvinenko, V., Nurmi, P.A., Often, M., Philippov, N., Sandstad, J.S. and Voytekhovsky, Y.L . (comp.) 2013. Metallic Mineral Deposit Map of the Fennoscandian Shield 1:2 000 000. Revised edition. Geological Survey of Finland, Geological Survey of Norway, Geological Survey of Sweden, The Federal Agency of Use of Mineral Resources of the Ministry of Natural Resources of the Russian Federation.

Kyläkoski, M. 2007. Nickel, Copper and Platinum-Group Element Ore Potential of the Jouttiaapa 1137 Formation, a ca. 2.1 Ga Continental Flood Basalt Sequence in the Peräpohja Belt, Northwestern Finland. Licentiate Thesis, Department of Geosciences, University of Oulu, 204 pp. (in Finnish with English abstract).

Kyläkoski, M., Hanski, E. and Huhma, H., 2012. The Petäjäskoski Formation, a new lithostratigraphic unit in the Palaeoproterozoic Peräpohja Belt, northern Finland. Bulletin of the Geological Society of Finland, 84, 85–120.

Nieminen, V., Skyttä, P., Piippo, S., Huovinen, I. and Kilpeläinen, T., 2014. The structure of the Kakari area with implications to the structural evolution of the Palaeoproterozoic Peräpohja Belt, Northern Finland. The 31st Nordic Geological Winter Meeting, Lund, Sweden, January 8-10, 2014.

Skyttä, P., Nieminen, V., Kilpeläinen, T., Piippo, S., Käpyaho, A., Lauri, L., Huovinen, I., Lehtilä, T. and Kinnunen, J., 2014. The structural control of mineral occurrences in the Peräpohja Belt, northern Finland. Finnish National Colloquium of Geosciences, March 19.-20. 2014, Espoo, Finland.

# X-ray computed micro-tomography: a holistic approach to metamorphic fabric analyses and associated mineralization

Mohammad Sayab[1], Jussi-Petteri Suuronen[2], Pentti Hölttä[1], Raimo Lahtinen[1], Niilo Karkkainen[1] and Aki Petteri Kallonen[2]

[1]Geological Survey of Finland, P.O. Box 96, FI-02151 Espoo, Finland
[2]Department of Physics, University of Helsinki, PO Box 64, 00014 Helsinki, Finland
Email: sayab.muhammad@gtk.fi

## 1. Introduction

Much of our knowledge about crust and upper mantle dynamics is based on the study of metamorphic minerals, their textures and associated microstructures (e.g., Sayab, 2008). Particularly, porphyroblasts represent a unique record of the pressure-temperature (P-T) evolution of a rock linked to its tectono-thermal history (e.g., Vernon, 2004). The large majority of this research is based on the study of petrographic (polished) thin sections with the optical microscope, SEM, or microprobe. An intrinsic limitation of these tools is their inability to directly visualize microstructures and associated metamorphic textures in three dimensions (3D). At best, the spatial 3D geometry of rocks can be inferred via the combination of 2D data from multiple thin sections. The traditional use of horizontal (H), P- and N-sections (parallel and normal to the stretching lineation, respectively) largely falls short in these situations. The lack of full 3D control commonly introduces ambiguity in microtectonic interpretations.

Recent technical advancements have added a new promising tool to existing microstructural methods: Computed micro-tomography (CT) with high energy X-rays. The main advantage of the technique is that it allows metamorphic microstructures and associated minerals to be directly visualized in 3D at optimal resolution (e.g., Huddlestone-Homes and Ketcham, 2010) thereby eliminating the interpretative procedures associated with conventional methods. This technique is non-destructive and provides detailed 3D spatial imagery of the internal architecture of a rock by measuring the attenuation of X-rays as they pass through different mineral phases (Ketcham and Carlson, 2001). In addition to 3D spatial images, unlimited serial cross-sections at different angles can be generated as a new kind of virtual petrographic sections. Here, we demonstrate the potential use of this new method and applied to drill core samples from the classical Orijärvi region and Uunimäki area, southern Finland. Through virtual scrolling, either horizontally or vertically, along or across the foliation using advance image processing software, the 3D shape of metamorphic fabrics can be visualized, and thus provides a new "holistic" approach for detailed microstructural analysis. We also show how the high resolution X-ray computed micro-tomography (HRXCT) is particularly well suited to resolve the spatial distribution of microstructural controls on sulfide minerals. Such data extrapolated to regional-scale structures is highly relevant to the targeting of ore deposits.

## 2. Sample description

Sample O1 is a 2.5 cm diameter, 14 cm long andalusite-mica schist, vertically drilled from the Orijärvi area, southwest Finland (Finnish National Grid coordinates: 6686250, 3308859). The drill core sample is characterized by a steeply ($78^{o}$) south dipping, E-W striking pervasive

foliation lies at an acute angle to S0. The foliation is associated with regionally developed upright folds formed as a result of a broadly N-S directed shortening phase of the early Svecofennian orogeny dated ca. 1875 Ma (Skyttä et al., 2006). In outcrop the main S1 foliation can be seen to be overprinted by a widely-spaced, subvertical S2 foliation striking NE-SW. Mineral assemblage such as andalusite and sillimanite in the studied sample clearly indicate high temperature (HT) amphibolite facies metamorphic conditions (Eskola, 1914).

Two phases of andalusite porphyroblasts have been recognized in the horizontal and vertical oriented thin sections (Figure 1). Porphyroblast rims include well aligned, mainly needle shaped inclusion trails that are generally continuous with the intensely developed matrix foliation. Porphyroblast cores are more densely populated with mineral inclusions but these are mainly equidimensional and do not exhibit a preferred orientation.

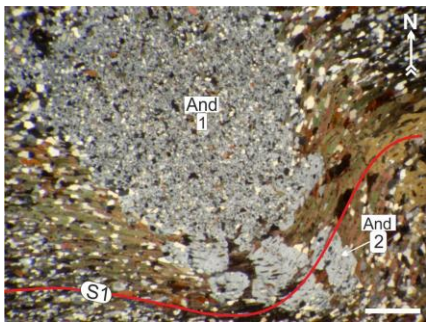


**Figure 1.** Oriented photomicrograph of horizontal thin section through the drill core. Andalusite core (And-1) preserves unoriented, mostly equidimensional inclusions, whereas rim (And-2) contains well aligned inclusions that can be followed into the matrix (S1).

Sample R41 is a 4.05 cm diameter and length, gabbroic rock and obtained from the borehole R41 of the Uunimäki area, representing depth of 89.63-89.73 meters. The inclination, with respect to horizontal surface, and azimuth of the borehole (R41) are 45° and 225, respectively.

## 3. X-ray computed micro-tomogrpahy

HRXCT can precisely image the interior of solid materials such as rocks. The scanner generates a series of grayscale radiographs of a given rock sample, which are then reconstructed into a 3D volumetric images. The gray value of each cubic volume element, or voxel, reflects the relative linear X-ray attenuation coefficient, which is dependent on the density and average atomic number of the mineral, and X-ray energy. The 3D volume can be viewed as individual cross-sectional images (slices) or a 3D rendering, and quantitatively analyzed with 3D image processing techniques.

The HRXCT used in this study is the Nanotom 180 (Phoenix|x-ray systems and Services, Germany, now part of GE Measurement Systems and Solutions) hosted in the University of Helsinki, Department of Physics. X-rays from a tungsten target were used with the X-ray tube voltage set to 160 kV, the beam current set to 120 µA, and 0.5 mm of copper used to filter the X-ray beam. For sample O1 and R41, voxel size of 14×14×14µm and 85×85×85µm were used, respectively.

## 4. 3D analyses of sample O1

The CT data was processed in Avizo®Fire software with built-in algorithms for 3D visualization and rendering. Contrasting grayscale values allowed to segment and separate andalusite porphyroblasts and their inclusions, sulfides, quartz and mica in the matrix. The

brightest grains are sulfides, followed by mica, and the darkest are andalusite and quartz (Figure 2). N-S and E-W vertical sections (Figure 2) cutting andalusite porphyroblast rims reveal steeply pitching S1 inclusion trails subparallel to matrix S1. Vertical and horizontal slices oriented perpendicular to the matrix foliation exhibit tight F1 folding of relic sedimentary bedding (S0) with steeply south-dipping axial planes parallel to S1.

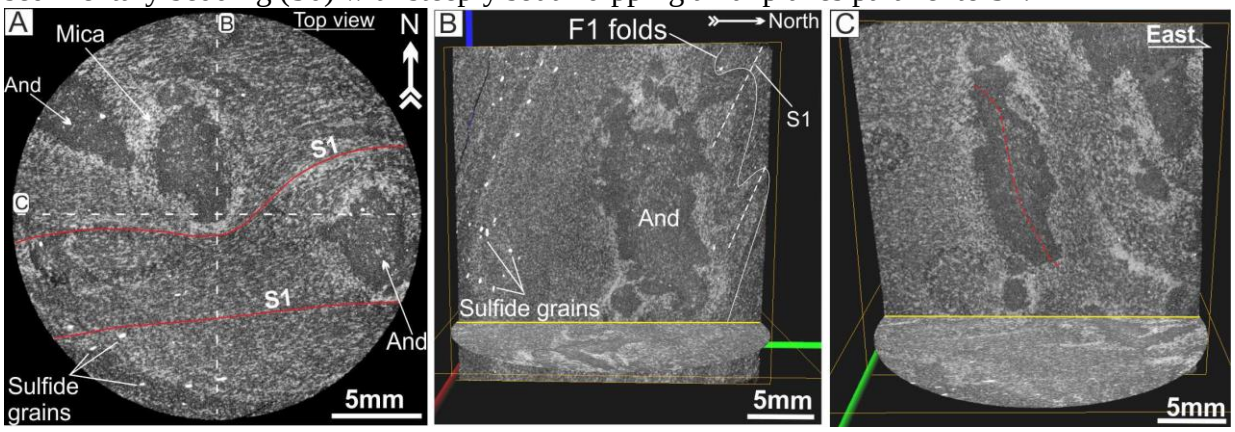


**Figure 2.** Different 3D representations of HRXCT data. (A) Horizontal slice showing three andalusite porphyroblasts localized in the northern layer versus sulfide grains in the southern layer. (B) Vertical slice perpendicular to the matrix foliation showing F1 folds. (C) Vertical slice parallel to the matrix foliation and through a porphyroblast rim with steeply pitching inclusion trails.

In all horizontal slices of the drill core, andalusite porphyroblasts are preferentially aligned WNW-ESE (Figure 2A), whereas the matrix foliation (S1) anastomose around them. The 3D imagery evidences two separate WNW-ESE striking layers within the drill core. The southern layer totally lacks porphyroblasts but contains numerous small sulfide grains (~100-1000µm in size) that are preferentially distributed along and orientated parallel to the matrix foliation (Figure 3A,B). The northern layer hosts andalusite porphyroblasts but only scarce sulfide grains.

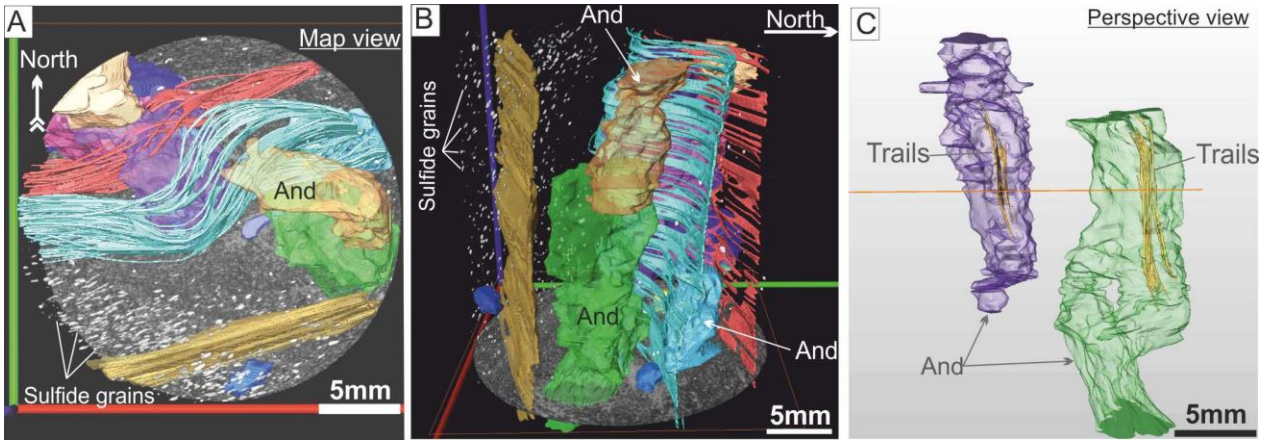


**Figure 3.** 3-D reconstruction of HRXCT data. Data is segmented and colored manually to differentiate objects of interest. (A-B) Map view of the drill core showing anastomose foliation around andalusite, whereas in the south the foliation is straight. 3D rendering of andalusite porphyroblasts (tabular shape), matrix foliation and distribution of sulfide grains in map (A) and perspective view (B). (C) Two andalusite porphyroblast with steeply pitching inclusion trails in their rim. Andalusites are elongated in vertical direction.

Andalusite porphyroblasts are mostly tabular but show strong elongation in vertical direction (Figure 3C). The largest porphyroblast measures 18×5×4mm and has a core containing un-oriented inclusions surrounded by a rim with well aligned inclusions (Figure 3). This microstructure indicates that prior to development of the steeply dipping foliation during F1 folding, no metamorphic fabric or a very weak one existed in the rock. Thus, initial rapid growth of andalusite-cores is indicated controlled by relatively high temperature metamorphism while a steeply dipping E-W striking regional foliation (S1) progressively developed, intensified against porphyroblast margins and was eventually included the rim zone.

## 4. 3D analyses of sample R41

In this drill core sample, the sulfide grains are spatially distributed along veins and fractures. The sulfide grains vary in size and shape, and show slight variations in their gray-scale values (Figure 4), indicating different types of sulfides. Orthogonal slices across the drill core exhibit complex fracturing network and associated mineralization.

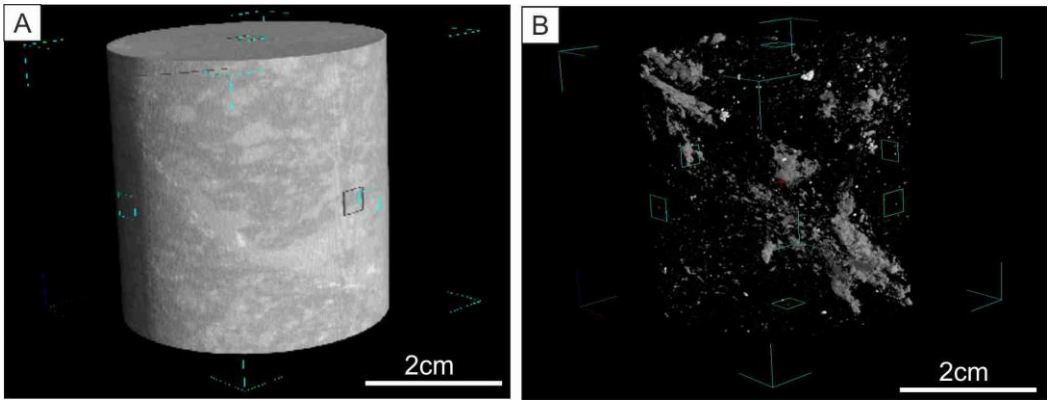


**Figure 4.** (A) 3D rendered volume of sample R41. (B) 3D distribution of sulfide grains.

## 5. Concluding remarks

X-ray computed micro-tomography is a relatively new promising tool in the field of geological sciences. Its applications are well-known and add significant knowledge in our understanding of geological phenomena at high resolution. Our new data is the first to report HRXCT results as applied to centimeter scale, poly-deformed, drill core samples to illuminate their internal architecture and revealed a number of in-situ 3D aspects, which are not possible via conventional methods.

## References:

Eskola, P., 1914. On the petrology of the Orijärvi region in southwestern Finland: bulletin de la Commission Géologique de Finlande, Vol. 40, 277 pages.

Huddlestone-Holmes, C. R., and Ketcham, R. A., 2010. An X-ray computed tomography study of inclusion trail orientation in multiple porphyroblasts from a single sample. Tectonophysics, 480, 305-320.

Ketcham, R. A., and Calrson, W. D., 2001. Acquisition, optimization and interpretation of X-ray computed tomographic imagery: applications to the geosciences. Computer & Geosciences, 27, 381-400.

Sayab, M., 2008, Correlating multiple deformation events across the Mesoproterozoic NE Australia using foliation intersection axes (FIA) preserved within porphyroblasts. Gondwana Research, 13, 331–351.

Skyttä, P., Väisänen, M., and Mänttäri, I., 2006. Preservation of Palaeoproterozoic early Svecofennian structures in the Orijärvi area, SW Finland – evidence for polyphase strain partitioning. Precambrian Research, 150, 153-172.

Vernon, R. H., 2004. A practical guide to rock microstructures, 606 p.

# Thermobarometric study on genesis of Ca-Ti-rich micas in shoshonitic lamprophyres in Fennoscandia

S. Sjöblom

Department of Natural Sciences, Geology and mineralogy, Åbo Akademi University, Turku, Finland,
E-mail: sonsjobl@abo.fi

The aim was to study the thickness of the lithosphere at the boundary between the Archean craton and Svecofennian Domain and the circumstances that dominated its lower parts during its formation. Studied material was a shoshonitic lamprophyre with feldspar and Ti-rich mica in matrix. The formation process was done in reverse and the circumstances were studied by using the needlelike titanite lamellae found in the biotites. The attempt was to find the ideal P/T-circumstances for the titanite to be forced back into the lattice. Experiments were done in the high-pressure laboratory of The Natural History Museum in Oslo with an End-loaded Piston-cylinder Apparatus. Results showed several kinds of re-crystallisations as was expected. The results indicated that the lamellae have formed in relatively low temperatures (800℃) and high pressures (2,5 GPa) which suggests that the genesis of the titanite lamellae has taken place in depths around 85 - 90 kilometres.

**Keywords:** Titanite, Fennoscandian shield, thermobarometer, lamprophyre, biotite, shoshonitic

## 1. Introduction

The study on lamprophyres at the boundary between the Archean craton and the Svecofennian Domain (Woodard 2010) (Figure 1) gave grounds to begin studies concerning the thickness of the lithosphere and the circumstances that dominated in its lower parts during the formation. It was possible to reverse the formation process and study the circumstances by using biotites from shoshonitic lamprophyres because of the needlelike titanite lamellae found inside each biotite crystal.

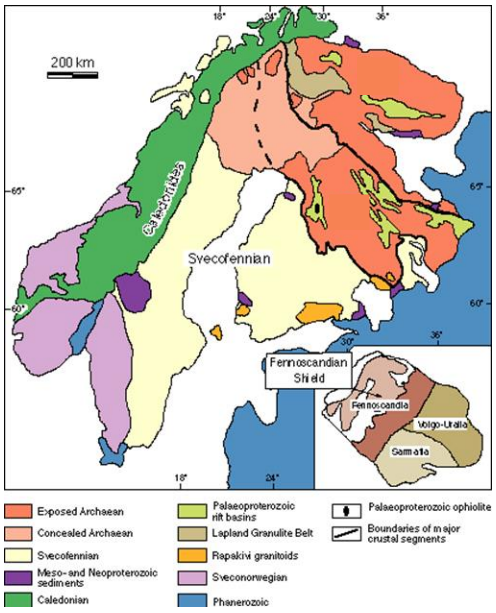


**Figure 1.** Simplified geological map of the Fennoscandian Shield. Modified after SVEKALAPKO Evolution of Palaeoproterozoic and Archaean Lithosphere by Sven-Erik Hjelt (Oulu), Stephen Daly (Dublin) and SVEKALAPKO colleagues. (www.geofys.uu.se)

The goal was to determine the limits for the circumstances that formed the examined lamprophyres. As the titanite would be forced back in the lattice, the result would be a homogenised Ca-Ti-rich biotite. The re-creation of the environment where Ca-Ti-micas were formed was therefore done in reverse compared to the actual genesis.

Similar lamprophyres from the Palaeoproterozoic era are found in several locations in Finland and in Russia (Eklund et al 1998, Woodard 2010), mostly occurring on the boundary areas between the Archean craton and the Svecofennian Domain (Woodard 2010). As a result of extension, the lamprophyres intruded the upper crust about 1,8 Ga ago (Eklund et al 1998). Despite metasomatism, the original composition can still be determined and therefore it gives exact information about the mantle it originated from.

## 2. Material

Studied material was a shoshonitic lamprophyre with feldspar and Ti-rich mica in matrix. The sampled dyke is located an island called Pieni-Vinkki in Lake Vuotjärvi, located in North Savo in Finland. The sample is a kind of a shoshonitic lamprophyre that has biotite as the dominant mafic mineral and feldspar as matrix phase, therefore it is termed a minette. The sampled bulk rock has a porphyritic nature with a fine-grained matrix (mainly consisting of biotite). Lamellae of titanite are visible in all sampled biotite grains.

Ca-Ti-rich mica was also found as phenocrysts (Woodard 2010). The study exploited the titanite lamellae that were found in each sampled biotite crystal. The distribution of the titanite-inclusions varied in each crystal, but quantitatively the amounts were enough that all the biotite crystals were usable for experiments.

## 3. Methods

Experiments were done in the high-pressure laboratory of The Natural History Museum in Oslo with an End-loaded Piston-cylinder Apparatus. Bulk rock analyses had been done in previous studies (Woodard 2010) and an estimation on the depth where the titanite lamellae have most likely formed into the biotites was calculated. Experiments in Oslo were done in varying temperatures (800-1100℃) and pressures (1-2,5 GPa). Studying the results of the experiments in a Scanning Electron Microscope (SEM) gave limit values for P/T-conditions that had been necessary for the titanites to form lamellae into the biotites.

## 4. Results

Homogenized mica seems to focus on an area where the conditions are under high pressure and relatively low temperature. Pressure on all the samples showing homogenisation is around 2.5 GPa and the temperatures stay under 1000℃. Results on the sample from 1000℃ show partial homogenisation despite the correlating time and pressure compared to the sample that was completely homogenised at 800℃. Therefore a pervasive and successful homogenisation requires that the temperature is significantly lower than 1000℃. According to the results the ideal temperature is more likely closer to 800℃. Pressure was a significant factor in the homogenisation process. Some indication of homogenisation was found on samples done at pressure of 2.0 GPa but they were not successful enough to be presented as homogenised micas.

The phase diagram by Thomsen and Schmidt with the minimum T for mica breakdown being 900℃ in 2.5 GPa (Woodard 2010) correlated with the results that were interpreted based on the experiments with PSA. No experiment was done in T(℃) = 900/P(GPa) = 2.5 but several experiments were done around it and the point that gave the most homogenised result was received in T(℃) = 800/P(GPa) = 2.5. At these circumstances some lamellae had gone back to the lattice while some showed shrinkage. Another sample showing incipient

homogenisation was found at T(℃) = 1000/P(GPa) = 2.5, which also correlates with the studies by Thomsen and Schmidt. Because every successful sample was done in 2.5 GPa it was possible to calculate the assumable depth for the genesis of the exsolutions to be around 85 – 90 kilometres (after Winter 2001). The results gained by this study also correlate with the results Kukkonen and Peltonen gained in their studies concerning xenolith-controlled geotherms (Kukkonen 1999). According to their results, as the pressure has been 2.5 GPa and the temperature around 800 °C, the formation depth of the titanite lamellae has been around 90 km (Figure 2).

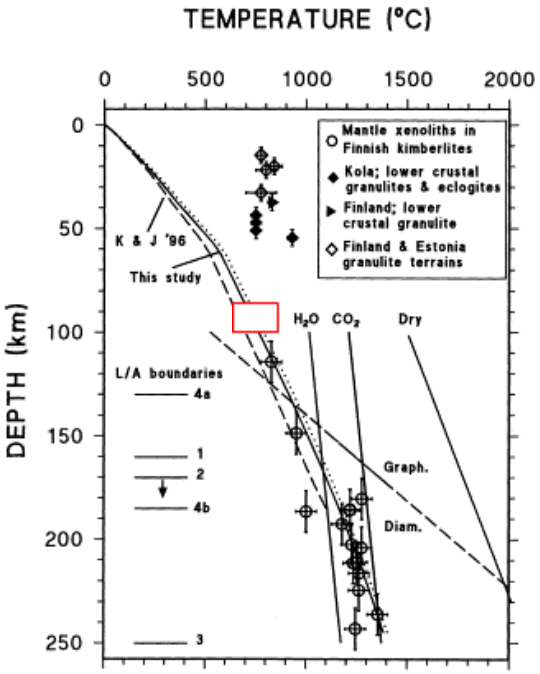


**Figure 2.** Geothermobarometry and geotherms, the result area of this study marked with a red box. (Modified after Kukkonen 1999)

## 5. Conclusions

Based on this study and the experiments, the following conclusions can be drawn:

1. High pressure at minimum 2.5 GPa is required to make the titanite lamellae to get into the lattice and produce a homogenised mica.
2. The temperature needs to be between 800 – 1000 °C degrees to enable homogenisation but to avoid melting of the lamellae.
3. The genesis of the titanite lamellae has taken place in depths around 85 - 90 kilometres.
4. The results of this study support previous definition of circumstances for mica breakdown.
5. A Piston-cylinder Apparatus and SEM are suitable equipment to carry out this type of experiments and to get results.

6. Fe and Mg contents of the experimented micas vary highly despite that the samples are from the same sampled area.

7. Based on the presence of some unexpected minerals it may have been in order to also experiment with bulk rock. Comparing possible differences in the results would require more experiments.

The titanite exsolution lamellae disappeared from the investigated micas at a minimum of 2.5 GPa and 800–1000 °C. This means that the 1760 Ma lamprophyres stem from a source situated at least 85-90 km depth with a temperature between 800 and 1000 °C.

**References:**

Eklund O., Konopelko, D.,Rutanen, H., Fröjdö, S. and Shebanov, A.D., 1998. 1.8 Ga Svecofennian post-collisional shoshonitic magmatism in the Fennoscandian shield. Lithos, 45, 87-108.

Kukkonen, I.T., and Peltonen, P., 1999. Xenolith-controlled geotherm for the central Fennoscandian Shield: implications for lithosphere-astenosphere relations. Tectonophysics, 304, 301-215.

Winter, J. 2001. An introduction to igneous and metamorphic petrology. Upper Saddle River, Prentice-Hall. 699 p.

Woodard, J., 2010. Genesis and Emplacement of Carbonatites and Lamprophyres in the Svecofennian Domain. Academic Dissertation, University of Turku, Finland. 175p.

# Bedrock structures controlling the spatial occurrence and geometry of glacial deposits; example from First Salpausselkä, Hyvinkäänkylä, Finland

Pietari Skyttä[1] and Kirsti Korkka-Niemi[2]

[1]Department of Geography and Geology, 20014 University of Turku, Finland
[2]Deparment of Geosciences and Geography, 00014 University of Helsinki, Finland
E-mail: pietari.skytta@utu.fi

This paper exemplifies how the location and geometry of glacial deposits in southern Finland have been controlled by deformation structures of the underlying bedrock. For this reason, future investigations related to the structure of the glacial deposits, which serve as significant aquifers, are encouraged towards an integrated approach linking the structures, and their reactivations, within the basement (bedrock) and the cover (Quarternary deposits).

**Keywords:** structural geology, shear zones, bedrock surface, qlacial deposits, digital elevation models

## 1. Introduction

The control of bedrock structures over the localisation of Quarternary deposits, in particular the glacial deposits, has been long known (Okko, 1962; Palmu, 1999). Due to the societal significance of many of the deposits which act as major aquifers, it is essential to understand not only the locations but also the volumes and internal structures of the deposits. For these reasons, this study aims at showing how interpretations on the regional-scale structures of the bedrock may be applied at more local scales in modelling the glacial deposits. In specific, we illustrate the linkage between the map patterns of the deposits and the discontinuities within the underlying bedrock as revealed by the morphology of the bedrock surface underneath the Quarternary deposits.

Furthermore, we investigate which types of deformation structures should be considered in aquifer modelling, and discuss how the discontinuities in glacial deposits could be linked with the geometry and kinematics of shear zone systems transecting the crust. This study utilizes GIS data freely available from public sources, including digital elevation models, and constraints on the topography of the bedrock surface derived from groundwater monitoring wells and local-scale gravity surveys from Salpausselkä I, Hyvinkäänkylä, southern Finland Breilin et al., 2004). The work has been conducted in digital 3D-modelling environment. The results of this study highlight the potential of, and the need for more systematic usage of structural geological expertise in modelling the glacial deposits.

## 2. Data and methods

The 10 m resolution digital elevation model (National Land Survey) overlain by the map of Quarternary deposits (Geological Survey of Finland) acts as the topmost layer in the modelling set-up (Fig.1C). Digital elevation model for the top surface of the bedrock, interpolated from groundwater monitoring wells and data from gravimetric surveys conducted between the monitoring wells has been available from the Geological Survey of Finland (GTK; Fig. 1C; Breilin et al., 2004).

The structural framework of the bedrock at local scales is based on lineament interpretation by Breilin et al. (2004) and at larger scales by the network of major shear zones

stemming from dextral transpression at approximately 1.83-1.80 Ga (Fig. 1A; Ehlers et al., 1993; Väisänen and Skyttä, 2007; Skyttä and Mänttäri, 2008). The available interpretations on the shear zone networks were specified and further developed using regional-scale aeromagnetic and bedrock maps (GTK; Fig. 1B). Moreover, lithological contacts and dip data to constrain their 3D-attitudes were digitized from the bedrock maps.

Data integration and further model building were carried out with MOVE™ 3D-modelling software package (Midland Valley Exploration Ltd.).

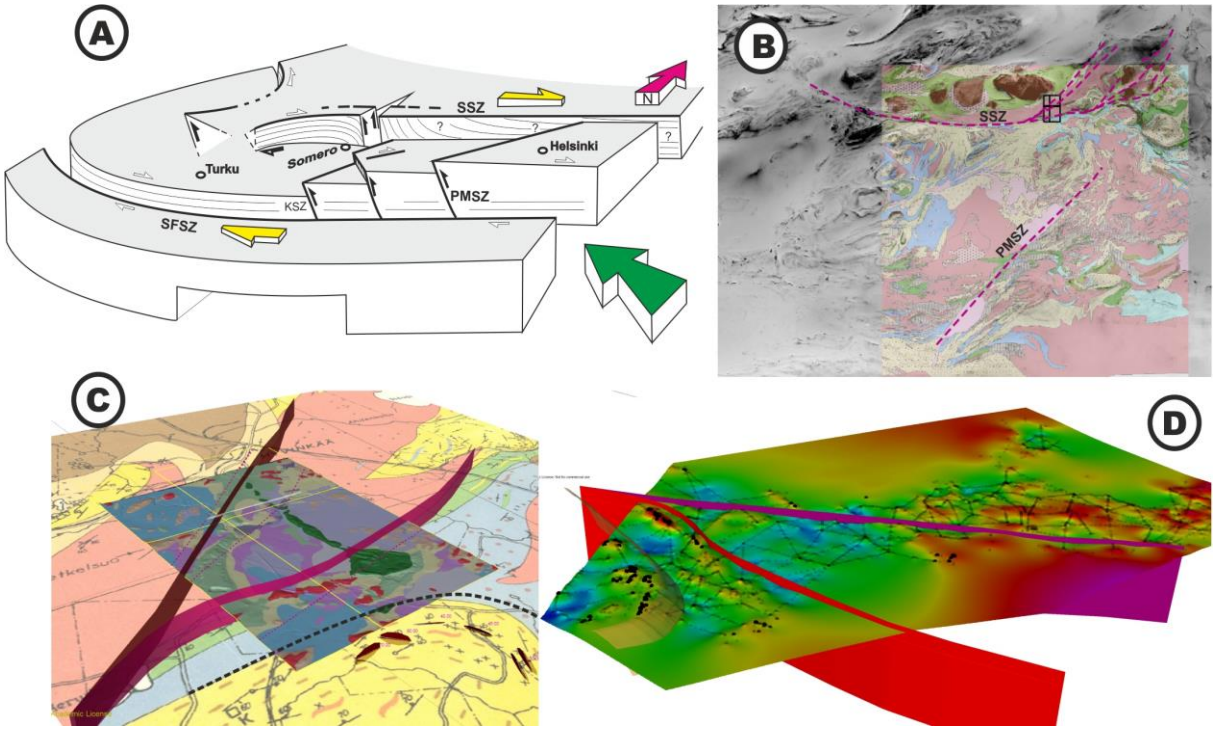


**Figure 1**. **A.** 3D-skecth on the shear zones of SW Finland (after Väisänen and Skyttä, 2007). KSZ, PMSZ, SFSZ, SSZ = Kisko, Porkkala-Mäntsälä (Pajunen, 2008), South-Finland (Torvela et al., 2008) and Somero Shear Zones. **B.** The largest shear zones interpreted on aeromagnetic and bedrock geology maps, the study area indicated by a rectangle. **C.** A 3D-visualization of two vertical faults along the horse-tail style termination of SSZ, shown on a digital elevation model overlain by the Qarternary deposits. The thick dashed = contact of the domal structure in the bedrock. View towards NE. **D.** Two faults, the contact of the domal structure in C., and digital elevation model of the bedrock surface interpreted from gravimetric surveys and drill hole data (black dots). Red and blue colours indicate high and low elevations, respectively. View towards NW. Geological and geophysical maps and the gravimetric data from the Geological Survey of Finland.

## 3. Results

There is a distinct correlation between the structures of the bedrock and quarternary deposits along the Somero Shear Zone, which according to the new interpretation presented here, displays a horse-tail style termination towards the east (Fig. 1B). The NE-striking branch coincides spatially with First Salpausselkä marginal formation whereas the location of the approximately E-W striking branch defines the termination of the N-S trending longitudinal esker as shown by its abrupt transition into a delta (Fig. 1C). The third clear correlation is shown by a smaller arch-shaped glacial deposit which location is controlled by the underlying bedrock dome (Fig. 1C, D).

The linkage between the location and geometry of the glacial deposits and the basement structures is further confirmed by the morphology of the bedrock surface: both branches of SSZ, initially modelled as vertical features, coincide with distinct linear depressions of the bedrock surface. Moreover, also the arch-shaped deposit follows a curved depression of the bedrock surface (Fig. 1D).

## 4. Discussion

The correlations between the basement (bedrock) and cover (Quarternary deposits) indicate that major orogenic shear zones were reactivated during the glacial events, and that there is a huge potential in applying structural geological expertice in modelling the derived deposits. Specifically, understading the network of major shear zones and their evolution aids in filtering the used local-scale lineament interpretations into geologically meaningful data sets for further modelling.

Besides aiding in recognition of changes in the deposit geometries, the bedrock structures may be used in compilation of digital elevation models of the bedrock surfaces. Hence, future work will attribute how to make use of the orientation data of bedrock structures as input parameters in surface interpolations. For example, we need to study how to apply interpolation algorithms with variable input parameters for adjoining sub-areas, e.g. defined by the indivdiual branches of Somero Shear Zone (Fig. 1). Furthermore, we need to evaluate whether and with which constraints the elevation model of the bedrock surface along the shear zones should be modified, i.e. should the steep dips of the continous elevation model be modified into distinct breaks, and could this be done automatically or manually. This question is also linked to the origin and evolution of the shear zones; what are the inferred geometries related to the shear zone terminations in the case of a strike-slip vs. a dip-slip zone, and how did the geometries control the later glacial/post-glacial reactivations? Furthermore, the significance of lithological contacts vs. shear zones as controlling the glacial deposits should be systematically evaluated at a scale broader than that of this investigation.

## Acknowledgements

Joni Mäkinen from the University of Turku and Jukka-Pekka Palmu from the Geological Survey of Finland are acknowledged for the Hyvinkäänkylä aquifer data and Midland Valley Exploration Ltd. for the use of MOVE™ modelling software under the Academic Software Initiative.

## References:

Breilin, O, Paalijärvi, M. and Valjus, T., 2004. Pohjavesialueen geologisen rakenteen selvitys I Salpausselällä Hyvinkään kaupungissa Nummenkärki - Suomiehensuo alueella. Geological Survey fo Finland, Investigation report Dec 14, 2004, 89 pp. (in Finnish)

Ehlers, C., Lindroos, A. and Selonen, O., 1993. The late Svecofennian granite-migmatite zone of southern Finland-a belt of transpressive deformation and granite emplacement. Precambrian Research 64, 295-309.

Okko, M., 1962. On the development of the First Salpausselkä, West of Lahti. Geological Survey of Finland, Bulletin - Bulletin de la Commission Géologique de Finlande.

Pajunen, M. (Ed.)., 2008. Tectonic evolution of the Svecofennian crust in southern Finland: a basis for characterizing bedrock technical properties. Geological Survey of Finland Special Paper 47, 326 pp.

Palmu, J-P., 1999. Sedimentary environment of the Second Salpausselkä ice marginal deposits in the Karkkila-Loppi area in southwestern Finland. Geologian tutkimuskeskus. Tutkimusraportti 148. Espoo: Geologian tutkimuskeskus. 91 p. (in Finnish).

Skyttä, P. and Mänttäri., I., 2008. Structural setting of late Svecofennian granites and pegmatites in Uusimaa Belt, SW Finland: Age constraints and implications for crustal evolution. Precambrian Research 164, 86–109.

Torvela, T., Mänttäri, I. and Hermansson, T., 2008. Timing of deformation phases within the South Finland shear zone, SW Finland. Precambrian Research, 160, 277-298.

Väisänen, M. and Skyttä, P., 2007. Late Svecofennian shear zones in southwestern Finland. GFF, 129, 55-64.

# Partial melting of Earth' rocks: field, analogue and numerical modelling approaches

A. Soesoo[1], P.D. Bons[2] and S. Hade[1]

[1]Tallinn University of Technology, Ehitajate tee 5, Tallinn, 19086 ESTONIA
[2]Dept. of Geosciences, Eberhard Karls University Tübingen, Wilhelmstr. 56, 72074 Tübingen, GERMANY
E-mail: alvar.soesoo@ttu.ee

Magma is generated by partial melting to form micrometre-scale droplets at the source and may accumulate into >100 km-scale plutons. Here we provide measurements of migmatitic leucosomes and granitic veins in drill cores from the Estonia, Labrador and SW Finland. Despite the differences in size and number of measured leucosomes and magmatic veins, differences in host rock types and metamorphic grades, the cumulative width distribution of the studied magmatic leucosomes/veins follows a power law with exponents mostly between 0.7 and 1.8. It has been suggested that magma batches in the source merge to form ever-bigger batches in a self-organized way. This leads to a power law for the cumulative distribution of magma volumes, with an exponent $m_V$ between 1 for inefficient melt extraction, and 2/3 for maximum accumulation efficiency as most of the volume resides in the largest batches that can escape from the source. If $m_V \geq 1$, the mass of the magma is dominated by small batches, in case $m$=2/3, about 50% of all magma in the system is placed in a single largest batch. Our observations support the model that the crust develops a self-organized critical state during magma generation. In this state, magma batches accumulate in a non-continuous, step-wise manner to form ever-larger accumulations. There is no characteristic length- or time scale in partial melting process or its products. Smallest melt segregations and >km scale plutons form the end members of a continuous chain of mergers of magma batches. The numerical MASC model incorporates this process in the evolution of magma chemistry to explain chemical variation in magmatic bodies and show how chemical variation can be generated from geochemically homogenous source rock. It can be shown quantitatively that tectonic forces can be partly responsible for chemical variation in magmatic products.

**Keywords:** partial melting, leucosome size distribution, power law, fractal, melt chemistry, self organization

## 1. Introduction

The Earth's crust is composed largely of igneous rocks, which formed through partial melting of crust and mantle. Melting processes have time scales in the order of millions of years and length scales up to hundreds of kilometers. One example is magma generation and transport, which is of first order importance for the differentiation and evolution of the Earth, and still is the main mass transfer process in the crust. It is known that a large number of geological objects show a power-law or fractal distribution. Fractals can be used in studies of mantle convection, lava flows, ore mineralization and partial melting products, etc. The width and spacing of migmatitic leucosomes as representatives of "frozen" partial melts in the crust will be statistically evaluated in this presentation.

The chemistry of early melt droplets is different from that of the emplacement level. Apart from the fact that different rocks produce magmas of different chemistry, the chemistry of early melt droplets can be altered during magma transport. Using MASC modelling (MASC=Melt Accumulation and Segregation Code), it will be shown how the magma batch chemistry can be altered during melt transport and accumulation.

## 2. Migmatites: leucosome width and fractals

Migmatite leucosome thicknesses were examined by measuring their width and spacing along line traverses or in drill core. The resolution of measurements is usually limited to 2 mm; leucosomes with thicknesses below this value were not included in the data. Here we provide

measurements of migmatitic leucosomes and granitic veins in drill cores from the Estonian Proterozoic basement and outcrops at Masku in SW Finland, and the Labrador peninsula, Canada. As shown in Figure 1, the widths of the migmatitic leucosomes follow a power law distributions Soesoo & Bons, 2013). Despite the differences in size and number of all measured leucosomes in different geological settings, differences in host rock types and formation conditions, the studied leucosome data set shows good power law distributions with exponents *m* usually between 0.7 and 1.9. It has been suggested that magma batches in the source merge to form ever-bigger batches in a self-organized way. This leads to a power law for the cumulative distribution of magma volumes, with an exponent $m_V$ between 1 for inefficient melt extraction, and 2/3 for maximum accumulation efficiency as most of the volume resides in the largest batches that can escape from the source. If $m_V \geq 1$, the mass of the magma is dominated by small batches, in case $m_V=2/3$, about 50% of all magma in the system is placed in a single largest batch.

In addition to the leucosome width distributions, the spacing of leucosomes can be analysed by the box-counting method, which gives the topological dimension of the migmatite structures and corresponds to the fractality in the strict sense. Knowing the power law size distribution for the leucosomes (melt batches) allows us to estimate the total volume of the melt phase, as well as the relative contributions of the largest batch and of the smallest batch to the overall partial melt budget of a magma system.

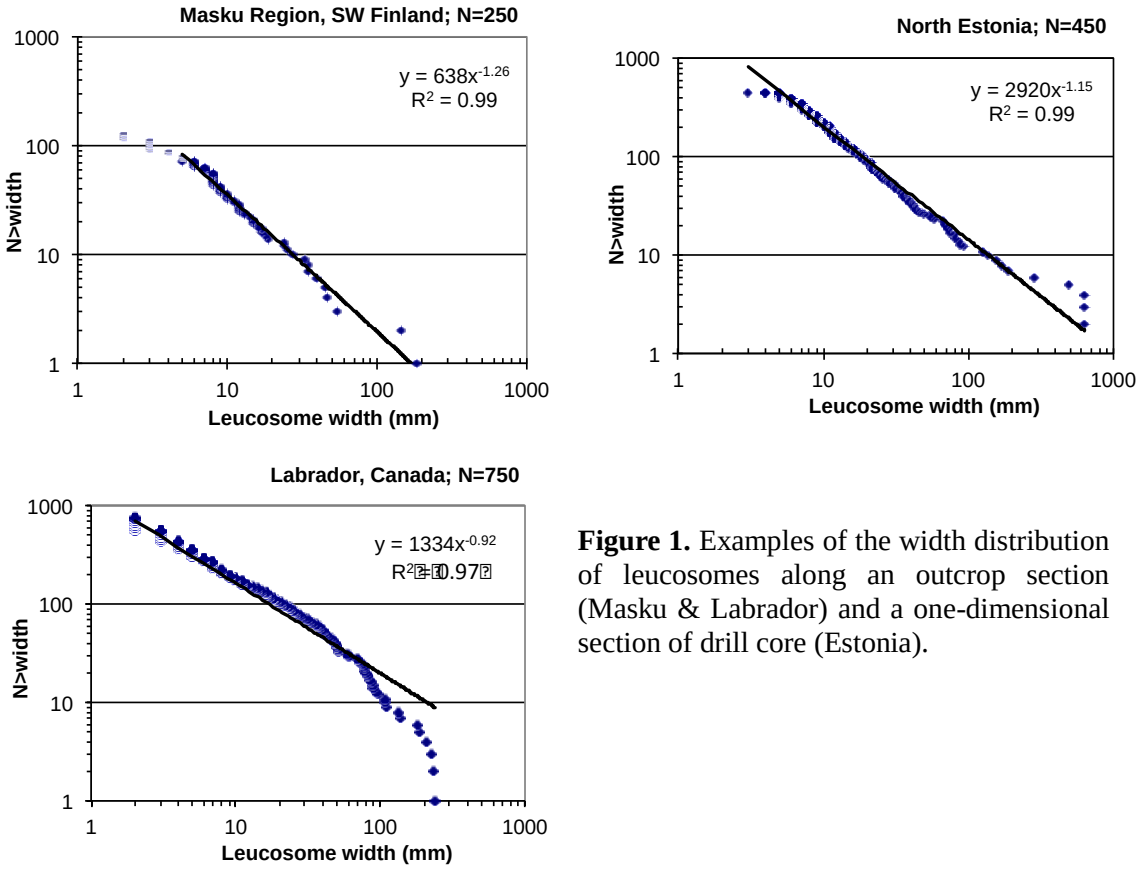


**Figure 1.** Examples of the width distribution of leucosomes along an outcrop section (Masku & Labrador) and a one-dimensional section of drill core (Estonia).

## 3. Analogue modeling of partial melting processes

In order to understand partial melting and melt transport, analogue experiments were conducted (Bons & van Milligen, 2001; Soesoo et al. 2004; Urtson & Soesoo, 2007). In the analogue model, the gradual formation of melt in a rock was simulated by the formation of

$CO_2$ gas in wet send, formed by fermentation of dissolved sugar. The simple experiment showed how the melt analogue – gas - could slowly diffuse out of the system below a certain gas production rate. The process of melt accumulation from a partially molten system or gas accumulation in the analogue system is traditionally viewed as porous flow through permeable media. However, the experiments clearly showed that gas batches also flows through fractures that move by propagation at one end and simultaneous closure at the other end. No interconnected fracture systems or critical melt fraction is needed. The movement and accumulation of melt batches can also trigger chain reactions of movement and accumulation - avalanches. Therefore, the large-scale melt transport through the rock is not diffusional, but ballistic and stepwise. The numerical and experimental experiments show that the melt systems develop towards a self-organised critical state, characterised by the emergence of scale invariant or fractal structures, such as the size distribution of melt batches, avalanches and escaping melt batches. This scale-invariant structure links the smallest leucosomes to the largest melt bodies or intrusions. The size of experimental batches follows power law or fractal statistics. The observed power law distributions of the gas batch sizes in the analogue experiment and leucosome widths in the migmatites allow to conclude that the behaviour of the liquid phase could be analogous in both experimental and natural liquid segregation systems.

**4. Numerical modelling of partial melting processes**

Most models for melt segregation and ascent do not explain transport and accumulation of melt as an interrelated system. A different approach on how melt dynamics can be described more adequately has been developed by using MASC model (Soesoo & Bons 1998; Bons et al. 2004). Our model, based on the assumption that melt batches reside in hydrofractures, explains both transport by hydrofracture propagation, and stepwise accumulation by melt batch merging. The model predicts that the system quickly develops into a critical state with self-organisation characteristics, where the melt distribution is organised in a self-similar way to allow discharge of any additional melt. These modelling results show that interaction between the melt and its melting environment is complicated and cannot be described meaningfully by any average values. The model can also be related to tectonic regime. At a lower strain rate it takes a longer time and more extensive melting of the source before the first melt batch leaves the source. A smaller percentage of melt is needed to reach extraction at a higher strain rate.

This stepwise melt transport and accumulation approach does not separate the process from source to emplacement in distinct phases, but instead links the smallest melt batch (leucosome) to the largest emplacement structure (batholith) in one single holistic system. The results are in good agreement with natural measurements and analogue modelling results.

**5. Chemistry of partial melts: a numerical approach**

Despite a large number of modern geochemical studies on partial melting there is a distinct need for models that can explain the observed geochemical variability. The MASC model can be applied in studies of chemical evolution of partial melting systems from micrometre to kilometre scales. The results show that geochemical variations within and between intrusive/extrusive complexes are not only caused by source rock composition and different melting percentages, but can also be due to other processes such as deformation and melt batch dynamics (Urtson & Soesoo, 2009; Fig 2). These results show how a single source may generate a large variation in the chemistry of magmatic products. This is in accordance with natural observations of variation in melt inclusions within igneous rocks.

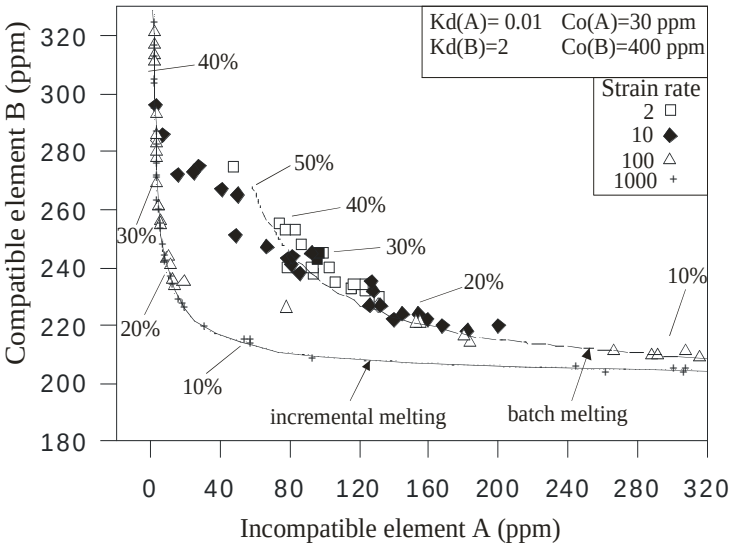


**Figure 2.** Incompatible vs. compatible element plot of melt batches derived during progressive melting of a metasedimentary source, modelled with MASC. Theoretical batch and fractional melting curves are for reference only. At high strain rate, the concentrations of elements in the melt follow the theoretical incremental melting curve, while at low strain rates, the melts show similarities with batch melting.

## 6. Conclusions

The natural migmatite leucosome measurements and analogue and numerical modelling results show that during melt segregation and transport the partial melt system is controlled by self-organisation and the topology of magmatic bodies can be described with a power law and the size/volume distribution shows fractal properties. Our observations support the model that the crust develops a self-organized critical state during magma generation. There is no characteristic length- or time scale in the partial melting process or its products. The MASC model allows to explain chemical variation in magmatic bodies and show how chemical variation can be generated from a geochemically homogenous source rock. It can be shown quantitatively that the tectonic regime can strongly influence the chemical variation in magmatic products.

## Acknowledgements

The study is supported by ESF grant No. 8963 and the Estonian Target Research Project No. SF0140016s09 to AS.

## References:

Bons, P.D. and van Milligen, B.P., 2001. A new experiment to model self-organized critical transport and accumulation of melt and hydrocarbons from their source rocks, Geology, 29, 919-922.

Bons, P.D., Arnold, J., Elburg, M.A., Kalda, J., Soesoo, A. and van Milligen, B.P., 2004. Melt extraction and accumulation from partially molten rocks, Lithos, 78, 25-42.

Soesoo, A. and Bons, P., 1998. Granite classification and the effect of deformation on the chemistry of granitic melts. Anorogenic and other granites of Proterozoic domains, Abstracts, Tallinn-Arbavere, Estonia, 42-43.

Soesoo, A. and Bons, P., 2013. Partial melting of Earth' rocks: fractals and analogue modelling approach, In (Ed. Perugini, D.) VI International Conference on Fractals and dynamic systems in Geosciences, Perugia, Italy 2013, pp. 71 - 72.

Soesoo, A., Kalda, J., Bons, P.D., Urtson, K. and Kalm, V. 2004. Fractality in geology: a possible use of fractals in the studies of partial melting processes. Proc. Est. Acad. Sci., Geol., 53, 13-27.

Urtson, K. and Soesoo, A., 2007. An analogue model of melt segregation and accumulation processes in the Earth's crust, Est. J. Earth Sci., 56, 3–10.

Urtson, K. and Soesoo, A., 2009. Stepwise magma migration and accumulation processes and their effect on extracted melt chemistry, Est. J. Earth Sci., 58, 246 - 258.

# Late Svecofennian mafic magmatism in southern Finland

Markku Väisänen[1], Charlotta Simelius[1,2], Hugh O'Brien[3], Mira Kyllästinen[1] and Jussi Mattila[4]

[1]Department of Geography and Geology, 20014 University of Turku, Finland
[2]Pöyry Finland Oy, Vantaa, Finland
[3]Geological Survey of Finland, FI-02151 Espoo, Finland
[4]Posiva Oy, Eurajoki, Finland
E-mail: markku.vaisanen@utu.fi

We present single-grain zircon U-Pb laser-ablation data from gabbroic rocks in three locations in southern Finland. In Ruissalo, Turku, the mafic intrusions are found within the Airisto shear zone with ages of c. 1.83-1.82 Ga. In Muurla, the c. 1.81 Ga granite cuts across the c. 1.83-1.82 Ga gabbro. In Salittu, Karjalohja, the 1.83-1.82 Ga mafic dyke crosscuts the picrite. These findings indicate heat transfer from the mantle to the crust during the lateorogenic stage.

**Keywords:** lateorogenic, mafic magmatism, heat source, shear zones, U-Pb, zircon, LA-MC-ICP-MS

## 1. Introduction

The Svecofennian orogeny in southern Finland has been divided into two main orogenies: the 1.89-1.87 Ga Fennian orogeny (synorogenic) and 1.84-1.80 Ga Svecobaltic orogeny (lateorogenic) intervened by the poorly known intra-orogenic period (Lahtinen et al., 2005). The lateorogenic stage is characterised by dextral transpression (Ehlers et al., 1993), culmination of high temperature metamorphism (Korsman et al. 1984, Väisänen et al. 2002, Mouri et al. 2005) and, consequently, large amount of lateorogenic anatectic granites (Figure 1). The onset of anatectic granite magmatism has recently found to have started at c. 1.85 Ga, i.e., during the intra-orogenic period (Kurhila et al. 2005, Kurhila et al., 2010, Väisänen et al., 2012). Until now, only one occurrence of lateorogenic mafic intrusion has been described (1838 ± 4 Ma Jyskelä gabbro; Pajunen et al., 2008)

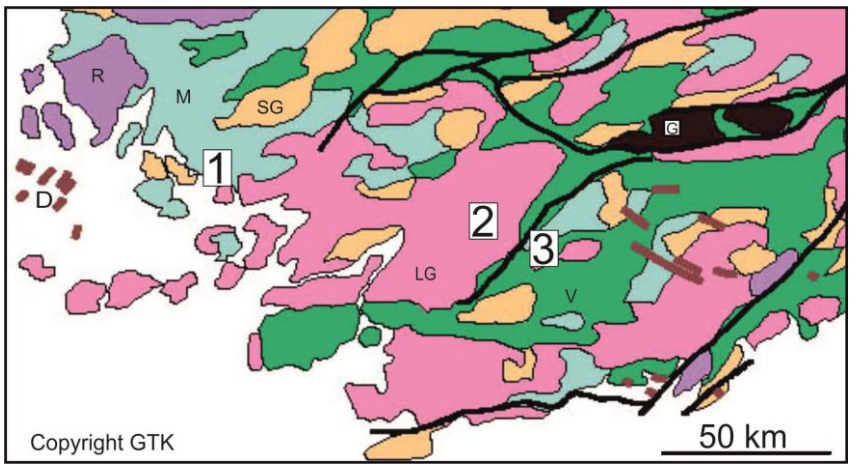


**Figure 1**. Geological map of SW Finland, modified after the 1:5 million map by the Geological Survey of Finland (1999: www.gtk.fi). Symbols on different colours and shades are: D=diabase dykes, G=gabbros, LG=lateorogenic granites, M=migmatitic mica gneisses, R=rapakivi granites, SG=synorogenic granitoids, V=volcanic rocks. Thick black lines=shear zones. Study targets are shown by numbers on white background; 1=Turku, Ruissalo; 2= Muurla, road cut; 3= Karjalohja, Salittu.

In this study we present new single-grain zircon ages from lateorogenic gabbroic rocks from three locations in southern Finland (Figure 1) from different geological environments. We also preliminary discuss some features of their geochemical compositions. The U-Pb analyses were performed using the LA-MC-ICP-MS techniques in the Finnish Geosciences Research Laboratory (SGL) at the Geological Survey of Finland, Espoo.

## 2. Study targets and their U-Pb zircon ages

### *2.1 Ruissalo, Turku*

In the western end of the Ruissalo Island, in the Saaronniemi Camping Place area, the N-S trending Airisto shear zone is exposed in two parallel sub-vertical shear zones located c. 300 m from each other. The shear zones are characterised by mylonites, brittle fracture zones and also pseudotachylites. Mafic intrusions, also affected by shearing, are found within the shear zones but not outside the zones. Two samples (RUIS1 and RUIS2) were taken from the gabbroic rocks located within the two branches of the shear zone (Simelius 2013).

Both of the samples gave, within errors, the same 1.83-1.82 Ga concordia ages. No older inherited ages were found in the data set.

### *2.2 Muurla, highway E-18 road cut*

Dark mafic intrusions and pink granites are exposed along a c. 400 m long road cut of the E-18 road at Muurla. Dikes from the granitic bodies cut across the gabbro. Both of these rock types are affected by narrow sub-horizontal shear zones. Two samples were taken from the gabbro and the granite (samples MGB and MGR; Kyllästinen, 2014).

The gabbro gave a concordia age of c. 1.83-1.82 Ga. The granite was slightly younger with a c. 1.81 Ga age. No older zircon populations were found from either of the samples.

### *2.3 Salittu, Karjalohja*

The Salittu formation within the Orijärvi area comprises mafic and ultramafic (picritic) volcanic rocks interpreted to have formed during rifting of the volcanic arc. The absolute age of the formation is unclear, but it overlies the c. 1.88 Ga volcanic arc rocks. In the Salittu village, the picrite is excavated for industrial raw material by Nordkalk Oy Ab. On the more mafic portion of the quarry wall, a lighter coloured mafic dike, c. 50-100 cm wide, crosscuts the picrite. The sample Salittu from the dike has a geochemical analysis number 127.2MV96 in Väisänen and Mänttäri (2002).

The mafic dike yielded a concordia age of c. 1.83-1.82 Ga. The zircons also contained two older ages of c. 1.86 Ga and 2.1 Ga but we interpret these as inherited zircons.

## 3. Geochemical data

Because the geochemical data on the 1.83-1.82 Ga mafic rocks are very limited, consisting only of the dated samples, only very general comments can be stated at this stage. One of the observations is that, although of the same age, the compositions of the Ruissalo, Muurla and Salittu intrusion are not similar. The Ruissalo samples show an enriched character resembling the intra-orogenic mafic rocks in SW Finland (Väisänen et al., 2012), whereas the Muurla and Salittu samples are more primitive (Figure 2) with higher Mg-numbers, Ni and Cr contents, but lower P, F, LREE contents.

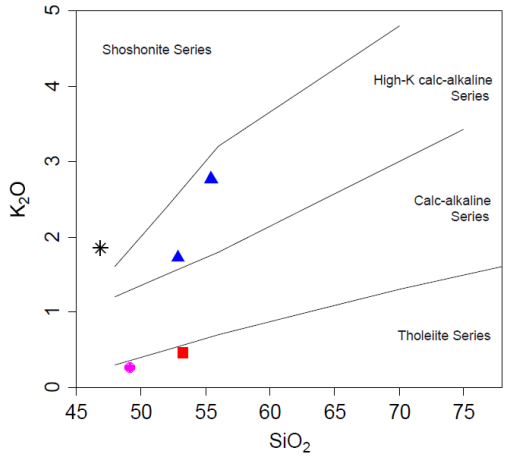


**Figure 2.** $K_2O$ *vs* $SiO_2$ diagram after Peccerillo and Taylor (1976). Symbols are: triangle=Ruissalo, square=Muurla, sphere=Salittu. For comparison a sample from the shoshonitic 1815 Ma Urusvuori monzogabbro (Rutanen et al., 2011) is shown with star symbol. Ruissalo samples fall within the high-K field whereas Muurla and Salittu fall within the tholeiitic field.

## 4. Discussion and conclusions

The present lateorogenic data and the data from the earlier intra-orogenic mafic intrusions (Mänttäri et al., 2006, Väisänen et al., 2012, Nevalainen, 2014) show that the mantle-derived magmatism was active throughout the Svecofennian orogeny in southern Finland. However, these findings are quite recent and their geodynamic implications are yet ambiguous since the important data on field relations, geochemistry and isotopic geology is still mostly lacking. Nevertheless, we propose that mafic intrusions with ages between c. 1.86-1.81 Ga are quite common throughout southern Finland and that more of such findings will emerge.

The Ruissalo intrusions are located within the steeply dipping Airisto shear zone and we thus infer that the early shearing played important role in the intrusion mechanism of the mafic magmas of the Ruissalo area. In general, shear zones may have acted as pathways to the mafic magmas to ascend through the thick, hot, ductile and partially molten crust during the lateorogenic stage. A gently dipping shear zone was also detected close to the Muurla gabbro (Aho et al., 2014), which supports this idea.

The heat source for the high temperature metamorphism in southern Finland is controversial. Schreurs and Westra (1986) proposed mafic intraplating, Korsman et al. (1999) mafic underplating and Lahtinen et al. (2005) evoked extensional tectonics. Kukkonen and Lauri (2009) modelled the heat budget and proposed that radioactive decay of the earlier granitoids led to crustal melting during the lateorogenic stage. Väisänen et al. (2012) emphasised the role of the mafic magmatism in transferring external heat from the mantle to the crust. There are now evidences from different sources, as discussed above, that the crust was intruded by mantle-derived magmas during the high-grade metamorphism at 1.85-1.81 Ga. Although the number of the so far discovered mafic intrusions and their areal extent is still quite low, they nevertheless inevitably show that mantle-crust interaction took place at the time. Our hypothesis is that the incremental heat flow from the mantle to the crust, combined with radioactive decay, gradually increased the crustal temperatures high enough to cause wide-spread crustal melting and the formation of migmatites and granites during the lateorogenic stage. The tectonic setting/settings for this is/are, however, uncertain, since the mantle-derived magmatism spans over the proposed episodic Svecofennian intra-orogenic, lateorogenic and postorogenic stages.

## Acknowledgements

We thank Yann Lahaye for his help in the SGL laboratory and Arto Peltola for the thin sections and zircon mounts. The Finnish Cultural Foundation, Varsinais-Suomi Regional Fund gave financial support.

## References:

Aho, R., Kauti, T., Penttinen, H., Skyttä, P. and Väisänen, M., 2014. A multi-disciplinary approach to unravel the tectonic setting of the bedrock in the Salo area, SW Finland. Lithosphere 2014 – 8th Symposium on the Structure, Composition and Evolution of the Lithosphere inFennoscandia. Programme and Extended Abstracts, Turku, Finland, November 4-5, 2014. Institute of Seismology, University of Helsinki, Report S-62, 1-4.

Ehlers, C., Lindroos, A., and Selonen, O., 1993. The late Svecofennian granite-migmatite zone of southern Finland-a belt of transpressive deformation and granite emplacement. Precambrian Research, 64, 295-309.

Korsman, K., Hölttä, P., Hautala, T. and Wasenius, P. 1984. Metamorphism as an indicator of evolution and structure of crust in eastern Finland. Geological Survey of Finland, Bulletin, 328, 40 p.

Korsman, K., Korja, T., Pajunen, M., Virransalo, P. and GGT/SVEKA Working group. 1999. The GGT/SVEKA transect: structure and evolution of the continental crust in the Paleoproterozoic Svecofennian orogen in Finland. International Geology Review, 41, 287-333.

Kukkonen, I.T. and Lauri, L.S. 2009. Modelling the thermal evolution of a collisional Precambrian orogen: High heat production migmatitic granites of southern Finland. Precambrian Research, 168, 233–246.

Kurhila, M., Andersen, T. and Rämö, O. T., 2010. Diverse sources of crustal granitic magma: Lu-Hf isotope data on zircon in three Paleoproterozoic leucogranites of southern Finland. Lithos, 115, 263–271.

Kurhila, M., Vaasjoki, M., Mänttäri, I., Rämö, T. and Nironen, M. 2005. U-Pb ages and Nd isotope characteristics of the lateorogenic migmatizing microline granites in southwestern Finland. Bulletin of the Geological Society of Finland, 77, 105–128.

Kyllästinen, M. 2014. Muurlan gabron ja graniitin zirkonien separointi, LA-MC-ICPMS- ikämääritykset ja geokemialliset koostumukset. LuK -tutkielma, Turun yliopisto, Maantieteen ja geologian laitos, 29 s.

Lahtinen, R., Korja, A. and Nironen, M. 2005. Palaeoproterozoic tectonic evolution. In: M. Lehtinen, P. A. Nurmi and O. T. Rämö, (eds.) Precambrian Geology of Finland — Key to the Fennoscandian Shield. Elsevier B.V., 481–532.

Mänttäri, I., Talikka, M., Paulamäki, S. and Mattila, J. 2006. U-Pb Ages of Tonalitic Gneiss, Pegmatite Granite, and Diabase Dyke, Olkiluoto Study Site, Eurajoki, SW Finland. Posiva Working Report 2006-12, 18 p.

Mouri, H., Väisänen, M., Huhma, H. and Korsman, K. 2005. Sm-Nd garnet and U-Pb monazite dating of high-grade metamorphism and crustal melting in the West Uusimaa area, southern Finland. GFF, 127, 123–128.

Nevalainen, J. 2014. Single-grain zircon U-Pb dating and geochemistry of the Moisio monzogabbro, Turku, SW Finland. M.Sc. Thesis. University of Turku, Department of Geography and Geology, 55 p.

Pajunen, M. Airo, M-L, Elminen, T., Mänttäri, I., Niemelä, R., Vaarma, M., Wasenius, P. and Wennerström, M. 2008. Tectonic evolution of the Svecofennian crust in Southern Finland. Geological Survey of Finland, Special Paper, 47, 15–160.

Peccerillo, R. and Taylor, S.R. 1976. Geochemistry of Eocene calc-alkaline volcanic rocks from the Kastamonu area, northern Turkey. Contributions to Mineralogy and Petrology, 58, 63–81.

Rutanen, H., Andersson, U.B., Väisänen, M., Johansson, Å., Fröjdö, S., Lahaye, Y. and Eklund, O. 2011. 1.8 Ga magmatism in southern Finland: strongly enriched mantle and juvenile crustal sources in a post-collisional setting. International Geology Review, 53, 1622-1683.

Schreurs, J. and Westra. L. 1986. The thermotectonic evolution of a Proterozoic, low pressure, granulite dome, West Uusimaa, SW Finland. Contributions to Mineralogy and Petrology, 93, 236-250.

Simelius, C. 2013. Airiston hiertovyöhyke – Duktiilista deformaatiosta hauraiden rakenteiden ympäristöksi. Pro Gradu -tutkielma. Turun yliopisto, Maantieteen ja geologian laitos, 93 s.

Väisänen, M. and Mänttäri, I. 2002. 1.90–1.88 Ga arc and back-arc basin in the Orijärvi area, SW Finland. Bulletin of the Geological Society of Finland, 74, 185–214.

Väisänen, M., Mänttäri, I. and Hölttä, P. 2002. Svecofennian magmatism and metamorphic evolution in southwestern Finland as revealed by U-Pb zircon SIMS geochronology. Precambrian Research, 116, 111–127.

Väisänen, M., Eklund, O., Lahaye, Y., O'Brien, H., Fröjdö, S., Högdahl, K. and Lammi, M. 2012. Intra-orogenic Svecofennian magmatism in SW Finland constrained by LA-MC-ICP-MS zircon dating and geochemistry. GFF,134, 99–114.

# Velocity Images of the Lithosphere and Structure of Fennoscandian Upper Mantle

L. Vecsey[1], J. Plomerová[1], H. Munzarová[1], V. Babuška[1] and LAPNET working group

[1]Institute of Geophysics, Academy of Sciences of the Czech Republic, Prague
E-mail: vecsey@ig.cas.cz

Passive seismological experiment LAPNET provided data for structural studies of the upper mantle beneath the northern part of Fennoscandia. We analyze body waves of earthquakes from teleseismic distances and retrieve both anisotropic and isotropic velocity images of the upper mantle. We present domain-like fabrics of the Precambrian continental lithosphere of northern Europe and map boundaries as well as thickness of the domains. The results clearly demonstrate that also the Archean mantle lithosphere consists of domains with consistent fabrics reflecting fossil anisotropic structures.

**Keywords:** lithosphere structure, upper mantle tomography, anisotropy, Fennoscandia

## 1. Introduction

The research benefiting from the LAPNET array aims at obtaining a 3D seismic model of the crust (Silvennoinen et al., 2014) and upper mantle (P- and S-wave velocity tomography models, positions of major boundaries in the crust and the upper mantle, and estimates of seismic anisotropy strength and orientation) in the northern Fennoscandian Shield, particularly beneath the Archean domain of Fennoscandia. The 3D model can be used to define spatial distribution and thickness of the Archean lithosphere for different purposes, e.g., for diamond prospecting. The 3D model of the crust and the upper mantle will also be used to improve registration and location of local earthquakes and understanding of mechanisms of seismicity in northern Fennoscandia.

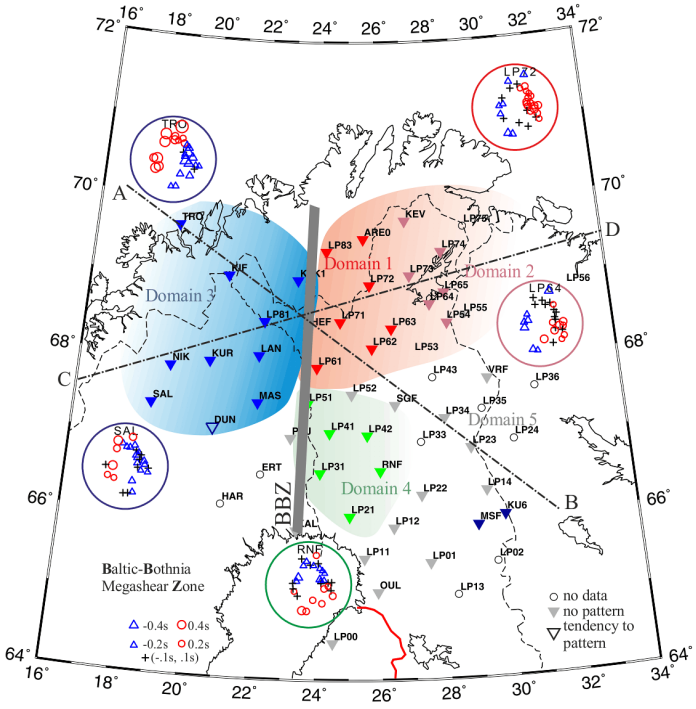


**Figure 1.** Seismic anisotropy from directional terms of relative P-wave residuals. Baltic-Bothnia megashear Zone (BBZ) copies boundary domains with similar anisotropy. Patterns of the P spheres delimit domains with similar anisotropic characteristics (Plomerová et al., 2011).

## 2. Results

Similarly to other regions of various tectonics and ages, the Archean mantle lithosphere is formed by domains with differently oriented fabrics reflecting fossil anisotropic structures (Babuška and Plomerová, 2006). The domains in the Archean part of the Fennoscandian Shield (Figure 1) are sharply bounded (see also Plomerová et al., 2011). While the Proterozoic-Archean contact (P-A) in the south-central Finland appears as a broad transition (Vecsey et al., 2007), the P-A contact in the north seems to be narrow. Boundary between the domains with distinct mantle lithosphere fabrics can be associated with the Baltic-Bothnia megashear Zone (BBZ).

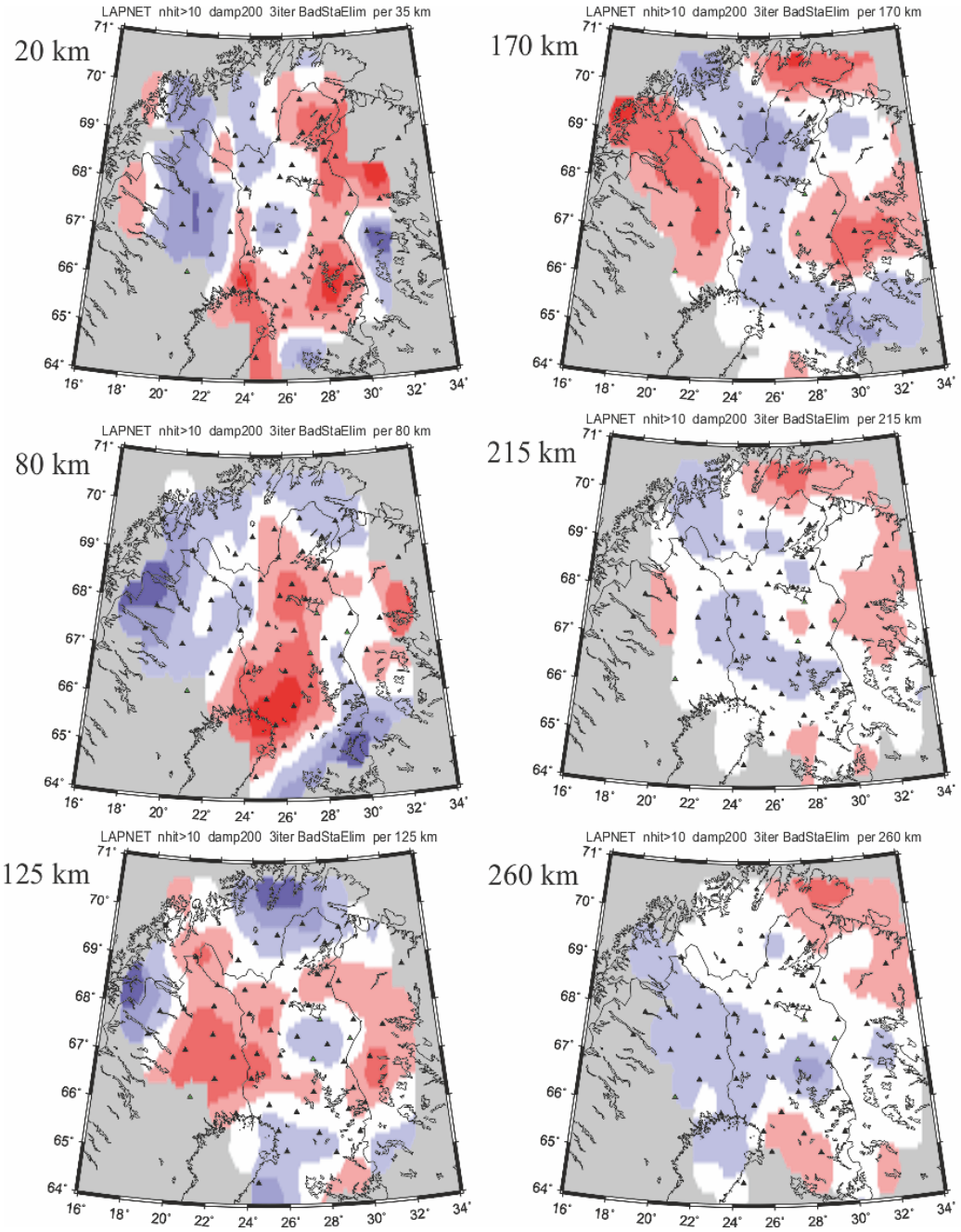


**Figure 2.** Tomography I from teleseismic P-wave relative travel times corrected for the crust.

Isotropic velocities in the Archean mantle lithosphere retrieved by standard tomography (Figs. 2, 3) appear to be lower than those in the Proterozoic part of the Fennoscandian Shield. Boundary between the two regions follows the surface trace of the BBZ. The westward shift of the boundary between regions with positive and negative velocity perturbations at depths around 125 km can indicate its inclination, similarly to the wedge like structure of the Proterozoic-Archean transition in the south-central Finland (Plomerová et al., 2006). Higher velocities around 170 km can be related to the lithosphere thickening towards the south-central Finland and along the P-A lithosphere contact beneath the middle part of the LAPNET array (Plomerová and Babuška, 2010).

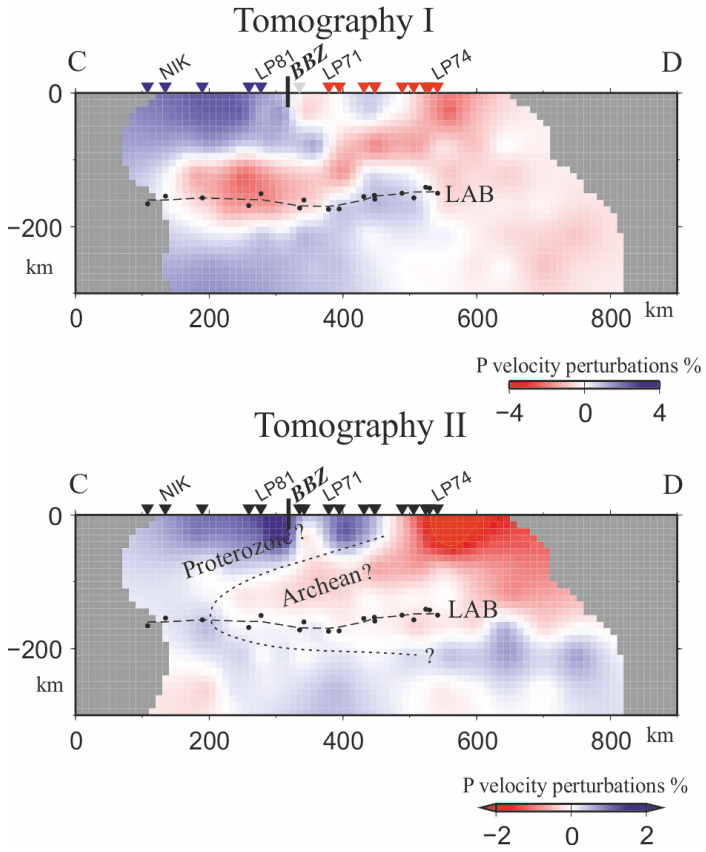


**Figure 3.** Cross-section CD (see Fig. 1) of tomography I (isotropic velocities) and tomography II (with additional corrections for seismic anisotropy; Plomerová and Babuška, 2010).

Combined analysis of 3D anisotropic structures retrieved by joint inversion of body-wave anisotropy parameters, based on P- and shear-wave anisotropic parameters, along with velocity perturbations imaged by standard isotropic regional tomography, advances our knowledge of the upper mantle structure, the lithosphere formation and its development with potential implications for 'intraplate' seismicity or deposits of raw materials. We concentrate on the lithospheric mantle structure and the upper mantle processes, which govern most of dynamic crustal features.

## References:

Babuška, V. and Plomerová, J., 2006. European mantle lithosphere assembled from rigid microplates with inherited seismic anisotropy. Phys. Earth. Planet. Inter., 158, 264-280.

Plomerová, J., Babuška, V., Vecsey, L., Kozlovskaya, E., Raita, T. and SSTWG, 2006. Proterozoic-Archean boundary in the upper mantle of eastern Fennoscandia as seen by seismic anisotropy. J. Geodyn., 41, 400-410.

Plomerová, J. and Babuška, V., 2010. Long memory of mantle lithosphere fabric - European LAB constrained from seismic anisotropy. Lithos, 120, 131-143.

Plomerová, J., Vecsey, L., Babuška, V. and LAPNET working group, 2011. Domains of Archean mantle lithosphere deciphered by seismic anisotropy – inferences from the LAPNET array in northern Fennoscandia. Solid Earth, 2, 303-313.

Silvennoinen, H., Kozlovskaya, E., Kissling, E., Kosarev, G., and POLENET/LAPNET working group, 2014. A new Moho boundary map for the northern Fennoscandian Shield based on combined controlled-source seismic and receiver function data. GeoResJ, 1-2, 19-32.

Vecsey, L., Plomerová, J., Kozlovskaya, E. and Babuška, V., 2007. Shear-wave splitting as a diagnostic of varying upper mantle structure beneath south-eastern Fennoscandia. Tectonophysics, 438, 57-77.

# Non-subduction geodynamics of the Neoarchean continental lithosphere: geochemical, isotopic and petrologic signatures of the Kolmozero-Voro'ya greenstone belt, Kola–Norwegian province, Fennoscandian Shield

A.B. Vrevsky

Institute of Precambrian Geology and Geochronology RAS, Makarova emb. 2, 199034, S-Petersburg, Russia
E-mail: a.b.vrevsky@ipgg.ru

This study presents new data on the geochemical and Sm–Nd isotope compositions, as well as the U–Pb age and geodynamic nature, of the Neoarchean basalt–andesite–dacite (BAD) association from the Kolmozero–Voron'ya greenstone belt. As it was first demonstrated by the example of the Neoarchean greenstone belt, the formation of BAD associations within a single Neoarchean greenstone structure may be explained by the long-lasting evolution of separate mantle and low continental crust sources not related to subduction processes.

**Keywords:** Neoarchean greenstone belt, Fennoscandia, andesite, Sm-Nd isotopic systematics, mantle plume, lithosphere, geodynamic.

## 1. Introduction

The petrology and geodynamic nature of calc-alkaline igneous complexes are one of the most acute problems of the genesis of a juvenile continental crust at the early stages of the Earth's evolution. Commonly, the basalt-andesite-dacite (BAD) associations of the Archean greenstone belts is considered to be a single indicator of subduction-accretion convergent geodynamic settings in which the continental crust of Archean granite-greenstone provinces was formed. Such volcanic complexes, including those of the Fennoscandian Shield, are suggested to indicate plate tectonic geodynamic scenarios because some of their isotopic-geochemical characteristics are similar to those of Phanerozoic adakitic and boninitic volcanic series (Martinet al., 2006; Puchtel et al., 1999; Svetov et al., 2004).

## 2. Geological background

The Polmos-Porosozero structure is the best-preserved part the >300 km long Uraguba-Kolmozero-Voronya Neoarchean greenstone belt which is located in the zone between the Murmansk and Central Kola domains of the Fennoscandian Shield. The volcanic-sedimentary complex of the structure consists of three units (Vrevskii et al., 2003). The lower terrigenous unit is mainly formed by garnet-biotite and biotite schists (metagreywackes). The lower part of the overlying volcanogenic unit is represented by metamorphosed pillow and massive tholeiitic-basalts and komatiitic lava with pyroclastic interbeds. Komatiite and tholeiite volcanics grade into a unit formed of interbeded basalts, andesite-basalts, andesites and dacites with textural signs of lava and tuffs without stratigraphic and tectonic unconformities. The basalt-andesite-dacite (BAD) unit also contains thin interlayers of greywackes, calcareous dolomite, BIF and carbonaceous schists. BAD association is uncomformably overlained by the upper terrigenous unite, which consists of high aluminous gneisses and schists with the lenses of polymictic conglomerates at the base of the section.

## 3. Geochemistry

The composition of BAD association generally corresponds to a normal alkalinity of calc-alkaline series. However, based on the variations in the major, trace and REE elements composition of intermediate volcanics, two geochemical groups, namely *andesite-I* and *andesite-II*, were identified. *Andesite-I* consists dominantly of andesite-basalt ($SiO_2$=55.3-56.6%), poor in $TiO_2$ (<0.5), have a normal Mg content ($mg^{\#}$=0.26-0.40). This type of volcanics belongs to a sodic calc-alkaline series and shows a strongly fractionated normalized LREE pattern $(Ce/Sm)_N$=2.38-2.82 and a weakly fractionated HREE pattern $(Gd/Yb)_N$=1.62-2.35(Fig.1, tabl.1). A second geochemical group (*andesite-II)* of andesitic and andesitic-dacitic volcanics ($SiO_2$=56.4-59.7%) is characterized by higher Mg (mg#=0.41-0.46), Ti, V and Ba concentrations and lower Sr, Cr, Co, Ni, Ti contents, as well as lower Ti/Zr and Zr/Y ratios. It shows a more potassic composition of alkalines. The normalized REE patterns of this group volcanics exhibit LREE depletion $(Ce/Sm)_N$=0.62–0.88) and slight HREE fractionation $(Gd/Yb)_N$=1.01–1.58)(Fig. 1, table 1), which is atypical of andesites. Unlike Archean and Phanerozoic adakitic associations, both types of andesites have a lower concentration of "indicator" elements such as Ba, Sr and Y and a lack of negative Nb anomaly $(Nb/La)_N$ =0.9–2.6) on spidergrams.

**Table 1.** Average composition of the BAD association from the Polmos-Porosozero structure.

| Components | 1 | 2 | 3 | Components | 1 | 2 | 3 |
|---|---|---|---|---|---|---|---|
| n | 7 | 7 | 4 | n | 7 | 7 | 4 |
| $SiO_2$ | 58,07 | 57,37 | 50,58 | Ti | 2481 | 3973 | 2061 |
| $TiO_2$ | 0,43 | 0,69 | 0,31 | Ti/Zr | 53,7 | 25 | 76 |
| $Al_20_3$ | 14,46 | 15,01 | 14,2 | Zr/Y | 6,5 | 3,7 | 2,4 |
| FeO* | 8,06 | 9,25 | 11,63 | Sr/Y | 15,9 | 6,6 | 9,1 |
| MnO | 0,16 | 0,13 | 0,22 | La | 13,51 | 2,47 | 1,57 |
| MgO | 5,64 | 4,61 | 8,41 | Ce | 29,03 | 7,33 | 3,84 |
| CaO | 7,63 | 7,08 | 8,93 | Pr | 3,67 | 1,16 | 0,61 |
| $Na_2O$ | 2,41 | 3,67 | 2,04 | Nd | 14,21 | 6,04 | 3,11 |
| $K_2O$ | 1,14 | 0,27 | 0,26 | Sm | 2,87 | 2,14 | 1,05 |
| $P_2O_5$ | 0,15 | 0,13 | 0,13 | Eu | 0,87 | 0,82 | 0,4 |
| $K_2O/Na_2O$ | 0,58 | 0,07 | 0,15 | Gd | 2,8 | 2,58 | 1,32 |
| Ba | 26,0 | 35,1 | 19,9 | Tb | 0,43 | 0,48 | 0,26 |
| Sr | 243,7 | 132,4 | 103 | Dy | 2,45 | 3,06 | 1,71 |
| Y | 15,3 | 20,1 | 11,3 | Ho | 0,49 | 0,67 | 0,4 |
| Zr | 99,29 | 74,04 | 27,1 | Er | 1,41 | 1,89 | 1,11 |
| Nb | 7,62 | 4,69 | 1,53 | Tm | 0,2 | 0,28 | 0,18 |
| Hf | 2,61 | 2,14 | 0,66 | Yb | 1,26 | 1,78 | 1,07 |
| V | 139,3 | 214,4 | 214,8 | Lu | 0,2 | 0,27 | 0,18 |
| Cr | 247 | 118 | 296 | (Nb/La)n | 0,9 | 2,56 | 1,1 |
| Co | 56,0 | 44,9 | 51,3 | (Gd/Yb)n | 1,81 | 1,21 | 1,12 |
| Ni | 171,8 | 63,8 | 133,3 | (Ce/Sm)n | 2,43 | 0,81 | 0,86 |

Note:(1) Andesites I; (2) andesites II; (3) basalts

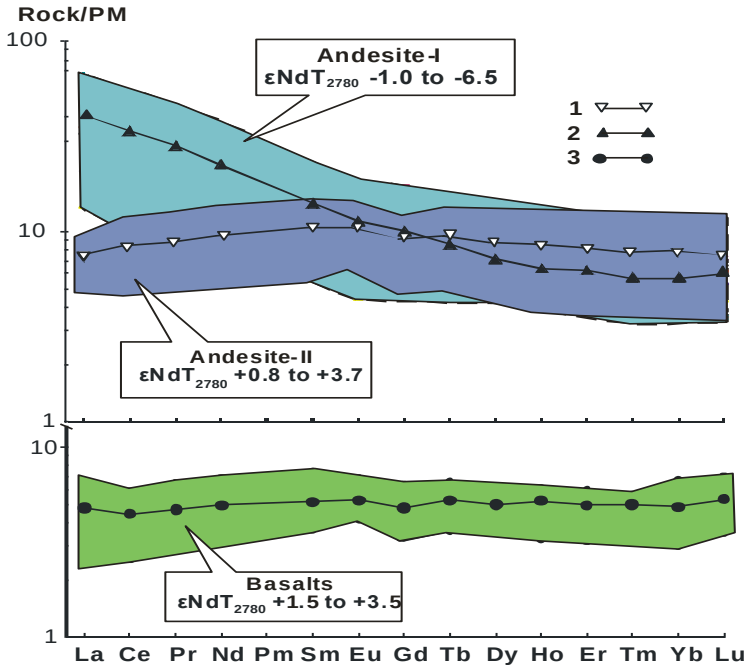


**Figure 1.** Primitive mantle–normalized REE distribution patterns in rocks of the BAD association from the Polmos–Porosozero structure. (1–3) average compositions: (1) andesites II, (2) andesites I, (3) basalts.

## 4. U-Pb zircon age data (SHRIMP II) and Sm-Nd isotopic systematic

The zircon population from andesites-I were analyzed for U–Pb isotope systematics (U-Pb SHRIMP II) and discordant upper intercept age of 2778.4±5.4 Ma (MSWD=0.75) was obtained. BAD association shows a significant variation in the initial $^{143}Nd/^{144}Nd$ ratios (Table 2). Andesite-I typically has $\varepsilon NdT_{2780}$ values varying from +0.8 to +3.7 and the Sm-Nd model age (TDM) from 3050 to 3235 Ma.

**Table 2.** Sm–Nd isotope data of the BAD association from the Polmos–Porosozero structure

| Sample | Rock type | Sm, ppm | Nd, ppm | $^{147}Sm/^{144}Nd$ | $^{143}Nd/^{144}Nd$ | $\varepsilon Nd_{T=2780}$ |
|---|---|---|---|---|---|---|
| 63-a | Basalt | 0,81 | 2,36 | 0,2121 | 0,513027 | +3,5 |
| 155 | Basalt | 1,44 | 4,32 | 0,2018 | 0,512826 | +1,8 |
| 161 | Basalt | 0,98 | 2,87 | 0,2069 | 0,512907 | +1,5 |
| 137 | Andesite II | 1,39 | 4,15 | 0,2024 | 0,512416 | -6,5 |
| 521 | Andesite II | 2,53 | 6,77 | 0,2263 | 0,513149 | -1,0 |
| 523 | Andesite II | 3,03 | 8,41 | 0,2175 | 0,512958 | -1,5 |
| 537-1 | Andesite I | 4,65 | 25,84 | 0,1118 | 0,511087 | +3,7 |
| 529 | Andesite I | 1,17 | 3,49 | 0,2024 | 0,512832 | +2,9 |
| 257-a | Dacite I | 2,16 | 10,97 | 0,1167 | 0,511200 | +0,8 |
| 240 | Andesite I | 2,91 | 13,37 | 0,1314 | 0,511454 | +1,1 |

Andesite-II shows isotopic and geochemical signatures ($\varepsilon Nd T_{2780}$-1.0 to -6.5), which dramatically differ from andesite-I. Andesite-II is suggested to be formed either from an "enriched" mantle (EMI-type) source or by the significant contamination of the primary melts by the continental crust.

## 5. Petrologic interpretation and discussion

In order to determine protolith of the andesite-II, geochemical modeling based on the trace element and isotopic characteristics and available experimental data (Condie, 2001, Petermann et al., 2003; Annen et al., 2006) was performed. The 3.59+0.42/–0.25 Ga model ages suggest that protolith of andesite-II primary melts had a prolonged evolutionary history of isotopic composition. The best fit solution for protolith is ancient (>3.5 Ga) basic eclogite with $^{147}Sm/^{144}Nd$=0.15, which nature can be interpreted as mafic melts underplated the lower crust. This possible lower crustal candidates was close in their Sm-Nd isotopic composition to the Paleoarchean amphibolites from the Voldozero terrain of the Fennoscandia Shield (Vrevskii et al., 2010) or the 4.28 Ga Nuvvuagittuq mafic complex of the Superior Province (O'Neil, Carlson, 2008).

## 6. Conclusions

The obtained data for the BAD association from the Neoarchean Polmos–Porosozero greenstone structure and the previously defined nature of the komatiite–tholeiite association (Vrevskii et al., 2003) can be interpreted in the context of geodynamic of plume–lithosphere interaction, not related to subduction processes. This mechanism of the juvenile crust formation agrees reasonably well with the concept (Condie, 2001) of a long-lived Archean mantle plume (>200 Ma) and is therefore sufficient for explaining the andesite-I data as being derived from melting of the peridotite mantle in a plume head enriched in the fluid components. Therefore, the primary basaltic melts are being the melting products of the hottest axial zone of the plume.

## References:

Annen, C., Blundy, J. D. and Sparks R. S. J., 2006. The Genesis of intermediate and silicic magmas in deep crustal hot zones, Journal of Petrology, 47, 505–539.

Condie, K.C. 2001. Mantle plumes and their record in the Earth History, Cambridge, 306 p.

Martin, H., Smith, R.H., Rapp, R., Moyend, J.-F. and Champione, D., 2005. An overview of adakite, tonalite-trondhjemite-granodiorite (TTG) and sanukitoid: relationships and some implications for crustal evolution, Lithos, 79, 1-24.

O'Neil, J., Carlson, R.W., Francis, D. and Stevenson, R.K., 2008. Neodymium-142 evidence for Hadean mafic crust, Science, 321, 1828–1839.

Petermann, M. and Hirschmann, M.M., 2003. Anhydrous partial melting experiments on MORB-like eclogite: phase relations, phase compositions and mineral+melt partitioning of major elements at 2–3 Gpa. Journal of Petrology, 44, 2173–2201.

Puchtel, I. S., Hofmann, A. W., Amelin, Yu. V., Garbe-Schonberg, C. D., Samsonov, A. V. and Shchipansky, A. A. 1999. Combined mantle plume-island arc model for the formation of the 2.9 Ga Sumozero-Kenozero greenstone belt SE Baltic Shield: isotope and trace element constraints. Geochimica et Cosmochimica Acta, 63, 3579−3595.

Svetov, S. A., Huhma, H., Svetova, A. I. and Nazarova, T. N., 2004. The oldest adakites of the Fennoscandian Shield, Doklady Earth Sciences, 397, 878−882.

Vrevskii, A. B., Matrenichev, V. A. and Ruzh'eva, M. S., 2003. Petrology of komatiites from the Baltic Shield and isotope geochemical evolution of their mantle sources, Petrology, 11, 532-561.

Vrevsky, A. B., Lobach-Zhuchenko, S. B., Chekulaev, V. P., Kovalenko, A. V., Arestova, N. A. 2010. Geological, petrologic, isotopic, and geochemical constraints of geodynamic models simulating formation of the Archean tonalite-trondhjemite-granodiorite associations in ancient cratons, Geotectonics, 44, 305-320.

# Orogen-parallel mass transport along the arcuate Himalayan front into Nanga Parbat and the western Himalayan syntaxis

D. M. Whipp, Jr.[1], C. Beaumont[2] and J. Braun[3]

[1]Department of Geosciences and Geography, University of Helsinki, Helsinki, Finland
[2]Department of Oceanography, Dalhousie University, Halifax, Canada
[3]ISTerre, Joseph Fourier University, Grenoble, France
E-mail: david.whipp@helsinki.fi

Quaternary rates of erosional exhumation in the western Himalayan syntaxis region are more than double those observed in the central Himalaya, which requires a local mass flux of crust into the base of the orogenic wedge that is higher than observed elsewhere along strike to sustain high topography. Analytical force balance calculations and 3D dynamic models of a generic arcuate convergent orogen with a syntaxis predict strain partitioning across the thrust front, providing an orogen-parallel mass flux into the model syntaxis that can balance very rapid rates of exhumation.

**Keywords:** strain partitioning, geodynamic modelling, obliquely convergent orogens, Himalayas, Tibetan Plateau

## 1. Introduction

Although the elevations of mountain peaks in the Nanga Parbat-Haramosh massif (NPHM), western Himalayan syntaxis region are comparable to elsewhere along strike, Quaternary rock exhumation rates are ~2-3 times faster than those observed in the central Himalaya (~11-13 mm/a; Whittington, 1996; Crowley et al., 2009; Whipp et al., 2007; Herman et al., 2010). The 'tectonic aneurysm' model (Zeitler et al., 2001) offers one possible mechanism by which a localized excess crustal mass can be supplied to balance very rapid surface erosion, but quantitative constraints on the source of the excess mass flux are lacking. Orogen-parallel mass transport owing to strain partitioning across the range-bounding thrusts is predicted to produce orogen-parallel shortening and crustal thickening in the syntaxis region (e.g., McCaffrey and Nabelek, 1998; Seeber and Pecher, 1998; Whipp et al., 2014), which is an alternative to the 'tectonic aneurysm' model. When strain is partitioned, the orogen-normal and orogen-parallel components of convergence are accommodated by separate thrust and strike-slip shear zones rather than by a single oblique thrust (e.g., Fitch, 1972). Analytical predictions for 2D infinite-length and 3D obliquely convergent orogens predict the convergence obliquity angle $\gamma$ (Figure 1a) and the respective strengths of the thrust and strike-slip shear zones that bound the orogenic wedge, and that of the wedge itself all influence partitioning behaviour (e.g., McCaffrey, 1992; Whipp et al., 2014). For a frictional plastic rheology with negligible rock cohesion, the strength of the shear zones will be controlled by the respective angles of internal friction $\phi$ of the shear zones and orogenic wedge. We build on the results of Whipp et al. (2014) using 3D mechanical models of an arcuate convergent orogen with a syntaxis (Figure 1) to explore the strain partitioning behaviour across an arcuate thrust front, quantify rates of translation of the orogenic wedge toward the model syntaxis, and determine rates of surface uplift in the model syntaxis.

## 2. Numerical model design

Strain partitioning behaviour and the resulting orogen-parallel mass transport is demonstrated using a 3D dynamic model of an arcuate convergent orogen bounded by two regions of orogen-normal convergence. The general model design is based on (Whipp et al., 2014); the

model comprises a mature orogen with a plateau underlain by a low-viscosity ($\eta = 10^{19}$ Pa s) middle-lower crust and an adjoining orogenic wedge. However, the geometry of predefined weak zones at the base and rear of the orogenic wedge, and the surface topography in the orogenic wedge have been modified to be arcuate with an arc radius of 256 km, rather than segmented linear. Velocity boundary conditions drive deformation in the model with an influx of crust into the orogen at 20 mm/a along one side of the model. The basal boundary conditions along the model base simulate subduction of the mantle lithosphere and we consider two subduction geometries: The segmented linear geometry from Whipp et al. (2014), and an arcuate subduction region geometry with an arc radius equal to that of the thrust front. The velocity boundary conditions and crustal weak zone geometries produce oblique convergence at obliquity angles of up to $\gamma = 45°$.

We explore the strain partitioning behaviour and the magnitude of orogen-parallel mass transport in the model by varying the strength of the weak zone at the rear of the orogenic wedge, and that of the wedge itself. Other than within the viscous region beneath the plateau, the crustal rheology is pressure-dependent frictional plasticity with a Mohr-Coulomb

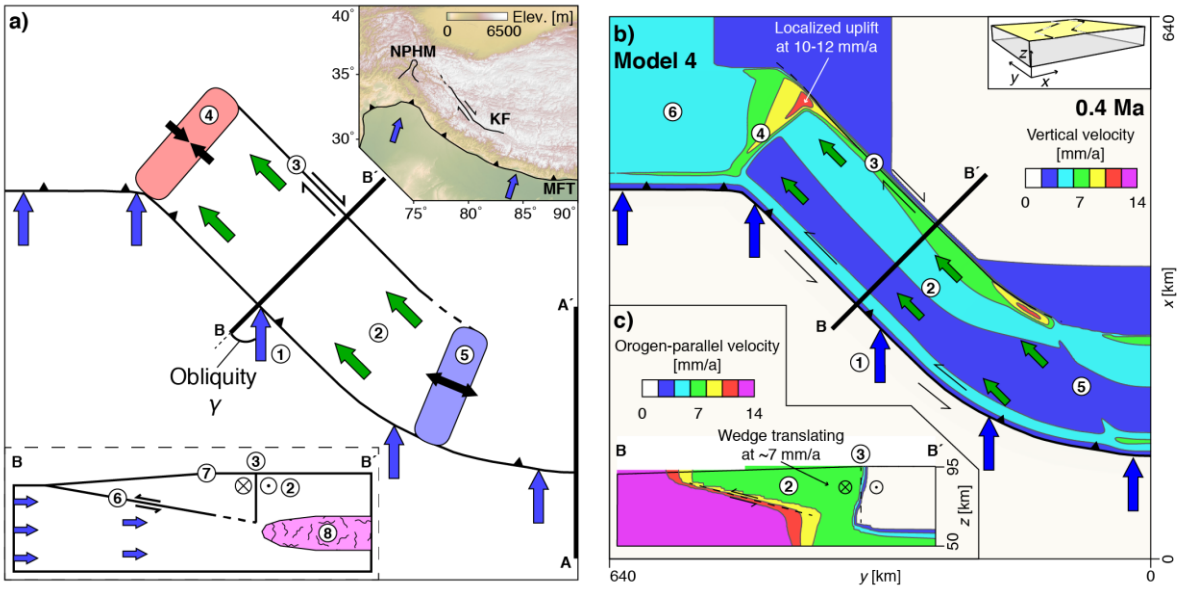


**Figure 1.** (a) Common features of an oblique convergent orogen with a syntaxis. In planform, features include: (1) Obliquity γ between the normal to the orogen-bounding structure and the convergence direction (blue arrows), (2) orogen-parallel (OP) mass transport owing to strain partitioning where convergence is oblique (green arrows), (3) a strike-slip structure at the rear of the orogenic wedge, (4) a shortening structure in the syntaxis region (pink region), and (5) a region accommodating OP extension (purple region). Lower inset: Common features of a large orogen with neighboring plateau include (6) a basal detachment structure with a shallow dip (~10°), (7) an average topographic slope that decreases to flat near the transition from the orogenic wedge to the plateau, and (8) a region of weak, viscous middle-lower crust. Upper inset: Topography of the western Himalaya, Tibetan Plateau and Pamirs with major tectonic features and approximate Indian plate motion vectors (blue arrows). KF: Karakoram fault, MFT: Main Frontal thrust, and NPHM: Nanga Parbat-Haramosh massif. (b) Surface uplift rates (background contours) and major features of Model 4 after 0.4 Ma. OP mass transport leads to uplift within the model syntaxis region at rates comparable to the NPHM.

failure criterion and a cohesion of 1 MPa. The basal shear zone is weak ($\phi_b$ = 2.5°) owing to prolonged shearing during growth of the orogen and dips at 10°. The respective angles of internal friction for the near-vertical rear shear zone and wedge are variable: $\phi_r$ = 1-5° and $\phi_w$=15-5°. The strengths of the rear shear zone and orogenic wedge are reduced via strain rate softening, where the angle of internal friction decreases linearly over a defined strain rate range. Elsewhere the crust has a constant angle of internal friction of $\phi_c$ = 15°, which assumes pore fluid pressure has reduced the crustal strength.

**3. Model results**

The observed strain partitioning behaviour in the arcuate geometry models is quite similar to that observed by Whipp et al. (2014), in spite of differences in both the topographic and crustal weak zone geometries, and the geometry of the basal subduction boundary conditions. A relatively strong rear shear zone ($\phi_r$ = 5°) prevents strain partitioning and oblique slip is favoured on the basal shear zone. Strain rate softening of the rear shear zone ($\phi_r$ = 5°→1°) and orogenic wedge ($\phi_w$ = 15°→5°) results in clear strain partitioning with orogen-parallel mass transport at ~7 mm/a and a well-developed orogen-normal trending shortening structure within the model syntaxis, where the obliquity angle γ decreases. The syntaxis shortening structure has localized uplift rates of ~10-12 mm/a (4 in Figure 1b). These results are nearly identical for the segmented linear and arcuate basal boundary conditions.

Interestingly, we observe the formation of a strike-slip shear zone cutting obliquely across the orogenic wedge at the section of the arcuate model geometry where the obliquity angle begins to increase in nearly an identical orientation to that observed by Whipp et al. (2014). This structure facilitates the transition from oblique slip to partitioned strain along strike in the arcuate orogen. The similarity in the position and structural orientation of this shear zone suggest it is a robust feature in models with a transition from orogen-normal to oblique convergence.

**4. Implications and conclusions**

In spite of the arcuate geometry of the orogenic wedge topography, orogen-bounding weak zones and boundary conditions, the general model behaviour we observe is very similar to that of an orogen with a linear oblique segment between two linear region of orogen-normal convergence (e.g., Whipp et al., 2014). The rates of orogen-parallel mass transport, conditions under which strain partitioning is observed and uplift velocities in the model syntaxis are all similar to the values reported by Whipp et al. (2014). This suggests that deformation on the shear zones that bound the orogenic wedge and within the wedge are controlled by the mechanical properties of the crust and not by the geometry of the basal boundary conditions. To some degree this is not surprising, since the basal boundary conditions are applied beneath the lateral edge of the viscous weak region underlying the orogenic plateau, which may slightly decouple them from deformation in the orogenic wedge in the upper crust. The boundary conditions are certainly important in driving strain partitioning via oblique convergence, but it appears the mechanical properties of the crust determine how the upper crust deforms.

In addition, the formation of the strike-slip fault system cutting obliquely across the orogenic wedge is notable not only because it forms in a similar position to its equivalent in models from Whipp et al. (2014), but also because it has a remarkably similar orientation to the recently recognized Western Nepal Fault System (WNFS) in the western Himalaya (Murphy et al., 2014). The WNFS is thought to form in the transition zone between oblique convergence along the Main Himalayan Thrust in the central Himalaya and partitioned strain

in the west. The consistent presence of a WNFS-like structure in models with partitioned strain supports the hypothesized role of the WNFS and suggests it is an important structural feature of the western Himalaya.

Lastly, in addition to the development of a structure similar to the WNFS, our models produce several important features observed in the Himalaya. When strain is partitioned, the sense of motion on the basal shear zone in the obliquely convergent parts of the model is nearly orogen-normal, which is consistent with observed fault slip vectors along the Himalayan arc (e.g., Molnar and Lyon-Caen, 1989). We also observe dextral slip on the rear shear zone (3 in Figure 1b), which is consistent with the sense of motion on the Karakoram fault. Finally, the uplift rates observed in the model syntaxis region are quite similar to the rates of Quaternary exhumation in the NPHM (e.g., Whittington, 1996; Crowley et al., 2009). Combined these observations suggest orogen-parallel mass transport as a result of strain partitioning is an alternative to the 'tectonic aneurysm' model that does not rely on rapid surface erosion to trigger rapid uplift.

**References:**

Crowley, J., Waters, D., Searle, M., and Bowring, S., 2009. Pleistocene melting and rapid exhumation of the Nanga Parbat massif, Pakistan: Age and P-T conditions of accessory mineral growth in migmatite and leucogranite: Earth and Planetary Science Letters, 288, 408–420.

Fitch, T., 1972. Plate Convergence, Transcurrent Faults, and Internal Deformation Adjacent to Southeast Asia and the Western Pacific: Journal of Geophysical Research, 77, 4432–4460.

Herman, F., Copeland, P., Avouac, J.-P., Bollinger, L., Mahéo, G., Le Fort, P., Rai, S., Foster, D., Pecher, A., Stüwe, K., and Henry, P., 2010. Exhumation, crustal deformation, and thermal structure of the Nepal Himalaya derived from the inversion of thermochronological and thermobarometric data and modeling of the topography: Journal of Geophysical Research, B, Solid Earth and Planets, 115, B6, B06407, doi: 10.1029/2008JB006126.

McCaffrey, R., 1992. Oblique Plate Convergence, Slip Vectors, and Forearc Deformation: Journal of Geophysical Research, B, Solid Earth, 97, B6, 8905–8915, doi: 10.1029/92JB00483.

McCaffrey, R., and Nabelek, J., 1998. Role of oblique convergence in the active deformation of the Himalayas and southern Tibet plateau: Geology, 26, 691–694.

Molnar, P., and Lyon-Caen, H., 1989. Fault plane solutions of earthquakes and active tectonics of the Tibetan Plateau and its margins: Geophysical Journal International, 99, 123–154.

Murphy, M.A., Taylor, M.H., Gosse, J., Silver, C.R.P., Whipp, D.M., and Beaumont, C., 2014. Limit of strain partitioning in the Himalaya marked by large earthquakes in western Nepal: Nature Geoscience, 7,38–42.

Seeber, L., and Pecher, A., 1998. Strain partitioning along the Himalayan Arc and the Nanga Parbat Antiform: Geology, 26, 791–794.

Whipp, D.M., Beaumont, C., and Braun, J., 2014. Feeding the "aneurysm": Orogen-parallel mass transport into Nanga Parbat and the western Himalayan syntaxis: Journal of Geophysical …,, doi: 10.1002/2013JB010929.

Whipp, D.M., Jr, Ehlers, T.A., Blythe, A.E., Huntington, K.W., Hodges, K.V., and Burbank, D.W., 2007. Plio-Quaternary exhumation history of the central Nepalese Himalaya: 2. Thermo-kinematic and thermochronometer age prediction model: Tectonics, 26, doi: 10.1029/2006TC001991.

Whittington, A., 1996. Exhumation overrated at Nanga Parbat, northern Pakistan: Tectonophysics, 260, 215–226.

Zeitler, P., Meltzer, A., Koons, P., Craw, D., Hallet, B., Chamberlain, C., Kidd, W., Park, S., Seeber, L., Bishop, M., and others, 2001. Erosion, Himalayan Geodynamics, and the Geomorphology of Metamorphism: GSA Today, 11, 4–9.

# Detrital zircon age record in sandstones from three Caledonian nappes in NE Finnmark, northern Norway

W. Zhang[1], D. Roberts[2] and V. Pease[1]

[1]Department of Geological Sciences, Stockholm University, 106 91 Stockholm, Sweden
[2]Geological Survey of Norway, PostBox 6315 Sluppen, 7491 Trondheim, Norway
E-mail: david.roberts@ngu.no

U-Pb detrital zicon age spectra are presented for six samples of sandstones from different formations in the Kalak, Laksefjord and Gaissa nappe complexes of the Finnmark Caledonides. The Early Neoproterozoic sandstones from the Kalak and Laksefjord nappes mostly show diverse population peaks within the range 2.0-1.0 Ga and, in conjunction with palaeocurrent data, are interpreted to derive from sourcelands in the Fennoscandian Shield to the 'south'. The Laksefjord samples also show peaks in the Neoarchaean at c. 2.9-2.6 Ga, sourced from rocks of those ages occurring in these northern shield areas today. Sandstones of Late Ediacaran to Early Cambrian age in adjacent formations in the Gaissa Nappe Complex show markedly different age spectra. One, derived from a southerly source, shows solely Neoarchaean to Palaeoproterozoic grains, whereas a sandstone derived from the northeast shows a wide spread of Mesoproterozoic zircons and a major peak at c. 550 Ma. This distribution and Ediacaran peak is interpreted to represent deposition in a Timanian foreland basin.

**Keywords:** U-Pb zircon data, Finnmark, provenance, Caledonian nappes, Timanide orogen

## 1. Geological setting

Varanger Peninsula in Finnmark, northeasternmost Norway, is somewhat unique in lying at the confluence of the Timanide and Caledonide orogenic belts. The main siliciclastic metasedimentary successions involved in these orogenies in this particular region range in age from Early Tonian or Late Stenian to Cambrian, also reaching up to Tremadocian on the nearby Digermul Peninsula (Figure 1). Extending from the southern Urals northwestwards to NE Norway and, by inference, offshore beneath the Caledonian thrust sheets, the NW-SE-trending Timanide accretionary orogen is characterised by peak deformation and metamorphism in the Timans of Russia at c. 580-550 Ma. By contrast, the northernmost parts of the Scandinavian Caledonides record two principal tectonothermal events, in Late Cambrian-Early Ordovician and Mid Silurian-Early Devonian times, involving the southeastward translation of extensive nappe complexes onto the Baltoscandian margin of the Fennoscandian Shield. The crystalline basement in this part of Finnmark and neighbouring areas of Finland and Russia comprises Neoarchaean gneissic granites and granodiorites, mostly 2.9-2.5 Ga, succeeded across strike to the southwest by the 2.0-1.9 Ga Lapland Granulite Belt, the latter deformed during the 1.95-1.77 Ga Svecofennian orogeny which affected vast areas of the shield farther south in Finland, Sweden and Norway. These various terranes also extend northwestwards beneath the Caledonian nappes.

In Finnmark, in recent years, U-Pb dating of detrital zircon has been reported from the Caledonian Kalak Nappe Complex (Kirkland et al., 2007, 2008) as well as from diverse formations on the Varanger and Digermul peninsulas (Roberts et al., 2008, Orlov et al., 2011, Roberts and Siedlecka, 2012, Wen et al., 2014 and in prep.). For the older, latest Stenian to Tonian sandstones of Varanger, with abundant palaeocurrent data indicating sources in the SE to SW quadrant, age peaks of c. 1.9-1.8 Ga and 2.8-2.7 Ga are clearly reflecting derivation from the exposed Palaeoproterozoic and Neoarchaean terranes on the shield. This is also the case for the oldest member of the autochthonous cover sequence of the Dividal Group (Wen et al., 2014). Younger Cryogenian formations, on the other hand, with sourcelands also to the south or southwest, are dominated by a wide spread of abundant zircon grains between 1.6

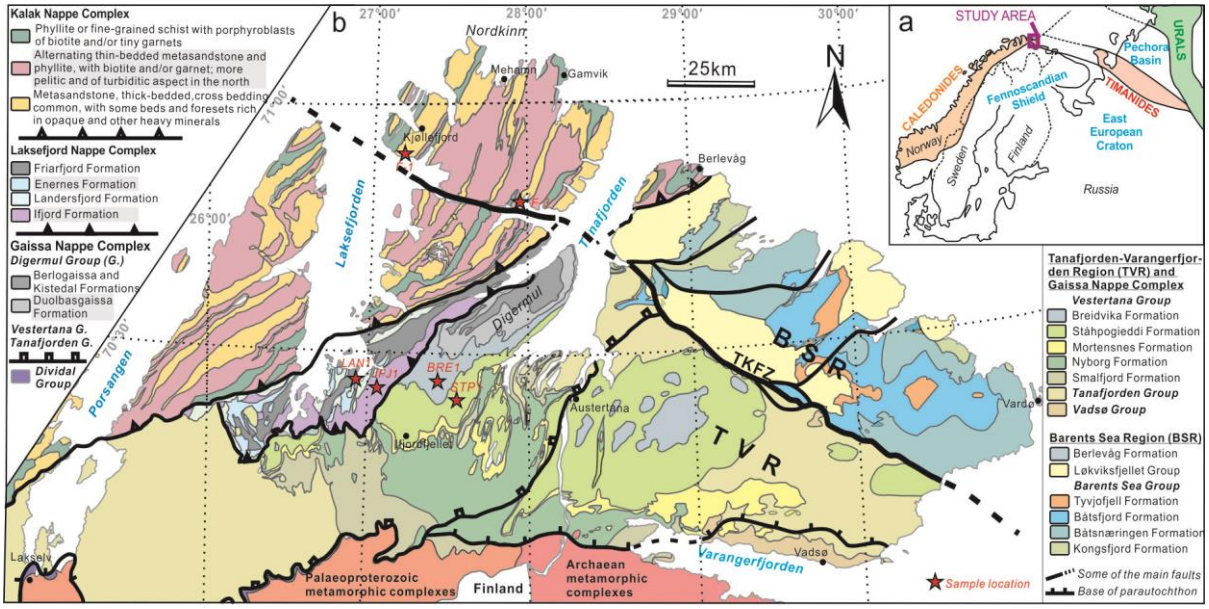


**Figure 1.** (a) Location of the Timanides and Caledonides, and the study area. (b) Simplified geological map of NE Finnmark showing the three main nappes and the sample localities. TKFZ-Trollfjorden-Komagelva Fault Zone.

and 0.9 Ga. Mesoproterozoic rocks of this age are either absent or poorly exposed in northern Fennoscandian today, thus providing a puzzle as to the sources of these profuse grains.

In the present contribution we deal specifically with detrital zircons from samples from different formations in the Kalak, Laksefjord and Gaissa nappe complexes, situated to the west of Varanger Peninsula (Figure 1). Both the Kalak and the Laksefjord nappe complexes are dominated by Neoproterozoic cross-bedded sandstones, with a basal polymict conglomerate in the latter case. Palaeocurrent data from thrust sheets in these nappes show a fairly unimodal sediment routing towards N-NW (Williams, 1974, Roberts, 2007), i.e., with sourcelands on the Fennoscanian Shield. For the Gaissa Nappe Complex, sources for the Ediacaran to Tremadocian sediments based on palaeocurrent data show a marked variability (Banks et al., 1971).

## 2. Sample locations

*Kalak samples*:

*F1*. Sandstone at Brenngamklubben, Dyfjord, southwestern coast of Nordkinn Peninsula; locality at coordinates NU50920 786570 on 1:50,000 map-sheet 'Kjøllefjord' 2236-4.

*F3*. Sandstone at Karibukta, near Ivarsfjord, southeastern coast of Nordkinn Peninsula; locality at NU53510 785550 on 1:50,000 map-sheet 'Hopseidet' 2236-1.

*Laksefjord samples*:

*LAN1*. Quartzitic sandstone from the Landersfjord Formation in Friarfjorden; locality at MU49895 781680 on 1.50,000 map-sheet 'Adamsfjord' 2135-1.

*IFJ1*. Sandstone matrix of the Gozavarre conglomerate, basal member of the Ifjord Formation; locality c. 3 km SW of Ifjord at NU50170 781565 on 1:50,000 map-sheet 'Ifjordfjellet' 2235-4.

*Gaissa samples*:

*STP 1*. Sandstone from the Manndraperelv Member of the Ståhpogieddi Formation, Vestertana Group; locality at NU51960 781350 on 1:50,000 map sheet 'Ifjordfjellet' 2235-4.

*BRE 1*. Sandstone from the lower member of the Breidvika Formation, Vestertana Group; locality at NU51600 781670 on 1:50,000 map sheet 'Ifjordfjellet' 2235-4.

### 3. U-Pb zircon analytical data and interpretations

*Kalak*: The two samples F1 and F3 show fairly similar age-spectral ranges between c. 2.0 and 1.0 Ga, though with peaks at slightly different times (Figure 2). F1 shows a main concentration of grains at c. 1.7-1.5 Ga with subsidiary peaks in Late Palaeoproterozoic and Late Mesoproterozoic time. For F3, a main spike occurs at 1.3-1.15 Ga with a less prominent peak in the 1.7 to 1.5 Ga range, tailing off towards 2.0 Ga. There are also indications of a few older grains, perhaps Neoarchaean. Maximum ages for the F1 and F3 successions are put at 1029 and 1124 Ma, respectively. In terms of provenance, and recalling the palaeocurrent data, the results point to input from the Palaeoproterozoic to Mesoproterozoic terranes in the northern Fennoscandian Shield. Comparing with the age spectra produced by Kirkland et al. (2007) from parts of the Kalak farther to the southwest, there are clear similarities, even with the appearance of a few Neoarchaean grains in the samples nearest the basal thrust plane of the Kalak Nappe Complex. A Baltican origin for the sediments in at least the lower thrust sheets of the Kalak thus appears convincing, thus opposing the suggestion of Kirkland et al. (2007) that the Kalak successions are totally foreign to Baltica.

*Laksefjord*: The samples LAN1 and IFJ1 show strongly disparate age spectra. Sample IFJ1 shows almost all 150 grains in the range 3.0-2.5 Ga, peaking at c. 2750 Ma (Figure 2). In this respect, it is relevant to mention the U-Pb zircon dating of a high-K granite from a slice of basement incorporated in the basal part of the Laksefjord Nappe Complex, which yielded an age of 2.85 Ga (Roberts and Gromet 2009). This granite is present as large clasts in the conglomerate and also occurs *in situ* in the Neoarchaean terrane south of Varangerfjorden. Thus, a fairly local source in the shield for the Ifjord Formation seems indisputable. Sample LAN1 displays a principal grain array between 2.0 and 1.0 Ga, not unlike the Kalak samples,

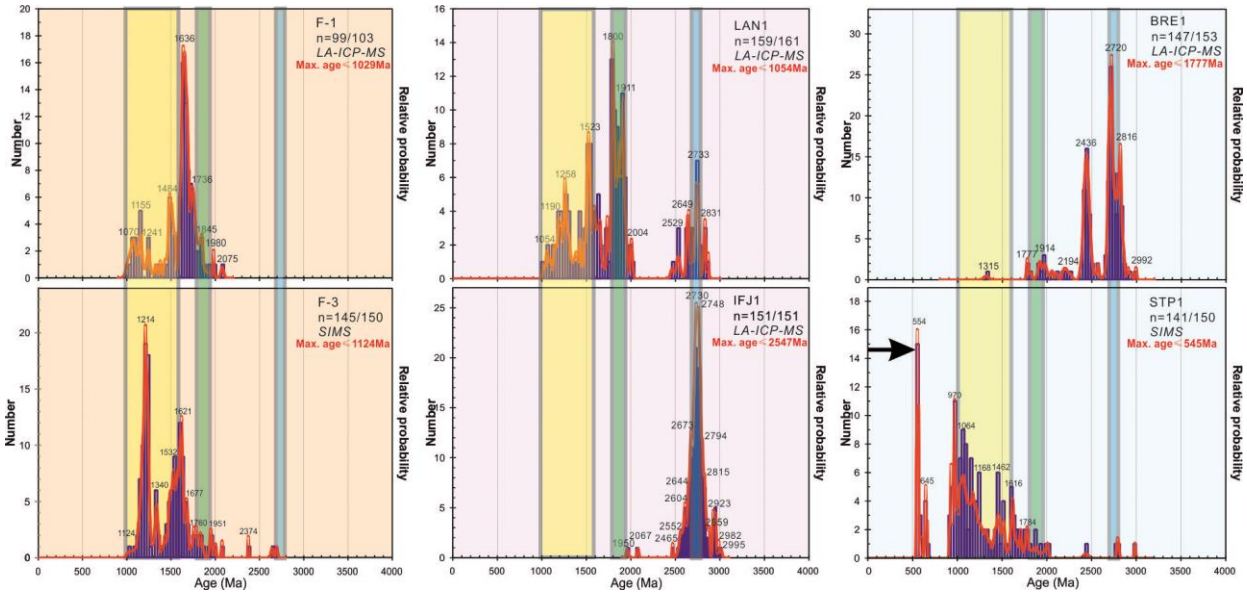


**Figure 2.** Probability density versus age (analysed age >1000 Ma, use $^{207}Pb/^{206}Pb$ ages; <1000Ma, use $^{206}Pb/^{238}U$ ages). The probability density plots exclude ages >10% discordant and high error (>10% uncertainty in $^{206}Pb/^{238}U$ or $^{206}Pb/^{207}Pb$ age). The number of grains indicated = those <10% discordant within uncertainties/the total number of analyses. Max. age = maximum age of two or more grains of the same age.

with a main, double-spiked peak at 1.9-1.8 Ga. In addition, there is a second cluster of grains in the range 2-9-2.5 Ga, peaking just below 2.8 Ga, which is reminiscent of the main peak and range in IFJ1. LAN1 clearly received detritus from the same Neoarchaean terrane as IFJ1, but also differs markedly in also having acquired abundant grains from a Late Palaeoproterozoic and Mesoproterozoic source terrane situated somewhere to the S-SW.

*Gaissa*: The two samples from the Gaissa allochthon show different age spectra despite the fact that the host formations have roughly the same, latest Ediacaran to earliest Cambrian age. BRE1 shows two major peaks at 2.8-2.7 and 2.4 Ga, with a few grains in the range 2.2-1.8 Ga (Figure 2). This sediment was clearly sourced in the Neoarchaean to Palaeoproterozoic terranes to the 'south', as also indicated by the palaeocurrent data. Sample STP1 has an age spectrum quite unlike that of BRE1, or indeed of any of our other samples. While showing a wide range of Mesoproterozoic grains, its principal feature is a major peak at c. 550 Ma. Along with the palaeocurrent evidence of having been sourced in the northeast, this clearly points to input from the Timanides. The formation is thus interpreted to represent deposition in a Timanian foreland basin (Gorokhov et al. 2002, Roberts and Siedlecka 2012, Wen et al. 2014). This is also the case for younger members of the Dividal Group (Andresen et al., 2014). The Mesoproterozoic input is likely to represent material recycled from the older, passive-margin successions occurring along the northern Timanian parts of Kola Peninsula or those now submerged offshore.

**References:**

Andresen, A., Agyei-Dwarko, N.Y., Kristoffersen, M., and Hanken, N.M., 2014. A Timanian foreland basin setting for the late Neoproterozoic-Early Palaeozoic cover sequences (Dividal group) of northeastern Baltica. Geol. Soc., London, Spec. Publ., 390, 157-175.

Banks, N.L., Edwards, M.B., Geddes, W.P., Hobday, D.K., and Reading, H.G., 1971. Late Precambrian and Cambro-Ordovician sedimentation in East Finnmark. Nor. Geol. Unders., 269, 197-236.

Gorokhov, I.M., Siedlecka, A., Roberts, D., Mel'nikov, N.N., and Turchenko, T.L., 2001. Rb-Sr dating of diagenetic illite in Neoproterozoic shales, Varanger Peninsula, northern Norway. Geol. Mag., 138, 541-562.

Kirkland, C.L., Daly, J.S., and Whitehouse, M.J., 2007. Provenance and terrane evolution of the Kalak Nappe Complex, Norwegian Caledonides: implications for Neoproterozoic palaeogeography and tectonics. Jour. Geol., 115, 21-41.

Kirkland, C.L., Daly, J.S., Chew, D.M., and Page, L.M., 2008. The Finnmarkian Orogeny revisited: an isotopic investigation in eastern Finnmark, Arctic Norway. Tectonophysics, 460, 158-177.

Orlov, S.Y., Kuznetsov, N.B., Miller, E. L., Soboleva, A.A., and Udorotina, O.V., 2011. Age constraints for the pre-Uralide-Timanide orogenic event inferred from the study of detrital zircons. Dokl. Earth Sci., 440, 1216- 1221.

Roberts, D., 2007. Palaeocurrent data from the Kalak Nappe Complex, northern Norway: a key element in models of terrane affliliation. Nor. Jour. Geol., 87, 319-328.

Roberts, D., Davidsen, B., and Slagstad, T., 2008. Detrital zircon age record of platformal and basinal Neoproterozoic sandstones from Varanger Peninsula, North Norway: a preliminary study. (abstract and poster) European Geosciences Union, General Assembly, Vienna, April 2008.

Roberts, D., and Gromet, L.P., 2009. A U-Pb zircon Archaean age for granitoid rocks in the Kunes Nappe, Laksefjord Nappe Complex, Finnmark, North Norway. Nor. Geol. Unders. Bull., 449, 1-8.

Roberts, D., and Siedlecka, A., 2012. Provenance and sediment routing of Neoproterozoic formations on the Varanger, Nordkinn, Rybachi and Sredni peninsulas, North Norway and Northwest Russia: a review. Nor. Geol. Unders. Bull. 452, 1-19.

Williams, G.D., 1974. Sedimentary structures in the amphibolite-facies rocks of the Bekkarfjord Formation, Laksefjord, Finnmark. Nor. Geol. Unders., 311, 35-48.

Zhang, W., Roberts, D., and Pease, V., 2014. Detrital zircon U-Pb analysis of Timanian passive-margin successions and Caledonian nappes in northern Norway and significance for Arctic reconstructions. (abstract and poster) European Geosciences Union, General Assembly, Vienna, May 2014.